Time-Compression Overlap-Add (TC-OLA) for Wireless Communications

by

Stephen Harrison
B.Eng., University of Victoria, 2009

A Dissertation Submitted in Partial Fulfillment of the
Requirements for the Degree of

DOCTOR OF PHILOSOPHY

in the Department of Electrical and Computer Engineering

Time-Compression Overlap-Add (TC-OLA) for Wireless Communications

by

Stephen Harrison
B.Eng., University of Victoria, 2009

Supervisory Committee

Dr. P. F. Driessen, Supervisor
(Department of Electrical and Computer Engineering)

Dr. W. Page, Departmental Member
(Department of Electrical and Computer Engineering)

Dr. G. Tzanetakis, Outside Member
(Department of Computer Science)

Supervisory Committee

Dr. P. F. Driessen, Supervisor
(Department of Electrical and Computer Engineering)

Dr. W. Page, Departmental Member
(Department of Electrical and Computer Engineering)

Dr. G. Tzanetakis, Outside Member
(Department of Computer Science)

ABSTRACT

Time-compression overlap-add (TC-OLA) is presented as a novel method of communications over a (wireless) channel, which is shown to have benefits over other methods in some applications. TC-OLA is initially explored in an experimental context using a custom wideband software-defined radio (SDR) to gain insight into some of the possibilities of this method. Basic analysis is developed showing the processing gain, transmitted spectrum, and behaviour in fading channels. The method is considered as a candidate for low power wide area network (LPWAN) applications, highlighting the equivalent channel property, channel averaging, and ability to handle more simultaneous users in the uplink than other schemes in this application area. The method is then considered as an alternative to single carrier frequency domain equalization (SC-FDE) for ultrawideband (UWB) applications, where the ability to reduce or eliminate the cyclic prefix (CP) overhead while still using frequency domain equalization (FDE) techniques is highlighted. Additional application areas for this technology are briefly considered, including cognitive radio and radar. The process of patenting this technology is outlined in an appendix. The issued patent can be found through the United States Patent and Trademark Office (USPTO) as U.S. Patent 9,479,216.

Contents

Supervisory Committee **ii**

Abstract **iii**

Table of Contents **iv**

List of Tables **ix**

List of Figures **x**

Acronyms **xiii**

Acknowledgements **xvii**

1 Introduction **1**

1.1 Claimed Advantages 2

1.2 Contributions 4

1.3 Outline 5

2 Novel UWB and Spread Spectrum System Using Time Compression and Overlap-Add Techniques **8**

2.1 Introduction 8

2.2 Literature Review 10

2.3 Theory of Operation 11

2.3.1 Time Compression and Overlap-Add 11

2.3.2 Windowing 13

2.3.3 Synchronization 15

2.3.4 Channel Effects 15

2.3.5 Interference Rejection 22

2.3.6 Extension to CDMA 22

2.3.7 Extension to TDMA 24
2.3.8 Complex Baseband and Real Passband Signals 24
2.3.9 System Implementation 26
2.4 Wideband SDR Implementation 27
2.4.1 Transmitter 29
2.4.2 Receiver 31
2.4.3 Experiments 34
2.5 USRP Implementation 37
2.5.1 Experiments 41
2.6 Conclusions and Future Work 46

3 Time-Compression Overlap Add: Description and Analysis 49
3.1 Introduction 49
3.2 Time-Shifting Model 50
3.2.1 AWGN Performance 53
3.2.2 Multipath Rayleigh Fading Performance 54
3.3 Digital Filter Model 56
3.3.1 Transmitted Spectrum 62
3.4 Conclusion and Future Work 67

4 Time-Compression Overlap Add for Low Power Wide Area Networks 68
4.1 Introduction 68
4.2 TC-OLA System Model 69
4.2.1 Code Division 72
4.2.2 Equivalence with DS/CDMA 73
4.3 Multiuser Performance Analysis 76
4.3.1 Generic Multipath Model 77
4.3.2 Matrix Notation 77
4.3.3 In Static Frequency Selective Channels 81
4.3.4 In Frequency Flat Fading 82
4.3.5 In Time-Varying Frequency Selective Channels 90
4.4 System Design and Results 91
4.5 Conclusion 95

5 Robust TC-OLA Reception with Frequency Domain Equalization for UWB Applications **98**
5.1 Introduction . . . 98
5.2 TC-OLA System Model . . . 100
5.3 Frequency-Domain Processing . . . 100
5.4 Simulation Results . . . 103
5.4.1 Indoor Channels . . . 104
5.4.2 Industrial Channels . . . 106
5.5 Conclusion . . . 108

6 Discussion and Future Work **109**
6.1 Perspectives on TC-OLA . . . 109
6.1.1 As a Matched Filter Communications System . . . 110
6.1.2 As a Spread Spectrum Method . . . 112
6.1.3 As a Multicarrier and Cyclic Prefix Block Processing Method 114
6.1.4 Sample Rearrangement and SC-FDMA . . . 115
6.2 System Parameter Relationships . . . 116
6.3 Multiple Access . . . 117
6.3.1 Time Division . . . 117
6.3.2 Code Division . . . 119
6.3.3 Frequency Division . . . 121
6.3.4 Multicarrier Code Division . . . 121
6.4 Circular TC-OLA . . . 122
6.5 Offset TC-OLA . . . 123
6.5.1 Phase and Frequency Synchronization . . . 125
6.5.2 Window Synchronization . . . 128
6.6 Timing Recovery . . . 130
6.6.1 Sample Frequency Offset . . . 131
6.6.2 Parameter Estimation . . . 131
6.7 Window Weighting . . . 132
6.7.1 Channel Inversion . . . 132
6.7.2 Window Discard . . . 134
6.8 Hardware Implementation . . . 135
6.9 Multiuser FDE . . . 139
6.10 Novel Applications . . . 140

6.10.1 Multiple Antenna Systems 140
6.10.2 Radar 141
6.10.3 Cognitive Radio 141
6.10.4 Audio Reverb 142
6.10.5 Hybrid Analog/Digital Broadcast 142
6.11 Conclusions 143
6.11.1 Patent Concepts 143
6.11.2 Analysis and Design Activities 144
6.11.3 Suggested Publications 146

7 Conclusions **148**

A Glossary of Symbols **150**

B Generic Multipath Model **153**

C Wideband SDR Receiver **155**
Software Usage Example 155
RFRB-SDR Design Document 158

D Patent Document **181**
Original Claims 181
First Office Action 189
Amended Claims 200
Notice of Allowability 211
Issued Patent 214

E Comparison of TC-OLA with RPMA **240**
E.1 Introduction 240
E.2 Uplink Capacity 240
E.2.1 Pole Capacity 241
E.2.2 Power Control 245
E.2.3 Scheduled vs. Random 245
E.2.4 Time-Dispersive Channels 246
E.3 Comparison of RPMA with Slotted ALOHA 247
E.4 TC-OLA Compatibility with RPMA 248

F Publishing Challenges **250**

F.1 Reviews of *Time-Compression Overlap Add for Low Power Wide Area Networks* 250

F.1.1 Editor's Comments 250

F.1.2 Reviewer 1 251

F.1.3 Reviewer 2 252

F.1.4 Reviewer 3 253

Bibliography **255**

List of Tables

Table 2.1 Example System Parameters for Figures 2.4-2.7 16
Table 2.2 System Parameters for Wideband SDR Implementation 28
Table 2.3 Experimental System Parameters 40
Table 2.4 Frequency Selective Channel Model 44

Table 5.1 Range of TC-OLA Parameters and Effective CP for $L_B = 256$. 104

Table A.1 General Symbols 152
Table A.2 Vectors and Matrices 152

List of Figures

Figure 2.1 Assembling a Stream of Non-Overlapping Segments 12
Figure 2.2 Assembling a Stream of Non-Overlapping Hanning Windows . 14
Figure 2.3 Effect of Frame Loss, Showing Drop in Output Amplitude . . 16
Figure 2.4 Static Two-Ray Channel Response 17
Figure 2.5 Time-Varying Two-Ray Channel Response, 10 Second Sweep . 18
Figure 2.6 Time-Varying Two-Ray Channel Response, 1 Second Sweep . 20
Figure 2.7 Time-Varying Two-Ray Channel Response, 0.1 Second Sweep 21
Figure 2.8 Basic Code Division Example 23
Figure 2.9 Basic Time Division Example 25
Figure 2.10 Simplified System Diagram 26
Figure 2.11 Signal Discontinuity Caused by Narrowband Interference . . . 27
Figure 2.12 Wideband SDR System Connection Diagram 29
Figure 2.13 Transmitted Frame Format 30
Figure 2.14 Receiver Digital Signal Processing Architecture 32
Figure 2.15 Received Samples, Timing Marker and Alignment Window . . 33
Figure 2.16 Impulse Response Averaged Over 8 Sweeps 35
Figure 2.17 Impulse Response Averaged Over 8 Sweeps, I/Q Crosstalk . . 36
Figure 2.18 Measured Power Delay Profile at 8, 14, and 20 Feet 38
Figure 2.19 USRP-Based System Hardware Connection Diagram 39
Figure 2.20 Recovered Impulse Response with Simple Wired Channel . . . 42
Figure 2.21 Recovered Impulse Response with Two-Ray Model 42
Figure 2.22 BER Floor vs. Maximum Doppler Frequency 43
Figure 2.23 BER Floor vs. Normalized Maximum Doppler Frequency . . . 45
Figure 2.24 BER Floor vs. Normalized Maximum Doppler Frequency . . . 47
Figure 2.25 BER Floor vs. Normalized Maximum Doppler Frequency . . . 47

Figure 3.1 TC-OLA Transmission Concept 51
Figure 3.2 Multirate Transmitter Process 56

Figure 3.3 Multirate Receiver Process 57
Figure 3.4 Equivalent Transmitter Process 58
Figure 3.5 Equivalent Transmitter Process for $R = 1$ 59
Figure 3.6 Equivalent Receiver Process for $R = 1$ 59
Figure 3.7 System Diagram 60
Figure 3.8 Alternate Receiver Structure 60
Figure 3.9 Alternate Interpolation Operation 61
Figure 3.10 Modified Upsampling Operation 61
Figure 3.11 Transmitter Structure for $R > 1$ 62
Figure 3.12 Output Spectrum and Envelope, $M = 12$, $R = 1$ 64
Figure 3.13 Output Spectrum and Envelope, $M = 96$, $R = 1$ 65
Figure 3.14 Output Spectrum and Envelope, $M = 12$, $R = 2$ 66

Figure 4.1 TC-OLA Transmit Operation, Sine Windows 70
Figure 4.2 TC-OLA Transmit Operation, Digital Symbols 71
Figure 4.3 TC-OLA–DS/CDMA Equivalence 75
Figure 4.4 Matrix Construction of Delayed Multipath Components 79
Figure 4.5 TC-OLA Matrix Permutation Operation 79
Figure 4.6 System Model (Matrix Formulation) 80
Figure 4.7 Interference Limit vs. Rician K Factor 86
Figure 4.8 SIR for Correlated Rayleigh Fading in Downlink 88
Figure 4.9 Selection Combining to Raise SIR Limit 90
Figure 4.10 Equivalent Tap Amplitude vs. Phasor Rotation Speed 92
Figure 4.11 Comparing TC-OLA and RPMA-like Systems in Downlink . . 94
Figure 4.12 Comparing TC-OLA and RPMA-like Systems in Uplink, Timing Uncertainty 96

Figure 5.1 TC-OLA Receiver for Frequency Domain Equalization 101
Figure 5.2 Alternate TC-OLA Receiver for Frequency Domain Equalization 102
Figure 5.3 Comparing TC-OLA and SC-FDE in CM1 105
Figure 5.4 Comparing TC-OLA Parameters in CM8 107

Figure 6.1 Unit-Energy Pulse Shape, Sine Window 110
Figure 6.2 Autocorrelation of Unit-Energy Pulse 110
Figure 6.3 Magnitude Spectrum of Pulse, Sine Window 111
Figure 6.4 Unit-Energy Pulse Shape, RRC Window 112

Figure 6.5 Magnitude Spectrum of Pulse, RRC Window 113
Figure 6.6 Magnitude Spectrum of Coded Pulse, RRC Window 114
Figure 6.7 Mapping TC-OLA to IFDMA 115
Figure 6.8 Time-Division Waveform with Two Users 118
Figure 6.9 Circular TC-OLA 122
Figure 6.10 Offset Window Functions, Constant Envelope 124
Figure 6.11 Offset TC-OLA Transmitter and Receiver, Alignment Delays . 125
Figure 6.12 Offset Windows with Relative Phase Angle 126
Figure 6.13 Offset TC-OLA Detector Circuit 127
Figure 6.14 TC-OLA Phase Synchronizer Circuit 128
Figure 6.15 Synchronization Waveform for Different Phase Offsets 129
Figure 6.16 TC-OLA Window Synchronizer 130
Figure 6.17 Analysis Weighting Function 133
Figure 6.18 Probability Density Function of Output SNR, Channel Inversion134
Figure 6.19 Output Signal and Noise Power for Consecutive Window Discard135
Figure 6.20 SNR Gain with Simple Discard Strategy 136
Figure 6.21 General Transmit Hardware 137
Figure 6.22 Transmit Hardware for Binary Digital Symbols 138
Figure 6.23 Receive Hardware 139

Figure E.1 TC-OLA Pole Capacity for $SNR_tgt = 5.5$ dB, $\frac{\mu_r^2}{\sigma_g^2} = 1$ 243
Figure E.2 TC-OLA Uplink Loading, Independent Rayleigh Fading 244

Acronyms

3G third generation

4G fourth generation

5G fifth generation

ADC analog-to-digital converter

AWGN additive white Gaussian noise

BER bit error rate

B-IFDMA block-interleaved FDMA

BPSK binary phase shift keying

cdf cumulative density function

CDMA code division multiple access

COLA constant overlap-add

CORDIC coordinate rotation digital computer

CP cyclic prefix

CR cognitive radio

CSI channel state information

DAC digital-to-analog converter

DFT discrete Fourier transform

DQPSK differential QPSK

DS/CDMA direct sequence CDMA

DSB-SC dual sideband suppressed carrier

DSSS direct sequence spread spectrum

EGC equal gain combining

FDE frequency domain equalization

FFT fast Fourier transform

FIR finite impulse response

FPGA field-programmable gate array

GPSDO GPS-disciplined oscillator

GSPS gigasamples per second

IBI interblock interference

IEEE Institute of Electrical and Electronics Engineers

IFDMA interleaved frequency division multiple access

IoT internet of things

ISI intersymbol interference

ISM industrial, scientific and medical

LFDMA localized FDMA

LPWAN low power wide area network

LTE long term evolution

M2M machine-to-machine

MIMO multiple input multiple output

MMSE minimum mean-square error

MRC maximal ratio combining

MSPS megasamples per second

OFDM orthogonal frequency division multiplexing

OLA overlap-add

OTN optical transport network

PAN personal area network

PAPR peak-to-average power ratio

pdf probability density function

PDH plesiosynchronous digital hierarchy

QAM quadrature amplitude modulation

QoS quality of service

QPSK quadrature phase shift keying

RF radio frequency

RFNoC RF network-on-chip

RPMA random phase multiple access

RRC root raised cosine

SC-FDE single carrier frequency domain equalization

SDH synchronous digital hierarchy

SDR software-defined radio

SINR signal-to-interference-and-noise ratio

SNR signal-to-noise ratio

SONET synchronous optical network

SUI Stanford University Interim

TCM time-compression multiplexing

TC-OLA time-compression overlap-add

TDE time domain equalization

TDM time division multiplexing

TDMA time division multiple access

USRP universal software radio peripheral

UWB ultrawideband

WCDMA wideband CDMA

ACKNOWLEDGEMENTS

I would like to personally thank:

Dr. Peter Driessen, for his mentorship, encouragement, insight, and all of the interesting conversations on a variety of topics over the years.

My committee members, Dr. George Tzanetakis and Dr. Wyatt Page, for providing valuable feedback in the candidacy exam.

Jerome Etwaroo and Dr. Aislinn Sirk, for their excellent handling of our patent application through the UVic technology transfer office.

All of the funding sources, including the NSERC Engage grant with Codan Radio Communications, Dr. Rodney Herring's atmospheric imaging project, Dr. Andrew Schloss' radiodrum project, the UVic Learning and Teaching Centre, the ELEC 365 laboratory TA position for Dr. Subhasis Nandi (RIP), graduate student awards, and others.

Grant Brydon (PMC-Sierra/Microsemi Corp.), for keeping me usefully employed through the bulk of this journey.

Tracey Coulter, for her continuous love and support.

Kitty Baby, for her additional "help".

Dr. Eric Manning, for chairing the Friday afternoon meetings.

Jonathon Pendlum (Ettus Research), for assistance with Zynq-related issues when developing the wideband SDR.

Kirk McNally, for his expertise in audio recording.

ELW402 Students Leonardo Jenkins, Duncan MacConnell, Steeve Bjørnson, Mike Cavallin, Görkem Çipli, Shawn Trail, Ahmed Fouad Ahmed Youssef and Peter Kremler.

Debbie Dergousoff, for sharing her home until she finished her Ph.D. and went off to live in Kyrgyzstan.

Paul Moquin and Ryoko Sano, for sharing their home until I finished my Ph.D. and went off to live in Penticton.

Time in Between, Lonesome Pine and the Riverside Bluegrass Band, for providing a creative outlet. Paul Moquin, Trevor Lantz, Megan Adams, Mike Brooks, Patty Castle, Amy Lounder, Dan Belgue, Angus MacKenzie, Eric Adams, James Whittall, Jeff Dill, Tad Ruszel and Ivonne Hernandez: Thanks for the good times and good tunes.

This document was typeset in LaTeX 2$_\varepsilon$ on Ubuntu Linux. Sublime Text 3 with the LaTeXing plugin was used for text entry, with Zotero integration for references and Subversion for revision control.

Simulation results were obtained from Python-based simulations using the NumPy and SciPy libraries. Long-running simulations were performed on Westgrid using the Python multiprocessing library.

Most data plots were generated using the matplotlib library under Python. Some plots in Chapter 2 were generated using GNUPlot. Technical drawings were created using Xfig, Inkscape, or Microsoft Visio.

Chapter 1

Introduction

The motivation for this entire body of work can be traced back to a single conversation with my supervisor, Dr. Peter Driessen, during an audio recording session for an unrelated array processing project. Having recently designed and built a working wideband software-defined radio (SDR), the details of which may be found in Appendix C, what novel radio applications were now accessible to us?

Wideband spectrum monitoring with focus on detection of rare events was one proposal, although with a sense that we were still only dealing with conventional narrowband signals and not using the bandwidth capability of the radio to its full potential. Well-known ultrawideband (UWB) modulation schemes were also considered, but these had already been studied in depth over the previous decade or more [1].

During this conversation, it emerged that one approach to the problem of generating a wideband signal in an SDR context is to simply play the source samples at a much higher sample rate. This leads to a time-compression effect on the signal, wherein we also run out of source material at a much faster rate. The concept of time compression is fundamental to a number of hierarchical digital data multiplexing schemes such as PDH, SONET/SDH, and OTN [2, 3]. It and has also been studied extensively in the analog domain [4–7] for multiplexing of speech signals. Along with these works, the 2003 patent entitled *Analog radio system with acoustic transmission properties* was soon discovered, which uses time compression and its corresponding frequency expansion effect as a solution to frequency-flat fading of voice signals transmitted over a radio channel [8].

Although multiplexing a plurality of signals is one use of time compression, we focused instead on the addition of redundancy to maintain signal quality. As we commonly work in both the audio and radio domains, it seemed natural to apply

the constant overlap-add reconstruction method found in audio processing references such as [9,10]. This is used both as a way to add redundancy and as a way to prevent the transmitter from running out of source material too quickly. The use of these two techniques together has been dubbed time-compression overlap-add (TC-OLA).

We consider TC-OLA as an entirely novel conception of how to transmit information over a channel. The concept is fundamentally different from well known amplitude, frequency and phase techniques and is also fundamentally different from code division multiple access (CDMA), orthogonal frequency division multiplexing (OFDM), and UWB impulse radio. However, we show later that some forms of TC-OLA are related to CDMA, OFDM, and interleaved frequency division multiple access (IFDMA) through time-domain sample rearrangement.

1.1 Claimed Advantages

The claimed advantages are summarized here, and will be elaborated in the following chapters.

Parameter Space. Analogous to the direct sequence spread spectrum (DSSS) processing gain ($\propto N$, the number of chips in the spreading sequence) we have a TC-OLA processing gain ($\propto \frac{M}{R}$, where M is the window size and R is the hop size, in samples). As the processing gain is based on a ratio, it is possible to manipulate the absolute value of M for different effects. We shall show that higher M gives better resistance to multiuser interference due to multipath while lower M can guard against higher Doppler spreads while maintaining the same bandwidth.

Processing Domain. In a multipath environment, a DSSS receiver uses multiple rake *fingers*, operating at the chip rate, to improve the SNR. The number of fingers is typically a hardware design parameter which may be over or under designed for any given scenario. With TC-OLA it is possible to equalize at the much lower message rate, using a software-based equalizer with a variable number of taps. This transfers some of the complexity from the hardware to the software.

Orthogonal Codes. Direct sequence CDMA (DS/CDMA) typically uses non-orthogonal codes in the uplink to guard against multipath and timing skew. The interfer-

ence penalty due to cross- and auto-correlation of the codes is accepted as a system design parameter. In TC-OLA we show that it is feasible to use orthogonal codes, even in the uplink, provided the timing can be constrained to within some percentage of the window size. With polyphase codes that are orthogonal at every offset the tolerance may be increased, with the added advantage that finding the start of the code sequence is not necessary.

Frequency Diversity. In OFDM the communications approach is to use multiple narrowband carriers which each transmit a subset of the total message symbols. Coding is used in almost all cases to prevent the overall BER from being dominated by the BER of the worst-performing carrier [11]. Frequency diversity is created by scheduling symbols from users onto carriers. Similar to MC-CDMA and IFDMA, TC-OLA can create frequency diversity without the overhead of scheduling.

Distributed Cyclic Prefix. OFDM maintains orthogonality of the carriers by adding a guard band or cyclic prefix (CP) to create a feasible FFT-based receiver and transmitter. With a CP on the order of the delay spread the block may need to be significantly longer than the delay spread to minimize loss due to the overhead. When using TC-OLA as a block-based processing system the distributed CP means windows can be on the order of the delay spread without excessive loss due to overhead.

Peak to average power ratio. Similar to SC-FDE schemes, TC-OLA can also have a favorable peak-to-average power ratio (PAPR) depending on the window shape and other signal characteristics.

Channel averaging. For a time-varying multipath channel, the TC-OLA receiver tends to reduce the magnitude of the taps. This helps to reduce the need to estimate the equivalent channel quickly and limit the noise enhancement of the equalizer.

Disparate Sources. TC-OLA is able to handle traffic from disparate sources provided they can be resampled to a common sample rate. For example, the system could handle sampled (analog) voice and digitally modulated data signals simultaneously.

1.2 Contributions

The academic contribution of this work is in the development and analysis of TC-OLA as a wireless communications technique. In Chapter 6 we connect this method to well-known concepts in the communications literature. Depending on the perspective, we can consider TC-OLA as a:

Matched-filter communications system. We present the overlap-add method as a matched filter communications system through the use of equivalent pulse shapes. The overlap-add process is in some sense a "distributed" correlation, where the samples being summed in the correlation are not contiguous in time.

Spread spectrum communications system. We find the equivalence between TC-OLA and DS/CDMA through choice of codes and a regular pattern of time-domain sample rearrangement. We derive the additive white Gaussian noise (AWGN) processing gain, which is shown to depend only on the TC-OLA spreading factor and not the window shape.

Multicarrier/block processing communications system. Similar to DS/CDMA, connections are shown to exist between TC-OLA, OFDM, and IFDMA when considering TC-OLA as a multicarrier communications system. IFDMA is seen to be the most similar modulation format, where a desired frequency-domain distribution of carriers results in a time-domain arrangement of samples that is similar to TC-OLA. Block-interleaved FDMA (B-IFDMA) is one frequency-domain generalization of IFDMA. We might consider TC-OLA with hop size greater than one sample as an analogous time-domain generalization.

Additionally, we consider TC-OLA as a wideband communications system. Time dispersion naturally comes into play when considering wideband channels. Below we describe two distinct classifications based on the relationship between delay spread and window size when considering TC-OLA in this context. Each class has a unique method of dealing with time dispersion due to multipath:

Short delay spread. When the delay spread is short relative to the window size, we make the approximation that the channel seen by the message signal is simply a frequency-compressed version of the wideband channel. This is supported through both experimental measurements and analysis, where the analysis has been developed with the introduction of a matrix permutation operator that

is specific to TC-OLA. This property makes it possible to equalize the recovered (despread) signal at the symbol rate using standard time-domain equalizer techniques (MMSE/DFE). This scenario is explored in Chapter 4.

Long delay spread. When the delay spread is long relative to the window size, we can apply frequency-domain equalization techniques. The equalizer is applied at the channel sample rate and is therefore very processing intensive. However, we note that no additional cyclic prefix (CP) overhead is added to operate in this manner. The receiver can adaptively select between two modes: one that tolerates longer delay spreads and one that is more efficient. This scenario is explored in Chapter 5.

Based on the two delay spread scenarios described above, we have targeted the use of TC-OLA toward two appropriate application areas, specifically:

Low power wide area network (LPWAN) technology. A multiuser star network is considered for low-throughput infrastructure monitoring applications. This is a use case for short delay spread operation, as the channel is characterized by low Doppler spread, long coherence time, and weak to moderate time dispersion. In this application we use orthogonal codes for multiple access, even with timing skew in the uplink. We consider a scheduled system, but without imposing strict arrival timing constraints. This scenario is explored in Chapter 4.

UWB technology. This considered as a use case for long delay spread operation. We consider communication over a high bandwidth point-to-point link, where the redundancy added by the TC-OLA transmit process is used to increase E_b/N_0 under the transmitted power constraints. CP overhead is eliminated while still being able to use SC-FDE techniques. This scenario is explored in Chapter 5.

1.3 Outline

The early exploratory work on this topic can found in Chapter 2, which originally appeared in the *IEEE Access* special section entitled *5G Wireless Technologies: Perspectives of the Next Generation Mobile Communications and Networking* [12]. In this chapter we present TC-OLA as a UWB and spread spectrum communications

method based on the idea of time compression. A sampled (analog) message signal is transmitted by modulating a carrier at a much higher sampling rate. Redundancy is added by dividing the signal into overlapping segments and transmitting each segment fast enough so that the segments no longer overlap. The original message signal is reconstructed by receiving and overlap-adding the segments.

A key feature of this scheme is that an *exact* sample rate match is not required to recover the signal intelligibly. This method is implemented in a custom wideband software defined radio, with good results in the presence of interference and multipath. This method represents a new concept and design approach and an advance in fundamental technology of the air interface physical layer that may be relevant to fifth generation (5G) wireless technologies.

The discoveries made while conducting research for Chapter 2 quickly led to the U.S. patent application and associated office actions which can be found in Appendix D. From this application, 27 of the original 41 claims were allowed in the first examination, including key independent claims. At the time of this writing, a total of 40 original and amended claims from the initial 41 were allowed by the USPTO and the patent has since been issued as U.S. Patent 9,479,216 [13].

Fundamental analysis of the system processing gain, equivalent system models, and the transmitted spectrum can be found in Chapter 3, which was originally presented at the *2015 IEEE Pacific Rim Conference on Communications, Computers and Signal Processing*. In this chapter the mathematical theory of TC-OLA for radio communications is presented. A simple time-shifting model is developed to explore performance in AWGN and simple multipath Rayleigh fading channels. Equivalent multirate filter structures for both the transmit and receive processes are developed and used to analyze the spectrum of the transmitted signal as it relates to the spectrum of the message signal.

In terms of practical applications, Chapter 4 looks at TC-OLA as a potential LPWAN technology for infrastructure monitoring and machine-to-machine (M2M) communications, a vital component of the 5G effort [14]. Results are compared with the well-designed random phase multiple access (RPMA) technology from Ingenu (previously On-Ramp Wireless), as the most similar existing LPWAN technology [15]. In this chapter a code-division variant of TC-OLA is proposed as an alternative physical layer scheme for LPWAN infrastructure monitoring applications. Analysis shows performance in flat fading channels is limited by Doppler spread while performance in static frequency-selective channels is limited by equalizer performance. Analysis

of time-varying frequency-selective fading highlights the channel averaging effect of TC-OLA. A TC-OLA system targeted toward low data rate monitoring applications is simulated using the Stanford University Interim (SUI) models developed for IEEE 802.16 (WiMAX) applications in the 2 GHz frequency range [16]. The system is compared with a CDMA system based on circular shifts of a Gold code as an approximation to an RPMA system. Simulation results show that TC-OLA can support a larger number of simultaneous users in the uplink as the practical number of users is not limited by random choice of chip offset, and is not limited by timing uncertainty or delay spread provided these values can be made small relative to the window size. Ability to equalize the channel at the message or symbol rate further improves the bit error rate (BER) and transfers complexity from a fixed number of hardware rake fingers to a software-defined equalizer. This chapter was considered for publication in *IEEE Transactions on Wireless Communications* but is now planned to be split into two or more separate articles.

Finally, we return to the original UWB motivation in Chapter 5, where TC-OLA is considered in a block-processing context with frequency domain equalization. In this chapter a variant of TC-OLA is proposed as an alternate physical layer scheme for UWB communications. Although the construction of the transmitted signal is identical to other TC-OLA applications, this work explores block-based receiver structures using frequency domain equalization (FDE) techniques that allow for a longer delay spread relative to the window size than time-domain TC-OLA processing. This method retains the advantages of single carrier frequency domain equalization (SC-FDE), such as lower PAPR, while reducing or eliminating the CP overhead in the case where block repetition is used to extend the link budget. Unlike overlap FDE, the CP overhead is eliminated without the increased processing load required to maintain a practically useful BER floor. For very high delay spread channels, such as CM8, a long effective CP length can be obtained without requiring a very long block length to maintain overhead efficiency. This chapter has been accepted for publication in *IEEE Communications Letters*.

Chapter 6 gathers up research paths that were explored but not published, and any ideas that were never explored. This can be considered a discussion on future work that may lead to additional publications or patent claims. Several recommendations are given in this chapter for future design and analysis activities, suggested publications, and patentable material.

Chapter 2

Novel UWB and Spread Spectrum System Using Time Compression and Overlap-Add Techniques

2.1 Introduction

In this chapter we present a spread-spectrum communications method which is distinctly different from UWB pulse radio techniques [1], multiband OFDM systems [17], direct sequence, frequency hopping, chirped, and time hopping spread spectrum techniques [18]. The method extends naturally to time division multiple access (TDMA) and can also leverage CDMA techniques [18]. This method represents a new concept and design approach and an advance in fundamental technology of the air interface physical layer that may be relevant to 5G wireless technologies.

This new communications method was conceived to take advantage of the wideband capabilities of a software-defined radio system using a 1.8 GSPS analog-to-digital converter (ADC). This system hardware was initially designed as a general-purpose experimentation platform and was adapted to implement this new method. Hardware with a lower sampling rate can also be used. In our approach, digital audio signal processing techniques (phase vocoder time stretching and pitch shifting) [9] are adapted for wireless communications.

The new method uses the idea of time compression where a sampled message signal is transmitted at a higher sampling rate. Robustness is achieved by dividing the signal into overlapping segments, transmitting the segments at a high enough sample

rate such that they no longer overlap, receiving these segments and reconstructing the message by overlap-adding the segments. The bandwidth spreading factor is the inverse of the fractional hop size, where the hop size is one minus the normalized amount of overlap relative to the segment length. The level of redundancy and robustness increases as the spreading factor is increased and hop size is decreased. For segments almost fully overlapping with overlap of all samples but one (a hop size of one sample), the spreading factor is equal to the segment length in samples. We refer to this scheme as TC-OLA.

As an example, for an audio signal (e.g. voice or modulated data waveform) sampled at 48 kHz, segment length of 1024 samples, and hop size of one sample, the samples are transmitted at 49.152 MSPS. The segments may be windowed tapering to zero at the edges, which helps to limit the transmitted bandwidth and relax the receiver's synchronization requirements. This wideband signal can be transmitted at baseband or on a carrier. The samples may be transmitted at an integer multiple N times 49.152 MSPS to obtain N TDMA channels.

One advantage of this scheme is that given a message source that is a sampled analog waveform, the transmitted samples need not be recovered exactly. The message signal is resampled at the receiver, so sample misalignment and slight clock drift will not significantly affect the quality of the recovered message.

Another advantage of the scheme is that loss of a single segment of samples only results in a drop in output amplitude. This effect is reduced as the spreading factor increases. Although this method does not improve the message SNR, it does provide a method to decorrelate interfering signals, with increasing tendency to "average out" the interference as the level of redundancy increases.

A third and important advantage of this scheme is the capability to spread any signal that would typically experience flat fading over a much wider bandwidth such that it experiences frequency-selective fading. Channel models for wireless links with carrier frequencies in the 1-10 GHz range may have delay spreads in the range 10^{-8} (indoor) to 10^{-5} (outdoor) seconds [19], [20]. Channel models for UWB channels typically have delay spreads in the 10^{-8} sec range [21]. Thus flat fades may occur over bandwidths up to about 100 MHz, so that spreading to bandwidths in the GHz range may be needed to ensure frequency selective fading. The wealth of literature on adaptive equalizers for frequency selective channels can then be used in receiver design. In the case of a time-varying frequency-selective channel, the overlap-add process naturally averages the effect of the channel response, so that adaptive equalizers

may not be required.

Applications of TC-OLA include mobile communications, UWB applications such as high data rate short range indoor wireless systems and personal area networks (PANs), as well as other systems such as infrastructure monitoring and fixed wireless links that may suffer from long flat fading outages that can be reduced by bandwidth expansion.

The TC-OLA method represents a new approach to the air interface physical layer that may be useful for 5G systems. A detailed performance comparison with existing air interfaces has not been done yet.

The remainder of this chapter is organized as follows. After a brief literature review in Section 2.2, in Section 2.3 we describe the theory of TC-OLA for a real baseband signal, including details of windowing and synchronization, followed by extensions to CDMA, TDMA and complex baseband and real passband signals. Section 2.4 describes the results obtained from a reference implementation using a custom wideband software defined radio with a 1.8 GSPS ADC that can accommodate UWB signal bandwidths. Section 2.5 describes a second reference implementation, using a 100 MSPS ADC in an off-the-shelf software defined radio (Ettus Research USRP N210). The test results in Sections 2.4 and 2.5 show good performance in the presence of simulated multipath and interference. Section 2.6 contains a discussion, conclusions and ideas for future work.

2.2 Literature Review

Some wireless communications systems use radio frequency bandwidths much wider than the message bandwidth. Examples include UWB pulse radio [1] and other UWB systems [17] as regulated with a spectral emission mask [22, 23]. Other examples include third generation (3G) wideband CDMA (WCDMA) [24], fourth generation (4G) long term evolution (LTE) [25] for mobile communications, and a system for fixed wireless infrastructure monitoring based on CDMA but optimized for low data rates with long spreading codes [26]. All of these systems minimize outages due to flat fading as a consequence of their wide bandwidth.

An early mention of the idea of time compression applicable to analog systems is found in [27] with more recent results in [7]. The idea of segmenting an analog voice signal and compressing the segments in time before transmitting them through the radio channel was found in [8] (after the present system was conceived). However,

the system of [8] is limited to voice transmission and does not include the idea of overlap-adding the segments or using complex baseband signals. The idea of analog time division multiplexing (TDM) for voice signals was described in [6].

The overlap-add (OLA) technique is common in audio signal processing where it is used as a method of analysis and resynthesis, time stretching and pitch shifting over short segments where the frequency content can be considered relatively constant from one segment to the next [9].

2.3 Theory of Operation

In this section, we describe the theory of TC-OLA for a real baseband signal, including details of windowing, and synchronization, channel effects on the message signal, interference effects, followed by extensions to CDMA, TDMA and complex baseband and real passband signals. Finally, we give a short overview of how the system is realized in practice.

2.3.1 Time Compression and Overlap-Add

A stream of data samples at some sample rate f_m is divided into a series of overlapping segments with a fractional hop size:

$$\delta = \frac{R}{M}, \tag{2.1}$$

where R is the hop size in samples and M is the length of the segment in samples (Figure 2.1). The samples may be sourced from an ADC, stored in a file or generated algorithmically. The overlapping segments are then reassembled into a stream of non-overlapping segments for transmission at some higher sample rate:

$$f_c \geq \frac{f_m}{\delta}, \tag{2.2}$$

with a ratio of frequencies

$$\beta = \frac{f_c}{f_m}. \tag{2.3}$$

This relationship ensures that each segment is compressed in time by a factor of β such that M samples at f_c occupy the same or less time as R samples at f_m. The distinction between δ and β is that the former specifies the redundancy added in the

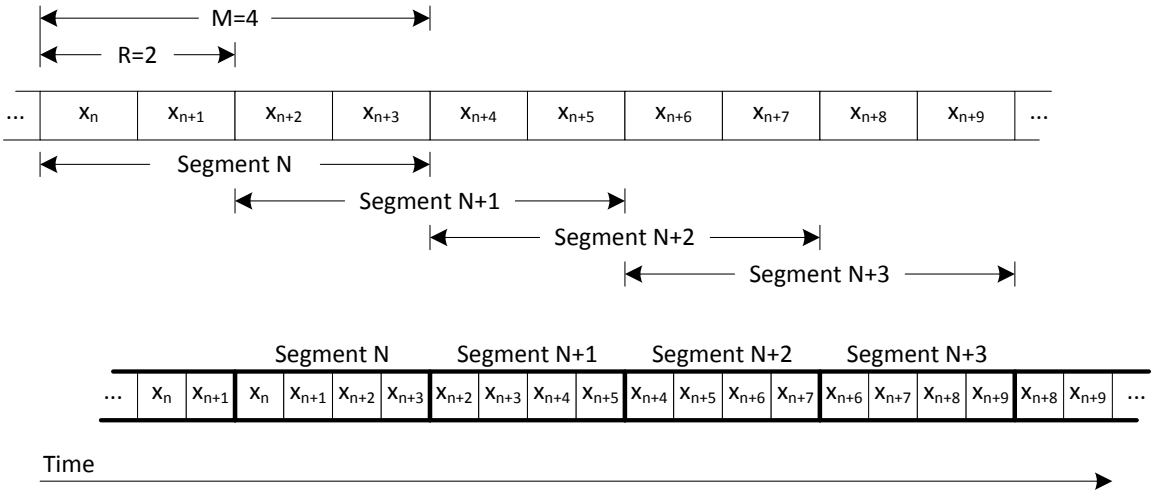

Figure 2.1: Overlapping segments at the lower sample rate assembled into a stream of non-overlapping segments at the higher sample rate.

transmission process while the latter specifies the spreading of the bandwidth. At minimum $\beta = \delta^{-1}$, but this is not the case for the practical implementations that we explore later on.

This process is illustrated pictorially in Figure 2.1 with the parameters $M = 4$, $R = 2$ and $\beta = \delta^{-1}$. Discounting (for now) any sharp discontinuities at the segment boundaries, the signal bandwidth is spread by a factor of β.

The receiver reverses this process by overlapping and adding the segments to reconstruct the original message signal scaled by a constant $k \propto \delta^{-1}$, due to the redundancy added in the transmission process.

2.3.2 Windowing

A window function that tapers to zero is applied to each transmitted segment to address practical concerns about synchronization of the segments at the receiver as well as limiting the transmitted bandwidth. Using a rectangular window without perfect synchronization at the receiver would result in sharp transients in the output (audible "glitches" in the case of an audio signal) where the segments are not perfectly aligned. The transmitted signal would also contain high frequency and therefore wide bandwidth transients at the segment boundaries.

The Hanning window:

$$w[k] = \frac{1}{2}\left(1 - \cos\left(\frac{2\pi k}{M-1}\right)\right) \tag{2.4}$$

is a natural choice as the windows sum to some constant positive integer

$$C = \sum_{i=-\infty}^{\infty} w\left[k - iR\right] \tag{2.5}$$

for any hop size R which satisfies the perfect overlap-add criteria

$$R = \frac{M}{2C}. \tag{2.6}$$

This window choice has a maximum fractional hop size of 0.5, leading to the doubling the receiver bandwidth to recover the message signal at unity gain. Figure 2.2 illustrates the series of window functions in the overlapping (top) and non-overlapping (bottom) forms.

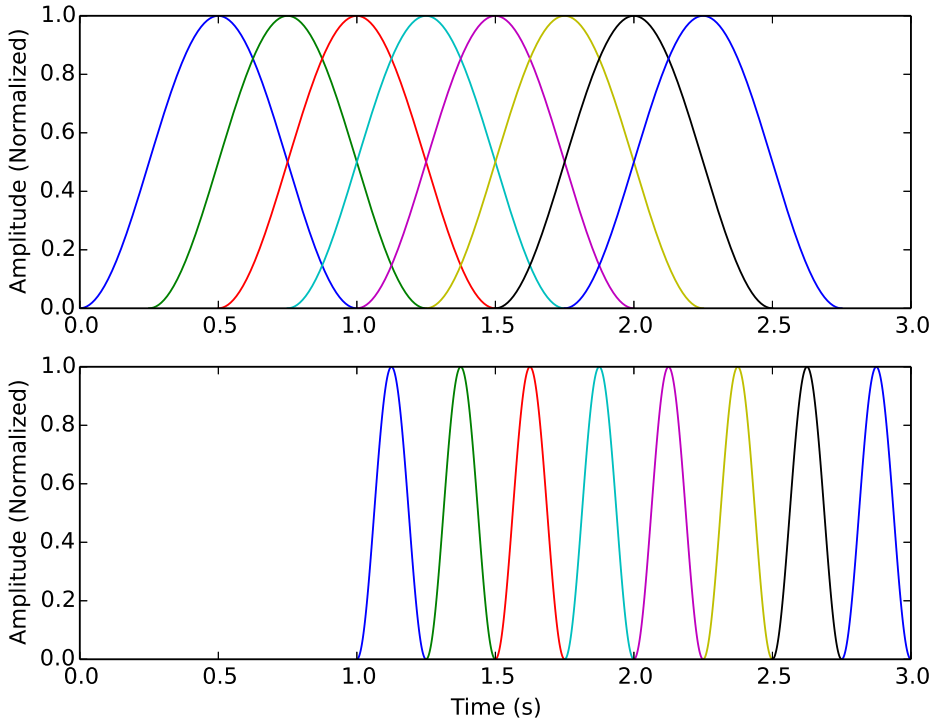

Figure 2.2: Overlapping Hanning windows with a fractional hop size of 25%, summing to $k = 2$ (top). The non-overlapping form that is transmitted over the channel is also shown (bottom).

2.3.3 Synchronization

A synchronization marker can be inserted between segments or groups of segments to aid in locating the start and end of each segment in the received sample stream. The transmit sample rate f_c must be increased to accommodate this insertion. Each timing marker then delineates a frame consisting of one or more segments. The marker that is added should have a strong correlation peak in order to locate the segments with minimum jitter. Segments from multiple interleaved sources can be identified with different timing markers or by including some modulated digital data with the timing marker. The system can also work without adding synchronization markers in some cases when complex signals are used as mentioned in Section 2.3.8 below.

In practice, f_m and f_c at the transmitter will vary slightly from f'_m and f'_c at the receiver. In an ideal system, the number of samples between timing markers could be used to estimate the transmitter's sample rate and modulate the receiver's sample rate accordingly. However, a key feature of this scheme is that an exact sample rate match is not required to recover the signal.

The effect of frame loss is tolerable in that it creates a momentary drop in the amplitude of the output signal as shown in Figure 2.3. This creates a kind of graceful degradation that is not typically present in digital schemes. The peak relative drop in amplitude is equal to 2δ when using the Hanning window.

To take advantage of this property the received segments may be weighted differently before the OLA operation to reduce the impact of segments that have been affected by deep fading or pulsed interference without greatly affecting the output signal.

2.3.4 Channel Effects

The receiver of the time-compressed signal process performs an expansion in time which is equivalent to a compression in frequency. Thus any channel impairments, including interference, will also be compressed in frequency. For example, Figure 2.4 (top) shows the response of a simple static two-ray channel model with equal power, delay of 16 μsec to a white noise input with bandwidth of 500 kHz. The nulls in this channel model are spaced by 62.5 kHz. The channel in this figure can be considered as complex baseband or as real passband where 0 Hz represents the center or carrier frequency.

In what follows, we consider a system with the parameters listed in Table 2.1. If

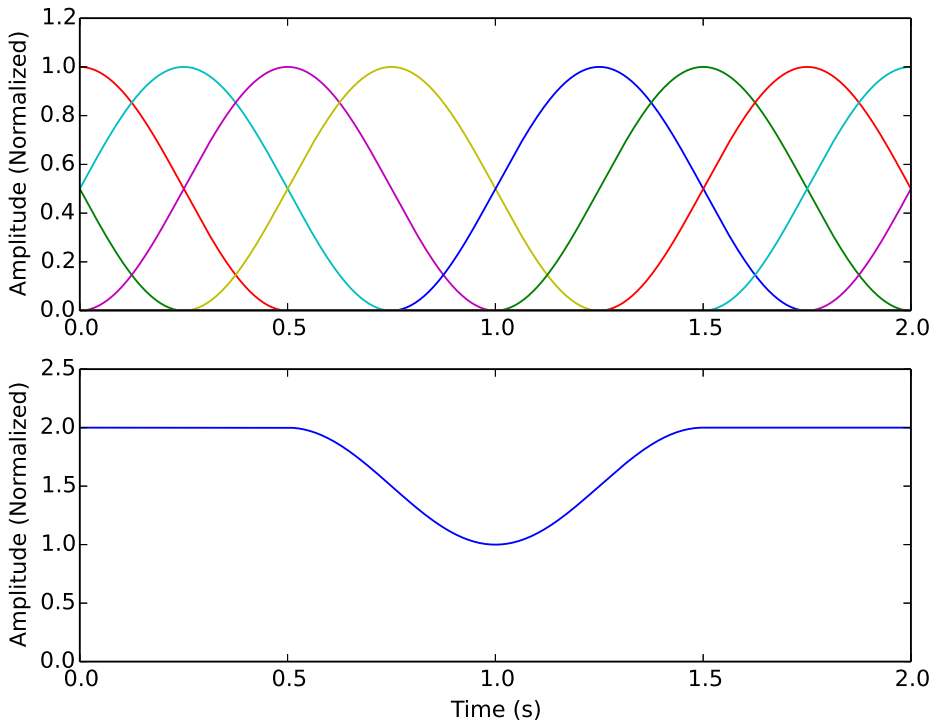

Figure 2.3: The frame centered at $t = 1.0$ s was not recovered (top), resulting in a drop in amplitude from 2.0 to 1.0 (bottom). In this example, the fractional hop size $\delta = 0.25$ and the peak relative drop in amplitude is 50%.

Parameter	**Value**
f_m (kHz)	8
f_c (kHz)	500
β	62.5
M	8,000
R	160
δ	0.02
Timing Marker (samples)	<2,000
Frame Length (samples)	10,000
Frame Period (ms)	20

Table 2.1: Example system parameters for Figures 2.4-2.7.

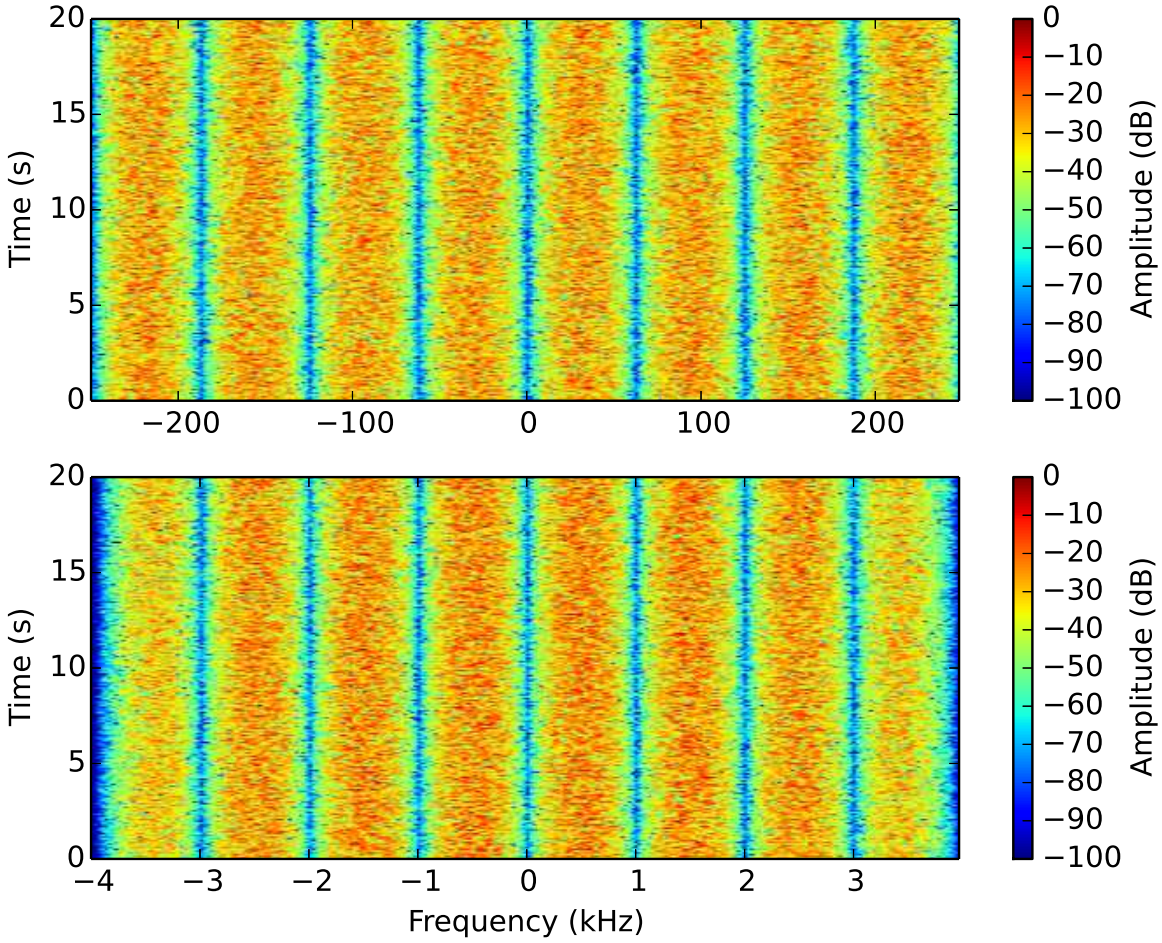

Figure 2.4: 500 kHz static two-ray model channel response with nulls spaced every 62.5 kHz (top) and effect on the (two-sided) 8 kHz output spectrum, showing nulls spaced every 1 kHz (bottom).

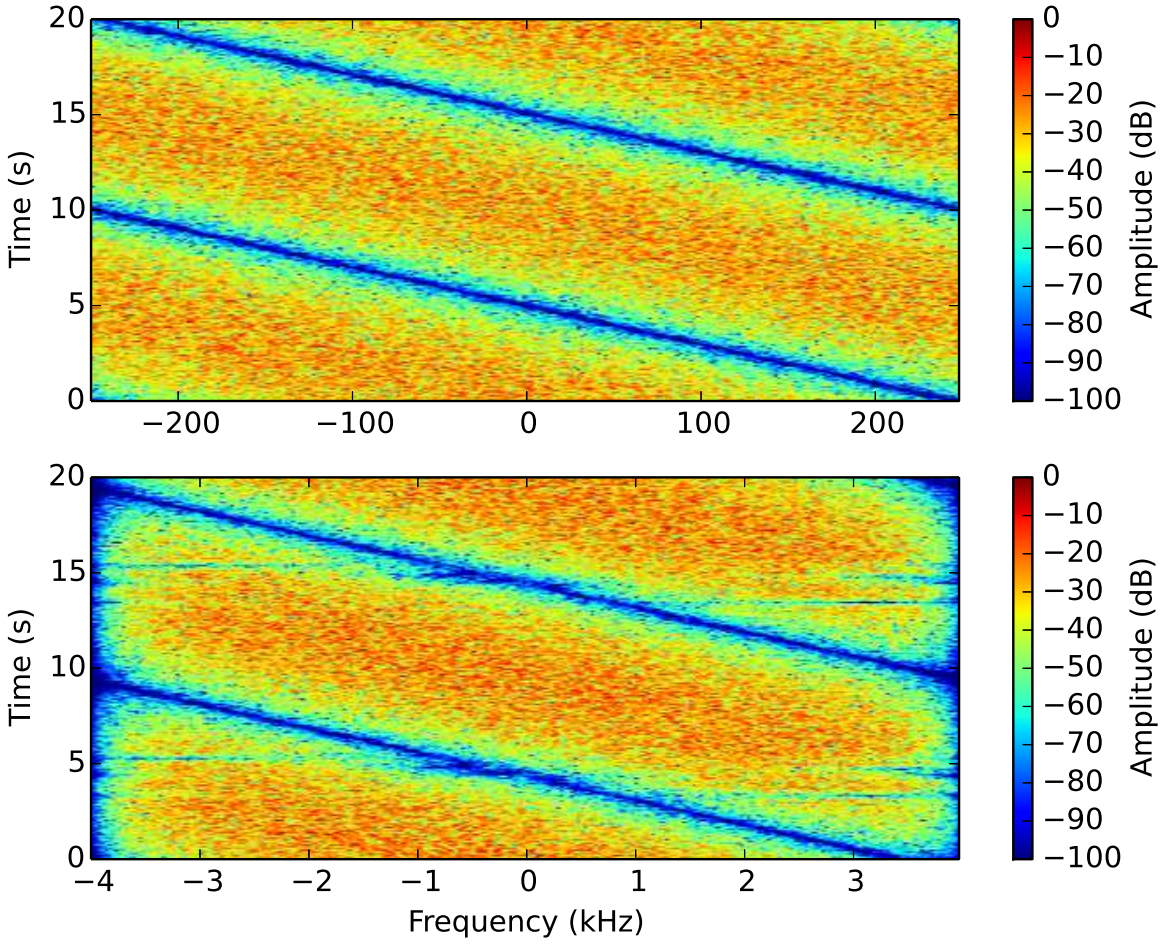

Figure 2.5: 500 kHz time-varying two-ray model channel response with null sweeping across every 10 seconds (top). Effect on (two-sided) 8 kHz output spectrum (bottom).

white noise of (one-sided) bandwidth 4 kHz is applied as the message input to this system and transmitted over this static two-ray channel, then the result will appear as in Figure 2.4 (bottom). The nulls are now spaced by 1 kHz, compressed in frequency by exactly the ratio of the sample rates. The averaging effect of the overlapping windows is not apparent in the figure because the channel is static.

We extend this discussion to time-varying frequency-selective channels by considering three different rates of time variation to provide some insight into the system behavior. The first case is where the channel is changing much slower than the averaging period $\frac{M}{f_m} = 1$ second. In this case, because the channel is relatively constant over the averaging period it is expected that the output response will track the channel response in time but compressed in frequency. This concept is shown in Figure 2.5, applied to the system of Table 2.1. We use an equal power two-ray model with a delay of 2 μsec. In this first case the phase of the second ray is rotated by 2π at a rate of 0.1 Hz such that the null sweeps linearly across the complex baseband channel every 10 seconds.

The second case is where the channel response changes faster than the averaging period but slow enough to be relatively constant over the frame period (20 msec). The minimum frame period is $\frac{M}{f_c} = 16$ msec but we have used a frame period of 20 msec to allow for a synchronization marker. In this case we start to see the averaging effect of the overlap-add process in the output although some similarities to the channel remain. This is illustrated in Figure 2.6, applied to the system of Table 2.1. This time the phase of the second ray is rotated at a rate of 1 Hz such that null sweeps linearly across the channel every second. It can be observed in Figure 2.6 (bottom) that the null in the output has been widened and is no longer as deep.

The third case is where the channel response changes much faster than the frame period. Again, using the system of Table 2.1, the second ray is rotated at a rate of 10 Hz such that the null sweeps linearly across the channel ten times per second. In this case it is expected that the channel response is no longer recognizable in the output as can be seen in Figure 2.7.

These three cases for a two-ray channel response were presented to gain an intuitive understanding of how the receiver with built-in averaging affects the end-to-end response as seen by the message signal. Other more realistic cases of time-varying frequency selective channel models include the above mentioned two ray model but with Rayleigh, Ricean or other fading statistics and specified Doppler spread on each ray [28]. More general frequency-selective channel models include multiple rays

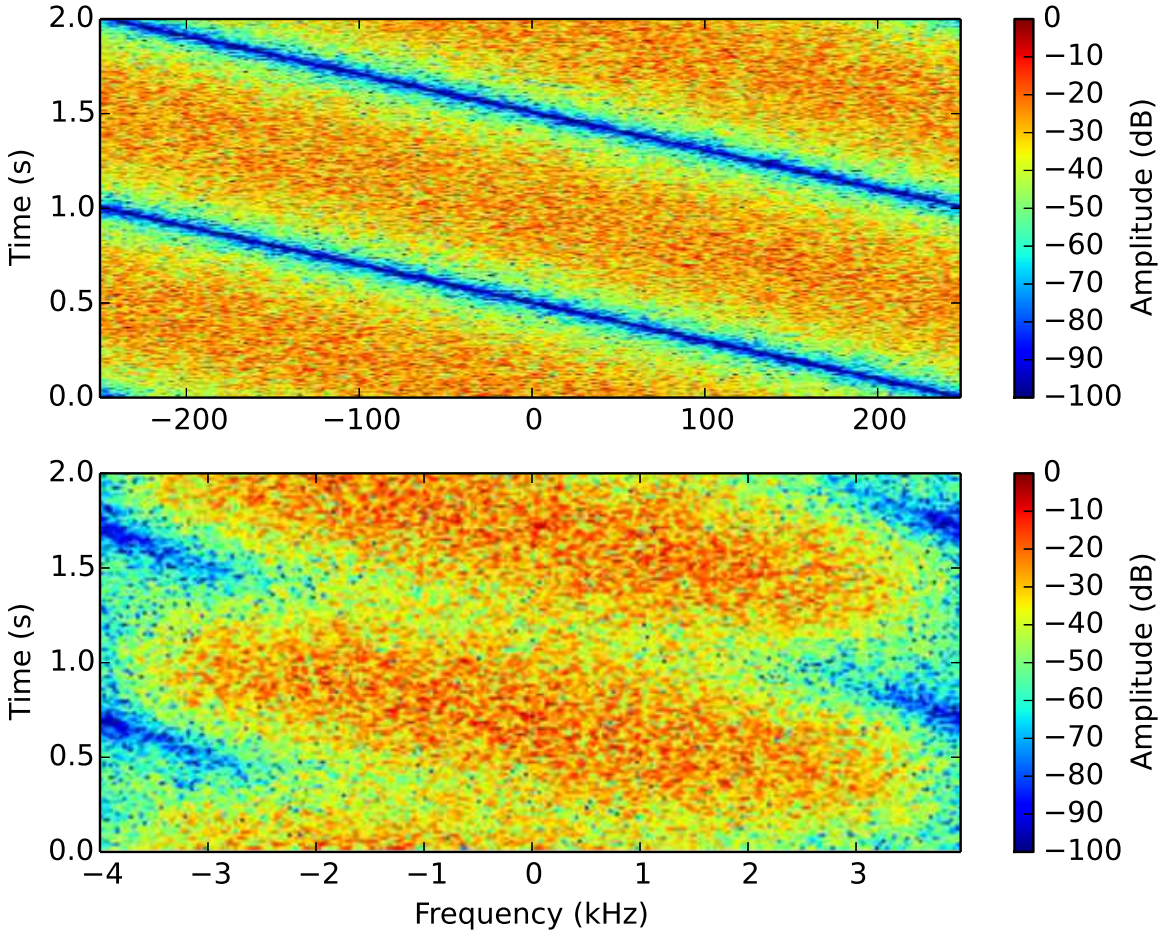

Figure 2.6: 500 kHz time-varying two-ray model channel response with null sweeping across every second (top) and effect on (two-sided) 8 kHz output spectrum (bottom).

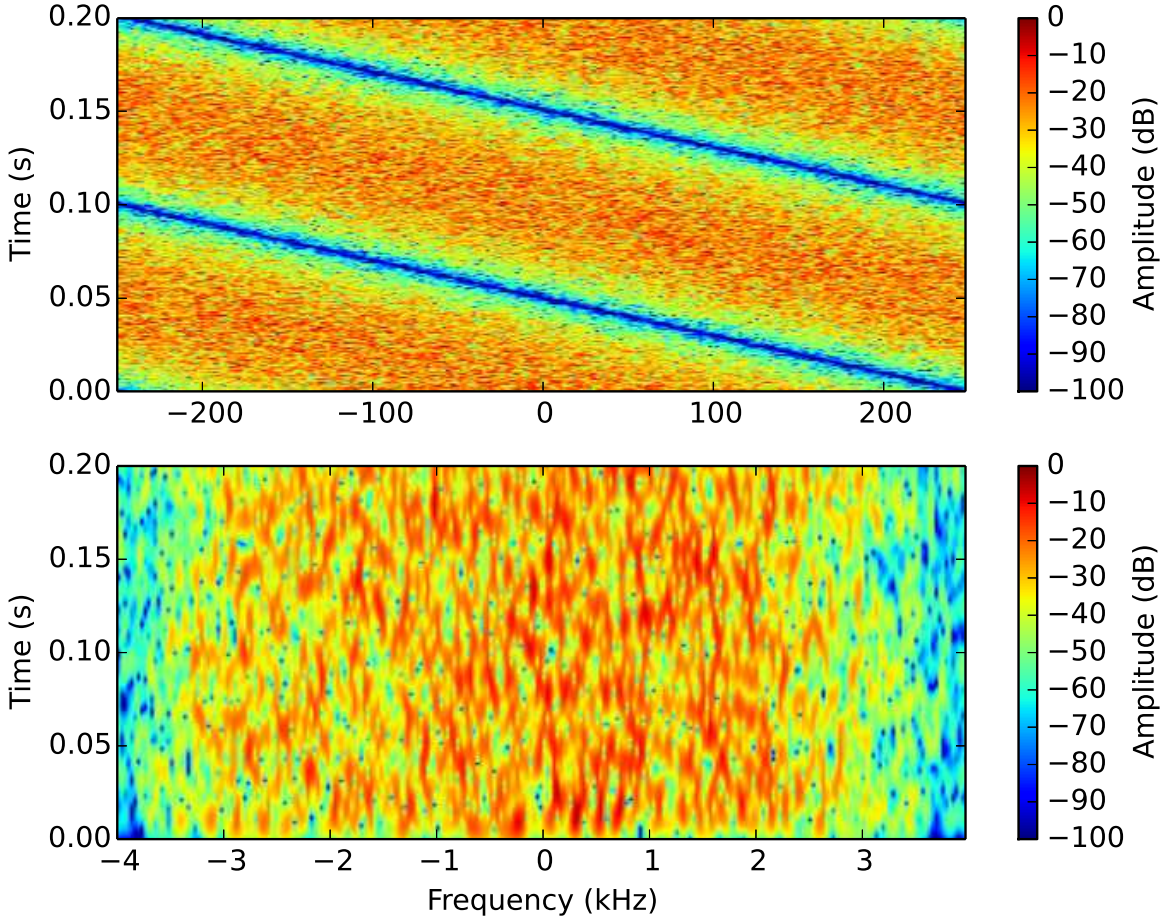

Figure 2.7: 500 kHz time-varying two-ray model channel response with null sweeping across 10 times per second (top). Effect on (two-sided) 8 kHz output spectrum (bottom).

(tapped delay line) each with a specified fading distribution (tap gain) and Doppler spread [19]. Models relevant to UWB are outlined in [29] with clusters of rays that may be resolvable with sufficient bandwidth and small scale fading that is Ricean with a large line of sight component. The response to these other channels as seen by the message signal is expected to depend on the fading parameters in a similar way.

2.3.5 Interference Rejection

Consider the case where the received segments have an interfering signal superimposed on them. Assume that the overlap-add process sufficiently decorrelates the interfering signal in each segment such that they can be assumed to add in power as with noise. In this case the interference power increases with k ($k \propto \delta^{-1}$) while the signal power increases with k^2. Therefore, the interference is rejected by a factor of k.

However, this assumption may not always be valid. For example, consider an interfering carrier where the interference adds up in phase in the overlap-add process. In this situation, the transmitter can mitigate the interference by applying a random or predetermined phase sequence to each segment. In the process of rotating each segment back to 0 degrees, the receiver effectively decorrelates the interfering carrier.

2.3.6 Extension to CDMA

In the case that multiple systems are transmitting on the same frequency, signals can be separated by applying a unique phase sequence to each transmitted segment. The opposite phase sequence is then applied to the segments at the receiver to rotate each segment back to 0 degrees. The sequences are chosen to maximize rejection of all interfering signals. Figure 2.8 illustrates this concept in a simple system with two transmitters operating with the same parameters. The sequence $\{1, 1\}$ is applied to the transmitted frames of X, while the sequence $\{1, -1\}$ is applied to the transmitted frames of Y. This allows the receiver for X to effectively cancel out Y.

This scheme can be extended to the set of sequences from the Hadamard matrix $\mathbf{H}(2^k)$ with the additional constraints that the number of signals to be transmitted is at most 2^k and the number of windows that overlap to produce each output sample must be an integer multiple of the sequence length. This can be expressed in terms of the fractional hop size as $\delta = \frac{1}{n2^k}$, where n is a positive integer. However, there are other ways to generalize this concept and it is not limited to binary phase sequences.

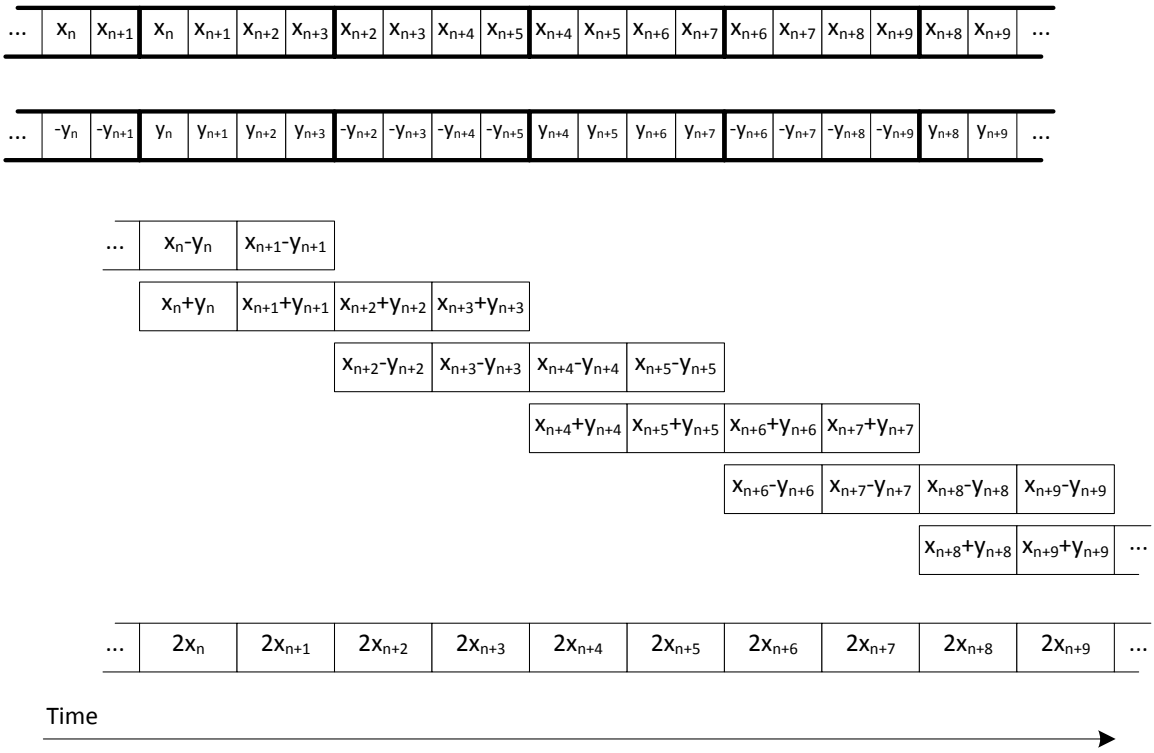

Figure 2.8: Two systems transmitting simultaneously. Signal X has the sequence $\{1, 1\}$ applied while signal Y has the sequence $\{1, -1\}$ applied to the transmitted frames. The sequence applied to Y causes it to be cancelled out in the receiver for X.

This scheme differs from DSSS in that application of the phase sequence does not significantly expand the transmitted signal bandwidth. In DSSS, the sequence is applied at the chip rate which is much higher than the symbol rate. In this scheme the sequence is applied at the frame rate, where each frame contains many samples.

2.3.7 Extension to TDMA

Allowing f_c to be greater than the minimum required in (2.2) provides some unused portion of time that can be used to interleave segments from additional sources. Stated another way, frequency f_c can be set to accommodate multiple signals, possibly with differing sample rates and fractional hop size parameters, where

$$f_c = \sum_{k=1}^{n} \frac{f_{m_k}}{\delta_k}. \tag{2.7}$$

This time interleaving is illustrated in Figure 2.9, where signal X uses the parameters $M = 4$ and $R = 2$ while signal Y uses the parameters $M = 3$ and $R = 1$. The sample rate of Y is 3/4 that of X. The output sample rate is therefore $f_c = \frac{17}{4} f_{m_x}$ application of (2.7).

2.3.8 Complex Baseband and Real Passband Signals

What has been described up to this point is a wideband real baseband signal. Using complex baseband and the corresponding real passband signals offers several extensions of TC-OLA:

- Creating an analytic complex baseband signal with a Hilbert transform, applying TC-OLA to I and Q separately, and upconverting to make a single sideband real passband signal.
- I/Q multiplexing two separate real baseband signals.
- Alternating the overlapping message windows between the I and Q channels.
- Offsetting the I and Q windows by 50% of the window size so that the amplitude nulls in the I channel and amplitude peaks in the Q channel occur at the same time. This offset will keep the envelope more constant and will also help to reduce I/Q crosstalk.

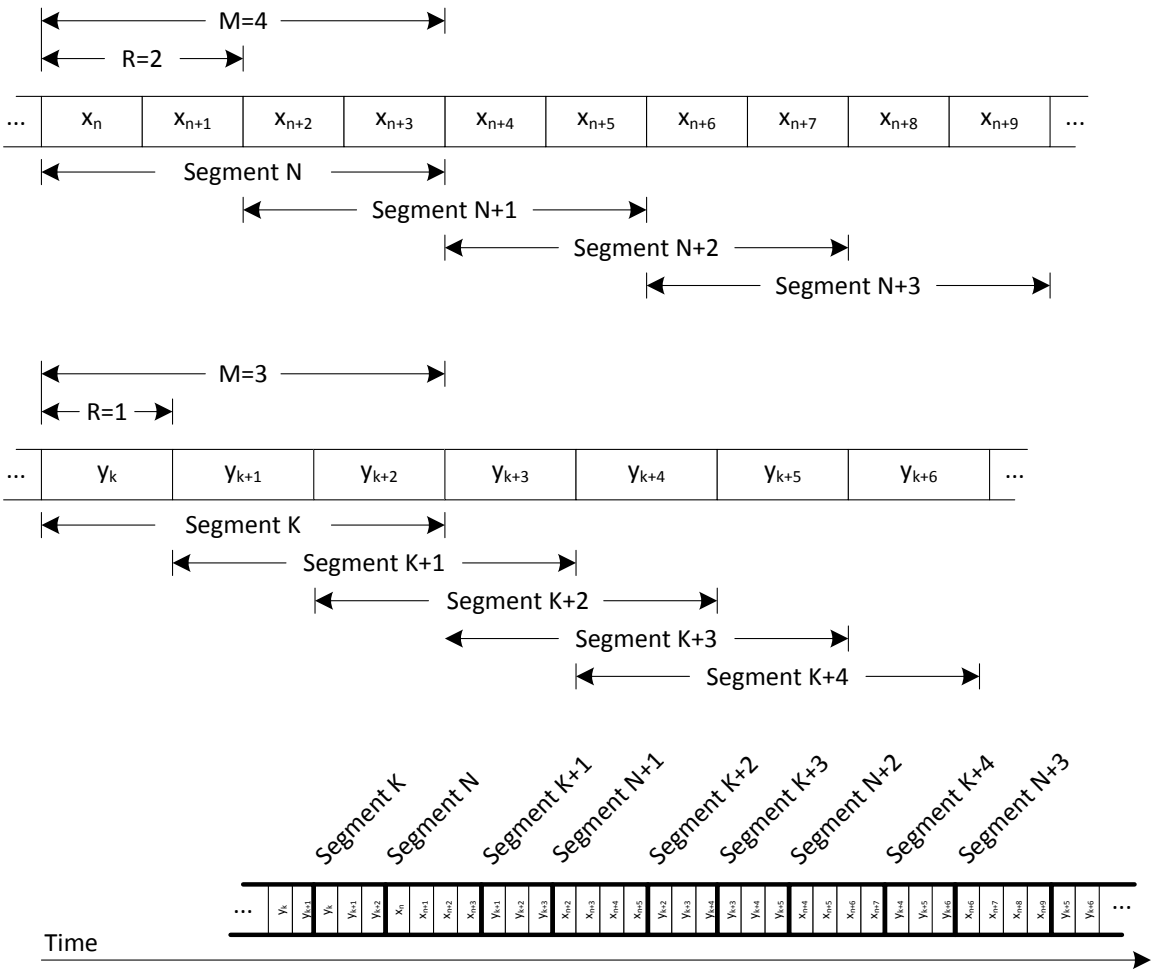

Figure 2.9: Time-domain interleaving from multiple sources. The sample rate of Y is 3/4 that of X. Rectangular windows are used for illustration purposes. Hanning windows could be used instead.

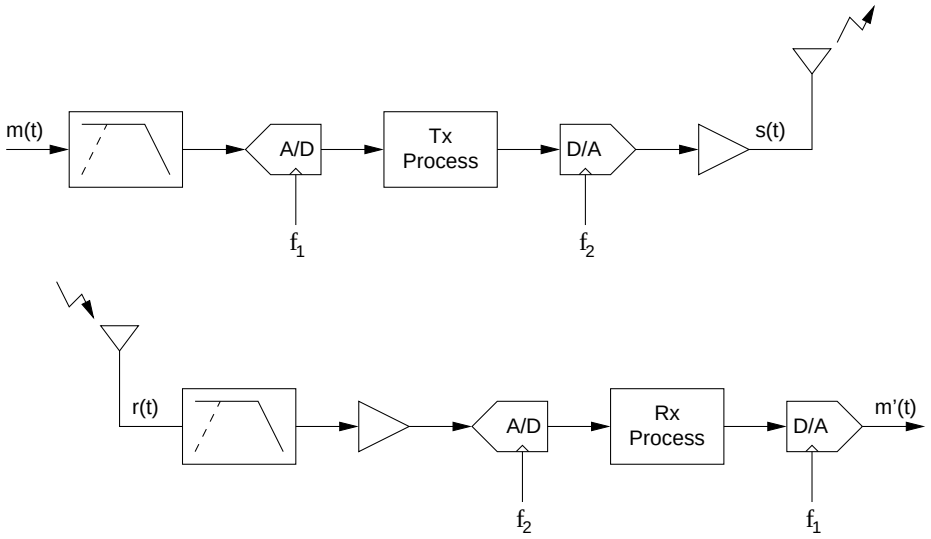

Figure 2.10: Simplified System Diagram.

- Not using frame alignment markers, since the periodicity of the windowed frames can define frame boundaries with sufficient accuracy.
- Applying the technique to the complex baseband output of a digital modulator such as quadrature amplitude modulation (QAM) or OFDM.

2.3.9 System Implementation

A simplified diagram of a general TC-OLA implementation not specific to particular hardware is shown in Figure 2.10. The transmit process frames the overlapping segments while the receive process synchronizes and performs the overlap-add reconstruction of the message signal. This is the model that the two reference implementations are based on.

In both implementations that follow, a square-root Hanning window is applied to the segments at both the transmitter and receiver, giving the desired Hanning window shape overall on the segments. At the transmitter it helps to reduce sharp transients at the segment boundaries, thus limiting the bandwidth of the transmitted signal. At the receiver, it helps to reduce transients caused by interfering signals which would be present if a Hanning window was applied at the transmitter and a simple rectangular window was applied at the receiver as shown in Figure 2.11.

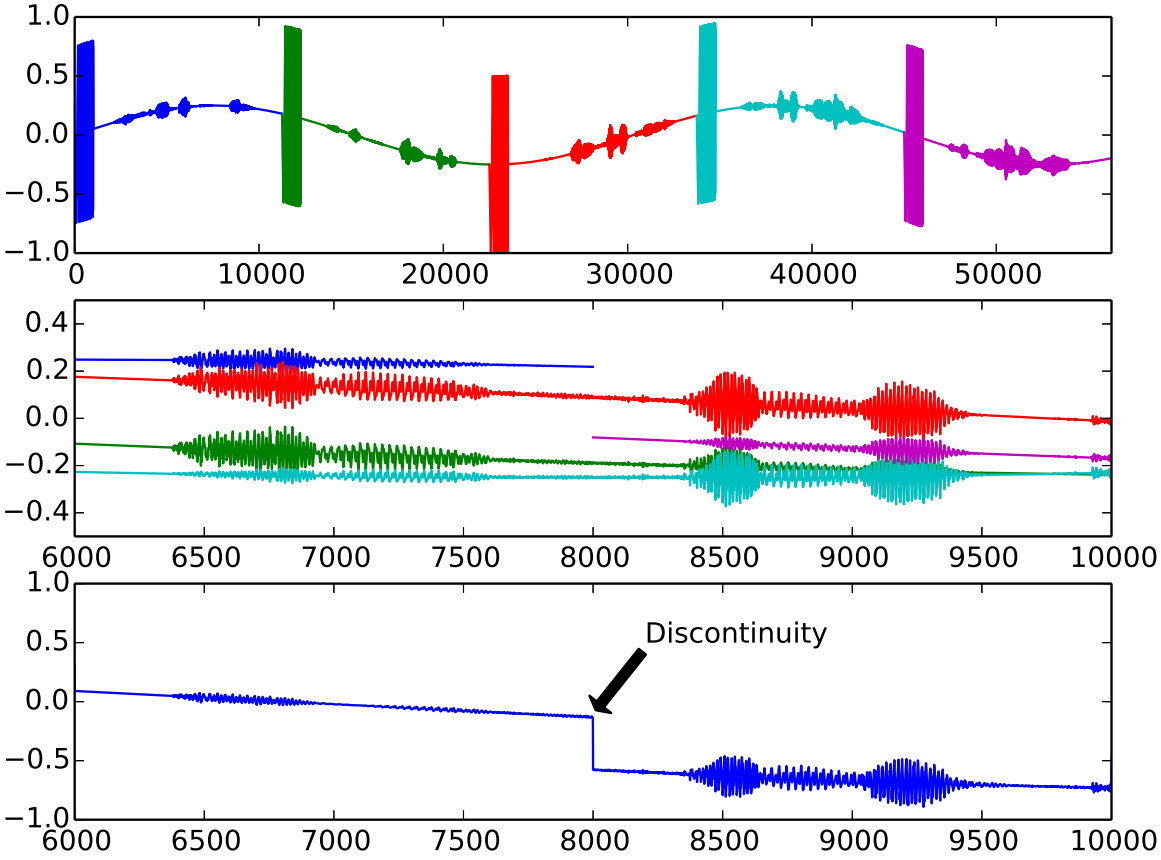

Figure 2.11: Received signal plus narrowband interference (top). Overlapped segments with rectangular window applied at receiver (middle). Discontinuity in the output caused by interference when a rectangular window is applied at the receiver (bottom). This discontinuity does not appear when a square-root Hanning window is applied to the segments at both the transmitter and receiver.

2.4 Wideband SDR Implementation

The proposed TC-OLA system can be scaled up to ultra wideband transmission using modern high-speed digital-to-analog converter (DAC)s and ADCs. Thus a wideband SDR was implemented as a testbed that can accommodate UWB signals with bandwidths greater than 500 MHz or greater than 20% of the center frequency [21].

The system parameters for this implementation are shown in Table 2.2. The ratio of the sample rates results in bandwidth spreading by a factor of $\beta = 28125$. In theory a system of this type could support a very high number of users in the TDM case or a very high level of redundancy. In our tests we simulate the TDM case.

A detailed diagram of the hardware interconnects is shown in Figure 2.12. The

Parameter	**Value**
f_m (kHz)	8
f_c (MHz)	225
β	28125
M	8,000
R	2,000
δ	0.25
Timing Marker (samples)	1,000
Frame Length (samples)	11,250
Frame Period (μs)	50
Processing Delay (ms)	2000

Table 2.2: System parameters for wideband SDR implementation.

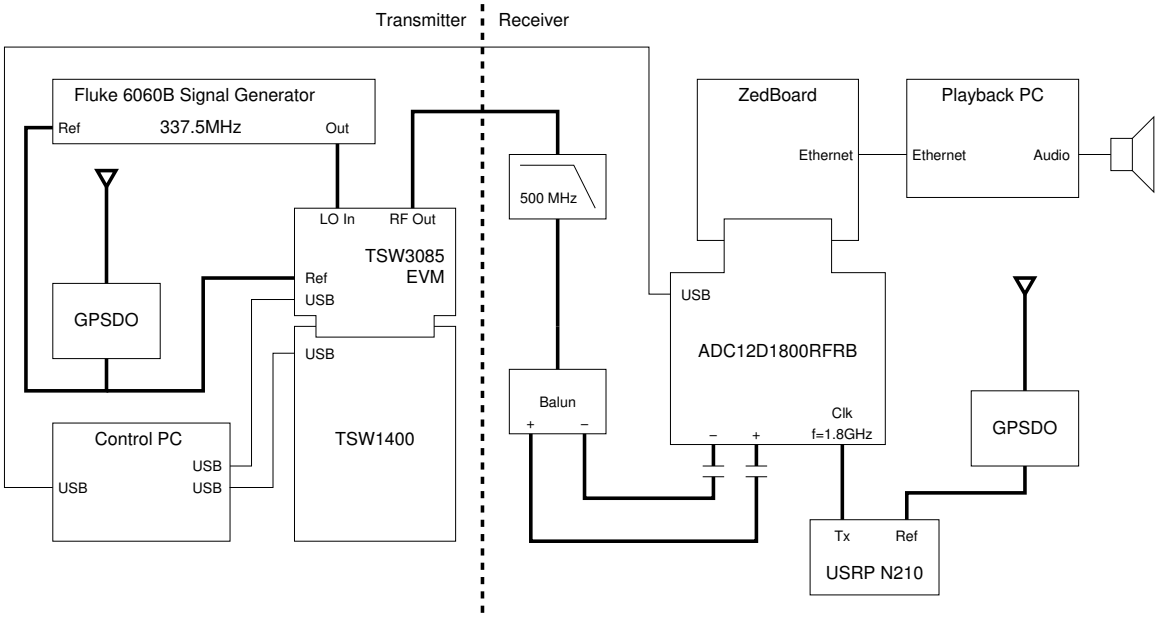

Figure 2.12: Wideband SDR connection diagram. USB Connection between Control PC and ADC12D1800RFRB is only required to load the FPGA image.

DAC and radio frequency (RF) signal generator are synchronized to one GPS-disciplined oscillator (GPSDO) on the transmitter side while the receiver uses a universal software radio peripheral (USRP) synchronized to a second GPSDO to generate a 1.8 GHz clock for the ADC. The transmit and receive hardware as well as the software are discussed in more detail in the following sections.

2.4.1 Transmitter

The TSW1400 evaluation platform from Texas Instruments [30] is used as a transmitter. It plays samples from a user-specified data file through the attached DAC at a configured rate.

To produce the data file, overlapping segments are cut from an 8 kHz mono audio file as per the system parameters in Table 2.2. Framing overhead and padding are added such that each frame contains 11250 samples. The frame overhead efficiency is 71% (8000/11250) and more efficient schemes could be developed. This was convenient scheme given the hardware constraints.

Figure 2.13 shows the transmitted frame format. The synchronization marker used is an exponential sine sweep [31] 1000 samples long. It should be noted that the choice of timing marker can be any sequence with good correlation properties. A

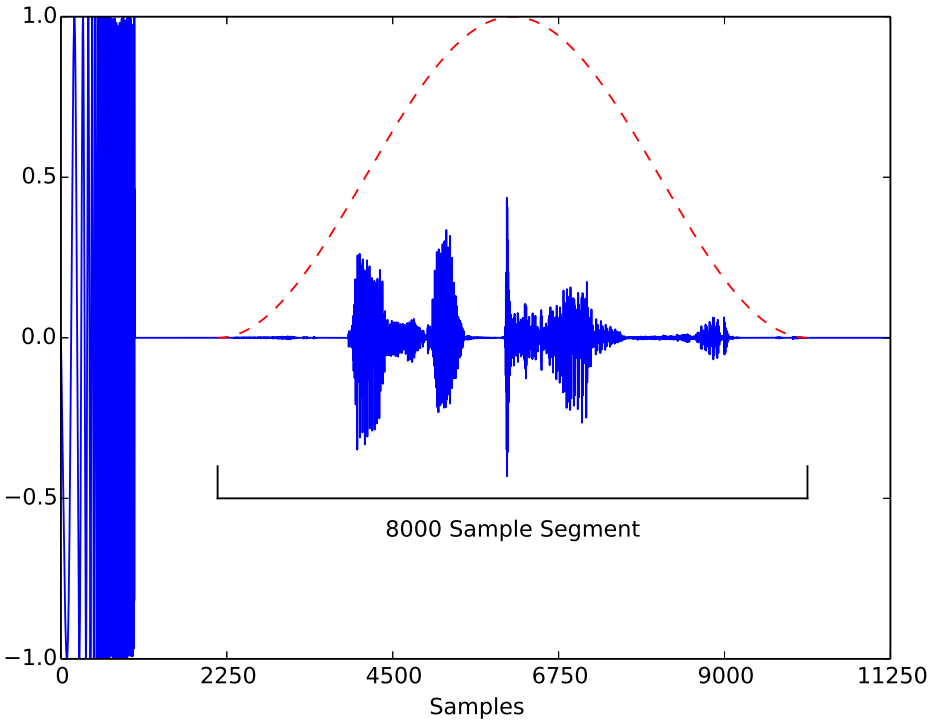

Figure 2.13: Transmitted Frame Format. The dashed line shows the Hanning window function relative to the sample segment.

Barker code sequence of length 13 modulated with binary phase shift keying (BPSK) was also used experimentally with good results.

These frames are played in a continuous loop through the DAC at $f_c = 225$ MHz, resulting in a frame time of 50μs, frame rate of 20k frames/sec, and bandwidth up to 112.5 MHz. An RF modulator is used to mix the output signal $s(t)$ with a carrier frequency fc = 337.5 MHz, creating a dual sideband suppressed carrier (DSB-SC) signal with bandwidth up to 225 MHz.

The bandwidth of this transmitted signal is UWB by the 20% criterion but not quite UWB by the 500 MHz bandwidth criterion. Hardware constraints of the present prototype system made it difficult to achieve this bandwidth without significant hardware modifications. The custom wideband SDR currently supports bandwidths up to 450 MHz, with potential up to 900 MHz using interleaved sampling. Transfer speeds to memory limit the bandwidth to 675 MHz at present. These limitations are not fundamental and could be overcome with more customized hardware.

2.4.2 Receiver

The receiver hardware consists of a ADC12D1800RFRB evaluation board from Texas Instruments [30] and a Zedboard from Digilent [32]. This combination of devices is used as a wideband direct-sampling software-defined radio with a sample rate of 1.8 GSPS. The field-programmable gate array (FPGA) images have been modified to include a digital down converter with decimation rates from ranging from 4 to 2048, as shown in Figure 2.14.

The capture controller is configured to capture buffers of 16384 samples, which is larger than the transmitted frame size as shown in Figure 2.15. This feature of the system allows the frame timing to be imprecise, as long as the timing marker consistently appears within the alignment window.

The capture timer is configured to capture every 0.24995 seconds, which results in a recovered sample rate slightly faster than the nominal audio playback rate of 8 kHz to prevent underruns in the audio playback hardware. Although the transmitter plays out the frames continuously in a loop, the receiver only captures every 4999th frame. For each received frame the transmitter must play through the loop an integer number of times, plus one frame. The 4998 frames transmitted in between are ignored.

In this system, the 4998 ignored frames could contain data from additional users. Therefore, this system simulates a TDM system supporting up to 4999 channels

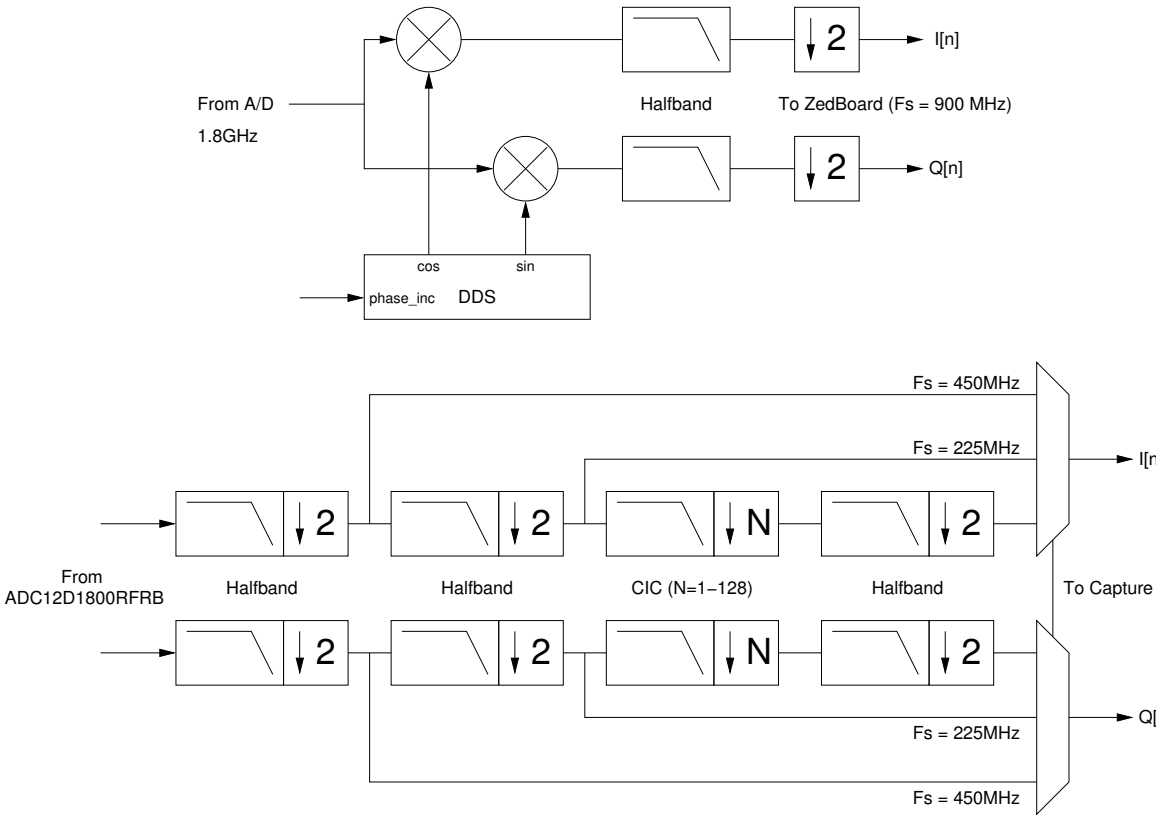

Figure 2.14: Receiver DSP Architecture. The ADC12D1800RFRB image was modified to include a bank of CORDIC processors and a halfband filter. The ZedBoard FPGA image was modified to include a series of halfband filters and a cascaded integrator-comb (CIC) filter.

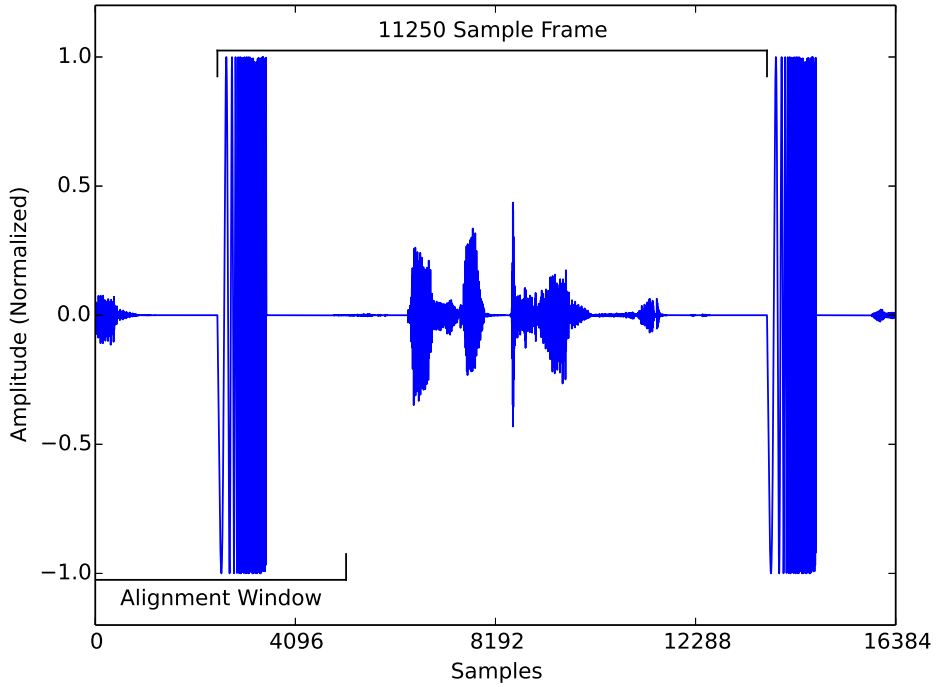

Figure 2.15: Received data showing the timing marker within the alignment window. Shown as a real signal for clarity, actual received data is complex.

where the receiver only processes one of the channels. To create a practical system supporting this many users, some kind of channel identifier needs to be included with the framing overhead.

The receiver software runs a tracking algorithm to center the frame in the capture buffer. The capture timer is manipulated until the timing marker is held stable within the alignment window. The phase and frequency offsets are then estimated from the timing marker. This estimate is used to compensate the frequency and phase offset in the audio samples. The extracted samples are then put into an overlap-add process to recover the original signal. The output from the overlap-add process is chunked into buffers of 1024 samples for live audio playback and capture.

2.4.3 Experiments

In the following experiments, we used a simple wired channel and an indoor wireless channel, and obtain early results demonstrating the feasibility of the new technique in a wideband setting.

The exponential sine sweep method [31] was used to estimate the impulse response of the wired channel as shown in (2.8), where $\mathcal{F}$ denotes the discrete Fourier transform (DFT) operation. The discrete-time signal $x[n]$ represents the exponential sine sweep. The discrete time signal $y[n]$ is the output of the overlap-add process.

$$h[n] = \mathcal{F}^{-1}\left(\frac{\mathcal{F}\left(y[n]\right)}{\mathcal{F}\left(x[n]\right)}\right) \tag{2.8}$$

The exponential sine sweep can be constructed as in the equations (2.9) to (2.11) below. It is often used to estimate impulse response in acoustic environments [31].

$$x[n] = \sin\left[K\left(e^{-nT_s/L} - 1\right)\right] \tag{2.9}$$

$$K = \frac{\omega_1 \tau}{\ln\left(\frac{\omega_1}{\omega_2}\right)} \tag{2.10}$$

$$L = \frac{\tau}{\ln\left(\frac{\omega_1}{\omega_2}\right)} \tag{2.11}$$

.

In this case, $x[n]$ is an 8-second sweep covering 20 Hz to 4 kHz that was generated

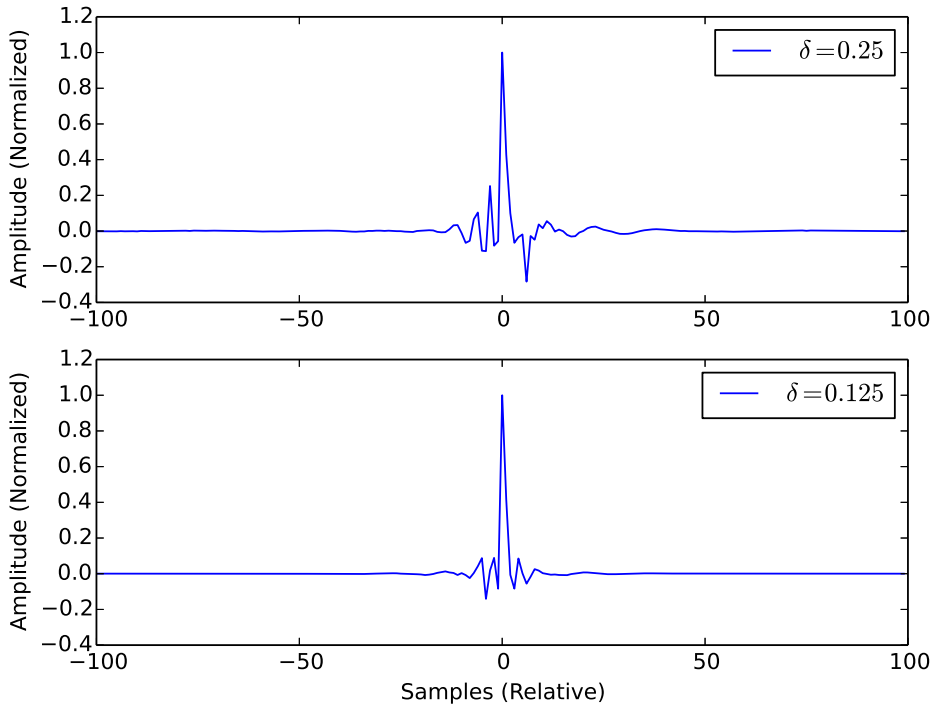

Figure 2.16: Averaged impulse response over 8 sweeps. Fractional hop size is 25% (top) and 12.5% (bottom).

at a sampling rate $f_m = 8$ kHz. Subjecting this signal to the entire process of segmentation, framing, transmission, recovery and reconstruction allows us to estimate the end-to-end impulse response as seen by the input signal. Figure 2.16 (top) shows an averaged impulse response over 8 trial sweeps. Although the impulse response varies significantly between trials, there are definitive features that appear in the average.

Working within the constraints of the current hardware setup, we can improve on this result by reducing the fractional hop size from $\delta = 0.25$ to $\delta = 0.125$ and adding an additional segment in quadrature with each frame as discussed earlier. Figure 2.16 (bottom) shows the resulting average impulse response, again over 8 trial sweeps. This result is significantly improved, evidenced by the reduced amplitude of side lobes relative to the peak.

However, zooming out further reveals additional peaks at ± 1000 samples as shown in Figure 2.17. This is indicative of crosstalk between the in-phase and quadrature segments which are separated by a hop size $R = 1000$ samples when $\delta = 0.125$.

The transmitter output was displayed on a spectrum analyzer and it was observed that the image rejection for a sine wave was only 15-20dB. This agrees with the impulse response obtained in Figure 2.17, where the crosstalk peaks are 15-20dB

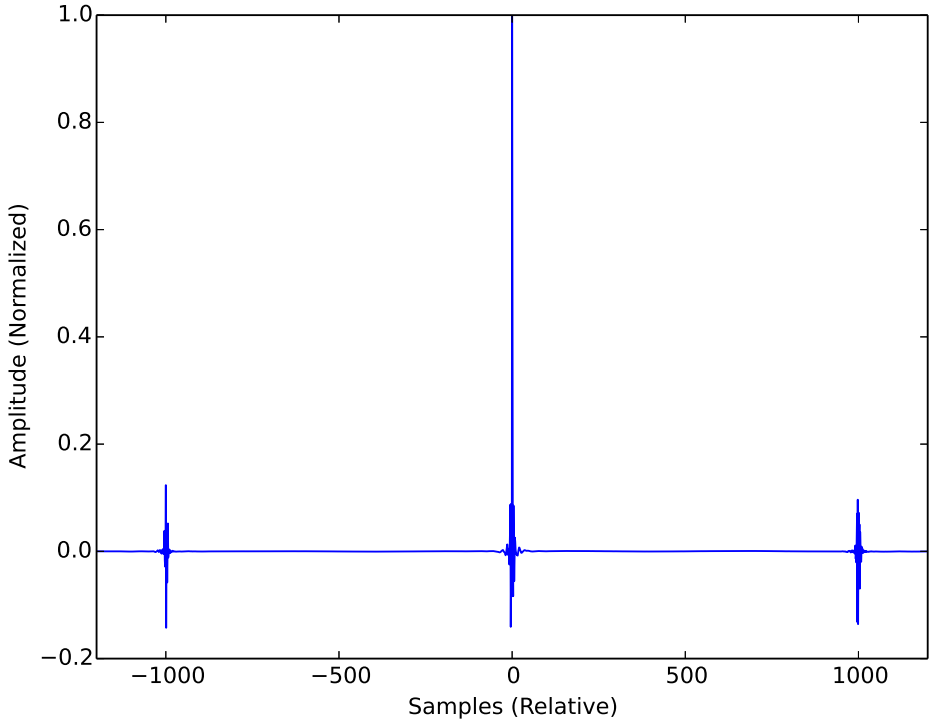

Figure 2.17: Averaged impulse response over 8 sweeps, with additional peaks at ±1000 samples indicating I/Q crosstalk.

down from the main peak. With careful tuning of the DAC's I/Q compensation this effect can be reduced if not eliminated.

To test the feasibility of this type of system over an indoor wireless channel, the wired channel was replaced with two wideband discone antennas designed for a minimum frequency of 600 MHz. The transmitter center frequency was changed from 337.5 to 1012.5 MHz, so that the transmitted signal occupies the bandwidth from 900 to 1125 MHz. The low pass filter in Figure 2.12 was exchanged for a suitable bandpass filter. Amplification was added such that the timing marker was received at a level of 10-20dB above other signals in the 225 MHz bandwidth and 30-40dB above the noise floor. The receiver is undersampling in this configuration, as the Nyquist frequency of the receiver is 900 MHz.

Testing was done in a lab environment of trapezoidal shape with windows on one side and with a door opening to an ancillary room. Signals were transmitted over line-of-sight paths with path lengths of 8, 14 and 20 feet. The 20 foot path originated from the ancillary room, with the doorway acting as a diffracting edge. The exponential sweep method was then applied as before to estimate the power delay profile of the channel. The results for all distances are shown in Figure 2.18 with maximum delay of 12 ms referred to f_m (observed by the message signal at audio frequencies) and 400 ns referred to f_c (observed at radio frequencies), with scaling factor $\beta = 28125$. A speech signal was transmitted over this system, and, as expected, was found to be intelligible with some reverberation at all distances.

The results were improved by expanding the receiver's capture buffer to capture four frames instead of one. Each segment is then received four times, similar in effect to reducing the fractional hop size by a factor of four. With all other parameters being equal, the level of background noise and interference in the output was estimated to be 6dB lower while the signal power remained the same, as expected. These results have demonstrated the feasibility of TC-OLA in a wideband setting. Testing the system at full UWB bandwidths in the unlicensed spectrum remains for future work.

2.5 USRP Implementation

In this section a USRP-based TC-OLA system using a 100 MSPS ADC [33] is described which, combined with the GNURadio software, provides a flexible experimentation platform. This implementation was used to quickly gather performance results for a TC-OLA system with various system parameters and channel models. These

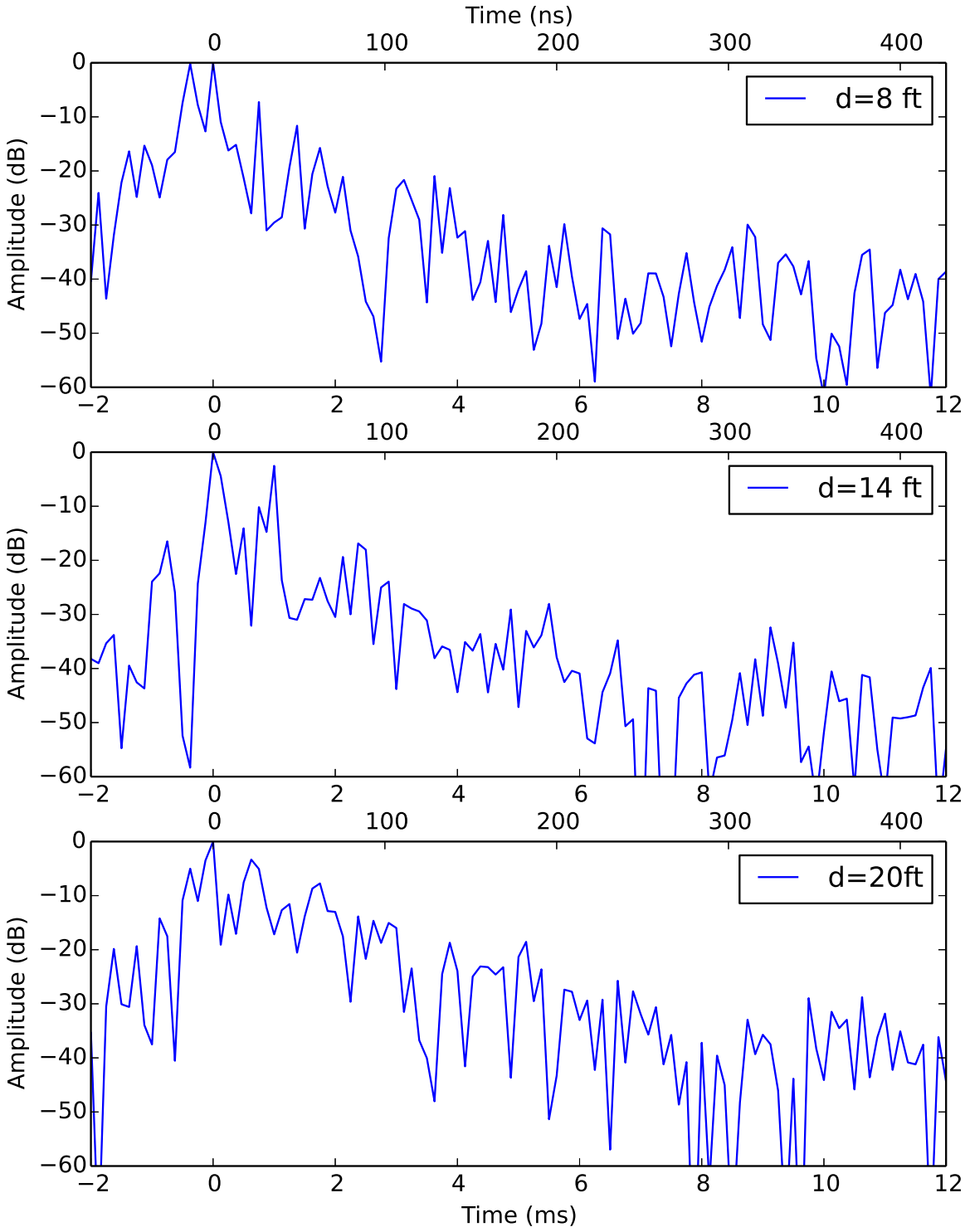

Figure 2.18: Power delay profile referred to the signal sample rate and transmitted sample rate for distances of 8, 14 and 20 ft.

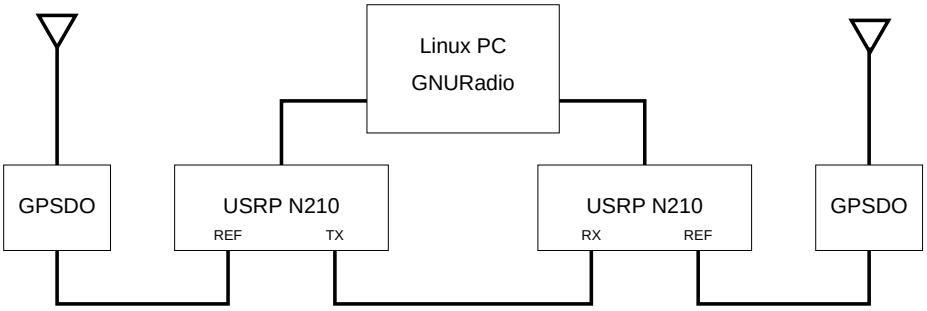

Figure 2.19: USRP-based system hardware connection diagram.

Parameter	**1**	**2**	**3**	**4**
f_m (kHz)	8	8	8	8
f_c (kHz)	500	500	200	200
β	62.5	62.5	25	25
M	8,000	384	8000	384
R	160	8	400	20
δ	0.02	0.02083	0.05	0.05208
Timing Marker (samples)	1000	64	1000	64
Frame Length (samples)	10,000	500	10,000	500
Frame Period (ms)	20	1	50	2.5
Processing Delay (ms)	2000	96	2000	96

Table 2.3: Experimental System Parameters.

results could not be conveniently obtained with the wideband system due to hardware constraints of the prototype. The USRP system uses modest time compression factors of either 25 or 62.5, much smaller than the factor 28125 for the wideband system, but sufficiently large to demonstrate aspects of the system performance.

A block diagram of this implementation is shown in Figure 2.19. The system consists of two commercially available USRP N210 software defined radios from Ettus Research [33] and two GPSDOs from Trimble Navigation [34].

All segment framing and message recovery were performed offline in software. This system was used to simulate the transmission of a single input signal with a high level of redundancy. The GNURadio software allowed us to simulate various channel scenarios quickly in a controlled and repeatable manner.

The USRPs are synchronized to the 10 MHz outputs of separate GPSDO units to provide a realistic simulation of frequency and phase offsets and drift between units located at different sites. LF front end cards covering 0-30 MHz and WBX front end cards covering 50 MHz-2200 MHz were available for these experiments.

A timing marker in the form of an exponential sine sweep begins each frame. Each segment is then padded with zeros on either side samples to create the desired frame length. The real baseband signal is then mapped to a passband DSB-SC at carrier frequencies of 10 MHz or 900 MHz depending on the equipped RF front end card. The system parameters for the experiments that follow were chosen as in Table 2.3 and will be referenced by their numbers in the following discussion.

The system parameters were chosen to explore the parameter space. Systems 1 and 2 as compared to systems 3 and 4 allow us to draw conclusions about varying

redundancy expressed by the fractional hop size δ. Systems 1 and 3 as compared to systems 2 and 4 allow us to draw conclusions about varying the frame size M.

Although the processing delays listed for systems 1 and 3 may be impractical for a two-way communication system this delay can be reduced to a reasonable level by substituting a series of shorter segments with the same total length and fractional hop size into each frame. However, this substitution may impact how the system interacts with the channel as shown in the next section.

2.5.1 Experiments

The exponential sine sweep method of impulse response estimation [31] was again applied to evaluate the response of simple wired channel to ensure the system is working correctly. Subjecting the sweep signal to the entire process of segmentation, framing, transmission, recovery and reconstruction allows us to estimate the end-to-end impulse response as seen by the input signal.

As expected, the end-to-end impulse response is very flat, except for some attenuation at high frequencies. This could be due to digital filters in the USRPs or cancellation due to jitter in window positioning. This result indicates that the transmission and recovery processes are not significantly affecting the message signal. The recovered impulse response as 10 MHz is shown in Figure 2.20. The same test at 900 MHz gave a similar result.

Additional signals that were tested with this basic configuration include two audio signals sampled at 8 kHz, wherein segments from the two sources were coded with columns from the Hadamard matrix $H(2)$ to create a simple CDMA signal. The channels were separated at the receiver with no perceptible crosstalk. In a sense, this is analogous to the CDMA downlink situation where all of the coded frames are transmitted in perfect synchronization. A static two-ray model was simulated in the transmission path using an finite impulse response (FIR) filter implemented in GNU-Radio having a second tap at 400 samples with an amplitude of -0.35. The channel impulse response was again estimated using the previously-described method. The recovered end-to-end impulse response agrees with the simulated channel parameters as shown in Figure 2.21.

To gain an intuitive understanding of this effect, an audio speech signal was transmitted through the system. The delay of 400 samples on the RF channel (800μs) manifests as an audible echo, delayed by 400 samples at the audio rate (50ms). This

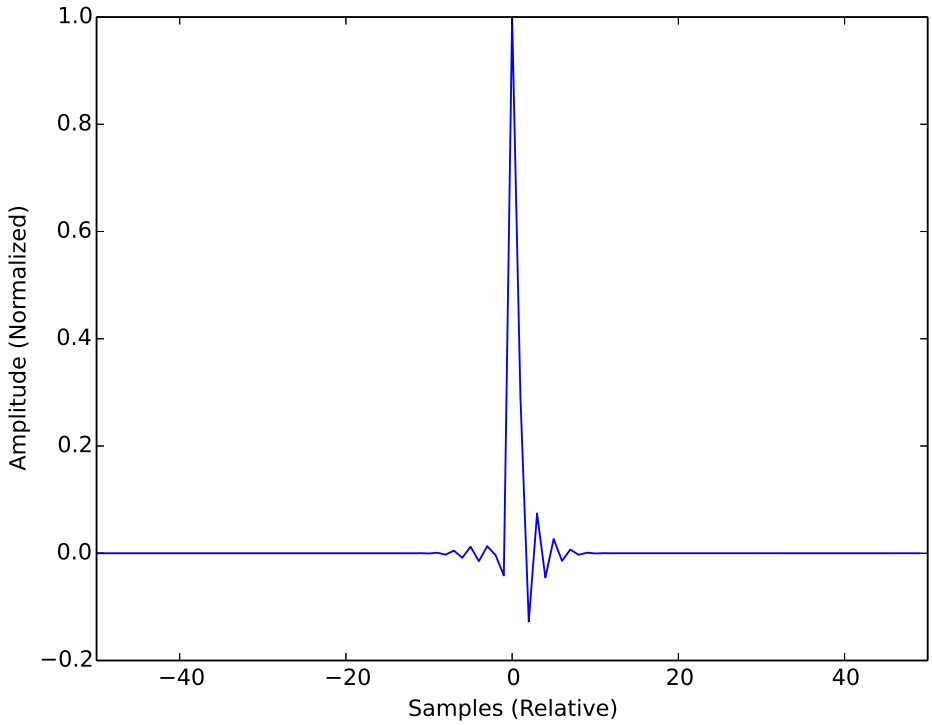

Figure 2.20: Recovered impulse response with simple wired channel.

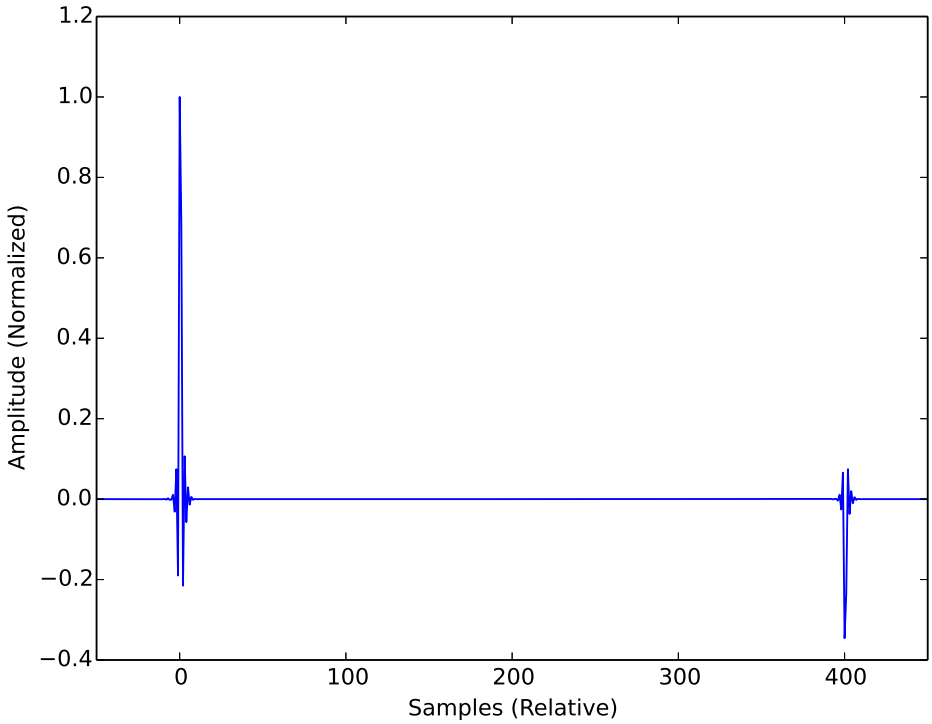

Figure 2.21: Recovered impulse response using two-ray model.

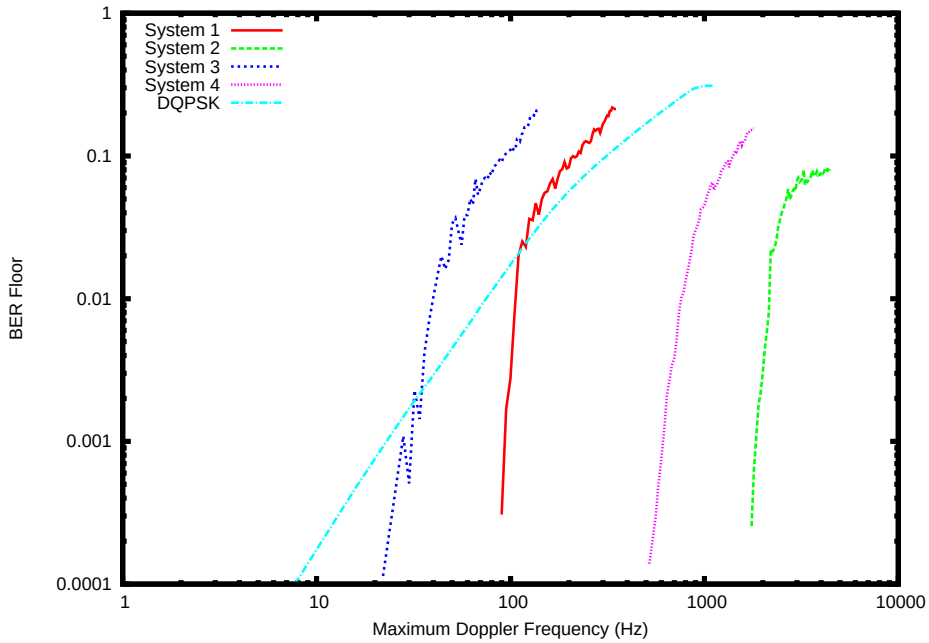

Figure 2.22: BER Floor vs. Maximum Doppler Frequency for DQPSK over Systems 1 through 4 subject to Rayleigh fading model.

is precisely as described by [8], as well as Figure 2.4, where the channel response is expanded in time by the ratio of sampling rates.

As we are using a short exponential sine sweep as a synchronization marker in this system, we can estimate and compensate for this channel on a frame-by-frame basis. First, an inverse filter h_{inv} is estimated from

$$h_{inv}[n] = \mathcal{F}^{-1}\left(\frac{\mathcal{F}\left(x[n]\right)}{\mathcal{F}\left(y[n]\right)}\right). \tag{2.12}$$

This filter is then applied to the samples of each received segment before the overlap-add process. The result is that the echo is removed from the audio speech signal.

There are several drawbacks to this approach, including poor estimation of the channel in a deep fade, frequency interpolation, and limitations on the channel delay relative to the frame length. An adaptive equalizer may provide better results. However, this method was shown to be able to adapt to a time-varying frequency-selective channel provided the channel is relatively constant over the frame period.

Up to this point we have only considered DSB-SC signals generated from real baseband sampled signals. However, this concept extends to complex baseband signals

Tap	**Delay (μs)**	**Power (dB)**
1	0	0
2	2	-3
3	4	-6

Table 2.4: Frequency Selective Channel Model.

as well. A differential QPSK (DQPSK) signal representing an 8000bps bit stream was modulated at 2 samples per symbol using the DQPSK modulator included with GNURadio 3.7.3. A segment of this modulated signal containing 250,000 bits was framed as per the frame lengths in Table 2.3 for transmission in order to test various channel scenarios.

First, a Rayleigh flat fading channel was simulated in the transmission path, using the model of [35] as represented in GNURadio version 3.7.3. This model was tested purely in simulation with no noise, allowing estimation of the BER floor with respect to the maximum Doppler frequency parameter of the model. The results for systems 1 through 4 are plotted against absolute maximum Doppler frequency in Figure 2.22. The BER floor of the DQPSK receiver in GNURadio 3.7.3 is plotted for reference.

The main observation is that systems with shorter frames perform better relative to the maximum absolute Doppler frequency in a Rayleigh flat fading scenario. This result is expected, and typically these types of performance tests are plotted against the normalized Doppler frequency. Figure 2.23 shows the same results with the Doppler frequency normalized to the frame time T_f.

From Figure 2.23 it is observed that similar BER floor performance is achieved relative to the normalized maximum Doppler frequency for similar values of fractional hop size δ. However, the slope of the BER floor curve below $f_D T_f = 2$ increases as the fractional hop size is decreased. This is an artifact of the timing recovery process, which operates correctly only when the phase shift over the window is less than π radians.

The frequency-selective case is now evaluated, as one of the primary goals of this scheme is to spread the bandwidth of the input signal enough that the channel becomes frequency selective rather than flat fading. To this end, the GNURadio 3.7.3 frequency selective channel model [36] was inserted into the simulation. This model adds a frequency-selective extension to the previously discussed Rayleigh fading model of [35]. The power delay profile is specified as in Table 2.4. Each tap fades

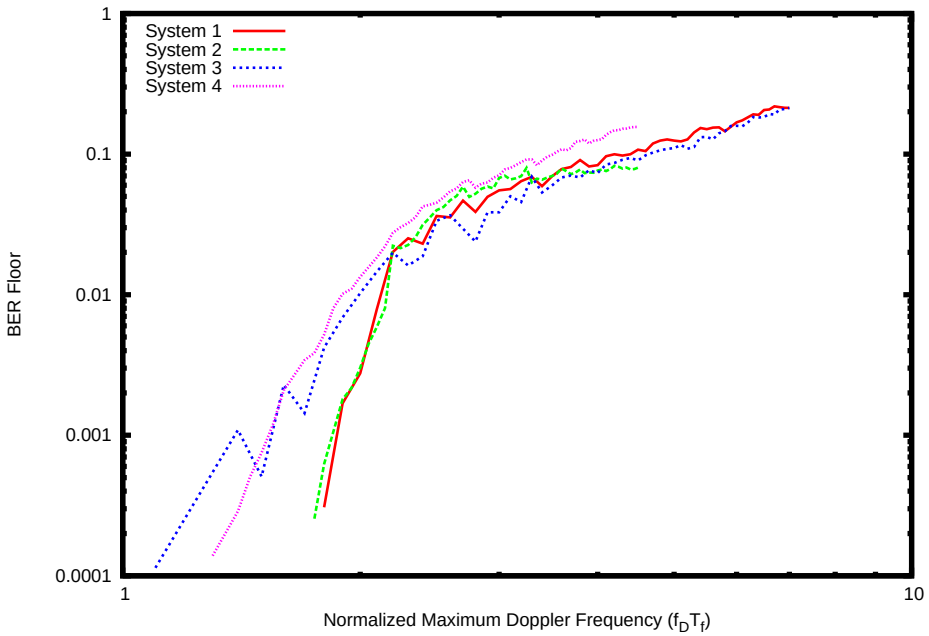

Figure 2.23: BER Floor vs. Normalized Maximum Doppler Frequency for DQPSK over Systems 1 through 4 subject to Rayleigh flat fading model.

independently but with the same maximum Doppler frequency applied to all taps.

The general result that can be observed is that the BER floor curves of Figure 2.22 shift to the left, reducing the upper limit of the Doppler frequency that can be tolerated. In the previous discussion (Figures 2.4-2.7) it was shown that the averaging effect of the overlap-add technique is reduced as the rate of change in the channel characteristic is reduced, thus affecting the BER floor at lower limit of the Doppler frequency graph. However, for very slow changes the previously-discussed channel estimation technique can be used.

Results for systems 1 and 2 are shown in Figure 2.24 which illustrates these features. Without channel estimation, the lower limit of the BER floor rises as the Doppler frequency approaches zero and the system becomes ISI-limited. With channel estimation, the result is degraded for higher normalized Doppler because the channel changes too quickly for the channel estimation to keep up. The upper limit of the BER floor has been shifted to the left with respect to the Rayleigh flat fading result. It appears that for this channel there is some useful range where the averaging effect dominates. For this channel it is between $f_D T_f \approx 0.03$ and $f_D T_f \approx 0.5$. There is also some range below which the estimation technique is useful. For this channel the estimation technique becomes useful below $f_D T_f \approx 0.033$. The combination of averaging and channel estimation covers the range for $0 \leq f_D T_f \leq 0.5$.

Figure 2.25 shows the same result plotted on an absolute scale. As lower Doppler spreads are typically accompanied by slower changes in frequency selective channels, it may be advantageous to alter the system parameters dynamically as a means of tuning the system to the channel conditions. By making a smooth transition from smaller frames to larger frames as the Doppler frequency decreases, it may be possible to keep the BER floor low without resorting to the complexity of channel estimation techniques. Although the channel estimation technique is shown to work well, it is expensive in terms of processing. From a system design perspective, it is sensible to leverage the built-in averaging effect of the overlap-add process to the fullest extent possible.

2.6 Conclusions and Future Work

In this chapter we have presented a time-compression overlap-add (TC-OLA) scheme for discrete-time signals where the level of redundancy and spreading factor can be varied by modifying the amount of overlap between segments of the message sig-

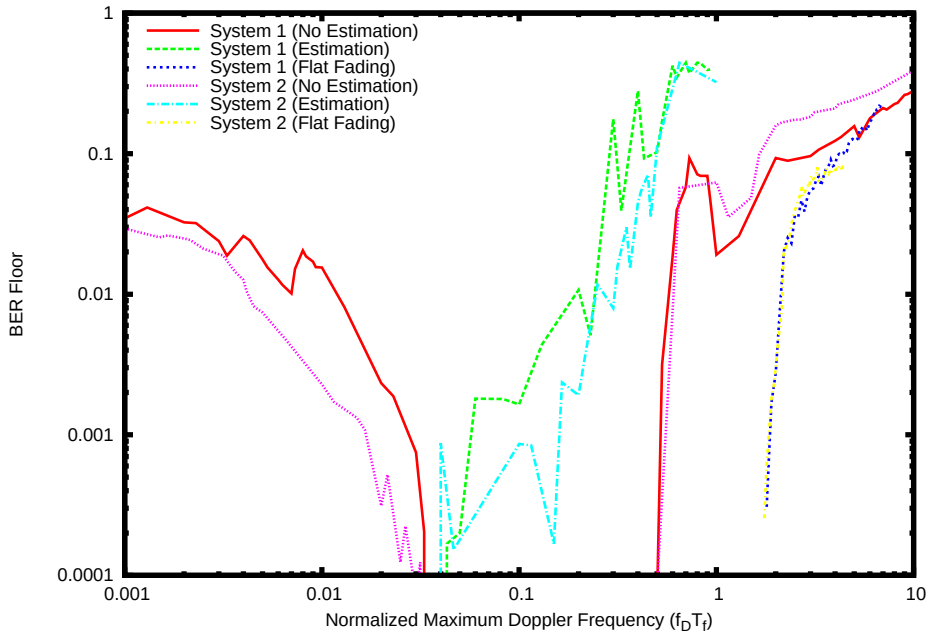

Figure 2.24: BER Floor vs. Normalized maximum Doppler frequency for systems 1 and 2 subject to frequency-selective channel of Table 2.3. Channel estimation can be used to extend the low range. Rayleigh flat fading results shown for reference.

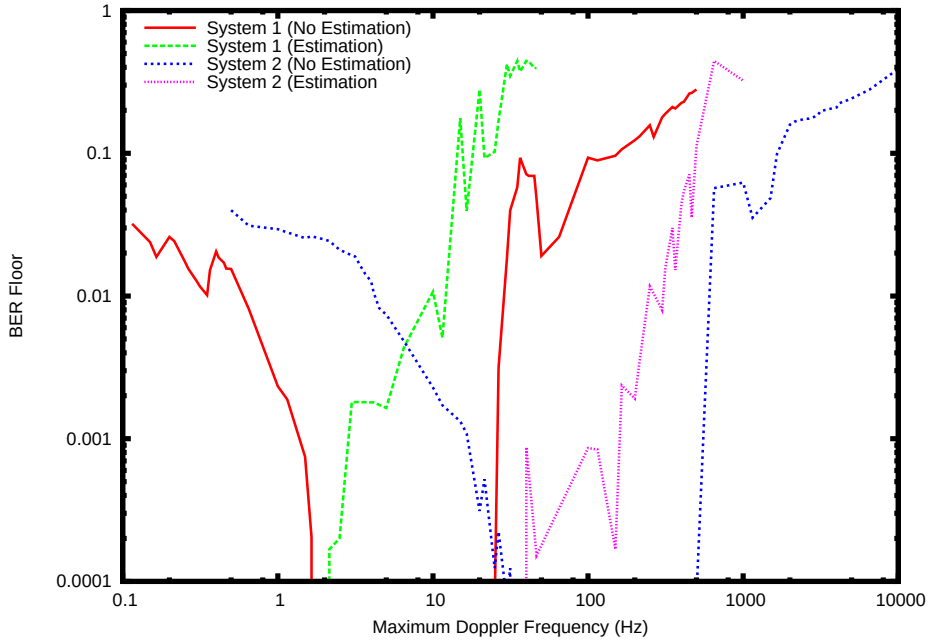

Figure 2.25: BER Floor vs. Maximum Doppler Frequency for systems 1 and 2.

nal [37]. This property could be applied dynamically with different strategies. For one example, the time compression factor δ could be changed to increase the signal bandwidth in order to overcome a temporary flat fading condition. Another example is a TDM system operating in a fixed bandwidth with a quality of service (QoS) mechanism where low priority traffic can be dropped in order to allocate more redundancy for high priority traffic as the channel condition degrades. To verify the operation of this TC-OLA scheme we have presented two implementations. It was shown that not only that sampled analog signals can be transmitted using TC-OLA but also that waveforms expressing digital modulation schemes generated algorithmically can be transmitted. The interference rejection property of TC-OLA was verified experimentally using the wideband implementation. Properties of TC-OLA in typical fading channel models have been explored. These results need to be expanded to understand the properties of the scheme in more varied scenarios, including outdoor channels and UWB channels at unlicensed power levels. Other future work includes a comparison with existing air interface physical layer communications in a 5G context. In this work we have presented a functional wideband SDR system which can receive and decode a wideband signal which is distinctly different from a UWB pulse radio. The receiver hardware was initially designed as a general-purpose experimentation platform that was able to implement this technique with several limitations. Ideally, the receiver would be redesigned to specifically implement this technique with minimal hardware limitations. Additionally, a more flexible transmitter must be designed that can support a wider range of the parameter space. Experiments could then be performed to better characterize the properties of this scheme over real wireless channels and in a system context with multiple users.

Chapter 3

Time-Compression Overlap Add: Description and Analysis

3.1 Introduction

TC-OLA is a spread-spectrum technique inspired by time compression multiplexing and overlap-add analysis/synthesis techniques, applied to software defined radio [12]. In a sense, TC-OLA can be considered the dual of DSSS. Where a DSSS system modulates the data with a high speed code [38], TC-OLA modulates a code with high speed data. In this work we assume a trivial code of $\{1, 1, ...\}$ in order to clearly illustrate some of the basic properties.

TC-OLA was initially motivated by an investigation into leveraging software defined radio technology combined with high speed DAC and ADC components to transmit and receive signals that could be considered UWB but would be different from pulse radio and OFDM UWB variants [12]. One aim of these types of systems is to spread the bandwidth sufficiently such that the transmitted signal experiences frequency-selective rather than flat fading. The TC-OLA solution is to simply play the source samples at a higher sample rate, effectively spreading the bandwidth by the ratio of the sample rates [8]. This technique is employed in time-compression multiplexing (TCM) systems, where the increased sample rate allows multiple channels to be multiplexed along with synchronization information [7, 27]. In a TC-OLA system the increased sample rate allows redundancy to be added to the message signal. Ideally the TC-OLA implementation is transparent to the underlying message signal, whether it is a sampled analog waveform or a digitally modulated waveform.

An experimental prototype wideband TC-OLA system (225MHz) using a pilot signal for synchronization and channel estimation was successfully implemented in Chapter 2. In order to improve the efficiency of the scheme, we seek to develop a system where time compression techniques are used to spread the bandwidth without the use of a pilot signal. Continuing from the experimental results reported in that chapter we develop two mathematical models of TC-OLA. The remainder of this chapter is organized as follows: Section 3.2 presents a model of the TC-OLA process based on time shifting, which is used to analyze the performance in AWGN and Rayleigh fading channels. Section 3.3 presents a model of the TC-OLA process based on multirate filter concepts, which is then used to analyze the transmitted spectrum.

3.2 Time-Shifting Model

A non-causal formulation of the TC-OLA transmit and receive processes is developed here based on time shifting of discrete time signals. In this formulation the message signal is recovered with no time delay, where in practice we expect some excess delay due to the TC-OLA process. This approach is inspired by the presentation in the audio signal processing literature. The distinct difference is that the windows of the message signal are not treated in isolation in the frequency domain before reconstruction. Instead they are formed into a new time domain signal at a higher sample rate by placing the windows end to end as shown in Figure 3.1. It is this series of windows which is transmitted through the radio channel. The receiver must determine the window boundaries and overlap the windows to recover an estimate of the original message signal.

The concept of window functions with a constant overlap-add property is central to TC-OLA. We shall define the window coefficients w_i for windows of even length M as in (3.1). Odd-length windows are also possible.

$$w_i = \sin\left(\frac{\pi\left(i+0.5\right)}{M}\right),\ 0 \leq i < M \tag{3.1}$$

Using this definition we may define a discrete time window function:

$$w[k] = \begin{cases} w_i|_{i=k} & : 0 \leq k < M \\ 0 & : otherwise \end{cases} \tag{3.2}$$

The window function is applied once by the transmitter and once by the receiver,

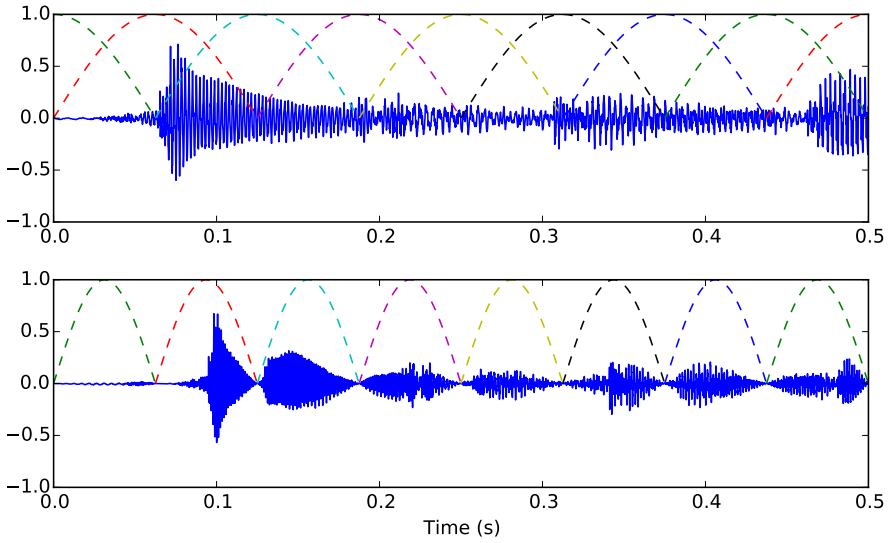

Figure 3.1: Top: Message signal sampled at f_m, showing overlapping window functions for reference. Bottom: Time-compressed series of non-overlapping windows to be transmitted through the radio channel at a sample rate of $f_c = \frac{M}{R} f_m$. Window functions shown for reference. In this example $\frac{M}{R} = 2$ but typically $\frac{M}{R} >> 2$.

giving an overall Hanning window shape. The constant overlap-add property for Hanning windows states that the overlapping windows sum to a constant C as in (3.3) for any hop size R that satisfies (3.4) [10].

$$C = \sum_{i=-\infty}^{\infty} w^2[k - iR] \tag{3.3}$$

$$R = \frac{M}{2C},\ C = 1, 2, 3... \tag{3.4}$$

Let k be the index variable for discrete time signals at rate f_m. Let j be the index variable for discrete time signals at rate $f_c = \frac{M}{R} f_m$. Let the message signal be $m[k]$ and the transmitted signal be $s[j]$. Let $s[j]$ be generated by repeatedly shifting the message signal $m[k]$ to the right by $M - R$ samples, each time applying the window function $w[k]$ which has been shifted to the right by M samples:

$$s[j] = \sum_{i=-\infty}^{\infty} w[j - iM]m[j - i(M - R)] \tag{3.5}$$

This discrete time waveform $s[j]$ is then converted to a continuous time baseband waveform $s(t)$ via an ideal DAC operating at sample rate f_c and optionally modulated onto a radio frequency carrier operating at f_c. Assume that the carrier frequency and phase are synchronized at the receiver. The downconverted signal is sampled by an ideal ADC which is synchronized with the sample clock of the transmitter DAC. The transmitted signal $s[j]$ arrives at the receiver via Q independent paths each with time-varying channel gain $x_q[j]$ and additive noise $n[j]$ as in (3.6). We assume for now that the delay of each path is an integer multiple of the window length M.

$$r[j] = \sum_{q=0}^{Q-1} x_q[j]s[j - qM] + n[j] \tag{3.6}$$

The message signal $m[k]$ is recovered by repeatedly shifting the received signal left by $M - R$ samples, each time applying the window function which has been shifted right by R samples:

$$\widehat{m}[k] = \sum_{i=-\infty}^{\infty} w[k - iR]r[k + i(M - R)] \tag{3.7}$$

Combining (3.5-3.7), we recognize that the summation of the window function $w[k]$ is invariant to a shift of M. In this case we also recognize that, due to the repetition within the TC-OLA signal, shifting the message signal $m[k]$ by M can be written equivalently as a shift of R:

$$\begin{aligned}\widehat{m}[k] = \sum_{q=0}^{Q-1} m[k-qR] \sum_{i=-\infty}^{\infty} w^2[k-iR]x_q[k+i(M-R)] \\ + \sum_{i=-\infty}^{\infty} w[k-iR]n[k+i(M-R)]\end{aligned} \tag{3.8}$$

By setting $n[j] = 0$, $x_0[j] = 1$ and $x_q[j] = 0|_{q>0}$ it is possible to show the perfect channel output of the TC-OLA process as in (3.9):

$$\widehat{m}[k] = m[k] \sum_{i=-\infty}^{\infty} w^2[k-iR]. \tag{3.9}$$

The summation in (3.9) indicates an overlapping series of Hanning windows. Given that (3.4) is satisfied:

$$\widehat{m}[k] = \frac{M}{2R} m[k] \tag{3.10}$$

From (3.10) it is clear that there is a gain associated with the overlap-add process that is dependent on the ratio of $\frac{M}{R}$ and on the overlap-add properties of the window function. This gain is exploited by TC-OLA to provide an effect analogous to the spreading gain in a DSSS system. This spreading gain can be used in link budget calculations when designing a TC-OLA system.

3.2.1 AWGN Performance

Let us now define $x_0[j] = 1$, $x_q[j] = 0|_{q>0}$ and $n[j]$ as an additive white Gaussian noise process with zero mean and variance σ_n^2:

$$\widehat{m}[k] = \frac{M}{2R} m[k] + \sum_{i=-\infty}^{\infty} w[k-iR]n[k+i(M-R)] \tag{3.11}$$

Let the output noise of the process be defined by a new random process $\widehat{n}[k]$ with zero mean and variance $\widehat{\sigma}_n^2$ by summing the scaled variances. Assuming the constant

overlap-add criterion is satisfied:

$$\widehat{\sigma}_n^2 = \sum_{i=-\infty}^{\infty} w^2[k - iR]\sigma_n^2 = \frac{M}{2R}\sigma_n^2 \tag{3.12}$$

The output signal to noise ratio is then:

$$SNR_{out} = \frac{\left(\frac{M}{2R}\right)^2 E\left[m^2[k]\right]}{\widehat{\sigma}_n^2} \tag{3.13}$$

$$= \frac{\left(\frac{M}{2R}\right) E\left[m^2[k]\right]}{\sigma_n^2} \tag{3.14}$$

The process gain can be computed by comparing the input SNR to the output SNR. The input SNR is:

$$SNR_{in} = \frac{E\left[\left(\sum_{i=-\infty}^{\infty} w[k - iM]\right)^2\right] E\left[m^2[k]\right]}{\sigma_n^2} \tag{3.15}$$

$$= \frac{\frac{1}{2}E\left[m^2[k]\right]}{\sigma_n^2} \tag{3.16}$$

The process gain is then:

$$G = \frac{M}{R} \tag{3.17}$$

$$= 10\ \log_{10}\left(\frac{M}{R}\right)\ dB \tag{3.18}$$

3.2.2 Multipath Rayleigh Fading Performance

Assume that TC-OLA carries the message signal $m[k]$ over a Rayleigh fading channel where the phase is recovered perfectly at the receiver but the fade rate is fast enough to be considered independent at a delay of $\frac{(M-R)}{f_c}$. These assumptions do not represent a practical situation but instead an extreme condition that allows us to estimate a lower bound on the effect of Rayleigh fading. Let us define $n[j] = 0$ and $x_q[j]$ as a Rayleigh random process with mean μ_q and variance σ_q^2. For this case we obtain from (3.8):

$$\widehat{m}[k] = \sum_{q=0}^{Q-1} m[k - qR] \sum_{i=-\infty}^{\infty} w^2[k - iR]x_q[k + i(M - R)] \tag{3.19}$$

For each q a new discrete random process $\widehat{x}_q[k]$ can be defined with mean $\widehat{\mu}_q$:

$$\widehat{\mu}_q = \sum_{i=-\infty}^{\infty} w^2[k - iR]\mu_q = \frac{M}{2R}\mu_q \tag{3.20}$$

and variance $\widehat{\sigma}_q^2$. Assuming the constant overlap-add criteria for a $\cos^4(\cdot)$ window shape is met[1]:

$$\widehat{\sigma}_q^2 = \sum_{i=-\infty}^{\infty} w^4[k - iR]\sigma_q^2 = \frac{3M}{8R}\sigma_q^2 \tag{3.21}$$

From this result we observe that the variance has been reduced relative to the mean by a factor of 25%. This is due to the overlap-add property of the $\cos^4(\cdot)$ window. In a more realistic scenario where the fading process is correlated between windows [39] we expect the output variance $\widehat{\sigma}_r^2$ to increase as uncorrelated measurements are more effective in predicting the mean[2].

Here we have also shown that the channel seen by the message signal has been transformed by the TC-OLA process. It was observed in [8, 12] that a delay of d samples at f_c is transformed into a delay of d samples at f_m for short delays relative to the window length M. Thus the channel response is compressed in frequency as the received signal is expanded in time. In this case taps at multiples of M samples in the channel have been transformed into taps at multiples of R samples in the output by the overlapping that occurs in the TC-OLA receive process. The overall system performance depends on how the receiver for the message signal $m[k]$ is affected by the transformed taps.

A full analysis of the channel transformation as well as a more general Rayleigh result including phase and correlation effects is deferred to Chapter 4.

[1]The constant overlap add criteria for $\cos^4(\cdot)$ windows was experimentally determined to be valid for any R that satisfies $R = \frac{M}{4K}$ $K = 1, 2, 3...$ and sums to $\frac{3M}{8R}$.

[2]The experimental results reported in [12] show that the BER floor rises as the normalized Doppler frequency f_D increases relative to the window time T_f beyond $f_D T_f = 2$. This analytical result contradicts the experimental result. We conclude and have confirmed experimentally that the rise in the BER floor is an artifact of the timing recovery scheme used in the experiment and not a fundamental property of the TC-OLA process.

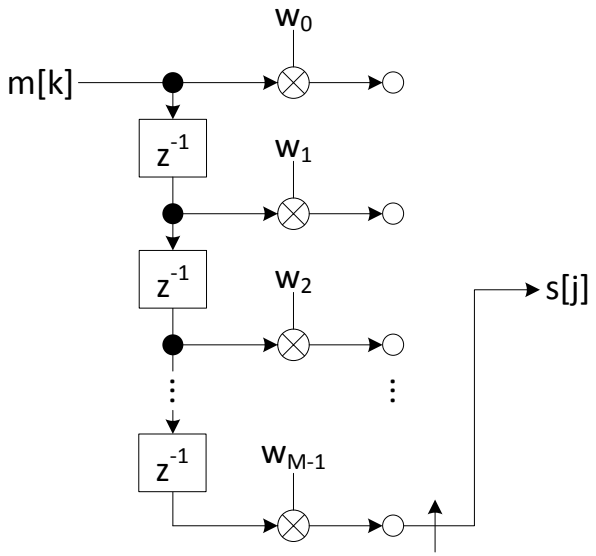

Figure 3.2: Transmit Process for $R = 1$. M output samples are produced on $s[j]$ for each input sample consumed from $m[k]$. Window coefficients w_i are as defined in (3.1).

3.3 Digital Filter Model

A causal digital filter formulation of the transmission process can be constructed from a simple description of the algorithm to generate a TC-OLA signal. First, apply the window function (3.1) to the most recent M samples at sample rate f_m. Transmit these samples at f_c then read in R new samples at f_m. The simple case where $R = 1$ can be modelled using a delay line and an M-phase commutator as shown in Figure 3.2. In this figure M input samples are produced at f_c for each sample input at f_m. The receive process is formed by the complement of the transmit process: apply the window function to the most recent M samples at f_c and add to the output buffer. Then shift the output buffer by R samples. In the simple case where $R = 1$, the receive process can be modelled as in Figure 3.3. It is clear that this process is the dual of the transmit process, formed by reversing all flow directions and exchanging junctions with summations [40].

By replacing the output commutator in the transmit process with the equivalent upsampling, delay and summation operations (Figure 3.4) and applying the noble identity [40] (Figure 3.5) it is possible to show that the transmit process for $R = 1$ is equivalent to upsampling the message signal by M followed by a FIR filter formed by the coefficients of the window function upsampled by $M - 1$. Figures 3.7 and 3.8

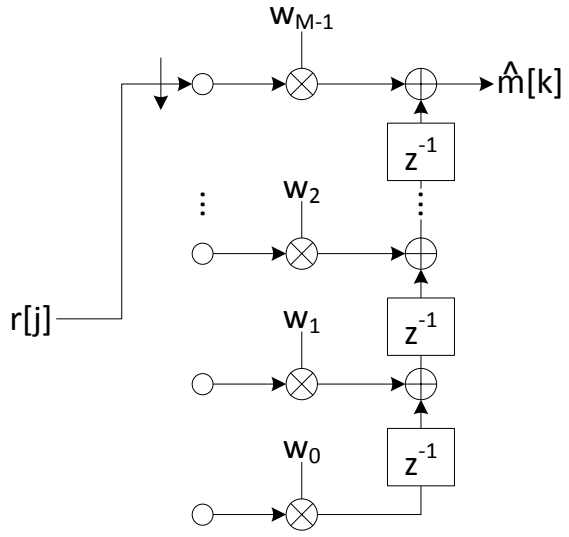

Figure 3.3: Receive Process for $R = 1$. One output sample is produced on $\widehat{m}[k]$ for every M input samples consumed from $r[j]$.

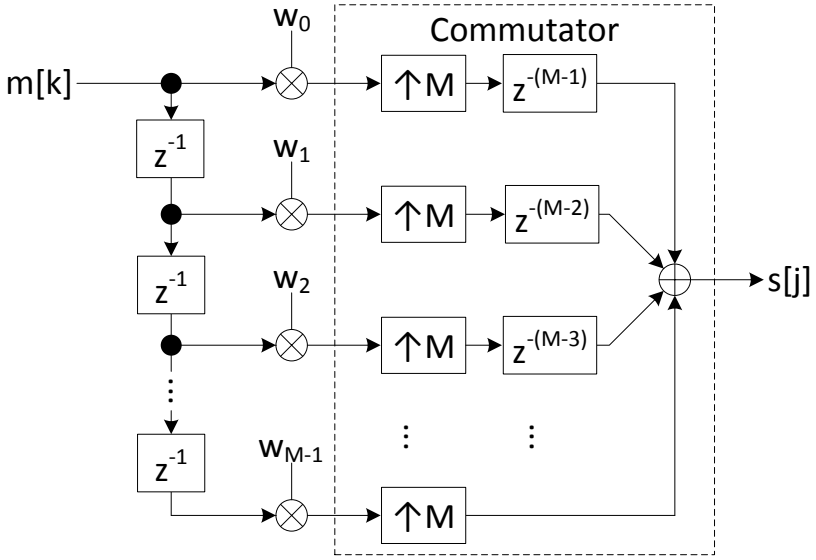

Figure 3.4: Transmit process for $R = 1$. The output commutator has been replaced by the equivalent upsampling, delay and summation operations.

refer to this equivalent filter as $H(z, M)$ where:

$$H(z, M) = \sum_{i=0}^{M-1} w_i z^{-(M-1)(i+1)} \tag{3.22}$$

An alternate receiver process, equivalent to Figure 3.3, can be constructed by the same filter followed by a downsampler (Figure 3.6). An assumption in this scheme is that the upsamplers in the transmitter are perfectly synchronized with the downsamplers in the receiver as shown in the system diagram of Figure 3.7. In practice the transmitter's upsampler state is unknown and must be estimated at the receiver. The alternate formulation of the receiver shown in Figure 3.6 allows easily replacing the final downsampler with a commutator (Figure 3.8) in order to simultaneously observe every possible commutator offset and choose the best one. The receiver structure shown in Figure 3.3 may have a programmable commutator offset, with the disadvantage of a delay while the change propagates through the system. The receiver structure shown in Figure 3.8 has the disadvantage that the FIR filter must operate at the higher f_c clock rate with many more delay elements, a concern for hardware implementations.

To generalize this process to the case of $R > 1$ it is useful to consider a modified upsampling operation where instead of stuffing $M - 1$ zeros between each sample,

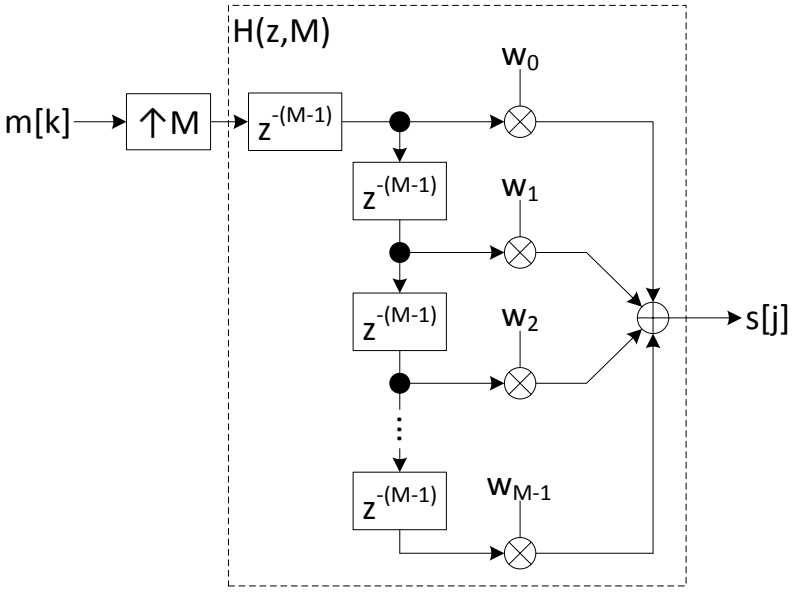

Figure 3.5: Transmit process for R=1, with upsampling referred to the input. The remainder of the process then takes the form of a finite impulse response (FIR) filter.

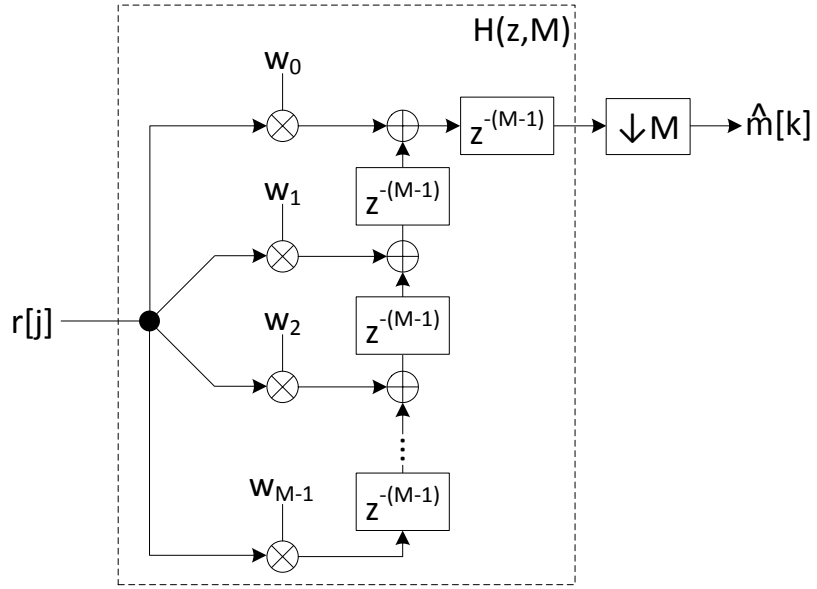

Figure 3.6: Receive process for R=1, with downsampling referred to the output. The remainder of the process then takes the form of a finite impulse response (FIR) filter. $H(z, M)$ is shown in the transposed form.

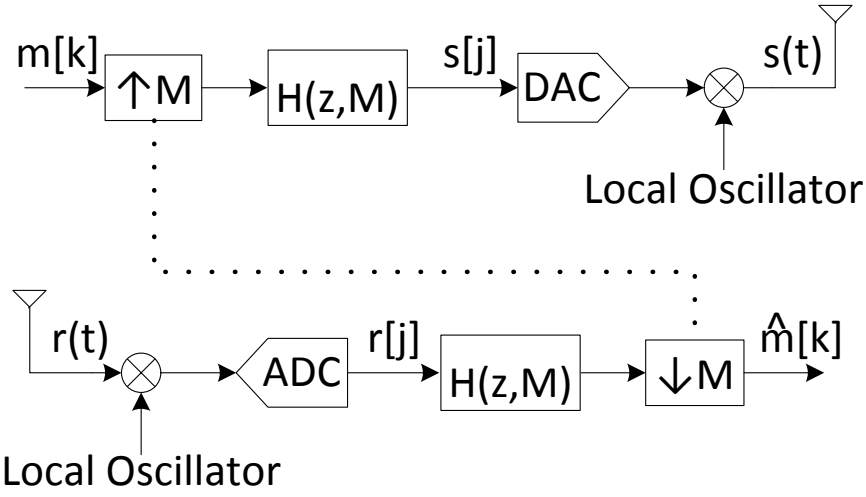

Figure 3.7: System diagram showing transmit and receive process for $R = 1$. The downsampler in the receive process must be correctly aligned to the upsampler in the transmit process. $H(z, M)$ is the transfer function of the equivalent FIR filter shown in Figures 3.5 and 3.6.

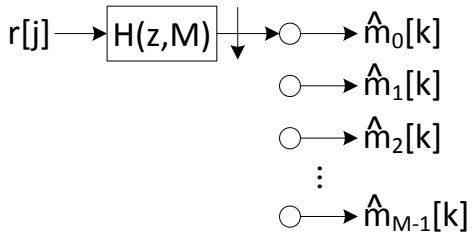

Figure 3.8: Flowgraph showing alternate receive structure for $R = 1$. By replacing the downsampler in Figures 3.6 and 3.7 with a commutator, all possible alignments can be observed simultaneously. $H(z, M)$ is the transfer function of the equivalent FIR filter shown in Figure 3.5 and 3.6.

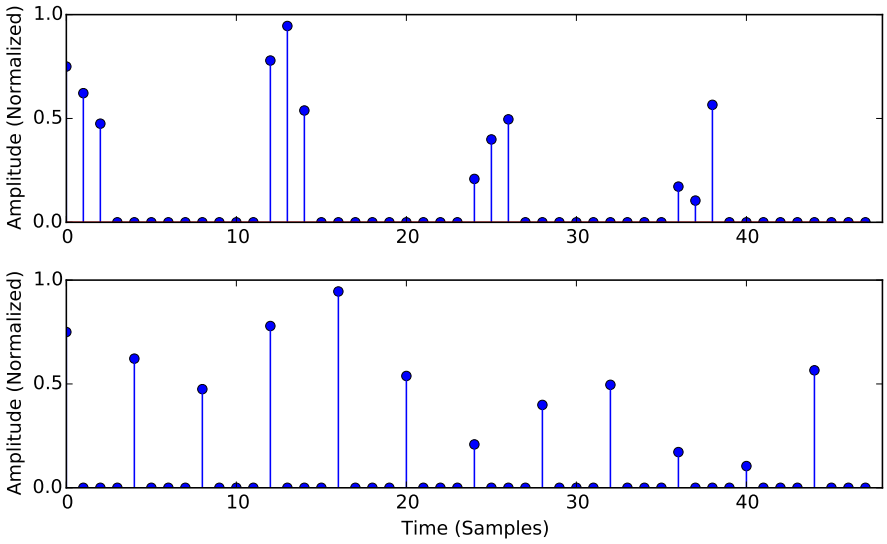

Figure 3.9: Top: With $M = 12$ and $R = 3$, stuffing $M - R = 9$ zeros between each group of R samples. $M/R = 4$. Bottom: Standard upsampling by 4 with the same input signal.

$M - R$ zeros are stuffed between each group of R samples as illustrated in Figure 3.9. This type of signal can be achieved by a commutator arrangement distributing the input across R phases, where each phase is upsampled by $\frac{M}{R}$, followed by another commutator as shown in Figure 3.10. All of the phases are then recombined by the output commutator. This clearly becomes the standard definition of upsampling when $R = 1$.

The generalized TC-OLA transmitter is formed by adding a filter element to each phase in Figure 3.10 to produce the structure of Figure 3.11. The filter coefficients for each phase are formed by taking every R^{th} coefficient for every $\phi = 0..R - 1$, as

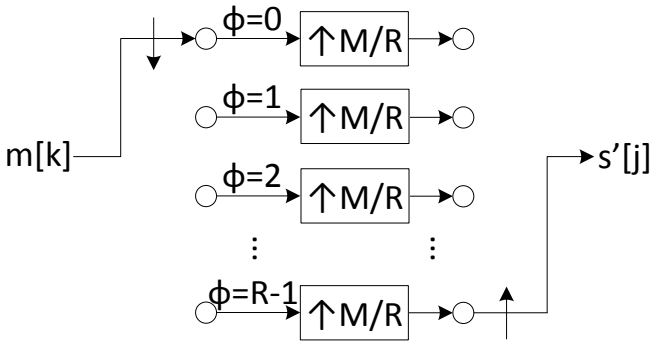

Figure 3.10: Flowgraph showing modified upsampling operation for $R > 1$. The input message signal is commutated across R phases, each of which is upsampled by M/R.

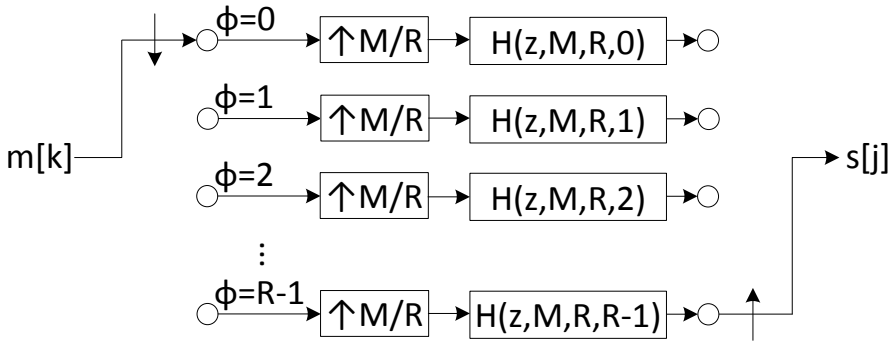

Figure 3.11: Transmitter structure for $R > 1$. The message signal $m[k]$ is distributed to R phases. Each phase is upsampled by M/R, while the filter for each phase is upsampled by $\frac{M}{R} - 1$. The result is then interleaved to produce the output $s[j]$.

with typical polyphase decomposition for FIR filters [40]. These coefficients are then interpolated by $\frac{M}{R} - 1$. The general equation for the filter of each phase is:

$$H(z, M, R, \phi) = \sum_{n=0}^{\frac{M}{R}-1} w_i|_{i=Rn+\phi} \, z^{-(\frac{M}{R}-1)(n+1)} \tag{3.23}$$

3.3.1 Transmitted Spectrum

The general case transmitter structure (Figure 3.11) can be analyzed using the $\mathcal{Z}$ transform properties of linearity, time shifting, downsampling and upsampling [41] to find an expression for the spectrum of the transmitted signal. Starting from the structure of Figure 3.10 we can replace the commutators with their equivalents to obtain:

$$S'(z) = \frac{1}{R} \sum_{\phi=0}^{R-1} \left[\sum_{p=0}^{R-1} e^{-j\frac{2\pi\phi p}{R}} M(z^{\frac{M}{R}} \cdot e^{-j\frac{2\pi p}{R}}) \right] z^{-\kappa} \tag{3.24}$$

where $\kappa = \frac{M}{R}\phi + R + \phi + 1$. Inserting the filter function $H(z, M, R, \phi)$ before the output commutator in Figure 3.11 we then have:

$$S(z) = S'(z)H(z^R, M, R, \phi) \tag{3.25}$$

For the simple case with $R = 1$, the ϕ parameter is set to zero:

$$S(z)|_{R=1} = M(z^M)H(z, M, 1, 0) \tag{3.26}$$

$$= M(z^M)H(z, M) \tag{3.27}$$

One way to interpret this result is that the spectrum of the message signal is interpolated M times while the spectrum of the window function is interpolated $M - 1$ times as per (3.22). In that sense, the transmitted spectrum is an $M - 1$ point approximation to the spectrum of the message signal. As M increases, this approximation improves. Figure 3.12 illustrates this concept. Figure 3.13 shows a TC-OLA system with $M = 96$, $R = 1$. Although the peaks of the transmitted signal are more closely spaced than in Figure 3.12 the peaks are also narrower.

At this point one may conclude that TC-OLA simply spreads the message signal into M evenly-spaced narrowband signals over a wider bandwidth. However, the $\mathcal{Z}$-domain model (3.25) indicates aliasing of the message signal within the transmitted spectrum when $R > 1$. The downsampling effect of the input commutator in Figure 3.11 causes the input spectrum to fold R times on each phase, resulting in an expected aliasing effect. The upsampler then duplicates this folded spectrum $\frac{M}{R}$ times. This results in as R-component spectrum for each phase as shown in Figure 3.14b for $M = 12$, $R = 2$. We observe here that each component has $\frac{M}{R}$ peaks which overlap slightly with the adjacent peak from another component to create M total peaks. Compare this with Figure 3.12 where the M peaks do not overlap and are thus quite narrow. As R increases so does the overlap between peaks, and this overlap has the effect of filling in the space in the transmitted spectrum. The ideal receive process cancels these aliases when the original signal is reconstructed.

In this section we have shown that input spectrum is expanded by a factor of $\frac{M}{R}$. Although the reproduction of the input spectrum is not exact, the approximation improves as $\frac{M}{R}$ increases. We have also shown that the value of R affects how the transmitted spectrum is constructed, independent of the ratio of $\frac{M}{R}$. This has implications for ongoing investigations on how frequency selective fading and narrowband interference affect TC-OLA systems.

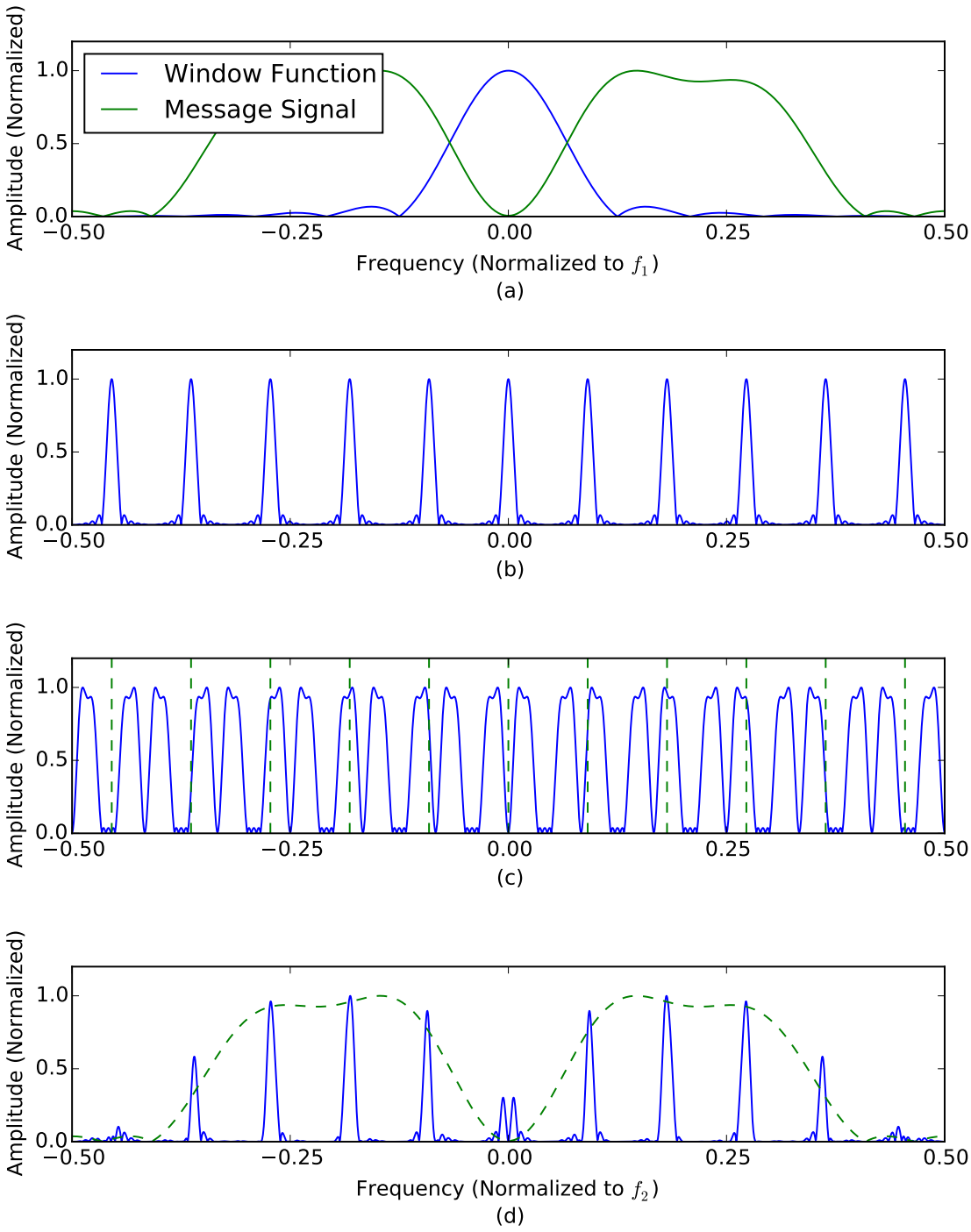

Figure 3.12: TC-OLA System with $M = 12$, $R = 1$. (a) Message signal and window function spectra. (b) Window function spectrum interpolated by $M - 1 = 11$. (c) Message signal spectrum interpolated by 12, showing center of interpolated window spectrum peaks for reference. (d) Transmitted spectrum, showing original message signal spectrum for reference.

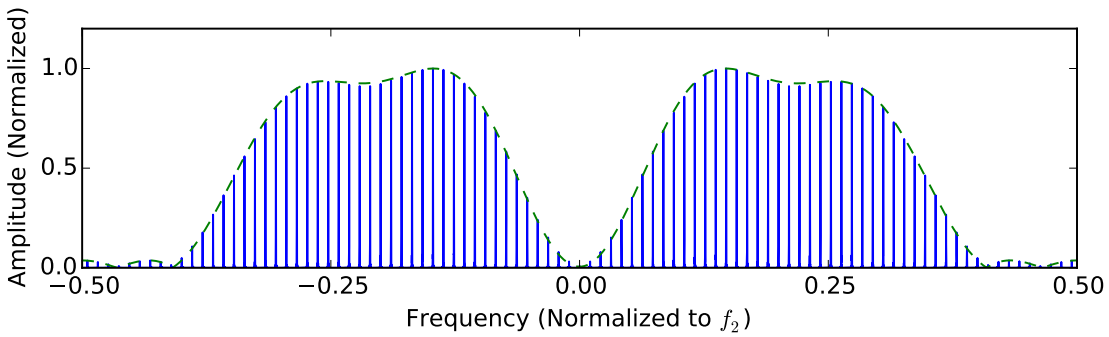

Figure 3.13: TC-OLA System with $M = 96$, $R = 1$. Transmitted spectrum, showing original message signal spectrum for reference.

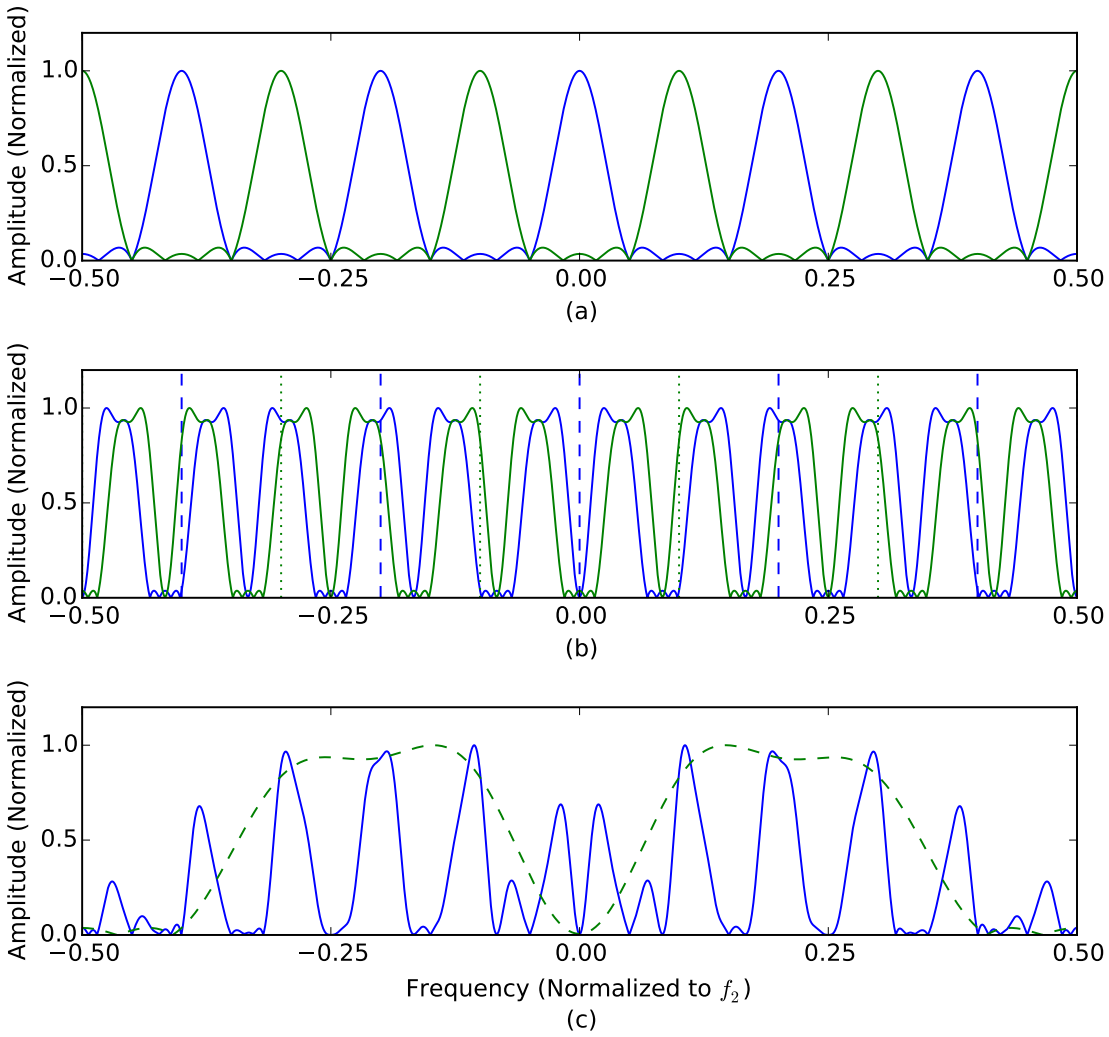

Figure 3.14: TC-OLA System with $M = 12$, $R = 2$. (a) Spectra of the 2 components of the window function. Each component is interpolated by $\frac{M}{R} - 1 = 5$ (b) Spectra of the 2 components of the input message signal, each interpolated by $\frac{M}{R}$. (c) Transmitted spectrum, showing original message signal spectrum for reference.

3.4 Conclusion and Future Work

In this chapter we have developed the mathematical background of a TC-OLA scheme that does not use a pilot signal for synchronization, although no method of timing recovery was presented. This new scheme was analyzed under ideal timing assumptions in AWGN and multipath Rayleigh fading channels. An equivalent multirate filter structure was presented in which the receiver can observe all synchronization offsets simultaneously. The transmitted spectrum was analyzed and shown to be an approximation of the message signal spectrum which improves as the spreading ratio increases.

Ongoing research on this communications mode includes the study of TC-OLA systems in more realistic multipath environments as well as impairments specific to TC-OLA such as commutator misalignment. A quadrature multiplexed variant with a method of phase, frequency and window timing recovery is in progress. We plan to make a full comparison of TC-OLA with multi-user DSSS systems, specifically CDMA systems.

Chapter 4

Time-Compression Overlap Add for Low Power Wide Area Networks

4.1 Introduction

Machine-to-machine (M2M) communications and internet of things (IoT) technologies form a significant portion of the 5G communications effort [14]. The IoT space covers a wide range of applications and technologies, from small personal area networks for connecting smart devices, to city-wide infrastructure monitoring networks. One solution for wide area coverage applications is to connect IoT devices to existing cellular infrastructure networks. These networks are not well matched to the needs of IoT devices in terms of data access patterns and mobility and not expected to scale up to supporting potentially thousands of devices per cell. As such, LPWAN technology has emerged as purpose-built alternative for wide area IoT access [42].

The LPWAN space can be partitioned into monitoring applications characterized by moderate latency and control applications characterized by low latency. Each of these categories may be partitioned again into mission critical or not depending on availability requirements. Here we focus on monitoring applications. Wideband wireless technologies in this space include Ingenu's patented RPMA technology operating in the 2.4 GHz industrial, scientific and medical (ISM) band [26], as well as the LoRa system based on chirp spread spectrum [42]. Narrowband systems including SIGFOX and Weightless are also considered to be LPWAN technologies. An industry perspec-

tive on the issues facing narrowband IoT (NB-IoT) can be found in [43], especially as it relates to the disadvantages of IoT over cellular infrastructure networks.

In this chapter we propose a code-division variant of TC-OLA [12,37,44] as an alternative physical layer scheme for LPWAN monitoring applications. This scheme has similar frequency spreading and robustness to narrowband interference as DS-CDMA with simple transmit and receive structures and orthogonal codes. It is possible to to perform time domain equalization (TDE) or FDE at the symbol rate in frequency selective channels as an alternative to rake receiver structures. The ability to equalize at the symbol rate makes it more feasible to use a software-defined equalizer, rather that a fixed number of rake fingers defined in hardware.

The remainder of this chapter is organized as follows. Section 4.2 presents the TC-OLA system model and the code division variant. Section 4.3 presents the equivalent channel model and analyzes the performance in static multipath, frequency flat fading, and some time-varying multipath cases that appeared experimentally in [12]. Section 4.4 presents a system design and experimental simulation results comparing with a system based on circular shifts of a Gold code as an approximation of an RPMA-like system. Section 4.5 presents our conclusions based on observations of the analysis and experimental results.

4.2 TC-OLA System Model

A baseband TC-OLA signal is generated for a message signal $m_u[k]$ sampled at the message rate f_m using (4.1) [44], where $w[k]$ is a window function of length M chosen such that $w^2[k]$ exhibits a constant overlap-add (COLA) property as in (4.2) when overlap added using hop size R. The change in indices from k to j indicates the change in sample rate from the message rate f_m to the channel rate f_c. The message signal may be a sampled analog (ie: voice) signal, modem signal, or digital symbols. In the latter case, pulse shaping occurs after the TC-OLA process.

$$s_u[j] = \sum_{i=-\infty}^{\infty} w[j - iM] m_u[j - i(M - R)] \tag{4.1}$$

$$\sum_{i=-\infty}^{\infty} w^2[k - iR] = \frac{M}{R} \mathrm{E}\left[w^2[k]\right] = C \tag{4.2}$$

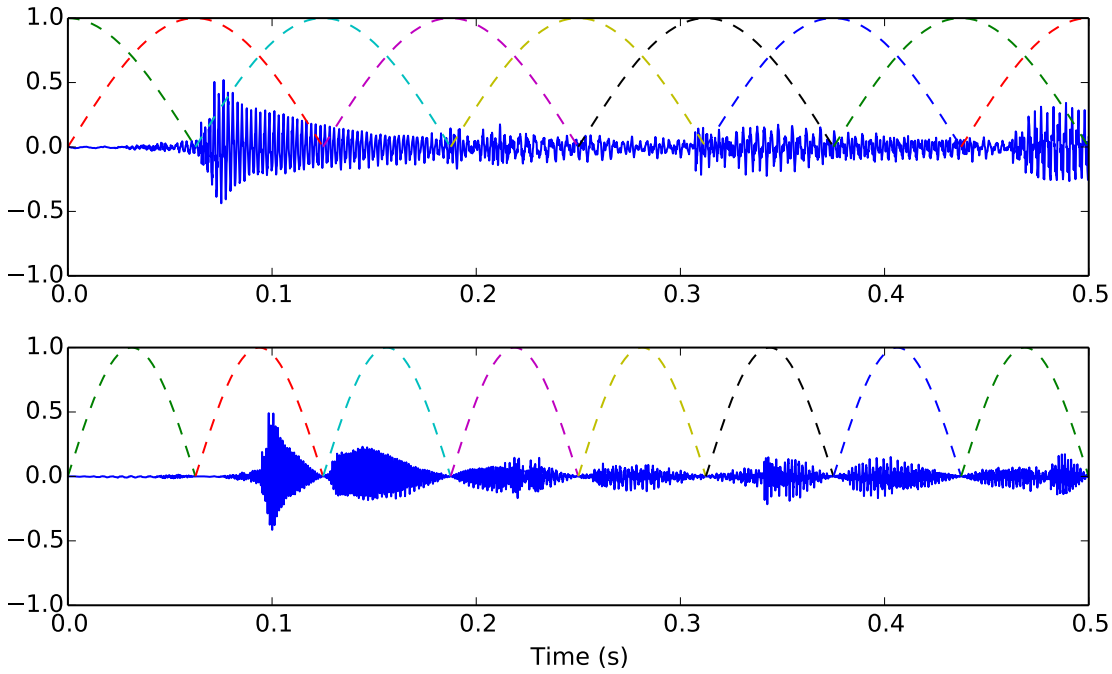

Figure 4.1: TC-OLA transmit operation. Message signal (top) sampled at message rate f_m, showing overlapping window functions for reference. Series of non-overlapping windows (bottom) to be transmitted through the radio channel at the channel rate $f_c = \frac{M}{R} f_m$ with window functions shown for reference. In this example $\frac{M}{R} = 2$ but typically $\frac{M}{R} >> 2$. Redundancy is added to the transmitted signal due to the overlap at the message rate.

A common window function is the *sine window* which we define in (4.3). Computation of $w^2[k]$ naturally results in a Hanning window, which is COLA for values of M and R that meet the constraint in (4.4) [10]. This type of window which tapers to zero at the edges is appropriate for sampled analog signals such as voice or modem. The TC-OLA transmit process is illustrated for sine windows in Figure 4.1.

$$w_{sine}[k] = \begin{cases} \sin\left(\frac{\pi(k+0.5)}{M}\right) & : 0 \leq k < M \\ 0 & : otherwise \end{cases} \tag{4.3}$$

$$R = \frac{M}{2K}, \;\; K = 1, 2, 3... \tag{4.4}$$

When the message signal is made up of digital symbols, as we shall do here, a rectangular window (4.5) is most appropriate, which is COLA for values of M and R

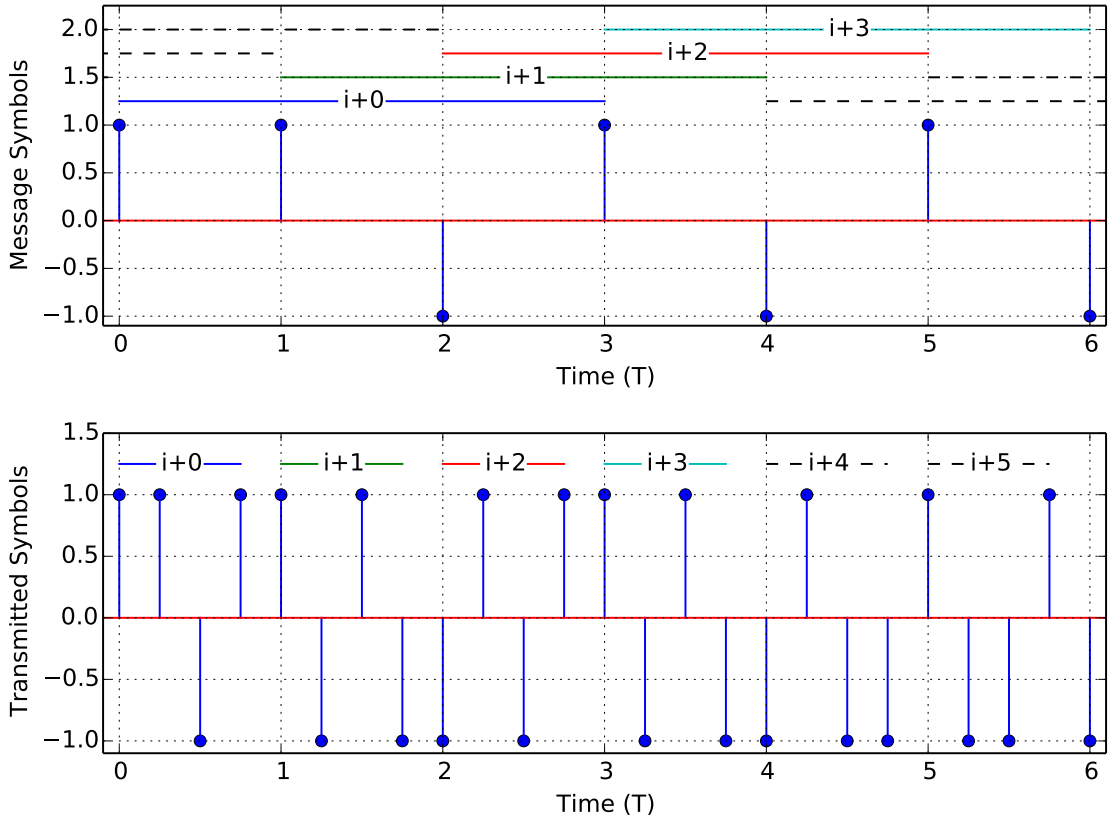

Figure 4.2: TC-OLA transmit operation using digital symbols. Message symbols (top) sampled at message rate f_m. Transmitted symbols (bottom) generated for $M = 4$, $R = 1$. The transmitted symbols are passed through a pulse shaping filter before transmitting through the channel. Rectangular window functions are shown for reference.

as in (4.6). In this case TC-OLA somewhat resembles the time-domain construction of IFDMA [45,46] although without the cyclic prefix (CP). In Chapter 5 we shall discuss how TC-OLA provides a distributed CP for robust block-based reception using the same signal construction. TC-OLA based on digital symbols is illustrated in Figure 4.2.

$$w_{rect}[k] = \begin{cases} 1 & : 0 \leq k < M \\ 0 & : otherwise \end{cases} \tag{4.5}$$

$$R = \frac{M}{K}, \;\; K = 1, 2, 3... \tag{4.6}$$

The transmitted signal is corrupted by the AWGN process $n[j]$ with variance σ_n^2.

The receiver performs the overlap-add process on the received signal using (4.7) to recover an estimate of the message signal $m_u[k]$ as in equation (4.8). Substituting (4.2) into (4.8) gives the estimate of the message signal as in (4.9), with the variance of the output AWGN process $\widehat{n}[k]$ computed as in (4.10).

$$\widehat{m}_u[k] = \sum_{i=-\infty}^{\infty} w[k - iR]\left(s_u[k] + n[k]\right) \tag{4.7}$$

$$\begin{aligned} &= m_u[k] \sum_{i=-\infty}^{\infty} w^2[k - iR] \\ &+ \sum_{i=-\infty}^{\infty} w[k - iR]n[k + i(M - R)] \end{aligned} \tag{4.8}$$

$$= Cm_u[k] + \widehat{n}[k] \tag{4.9}$$

$$\widehat{\sigma}_n^2 = \sum_{i=-\infty}^{\infty} w^2[k - iR]\sigma_n^2 = C\sigma_n^2 \tag{4.10}$$

4.2.1 Code Division

A code division TC-OLA scheme can be described mathematically as in (4.12) by modifying (4.1) to add the code symbol $a_{i,u}$. The code symbol is associated with the i^{th} transmitted segment of the message signal associated with the u^{th} user. In a sense, TC-OLA can be considered the dual of DSSS. Where a DSSS system modulates the data with a high speed code [38], TC-OLA modulates a code with high speed data.

$$s_u^{(c)}[j] = \sum_{i=-\infty}^{\infty} a_{i,u} w[j - iM] m_u[j - i(M - R)] \tag{4.11}$$

$$s^{(c)}[j] = \sum_{u=0}^{N-1} s_u^{(c)}[j] \tag{4.12}$$

The receiver for a specific user t can be described by modifying (4.8) as in (4.13), where in general $b_{i,t}$ is the code symbol associated with the i^{th} received segment of the message signal associated with the t^{th} user. In practice $b_{i,t} = a_{i,t}^*$ is used to recover the message signal for user t and this is the only case considered in this chapter as in (4.14).

$$\widehat{m}_t[k] = \sum_{i=-\infty}^{\infty} b_{i,t} w[k - iR] s^{(c)}[k + i(M - R)] \tag{4.13}$$

$$= \sum_{u=0}^{N-1} m_u[k] \sum_{i=-\infty}^{\infty} a_{i,u} a_{i,t}^* w^2[k - iR] \tag{4.14}$$

The code may be any general polyphase sequence. Ideally $a_{i,u}$ are chosen from a mutually orthogonal set such that

$$\sum_{i=-\infty}^{\infty} a_{i,u} a_{i,t}^* w^2[k - iR] = C\delta[u - t], \tag{4.15}$$

where one possibility is the set of codes from the Hadamard matrix $H(\cdot)$ and another is a set of linear phase rotations constructed such that an integer number of cycles are completed in $\frac{M}{R}$ windows. The advantage of using linear phase rotations is that it is not necessary to acquire the start of the code sequence, as any offset o in $a_{i,u} a_{i-o,u}^*$ only manifests as a phase shift at the output.

4.2.2 Equivalence with DS/CDMA

In the ideal case the matched filter detector for DS/CDMA represents a correlation of the code with a perfectly aligned copy of itself. In discrete time the correlation can be described as the summation of the product of the two codes. Consider a DS/CDMA system with N users receiving message signal $x_t[k]$ with spreading sequence $s_{i,t} \in \{+1, -1\}$ that has N_c chips. Neglecting any other system impairments, the estimate of the sample $x_t[k]$ is

$$\widehat{x}_t[k] = x_t[k] \sum_{i=1}^{N_c} s_{i,t}^2 + \sum_{\substack{u=1 \\ u \neq t}}^{N} \sum_{i=1}^{N_c} s_{i,t} s_{i,u} x_u[k] + \sum_{i=1}^{N_c} s_{i,t} n_{i,t} \tag{4.16}$$

$$= N_c x_t[k] + \sum_{\substack{u=1 \\ u \neq t}}^{N} \sum_{i=1}^{N_c} s_{i,t} s_{i,u} x_u[k] + \sum_{i=1}^{N_c} s_{i,t} n_{i,t} \tag{4.17}$$

which can be compared with the AWGN model of a TC-OLA system with N users

$$\begin{aligned}\widehat{m}_t[k] &= m_t[k] \sum_{i=-\infty}^{\infty} |a_{i,t}|^2 w^2[k-iR] \\ &\quad + \sum_{\substack{u=1 \\ u\neq t}}^{N} \sum_{i=-\infty}^{\infty} a_{i,u} a_{i,t}^* m_u[k] w^2[k-iR] \\ &\quad + \sum_{i=-\infty}^{\infty} a_{i,t}^* n_t[k+i(M-R)] w[k-iR] \end{aligned} \tag{4.18}$$

$$\begin{aligned}&= C m_t[k] \\ &\quad + \sum_{\substack{u=1 \\ u\neq t}}^{N} \sum_{i=-\infty}^{\infty} a_{i,u} a_{i,t}^* m_u[k] w^2[k-iR] \\ &\quad + \sum_{i=-\infty}^{\infty} a_{i,t}^* n_t[k+i(M-R)] w[k-iR] \end{aligned} \tag{4.19}$$

The equation may be rewritten for $w[k] = w_{rect}[k]$ to obtain the summation in terms of $\frac{M}{R}$ as

$$\widehat{m}_t[k] = C m_t[k] + \sum_{\substack{u=1 \\ u\neq t}}^{N} \sum_{i=0}^{\frac{M}{R}-1} a_{i,u} a_{i,t}^* m_u[k] + \widehat{n}[k] \tag{4.20}$$

and we note the similarity with (4.17).

As an example, a TC-OLA system using rectangular windows with $M = 4$, $R = 1$, input sequence x_n, and a code sequence $\{a_0, a_1, a_2, a_3\}$ is shown in Figure 4.3. Using a regular pattern of sample rearrangement, this can be shown to be equivalent to a CDMA system where the code sequence is circularly shifted by one chip every R symbols. By resolving this shift it is easy to show that we obtain a standard DS/CDMA sequence.

Where the processing gain in DS/CDMA is proportional to the number of chips in the spreading sequence, the TC-OLA processing gain is proportional to $\frac{M}{R}$ and is independent of the window shape, assuming the COLA property is satisfied.

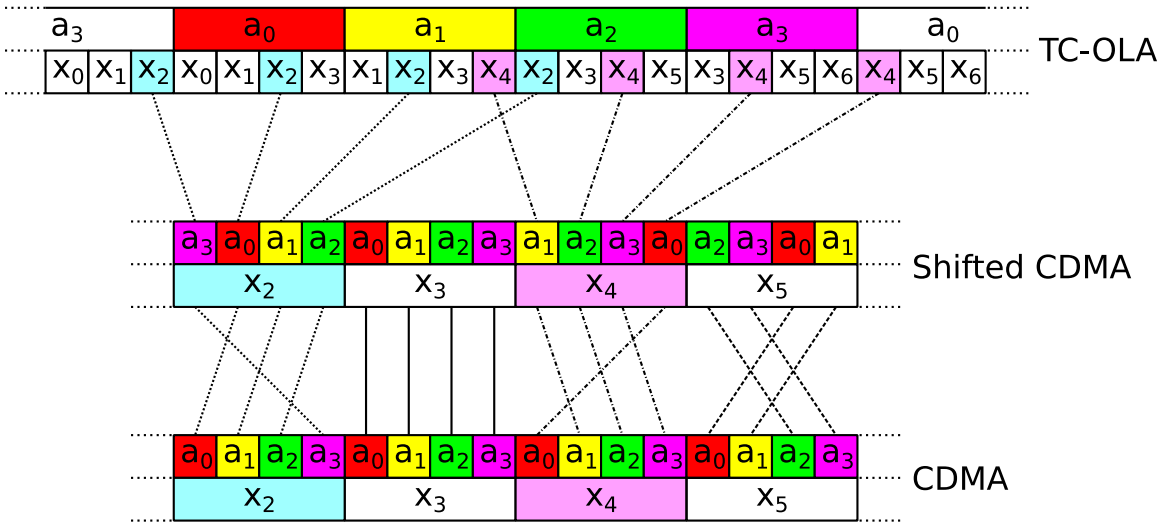

Figure 4.3: TC-OLA–DS/CDMA equivalence. In this figure x_i represents the data symbols and a_i represents the code symbols. By applying a regular pattern of sample rearrangement to the TC-OLA signal we obtain a version of CDMA where the code is circularly shifted by one chip every R data symbols (here $R = 1$). By resolving the shift we obtain a standard DS/CDMA sequence.

$$SNR_{out} = \frac{C^2 \, \mathrm{E}\left[m^2[k]\right]}{\widehat{\sigma}_n^2} \tag{4.21}$$

$$= \frac{C \, \mathrm{E}\left[m^2[k]\right]}{\sigma_n^2} \tag{4.22}$$

$$SNR_{in} = \frac{\mathrm{E}\left[w^2[k]\right] \mathrm{E}\left[m^2[k]\right]}{\sigma_n^2} \tag{4.23}$$

$$G = \frac{SNR_{out}}{SNR_{in}} = \frac{C}{\mathrm{E}\left[w^2[k]\right]} = \frac{M}{R} \tag{4.24}$$

$$= 10 \, \log_{10}\left(\frac{M}{R}\right) \, dB \tag{4.25}$$

Here we have shown that TC-OLA and DS/CDMA waveforms are essentially the same in the ideal case and have the same processing gain in AWGN channels. The differences in performance are in the details of behaviour in fading, multipath, and timing recovery.

4.3 Multiuser Performance Analysis

This section begins with the description of the generic baseband equivalent multipath fading model. To simplify the analysis in multipath we develop a matrix notation for the model in 4.3.2. The model is constrained for static multipath in 4.3.3 to highlight the frequency compression aspect of TC-OLA, the property that allows the channel to be equalized at the symbol rate rather than the chip rate. The model is then constrained to consider Rician flat fading in 4.3.4. In this configuration the interference limit in fading is derived. The near/far problem as it manifests in TC-OLA is also considered. Finally, a frequency-selective time-varying scenario that was considered experimentally in [12] is considered in analytically in 4.3.5 to highlight the channel averaging aspect of TC-OLA. In the next section we consider practical channel models that are relevant to the LPWAN application area.

4.3.1 Generic Multipath Model

To study the system performance and behaviour in a variety of scenarios we assume a generic discrete-time multipath channel with $P[i]$ *resolvable* multipath components, each with independent time-varying complex gain $g_{n,u}[i]$ with excess phase $\angle g_{n,u}[i] = \phi_{n,u}[i]$, and excess path delay $\tau_{n,u}[i]$. The excess phase and delay are referred to the 0^{th} multipath component of the received signal from user t such that the equivalent channel model for user t is written as in (4.26). More details can be found in Appendix B.

$$c_{t,u}[j,i] = \sum_{n=0}^{P_u[i]} g_{n,u}[i]\delta[j - \tau_{n,u}[i]] \tag{4.26}$$

In the uplink scenario, where each user arrives at the base station through an independent channel, the received signal for user t can be generally described as

$$r_t[j] = \sum_{u=0}^{N-1} c_{t,u}[j,i] * s_u[j] + n[j]. \tag{4.27}$$

4.3.2 Matrix Notation

The analysis of TC-OLA in multipath channels was patterned after the DS/CDMA analysis in [47] where the equations are developed as the sum of three terms (desired signal, interference, and noise), similar to a continuous-time version of (4.16)-(4.17). To simplify the analysis we develop a matrix notation for the receiver for the simple case where $R = 1$. In this case we produce 1 new sample of $\widehat{m}_t[k]$ per received window, and as such $i = k$. In general R samples of $\widehat{m}_t[k]$ are produced per received window and therefore $i \neq k$.

Let the M-element column vector $\mathbf{m}_{i,u}$ representing the i^{th} segment of the message signal $m_u[k]$ be written

$$\mathbf{m}_{i,u} = \begin{bmatrix} m_u[i] & \dots & m_u[i+M-1] \end{bmatrix}^T. \tag{4.28}$$

Let the $M \times M$ matrix $\mathbf{W}$ representing the window function $w[k]$ be written

$$\mathbf{W} = \begin{bmatrix} \mathbf{w} & \dots & \mathbf{w} \end{bmatrix}, \tag{4.29}$$

where $\mathbf{w}$ is the M-element column vector representing the window function.

Let the $M \times M$ diagonal matrix $\mathbf{A}_{i,u}$ represent the set of code symbols for user u be written

$$\mathbf{A}_{i,u} = diag\left(\begin{bmatrix} a_{i,u} & \dots & a_{i-M+1,u} \end{bmatrix}\right). \tag{4.30}$$

Let the $M \times M$ matrix $\mathbf{S}_{i,u}$ representing the M most recently transmitted windowed segments be written

$$\mathbf{S}_{i,u} = (\begin{bmatrix} \mathbf{m}_{i,u} & \dots & \mathbf{m}_{i-M+1,u} \end{bmatrix} \circ \mathbf{W})\mathbf{A}_{i,u}, \tag{4.31}$$

where $\circ$ is the Hadamard (point-wise) product.

Let the $M \times M$ diagonal matrix $\mathbf{G}_{i,u}^{(n)}$ represent the set of channel block gains for path n of user u be written

$$\mathbf{G}_{i,u}^{(n)} = diag\left(\begin{bmatrix} g_{n,u}[i] & \dots & g_{n,u}[i-M+1] \end{bmatrix}\right). \tag{4.32}$$

The effect of the overlap-add process on delayed paths is illustrated in Figure 4.4 as a sample offset between the transmitted and received window functions. We equate this with the matrix permutation operation illustrated in Figure 4.5 which is valid for $|\tau| < M$ samples. To assist with the analysis of multipath components we define this matrix permutation operation on an arbitrary matrix $\mathbf{S}$ as

$$\mathbf{P}^{\tau}(\mathbf{S}) = mat(\mathbf{C}^{\tau} vec(\mathbf{SD}))\mathbf{D} \tag{4.33}$$

where $\mathbf{D}$ is the exchange or backward identity matrix, $vec(\cdot)$ creates a column vector from the columns, $\mathbf{C}$ is the cyclic permutation matrix, and τ is the delay in samples. For $\tau = 0$, $\mathbf{P}^0(\mathbf{S}) = \mathbf{S}$. Another example of a matrix permutation operator used in communications analysis can be found in [48].

The structure of the TC-OLA signal aligns the samples to be added along the diagonal of $\mathbf{S}_{i,u}$, from which we can receive the estimate of the message signal $\widehat{m}_t[k]$ as

$$\begin{aligned} \widehat{m}_t[i] = &\sum_{u=0}^{N-1} \sum_{n=0}^{P_u[i]-1} tr\left(\mathbf{P}^{\tau_{n,u}[i]}\left(\mathbf{S}_{i,u}\right)\mathbf{G}_{i,u}^{(n)}\mathbf{A}_{i,t}^{*} \circ \mathbf{W}\right) \\ &+ \widehat{n}[i] \end{aligned} \tag{4.34}$$

by summing over the user index u, the path index n, and applying the code matrix

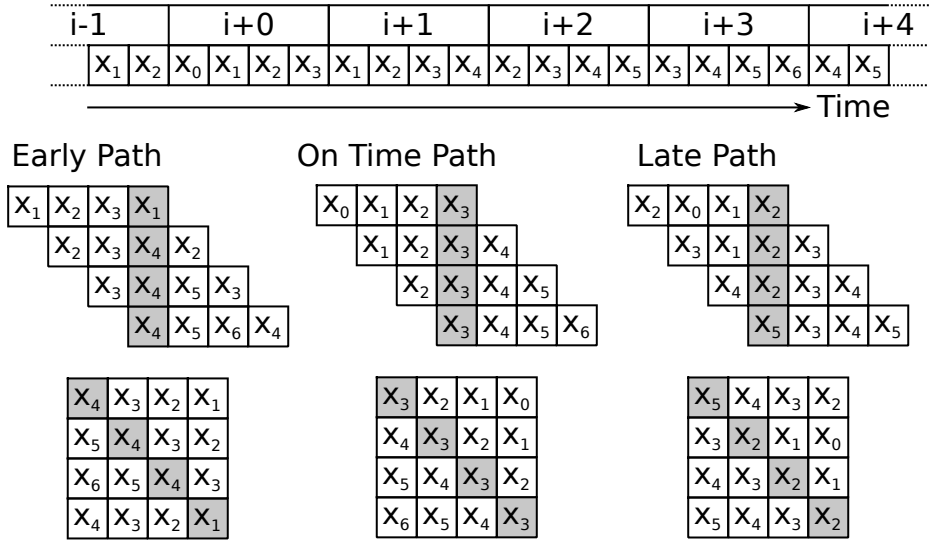

Figure 4.4: Illustrating the effect of delayed paths on the output signal by showing the overlap-add process. Results are shown for early ($\tau = -1$), on time ($\tau = 0$), and late ($\tau = 1$) arrivals. Overlap-add interpretation with summation over columns as presented in [12] is shown. The lower row shows formation of the matrix $\mathbf{S}$. Inspecting the trace of the matrix on the bottom right shows how the output is made up three late and one early sample. The proportions depend on τ but there are only ever two components.

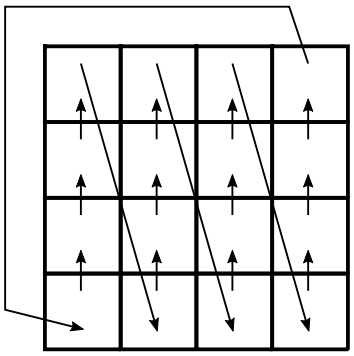

Figure 4.5: Matrix permutation operation $\mathbf{P}^{-1}(\cdot)$ described by (4.33). Note that the resulting matrix is not exactly the same as those shown in Figure 4.4, with some differing off-diagonal elements. However, the trace remains the same for $|\tau| < M$.

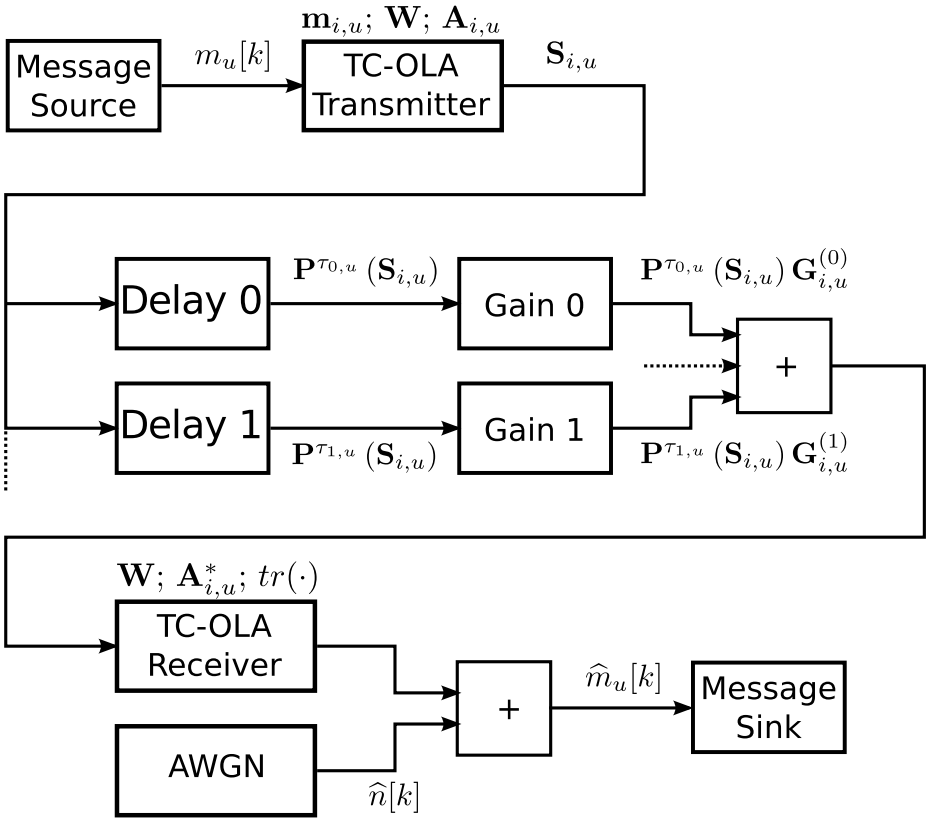

Figure 4.6: Labelled block diagram of the system model described in (4.34).

$\mathbf{A}_{i,t}$ for user t to all signals. The placement of $\mathbf{W}$ and $\mathbf{A}_{i,t}^{*}$ outside the permutation operator imply that they are aligned with the 0^{th} multipath component from user t and not necessarily aligned with the window boundaries of the delayed copy. As we have assumed block fading, it seems no less realistic to place $\mathbf{G}_{i,u}^{(n)}$ outside the permutation operator for convenience. In this work we assume rectangular windows and as such $\mathbf{W} = \mathbf{1}_{\mathbf{M}\times\mathbf{M}}$ is omitted from further analysis.

Equation (4.34) completely describes the received message signal in relation to the generic received uplink signal model in (4.27) for multipath delays of $|\tau| < M$ samples with $R = 1$. This general equation is constrained in the following sections for scenarios such as static multipath, frequency-flat fading, and frequency-selective fading. By adding these constraints different simplifying assumptions can be made in the analysis. A labelled system block diagram showing the signal flow through the system model is given in Figure 4.6.

4.3.3 In Static Frequency Selective Channels

The typical low mobility of nodes in an LPWAN application leads to channel models characterized by very low Doppler spread [19]. As such we are motivated to investigate the performance of TC-OLA in static multipath as a rough approximation to this scenario over a short observation period.

In a static multipath model we assume that P_u, $g_{n,u}$, and $\tau_{n,u}$ in (4.34) no longer depend on i. With some simplification we obtain

$$\begin{aligned}\widehat{m}_t[i] = & M g_{0,t} m_t[i] \\ & + \sum_{n=1}^{P_t-1} g_{n,t} tr\left(\mathbf{P}^{\tau_{n,t}}\left(\mathbf{S}_{i,t}\right)\mathbf{A}_{i,t}^{*}\right) \\ & + \sum_{\substack{u=0 \\ u\neq t}}^{N-1}\sum_{n=0}^{P_u-1} g_{n,u} tr\left(\mathbf{P}^{\tau_{n,u}}\left(\mathbf{S}_{i,u}\right)\mathbf{A}_{i,t}^{*}\right) \\ & + \widehat{n}[i]\end{aligned} \tag{4.35}$$

where the received signal is described by four terms. These are the desired signal, delayed components of the desired signal, delayed components of all other users, and noise. In a downlink scenario where $\tau_{0,u} = 0$ we can also expect

$$tr\left(\mathbf{P}^{\tau_{0,u}}\left(\mathbf{S}_{i,u}\right)\mathbf{A}_{i,t}^{*}\right) = tr\left(\mathbf{S}_{i,u}\mathbf{A}_{i,t}^{*}\right) = 0 \tag{4.36}$$

which further simplifies the third term.

By inspection of the permutation operation $\mathbf{P}^{\tau}(\cdot)$ and the matrix form of $\mathbf{S}$ illustrated in Figure 4.4 we conclude that

$$\begin{aligned}tr\left(\mathbf{P}^{\tau_{n,t}}\left(\mathbf{S}_{i,t}\right)\mathbf{A}_{i,t}^{*}\right) = M\,[&\alpha_{n,t} m_t[i-\tau_{n,t}] \\ &+ \beta_{n,t} m_t[i+M-\tau_{n,t}-1]]\end{aligned} \tag{4.37}$$

where

$$\alpha_{n,t} = \frac{M-|\tau_{n,t}|}{M}, \beta_{n,t} = \frac{|\tau_{n,t}|}{M}. \tag{4.38}$$

This form is indicative of an equivalent channel model seen by the message signal at the receiver output consisting of a regular delayed path and an early "pre-echo" path. From the first two terms of (4.35) with (4.37) and replacing $m_t[k]$ with $\delta[k]$ we

infer the equivalent channel $\widehat{c}_t[k]$ as

$$\begin{aligned}\widehat{c}_t[k] = M[g_{0,t}\delta[k] + \sum_{n=1}^{P-1} g_{n,t}\left(\alpha_{n,t}\delta[k-\tau_{n,t}]\right. \\ \left. + \beta_{n,t}\delta\left[k+M-1-\tau_{n,t}\right]\right)].\end{aligned} \tag{4.39}$$

If the window size is much larger than all significant delayed paths ($M >> \tau_{n,t}\forall n$) then we may neglect $\beta_{n,t}$ and write

$$\widehat{c}_t[k] \approx M\left[g_{0,t}\delta[k] + \sum_{n=1}^{P-1} g_{n,t}\alpha_{n,t}\delta[k-\tau_{n,t}]\right]. \tag{4.40}$$

The estimate of the message signal is then

$$\widehat{m}_t[k] = m_t[k] * \widehat{c}_t[k] + \widehat{n}[k] + \widehat{i}_{t,t}[k] + \sum_{\substack{u=0 \\ u\neq t}} \widehat{i}_{t,u}[k] \tag{4.41}$$

where the added interference term $\widehat{i}_{t,t}[k]$ represents the effect of the approximation $\beta_{n,t} \approx 0$ and $\widehat{i}_{t,u}[k]$ represents the interference from user u. This interference can also be expected to be small when $M >> \tau_{n,u}$.

This section illustrates the frequency compression aspect of TC-OLA which allows the message signal to be equalized at the message rate f_m. Inspection of (4.40) shows that the channel $\widehat{c}_t[k]$ seen by the message signal approaches $c_{t,t}[j]$ from (4.26) as $\frac{\tau}{M}$ approaches zero, although it is referenced to a lower sampling rate resulting in frequency compression of the channel. This was observed experimentally in [12] and represents the main intent of the invention in [8]. Assuming the interference terms are negligible the performance of TC-OLA in static multipath will be limited by the performance of the equalizer for $\widehat{c}_t[k]$.

4.3.4 In Frequency Flat Fading

Several models relevant to fixed wireless monitoring applications have a strong Rician (or Rayleigh) main path followed by additional delayed paths [19]. When the delayed paths are strongly attenuated the channel is only weakly frequency selective and the behaviour of the main path dominates the performance at low SNR. As such we are motivated to study the performance of TC-OLA in the frequency-flat fading regime.

We constrain (4.34) with $P = 1$ such that each channel consists of a single path $n = 0$. A block fading model for this path is given as $g_{0,u}[i] = X + jY$, where $X \sim \mathcal{N}\left(\mu_x, \sigma_g^2\right)$ and $Y \sim \mathcal{N}\left(\mu_y, \sigma_g^2\right)$. The envelope $|g_{0,u}[i]|$ is Rician distributed when $\sqrt{\mu_x^2 + \mu_y^2} > 0$ and Rayleigh distributed when $\mu_x = \mu_y = 0$.

With no delayed multipath components the model in (4.34) simplifies to

$$\widehat{m}_t[i] = \sum_{u=0}^{N-1} tr\left(\mathbf{S}_{i,u}\mathbf{G}_{i,u}\mathbf{A}_{i,t}^*\right) + \widehat{n}[i]. \tag{4.42}$$

Lacking any other information, it is fair to assume that the base station transmits all messages with equal power P_m

$$\mathrm{E}\left[m_u^2[k]\right] = P_m \forall u \in \{1..N\}. \tag{4.43}$$

The signal power for user t is then

$$P_{sig} = \mathrm{E}[tr\left(\mathbf{S}_{i,t}\mathbf{G}_{i,t}\right)^2] = \left(\frac{M}{R}\right)^2 \mu_r^2 P_m \tag{4.44}$$

given that $a_{i,t}a_{i,t}^* = 1$ and applying a Gaussian approximation for the mean of the summation of a large number of Rician variables [49].

Downlink Performance

In the downlink direction (from the base station to a particular users) all received signals $s_u[j]$ experience the same channel. The received signal model in (4.34) can be constrained for this case by setting

$$c_{t,u}[j,i] = c_{t,t}[j,i] \forall u \in \{0..N-1\}. \tag{4.45}$$

By simplifying for the above constraint we obtain

$$\widehat{m}_t[i] = \sum_{u=0}^{N-1} tr\left(\mathbf{S}_{i,u}\mathbf{G}_{i,t}\mathbf{A}_{i,t}^*\right) + \widehat{n}[i]. \tag{4.46}$$

An expression for the interference power is obtained by summing over all remaining users

$$P_{int} = \sum_{\substack{u=1 \\ u \neq t}}^{N-1} \mathrm{E}\left[tr\left(\mathbf{S}_{i,u} \mathbf{G}_{i,t} \mathbf{A}_{i,t}^{*} \right)^2 \right] \tag{4.47}$$

$$= \frac{M}{R} (N-1) \sigma_r^2 P_m. \tag{4.48}$$

Combining (4.10), (4.44) and (4.48) we derive an expression for the average downlink signal-to-interference-and-noise ratio (SINR) $\bar{\gamma}$ as

$$\bar{\gamma} = \frac{\left(\frac{M}{R}\right)^2 \mu_r^2 P_m}{\frac{M}{R}\sigma_n^2 + \frac{M}{R}(N-1)\sigma_r^2 P_m} \tag{4.49}$$

$$= \frac{\frac{M}{R}\mu_r^2 P_m}{\sigma_n^2 + (N-1)\sigma_r^2 P_m}. \tag{4.50}$$

Uplink Performance

In the uplink direction from user u to the base station, the base station receiver experiences a different channel for each user. From the interference term (4.48) for the downlink we can imagine how the near/far problem manifests in the TC-OLA uplink. The interference term will dominate at the receiver if $\mathrm{E}\left[m_u^2[k]\right]|_{u \neq t} >> \mathrm{E}\left[m_t^2[k]\right]$ *and* orthogonality between users is lost due to fading. To limit this issue we assume that the *average* channel power gain is known to the mobile station and that a power control scheme can be implemented such that signals arrive at the base station receiver with equal average power P_m. We choose not to investigate the near/far problem further is this work.

Using a simplistic model where the phase recovery of user t does not affect the Rician distribution of user u, an expression for the interference power in the uplink can be written

$$P_{int} = \frac{M}{R} (N-1) \sigma_g^2 P_m. \tag{4.51}$$

This model holds when $R \approx 0$ or $R >> \sigma_g^2$. The intermediate case may be addressed in simulation or later analysis.

Combining (4.10), (4.44) and (4.51) gives an expression for the average SINR $\bar{\gamma}$

in the uplink

$$\bar{\gamma} = \frac{\frac{M}{R}\mu_r^2 P_m}{\sigma_n^2 + (N-1)\,\sigma_g^2 P_m}. \tag{4.52}$$

In comparison with the downlink equation in (4.50), we note that the interference term in the uplink is different in that it contains the complex Gaussian channel variance rather than the Rician channel variance resulting from the channel envelope. This is the cause of the lower expected performance in the uplink direction in TC-OLA.

Interference Limit

To gain some insight about the limitations of the system, we set the channel noise power $\sigma_n^2 = 0$ in (4.50) and examine the signal to interference ratio (SIR). Assuming that the system accommodates the maximum number of orthogonal users $N = \frac{M}{R}$

$$\bar{\gamma} = \frac{\frac{M}{R}\mu_r^2}{\left(\frac{M}{R} - 1\right)\sigma_r^2} \approx \frac{\mu_r^2}{\sigma_r^2} \tag{4.53}$$

where (4.53) relies on the approximation $\frac{M}{R} - 1 \approx \frac{M}{R}$. In Rician fading with factor K we obtain

$$\bar{\gamma} \approx \frac{\pi L_{1/2}^2(-K)}{4 + K - \pi L_{1/2}^2(-K)}, \tag{4.54}$$

where

$$L_{1/2}(x) = e^{x/2}\left[(1-x)\,I_0\left(\frac{-x}{2}\right) - xI_1\left(\frac{-x}{2}\right)\right], \tag{4.55}$$

and $I_n(x)$ is the modified Bessel function of the first kind of order n [50]. Similarly for the uplink we obtain

$$\bar{\gamma} \approx \frac{\pi}{2} L_{1/2}^2(-K). \tag{4.56}$$

This result shows that the system performance is interference-limited at high SNR in fading. The interference limit creates a BER floor that limits the performance of any digital message signal [47]. In the limiting case of independent Rayleigh block fading ($K = 0$) with rectangular windows we can asymptotically approach an average

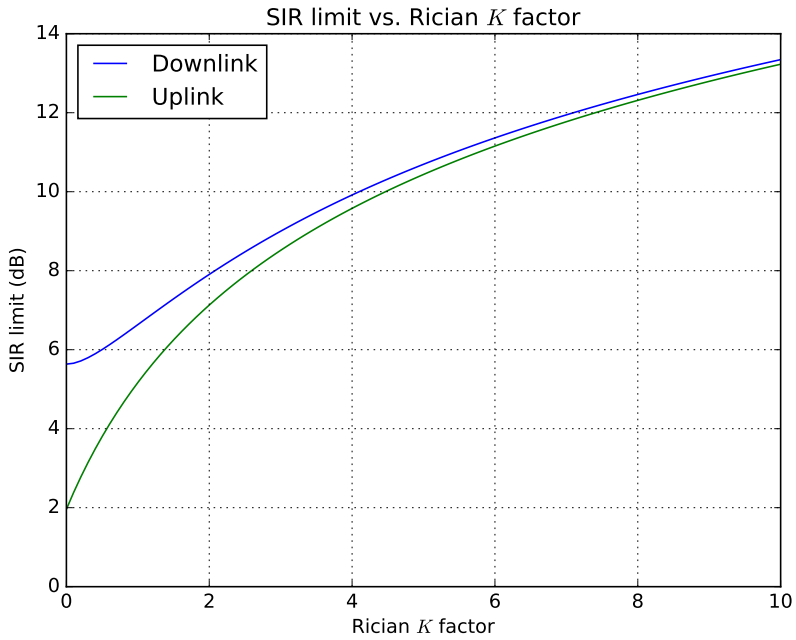

Figure 4.7: Interference limit vs. Rician K factor for a maximum number of users in the uplink and downlink with rectangular windows.

SIR of

$$\bar{\gamma}|_{K=0} \approx \frac{\pi}{(4-\pi)} \approx 5.63\,dB \tag{4.57}$$

in the downlink and

$$\bar{\gamma}|_{K=0} \approx \frac{\pi}{2} \approx 1.96\,dB \tag{4.58}$$

in the uplink. Equations (4.54) and (4.56) are plotted in Figure 4.7 showing the SIR limit against the Rician K factor.

The uplink interference limit for uncorrelated Rayleigh fading is significantly lower than the downlink without any channel state information (CSI). However, uncorrelated fading represents a worst case scenario where the orthogonal code properties have no effect and we can only rely on the central tendency of a Gaussian random variable to separate the users. To gain any advantage from the orthogonal coding there must be some correlation between fading values and/or between channels.

Correlated Fading

To make the independent block fading assumption more realistic we consider correlated Rayleigh block fading, with autocorrelation as described by Jakes [39]. The Doppler frequency f_d is normalized to the window period $T_w = \frac{M}{f_c}$. The fading autocorrelation function can then be written

$$R(n) = J_0(2\pi f_d T_w n) \tag{4.59}$$

with $n \in \{..., -1, 0, 1, 2, ...\}$ where $J_0(\cdot)$ is the zeroth-order Bessel function of the first kind.

For the system described above we expect the SIR to increase as the fading becomes more correlated. We can extend (4.48) to incorporate the autocorrelation function (4.59) as

$$P_{int} = P_m \sigma_r^2 \sum_{u=1, u\neq t}^{N} \left(\sum_{j=-\frac{M}{2R}}^{\frac{M}{2R}} \sum_{l=-\frac{M}{2R}}^{\frac{M}{2R}} a_{i+l,u} a_{i+j,t}^* R(|l-j|) \right)^2 \tag{4.60}$$

for the downlink and by replacing σ_r with σ_g for the uplink. This function is plotted against normalized Doppler frequency for the downlink in Figure 4.8. The same figure can be produced for the uplink by shifting the results down to the interference limit in (4.58). The SIR follows a -20 dB/decade slope and we estimate the intercept with the interference limit as $f_D T_w \approx \frac{R}{2M}$ in both the uplink and the downlink.

Correlated Channels

Correlation between the different channels experienced by the base station receiver in the uplink, regardless of the fading autocorrelation function, also raises the SIR limit. For uncorrelated Rayleigh fading the SIR rises from the 1.96 dB figure toward the 5.63 dB figure derived for the downlink as the correlation approaches 1.0.

Supported Number of Users

Rearranging (4.50) gives an expression for the number of users that can be supported for a given average SINR. This assumes that the Doppler frequency is not low enough

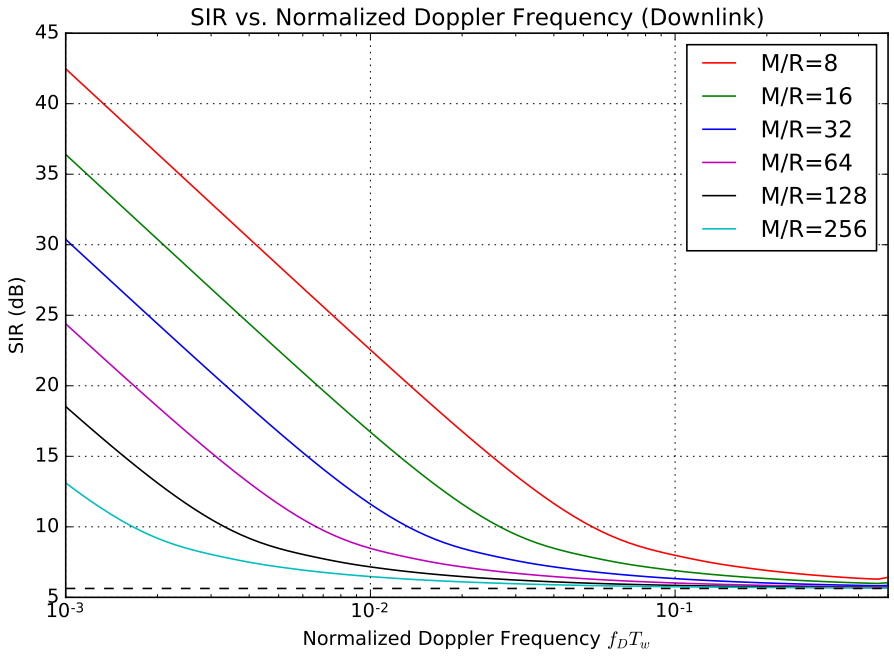

Figure 4.8: Signal to interference ratio (SIR) for correlated Rayleigh fading in the downlink with linear phase codes. The uplink curve is simply shifted from the 5.63 dB interference limit in (4.54) down to the 1.96 dB interference limit in (4.58).

to move away from interference limit, that is to say $f_D T_w > \frac{R}{2M}$. Thus it is more relevant to higher spreading factors as the intercept frequency gets lower as M/R increases as in Figure 4.8. In the downlink we obtain

$$N(\bar{\gamma}) = \frac{M}{R}\frac{\mu_r^2}{\bar{\gamma}\sigma_r^2} - \frac{\sigma_n^2}{\sigma_r^2 P_m} + 1 \tag{4.61}$$

and similarly rearranging (4.52) for the uplink we obtain

$$N(\bar{\gamma}) = \frac{M}{R}\frac{\mu_r^2}{\bar{\gamma}\sigma_g^2} - \frac{\sigma_n^2}{\sigma_g^2 P_m} + 1. \tag{4.62}$$

Assuming the uplink is interference-limited we obtain

$$N(\bar{\gamma}) = \frac{M}{R}\frac{\mu_r^2}{\bar{\gamma}\sigma_g^2} + 1. \tag{4.63}$$

Pole Capacity

Similar to DS/CDMA, TC-OLA systems have the concept of pole capacity, caused by each user's need to maintain a target SINR in the uplink [51]. To obtain an expression for pole capacity we rearrange (4.52) in terms of averaged received power P_m

$$P_m = \frac{\bar{\gamma}\sigma_n^2}{\frac{M}{R}\mu_r^2 - \bar{\gamma}(N-1)\sigma_g^2} \tag{4.64}$$

and note that the denominator of this expression goes to zero when the number of users reaches the value in (4.63). At this point, the power required to close the link at the desired SINR is infinite. However, we note that unlike DS/CDMA, the pole capacity is expected to vary with fading conditions. In DS/CDMA the pole capacity arises from the cross-correlation properties of the chosen spreading sequences and is typically a fixed system parameter.

The pole capacity results here could be developed for specific frame formats and codes in order to find the link SNR that maximizes packet throughput. We have not made this comparison and choose to focus on the raw BER results at this point. A discussion considering a TC-OLA system with specific frame formats and codes is given in Appendix E.

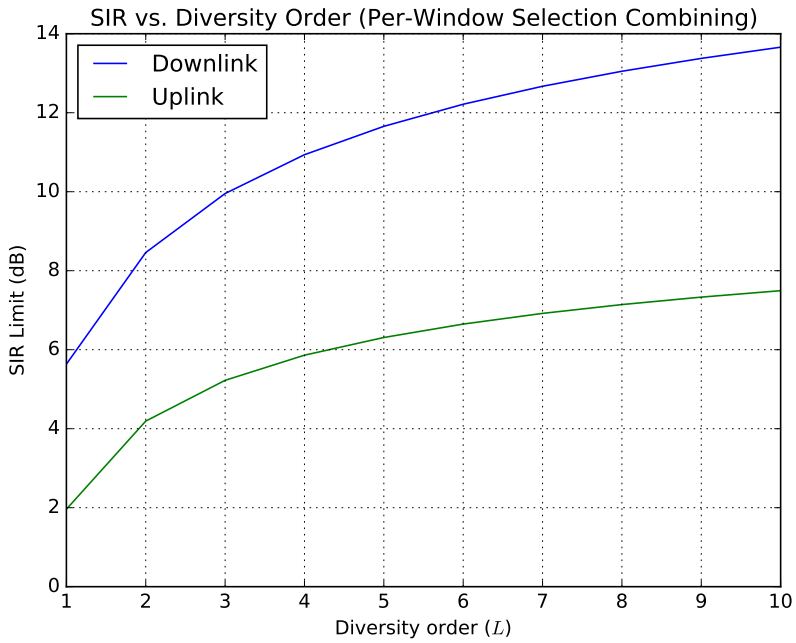

Figure 4.9: Use of selection combining to raise the SIR limit in independent Rayleigh fading (Rectangular Windows).

Selection Combining

Another way to raise the interference limit in flat fading is through receiver diversity. By applying the basic order statistics results [52] it is possible to get a result for per-window selection combining of L paths. The results are plotted in Figure 4.9 for orders up to $L = 10$ for rectangular windows in independent Rayleigh fading.

As with the previous analysis, the downlink benefits the most as it sees both an increase in the mean and a decrease in the variance. The uplink sees only the increase in the mean, but this is significant and even low orders can greatly improve the performance. From Figure 4.9 we observe that increasing the selection combining diversity to $L = 4$ in the uplink gives a similar performance as the downlink without diversity. More advanced diversity schemes such as maximal ratio combining (MRC) are expected to give even better performance gains.

4.3.5 In Time-Varying Frequency Selective Channels

We wish to evaluate TC-OLA performance in frequency selective fading channels such as the SUI channel models [19]. To gain some insight into how a range of

channel parameters affects performance, we look at how TC-OLA is affected by an equal-power two-ray model with the rotation period of the delayed path either much slower, similar to, or much faster than the TC-OLA averaging period ($\approx \frac{M^2}{R}$ samples at f_c). We considered this model experimentally in [12] and here we revisit these cases analytically.

To start, we constrain (4.34) with $g_{0,t} = 1$, $g_{1,t}[i] = e^{\imath\Omega i}$ and $\tau_1 = 1$ to obtain

$$\begin{aligned}\widehat{m}_t[i] = &\frac{M}{R} g_{0,t} m_t[i] \\ &+ tr\left(\mathbf{P}^1\left(\mathbf{S}_{i,t}\right)\mathbf{G}_{i,t}^{(1)}\mathbf{A}_{i,t}^{*}\right) \\ &+ \widehat{n}[i]\end{aligned} \tag{4.65}$$

For large M we can make the approximation $\beta_{1,t}[i] = 0$ as in (4.40) and estimate the equivalent tap coefficient $\alpha_{1,t}[i]$ as the sum of the gain $g_{1,t}[i]$ over the range of windows which overlap

$$\alpha_{1,t}[i] = \sum_{j=-\frac{M}{2R}}^{\frac{M}{2R}} e^{-\imath\Omega(i+j)}, \tag{4.66}$$

to create the equivalent channel in the same manner as (4.39)

$$\widehat{c}_t[k] = \frac{M}{R}\delta[k] + \alpha[i]\delta[k-1]. \tag{4.67}$$

The magnitude of the equivalent tap coefficient versus rotation speed normalized to the reciprocal of the averaging period is plotted in Figure 4.10 with the points we have discussed shown. In this section we have shown how the severity of time-varying multipath taps can be naturally reduced by the overlap-add process.

4.4 System Design and Results

In this section we consider TC-OLA performance over frequency selective channel models that are applicable to LPWAN deployment and obtain results by simulation. Consider a TC-OLA system with a message rate $f_m \approx 977$ sym/sec and a spreading gain of 1024, resulting in a channel rate $f_c = 10^6$ chips/sec before pulse shaping. After pulse shaping the system has a nominal bandwidth of $B = 2$ MHz. This TC-OLA

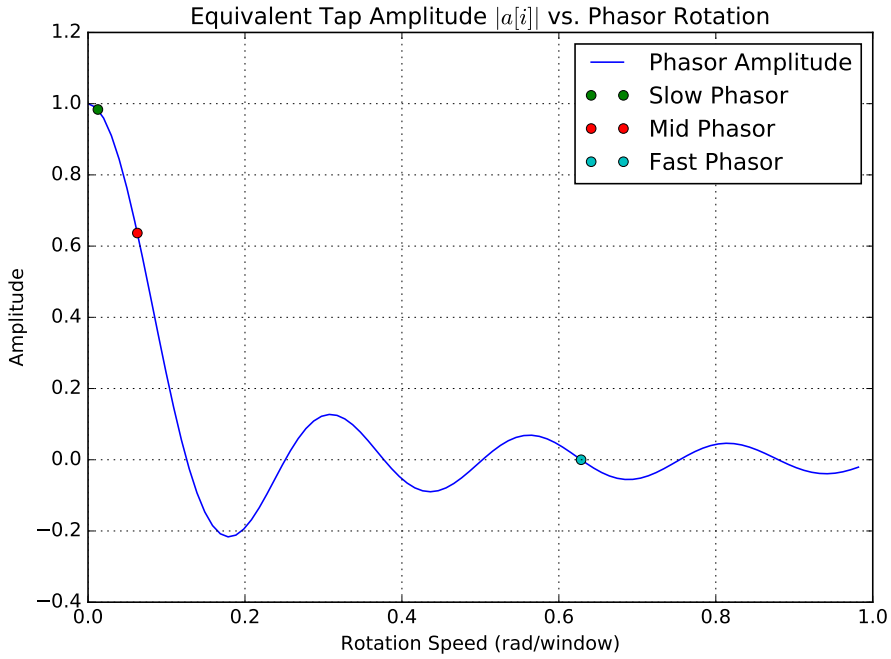

Figure 4.10: Equivalent tap amplitude vs. Phasor rotation speed.

system shall use rectangular windows and orthogonal polyphase sequences to separate users.

We shall compare this with a CDMA system based on circular shifts of a Gold code of length $2^N - 1 = 1023$, as an approximation to an RPMA-like system [26]. This system can theoretically support a maximum of 1023 users by utilizing every chip offset using the orthogonal properties of preferred pairs of Gold codes [47]. However, time-dispersive channels are expected to reduce the practical limit of the number of supported users. Further, timing uncertainty in the uplink is expected to reduce the practical limit further as multiple users may arrive at the base station with the same effective chip offset.

We also note that a rake receiver is of no benefit in this scenario when all chip offsets are occupied. It is of course possible to use different spreading codes for each user in the downlink in order to make use of rake receiver structures. However, this adds cost and complexity to the endpoint.

In the downlink we assume all signals are transmitted synchronously and experience the same channel upon arrival at the receiver of user t. Further, we assume that phase and chip timing of the aggregate signal are recovered perfectly at the receiver for user t. An minimum mean-square error (MMSE) equalizer is applied at the TC-OLA receiver output based on an estimate of the channel response based on the averaging effect described in 4.3.5. The systems are simulated in the SUI channel models as in [19] for 1023 users. Simulation results shown in Figure 4.11 are averaged over 1000 trials of 1000 symbols each with different random seeds for each trial.

From these results we observe that the BER is dominated by the fading distribution up to a BER floor although the TC-OLA system sees a modest gain due to the equalizer. As the channel becomes more time dispersive the equalizer in the TC-OLA system can provide more benefit while the RPMA-like system suffers more interference between users.

In the uplink we assume each signal arrives with a uniformly distributed timing uncertainty of $\pm\tau$ chips and that each signal experiences a different channel upon arrival at the base station receiver. Further, we assume that each signal arrives at the base station with equal average power and that phase and chip timing of the signal from user t is recovered perfectly at the base station.

For the RPMA-like system assume that the transmission timing uncertainty and random chip offset chosen by each endpoint form a uniform random variable $X \sim U(1, N_c)$ and that a new random value is chosen each time, such that each transmission

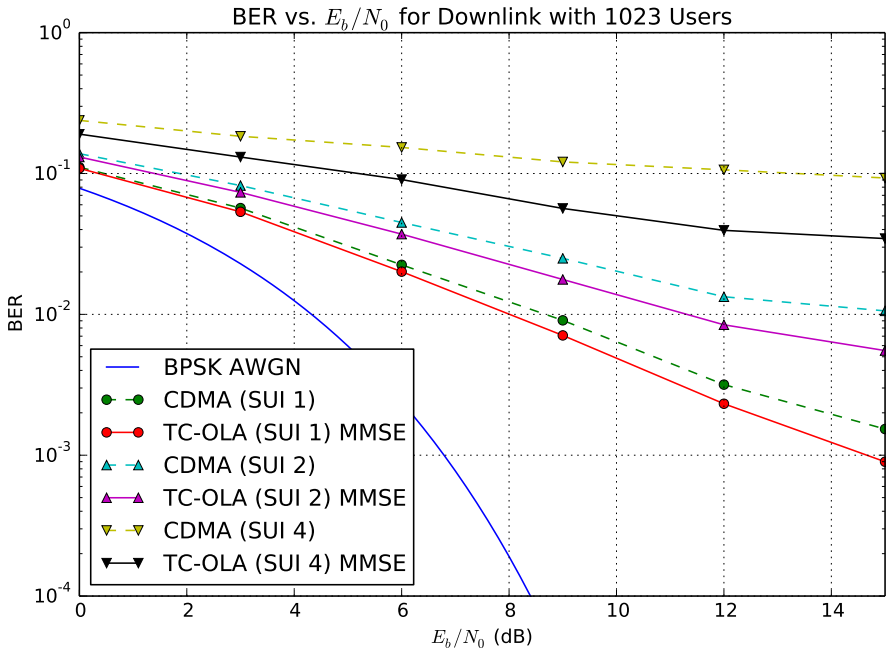

Figure 4.11: Raw BER in simulated downlink scenario comparing TC-OLA and RPMA-like systems with 1023 simultaneous users in SUI models 1, 2, and 4.

is independent [53]. From these assumptions we derive the uplink efficiency as

$$\eta = N\frac{1}{N_c}\left(1-\frac{1}{N_c}\right)^{N-1} \tag{4.68}$$

based on the probability of collision. We note that this expression is familiar as being the efficiency of slotted ALOHA [54], and see that in the limit with $N = N_c$ we obtain a peak efficiency of $e^{-1} \approx 0.37$. More details are available in Appendix E.3.

The use of randomly selected chip offsets avoids the complexity of trying to accurately schedule the chip offset of each user in the uplink. To view this deterministically we could expect that the number of users that can be reliably received with timing uncertainty $\pm\tau$ chips is limited as in (4.69). As the number of users is increased to N_c then reliable operation is not guaranteed unless timing uncertainty can be reduced to zero.

$$N_{max,\tau} \approx \frac{N_c}{2\tau} \tag{4.69}$$

However, the low Doppler spread (high fading correlation) and low timing uncertainty relative to the window size in the SUI models play to the strengths of TC-OLA. We are able to receive with 1023 users in the uplink with only a small interference penalty due to timing offsets. To illustrate this point further, we show simulated uplink results for a range of timing uncertainty in Figure 4.12. For the 7 km cell radius proposed in [19] the average round trip propagation time is $\approx 23.3\mu s$, translating to a uniformly distributed timing offset of $\tau \in [-24 \ldots 24]$ chips for our system. We have shown chip offsets as high as ± 64 chips with only a small BER penalty. The main observation is that the BER floor moves up at the spread of timing offsets increases.

4.5 Conclusion

A code-division variant of TC-OLA has been proposed as an alternative physical layer format for LPWAN monitoring applications. The original design concept was based on the time-compression overlap add approach, but can be described as in 4.2.2 as a time-domain rearrangement of the chips of a CDMA signal. However, we have shown that TC-OLA has better raw BER performance than a CDMA system based on circular shifts of a Gold code in time dispersive channels with a large number of users. The critical difference between TC-OLA and the RPMA-like system in this

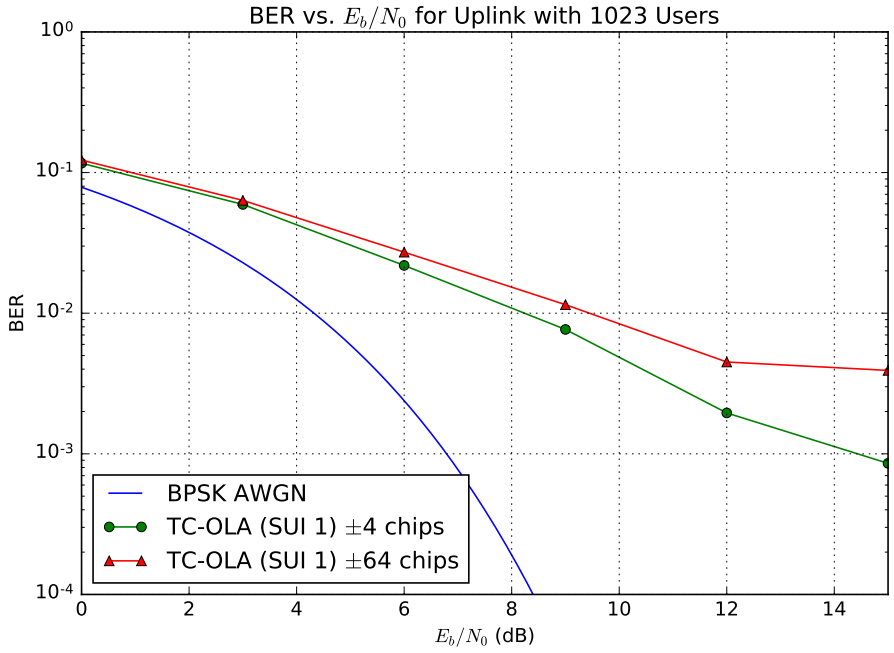

Figure 4.12: Simulated uplink scenario showing TC-OLA system with 1023 users SUI model 1 with a range of timing uncertainty. From this result we observe that greater timing uncertainty reduces the performance and leads to a higher BER floor.

scenario is that the practical number of users in the TC-OLA uplink is not limited by timing uncertainty and delay spread, provided these values can be made small relative to the window size. This allows the system designer to relax the timing requirements in the uplink.

The ability to perform channel equalization at the symbol rate is an added benefit that gives modest BER gains and transfers complexity from hardware rake fingers at the chip rate to software equalization at the message or symbol rate. In the example in the previous section a 1024-point FFT/IFFT is required every 1.05 seconds to apply the FDE technique. To apply the TDE technique requires a digital filter with suitable number of taps operating at the symbol rate of 977 sym/sec. These modest requirements should allow for a range of dynamic software-based equalization schemes.

We have not applied non-linear (decision feedback) equalization here but it may be possible to further reduce the BER using this technique. The matrix notation presented here for $R = 1$ can be generalized to $R > 1$ by considering R subsamplings of the received signal similar to the equivalent filter realization in [44]. Other future work includes analysis of frequency and sample rate offsets, the effect of phase recovery on the interference limit in Rician channels, and further investigation of the near/far problem as it manifests in TC-OLA.

Chapter 5

Robust TC-OLA Reception with Frequency Domain Equalization for UWB Applications

5.1 Introduction

Typical "impulse radio" ultrawideband (UWB) communications schemes use very short pulses with bandwidths exceeding 500 MHz to communicate at very low power levels over short distances [55]. Other systems proposed as UWB physical layer standards use variations of direct-sequence spread spectrum (DS-UWB) [56] or multiband orthogonal frequency division multiplexing (MB-OFDM) [57] to achieve the prescribed bandwidth.

Research interest surrounding UWB communications appears to be in decline since about 2010 [58]. However, the band between 3.1 and 10.6 GHz remains authorized for use by unlicensed UWB devices operating within the FCC limits [23]. This provides an opportunity for alternate communications schemes to operate in this band. One such scheme that may be able to utilize this band is time-compression overlap-add (TC-OLA), where early results used a custom software-defined radio (SDR) to transmit and receive a signal occupying a 225 MHz bandwidth in an indoor laboratory environment [12].

Single carrier frequency division multiple access (SC-FDMA) emerged as an alternative to OFDMA that is used in the LTE uplink [59] and results in similar performance with a lower peak to average power ratio (PAPR) than OFDM. A variant

of SC-FDMA called interleaved FDMA (IFDMA) where all subcarriers are equally spaced in frequency results in a similar time-domain construction to TC-OLA [45,46]. These schemes rely on single carrier frequency domain equalization (SC-FDE) techniques to remove channel-induced ISI but require the insertion of a cyclic prefix (CP) typically on the same order as the delay spread of the channel [60] such that circular convolution can be performed using the fast Fourier transform (FFT). The CP insertion reduces the overall efficiency of the scheme. An analysis of overlap FDE, a block-based reception technique that does not use CP insertion, is given in [61]. SC-FDE with CP techniques were investigated in a UWB context in [62], which states that a block may be transmitted multiple times to improve the received signal to noise ratio. While this is true, it does not eliminate the proposed 25% overhead introduced by the CP.

In this chapter we propose a variant of TC-OLA [12,37,44] as an alternate physical layer scheme for UWB applications. The redundancy added by TC-OLA, equivalent to block repetition proposed in [62], is used to extend the link budget when operating under the power constraints defined by FCC regulations [23]. To evaluate the performance we consider the UWB channel models developed by the IEEE 802.15.3a working group [21]. An important and novel feature of TC-OLA is the distributed CP property which makes it possible to create a robust SC-FDE scheme with zero CP overhead when the TC-OLA spreading factor $\frac{M}{R} \geq 3$. It can also operate in harsher industrial channel models such as CM8 [21] without requiring a very large block size to offset the effect of a long CP or suffering a low efficiency. The ability to use block-based SC-FDE techniques without any modification to the TC-OLA signal format is an attractive advantage of this combination. Another novel feature of this combination is the ability to switch between two proposed receiver modes with the same transmitted spreading factor to achieve greater efficiency (greater processing gain, receive sensitivity) or greater tolerance to delay spread, depending on channel conditions.

The remainder of this chapter is organized as follows. Section 5.2 presents the TC-OLA system model and the basic method. Section 5.3 details how frequency-domain equalization of TC-OLA is performed. Section 5.4 presents a system design and experimental simulation results comparing with a typical SC-FDE system, including specific examples and parameter choices. Section 5.5 presents our conclusions based on observations of the analysis and experimental results.

5.2 TC-OLA System Model

A baseband TC-OLA signal is generated for a message signal $m[k]$ sampled at the message rate f_m using (5.1) [44], where $w[k]$ is a window function of length M chosen such that $w^2[k]$ exhibits a constant overlap-add (COLA) property as in (5.2) when overlap-added using hop size R. The change in indices from k to j indicates the change in sample rate from the message rate f_m to the channel rate $f_c = \frac{M}{R} f_m$, where $\frac{M}{R}$ represents the TC-OLA spreading factor. The message signal may be a sampled analog (ie: voice) signal, modem signal, or digital symbols. In the latter case, pulse shaping occurs after the TC-OLA process.

$$s[j] = \sum_{i=-\infty}^{\infty} w[j - iM] m[j - i(M - R)] \tag{5.1}$$

$$\sum_{i=-\infty}^{\infty} w^2[k - iR] = \frac{M}{R} \mathrm{E}\left[w^2[k]\right] = C \tag{5.2}$$

The details of TC-OLA using sine windows may be found in [12, 44]. When the message signal is made up of digital symbols, as we shall do here, a rectangular window (5.3) is most appropriate, which is COLA for values of M and R as in (5.4). TC-OLA based on digital symbols is illustrated in Figure 4.2.

$$w_M[k] = \begin{cases} 1 & : 0 \leq k < M \\ 0 & : otherwise \end{cases} \tag{5.3}$$

$$R = \frac{M}{K}, \ K = 1, 2, 3... \tag{5.4}$$

5.3 Frequency-Domain Processing

In time-domain TC-OLA processing the signal is overlap-added as in (5.5), where $c[j]$ in (5.6) is the discrete-time channel model and $n[j]$ is an additive white Gaussian noise (AWGN) process with zero mean and variance σ_n^2. In Chapter 4 it was shown how this method effectively frequency-compresses the channel response.

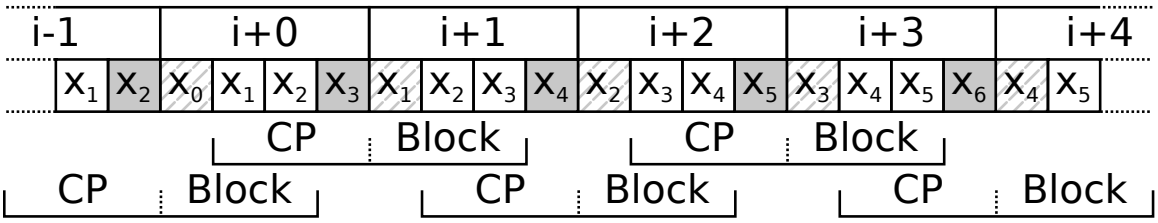

Figure 5.1: Illustrating construction and block-based reception of TC-OLA with $M = 4$, $R = 1$. Shaded symbols act only as CP symbols while the hatched symbols act only as block symbols. All other symbols act as both CP and block.

$$\widehat{m}[k] = \sum_{i=-\infty}^{\infty} w[k - iR]r[k + i(M - R)] \tag{5.5}$$

$$r[j] = s[j] * c[j] + n[j] \tag{5.6}$$

While this was shown to work well when the channel response is short relative to the window size, another solution is needed when the channel response is long relative to the window size. As such we consider the block-processing receiver method illustrated in Figure 5.1 and a frequency-domain equalization scheme such as MMSE. When processed in this manner the maximum AWGN processing gain is

$$G = \frac{M}{R} - 1, \tag{5.7}$$

rather than $G = \frac{M}{R}$ as with time-domain TC-OLA processing [44]. Referring to Figure 5.1, this is because R shaded symbols at the end of each window are only treated as part of the CP and do not contribute to the processing gain. With this construction the efficiency is

$$\eta = \frac{M - R}{M} \tag{5.8}$$

with an effective CP length L_{CP} and block length L_B of

$$L_{CP} = L_B = M - R. \tag{5.9}$$

This construction works down to the minimum $\frac{M}{R} = 2$, but gives a very poor efficiency unless $M >> R$.

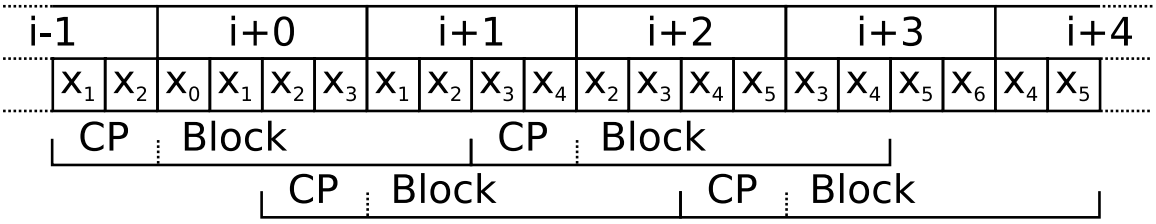

Figure 5.2: Illustrating construction and block-based reception of TC-OLA with $M = 4$, $R = 1$. At the expense of a longer block length and a shorter effective CP length the CP overhead present in Figure 5.1 can be eliminated. The new $L_{CP} = 2$ (was 3) while the new $L_B = 6$ (was 3). However, there is no longer any CP overhead: all received samples contribute to the processing gain.

At the expense of reducing the effective CP length and increasing the block length it is possible to create a scheme with no CP overhead as shown in Figure 5.2. The effective CP length in this construction is

$$L_{CP} = M - 2R \tag{5.10}$$

and the block length L_B is

$$L_B = 2(M - R). \tag{5.11}$$

The final $M - 2R$ samples of the block are discarded after applying the equalizer, and because of this the computational load is slightly higher. This construction requires that $\frac{M}{R} > 2$. From an implementation viewpoint, we would also like to constrain L_B in either method to a power of 2 for processing using the fast Fourier transform (FFT).

The ability to use block-based SC-FDE techniques without any modification to the signal format is an attractive advantage and a novel feature of TC-OLA. The decision of which method to use can be left up to the receiver, and requires no change in the transmitted signal. For the same spreading factor, the method of Figure 5.1 has a longer effective CP and shorter block length than the method of Figure 5.2. Thus it is tolerant of longer delay spreads and has less stringent timing recovery requirements. The receiver may switch to the method of Figure 5.2 if channel conditions allow, increasing the realized processing gain from $\frac{M}{R} - 1$ to $\frac{M}{R}$.

To perform the frequency-domain equalization (FDE), the FFT is taken over each block and the equalizer taps $\mathbf{C}_i$ are applied. The inverse FFT is taken of the result, which is then overlap-added with previous results to form the final output. The

received signal can be written as

$$\widehat{m}[k] = \sum_{i=-\infty}^{\infty} w_M[k - iR]\rho_i, \tag{5.12}$$

$$\rho_i = \mathcal{F}^{-1}\{\mathbf{C}_i \circ \mathcal{F}\{w_{L_B}[k - iR]r[k + i(M - R)]\}\}, \tag{5.13}$$

where $\mathcal{F}\{\cdot\}$ is the FFT operator and $\circ$ is the point-wise (Hadamard) product. Note that we have used a rectangular window of length L_B to prepare the block for the FFT and a window of length M for the overlap add process. In construction of Figure 5.1 the window $w_M[\cdot]$ has no effect as $M > L_B$ and in the construction of Figure 5.2 this window is used to trim the block back to the window size.

The equalizer taps $\mathbf{C}_i$ are computed as

$$\mathbf{C}_i = \frac{H_i}{|H_i|^2 + \frac{N_0}{2E_b}}, \tag{5.14}$$

where E_b is the energy per bit, N_0 is the one-sided noise power spectral density, and $\mathbf{H_i}$ is the length L_B FFT of the channel impulse response (CIR) associated with window i.

Interblock interference (IBI), a symptom of too short CP length relative to delay spread, tends to distort symbols near the beginning of the block in SC-FDE systems [62]. As can be seen in Figure 4.2, the construction of TC-OLA naturally shifts symbols through different positions within successive FFT blocks. We reason that this effect helps to average the distortions due to IBI over a larger number of symbols.

5.4 Simulation Results

For the simulations done here we choose the same parameters as the SC-FDE system of [62], namely RRC pulse shaping with symbol duration $T = 2\,\text{ns}$ and rolloff $\beta = 0.5$. The simulation sample rate is 4 GHz. We assume that block timing is recovered and that the channel is estimated perfectly at the receiver.

M/R	M	R	L_{CP}
3	192	64	64
5	160	32	96
9	144	16	112
17	136	8	120

Table 5.1: Range of TC-OLA parameters and effective CP for $L_B = 256$.

5.4.1 Indoor Channels

In the first experiment we apply the construction of Figure 5.2 to the indoor channels CM1 and CM3. The parameters we choose for the TC-OLA system are $M = 192$, $R = 64$, such that the effective block length L_B is

$$L_B = 2(M - R) = 256, \tag{5.15}$$

and the effective CP length L_{CP} is

$$L_{CP} = M - 2R = 64. \tag{5.16}$$

We note that the TC-OLA spreading factor is $\frac{M}{R} = 3$ which is the minimum for this method, and extends the link budget by 4.77 dB. This system has an effective bit rate of 167 Mbps. The comparable SC-FDE system uses the parameters from [62], with the block size of 256 and the CP length of 64. This system has an effective bit rate of 133 Mbps when using the equivalent block repetition rate of 3.

Simulation results comparing these two systems for CM1 are shown in Figure 5.3, while additional simulations (not shown) have confirmed a similar effect for CM2 and CM3. The SC-FDE results have included the CP overhead in computing E_b/N_0. The main observation we make from this result is the expected gain in E_b/N_0 and bit rate from the elimination of the CP overhead.

One way to explore the parameter space is to hold the effective block length L_B constant and increase the processing gain. This increases the effective CP length thus increasing the maximum tolerable delay spread. We do this if it is not practical to change the FFT size. Table 5.1 list the results for a constant block length of $L_B = 256$.

To analyze the difference in computational load we assume that computation of the FFT dominates the processor. The SC-FDE system requires a number of operations

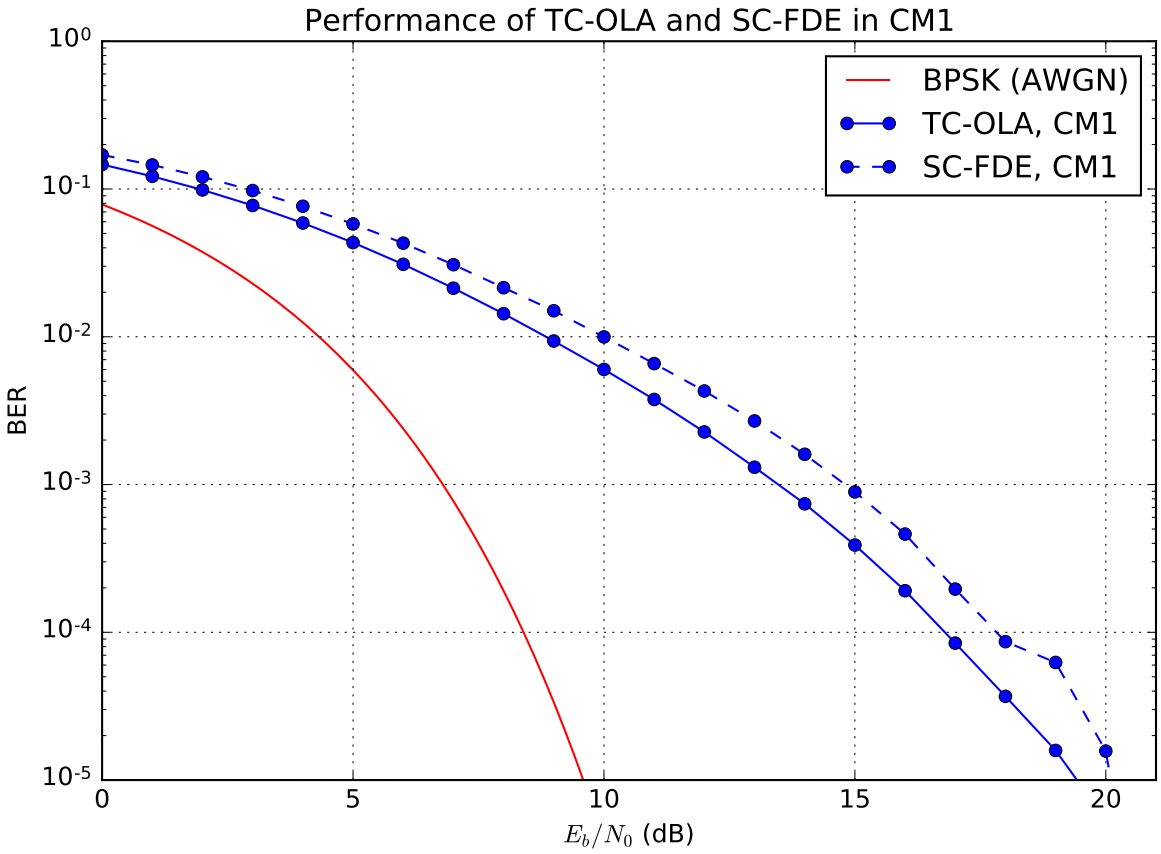

Figure 5.3: Comparing the performance of TC-OLA and SC-FDE in CM1. Both systems use an effective block size of 256 and CP length of 64. We observe the expected increase in efficiency as the CP overhead has been eliminated. Additional results for CM2 and CM3 (not shown) confirm a similar result.

proportional to

$$\frac{M}{R} L_B \log_2 L_B \tag{5.17}$$

while the TC-OLA system requires

$$\frac{L_B}{R} L_B \log_2 L_B, \tag{5.18}$$

which reduces to

$$2\left(1 - \frac{R}{M}\right). \tag{5.19}$$

This tends to a maximum of 2 as R becomes small relative to M. In return for this increased computational load we are increasing the effective CP length. If our goal is to maintain a certain CP length corresponding to particular channel delay spread then we might consider a smaller block length when increasing the processing gain.

5.4.2 Industrial Channels

In the second experiment we consider the industrial non-line of sight (NLOS) channel CM8. The construction of Figure 5.1 is used with $\frac{M}{R} = 5$ to extend the link budget. Although this scheme is only 80% efficient by application of (5.8), an effective CP length of 256 can be obtained with an FFT block length of 256. The SC-FDE system of [62] requires a block length of 1024 to maintain the same efficiency. Conversely, we could design a TC-OLA system based on the method of Figure 5.2 with a block length of 1024 and an effective CP length of 256 using $\frac{M}{R} = \frac{768}{256} = 3$. This method is 100% efficient for the same CP and FFT block length as the SC-FDE system.

Additionally, increasing the spreading ratio $\frac{M}{R}$ while maintaining the effective CP length results in both an increase in overhead efficiency and extension of the link budget at the expense of effective bit rate, which can be calculated as $\frac{1}{T}\frac{R}{M}\eta$. Results for CM8 are shown in Figure 5.4 for a range of spreading ratios. When the effective CP length is reduced below the channel length an expected BER floor is observed. When the spreading ratio is increased while maintaining the CP length we observe the expected increase in overhead efficiency.

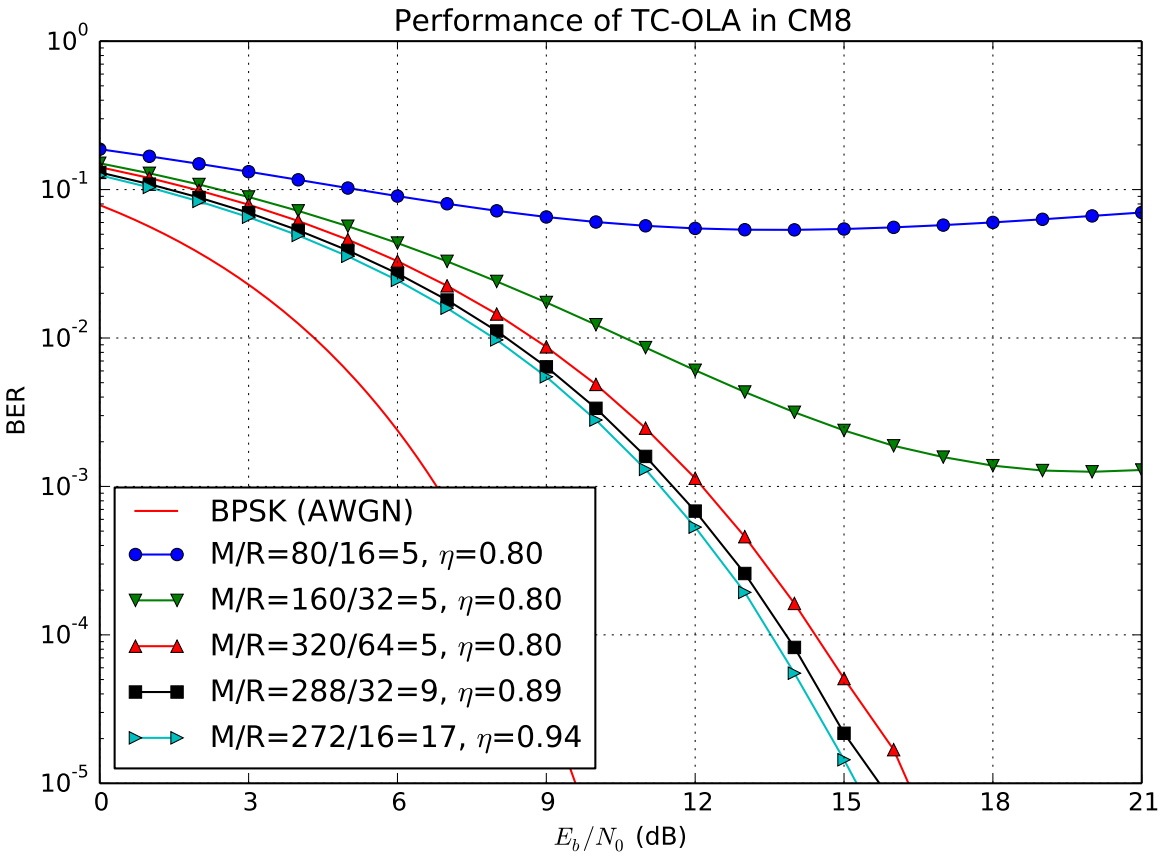

Figure 5.4: Results in CM8 for a variety of CP lengths and spreading ratios. The typical delay spread of CM8 channels is $\tau_{RMS} = 89$ns [21], from which we estimate the required CP length as $3\tau_{RMS} = 267$ns [47]. The first two TC-OLA scenarios listed here have CP lengths of 64 (128 ns), 128 (256 ns), while the remainder have a CP length of 256 (512 ns). The effective bit rate of the first three scenarios is 80 Mbps, while the remaining two scenarios have effective bit rates of 49.4 Mbps and 27.7 Mbps respectively.

5.5 Conclusion

In this work we assume that our model TC-OLA and SC-FDE systems are equally capable of acquiring block timing and estimating the channel. In comparison with overlap FDE, which requires no CP overhead or block acquisition, it is much more complex. However, overlap FDE comes with a BER floor that can only be reduced through a higher processing load [61]. The TC-OLA scheme proposed here represents a compromise with no or low effective CP overhead and similar processing load to SC-FDE. Unlike overlap FDE, the CP overhead is eliminated without the increased processing load required to maintain a practically useful BER floor. However, these gains can only be achieved through a TC-OLA spreading factor $\frac{M}{R} \geq 3$.

In time-domain TC-OLA processing the equalizer is applied after the overlap-add process. In this case some information about the channel is lost as the time-varying components of the channel tend to be averaged out by the overlap-add process [12], although the complexity and processing load is much lower. In the case we discuss here, no information is lost assuming the channel can be accurately estimated at some rate of change slower than the block rate. This assumption is thought to be valid for most UWB channel model applications. Measurement and modelling campaigns have focused on the static CIR measurement, with some analysis on the effects of body shadowing effect (BSE) or other dynamic obstructions in the environment [63].

Block-based reception of TC-OLA with frequency-domain equalization has been proposed as an alternative physical layer scheme for UWB applications. In addition to the advantages of SC-FDE methods such as lower PAPR [62], the particular advantage of this scheme is that the CP overhead can be reduced or eliminated when the redundancy added by TC-OLA is used to extend the link budget under the transmitted power constraints defined by the FCC. As an example, assuming a CP overhead of 25%, this can be the difference between 100 Mbps and 125 Mbps when a spreading factor of 4 is used to extend the link budget by 6 dB.

Chapter 6

Discussion and Future Work

In the course of the research work on this topic several ideas were investigated that are not represented in any article submitted for publication. This chapter captures these ideas as they may lead to additional discussion, patent claims, or future publications.

6.1 Perspectives on TC-OLA

Overlap-add is used in signal processing as a way to apply a known FIR filter $h[k]$ to a long sequence $x[k]$. This is done by breaking up the convolution into multiple convolutions of $h[k]$ with short segments of $x[k]$. TC-OLA applies an unknown wideband channel response $h[j]$ to a narrowband signal $x[k]$ using the overlap-add method. The wideband channel response is only accessible due to the bandwidth expansion that results from creating the higher sample rate stream $s[j]$ from short segments of $x[k]$. The overlap add process, in turn, restores the drop in SNR that results from the bandwidth expansion. This perspective lends a simple elegance, showing how each component of the method is interdependent.

This section summarizes some perspectives on TC-OLA that were presented throughout the previous chapters. Here we look at TC-OLA as matched filter communications system, a spread spectrum system, and a block processing system. In the end, we look at time-domain sample rearrangement as a recurring theme and a method of connecting TC-OLA to other existing communications schemes.

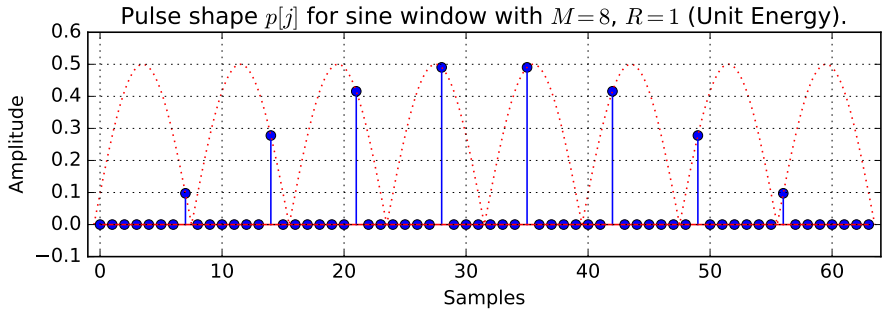

Figure 6.1: Unit-energy pulse shape $p[j]$ for sine window with $M = 8$, $R = 1$. Window function shown in dotted line for context.

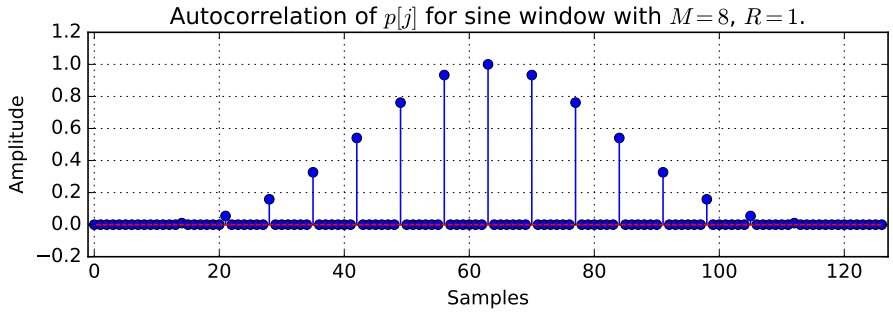

Figure 6.2: Autocorrelation of $p[j]$ for sine window with $M = 8$, $R = 1$. The correlation peak of 1.0 indicates that we have captured the energy in the transmitted pulse.

6.1.1 As a Matched Filter Communications System

The filter equation (3.22) in Chapter 3 allows us to write an equation for the equivalent pulse shape $p[j]$. From inspection of (3.23) we observe that there are actually R pulse shapes which are simply different subsamplings of the window shape as in (6.1).

$$p_\phi \left[\left(\frac{M}{R} - 1 \right) k \right] = w \left[Rk + \phi \right], \, \phi \in [0 \ldots R-1] \tag{6.1}$$

The normalized (unit energy) pulse shape for sine windows with $M = 8$, $R = 1$ is shown in Figure 6.1 in the context of the window functions that it occupies. The autocorrelation of $p[j]$ is shown in Figure 6.2 with a peak of 1.0, indicating that the energy in the pulse has been captured.

Note that in practice it may not be feasible to correlate over such a long pulse shape as we only expect the channel to be quasi-static over one window period. We

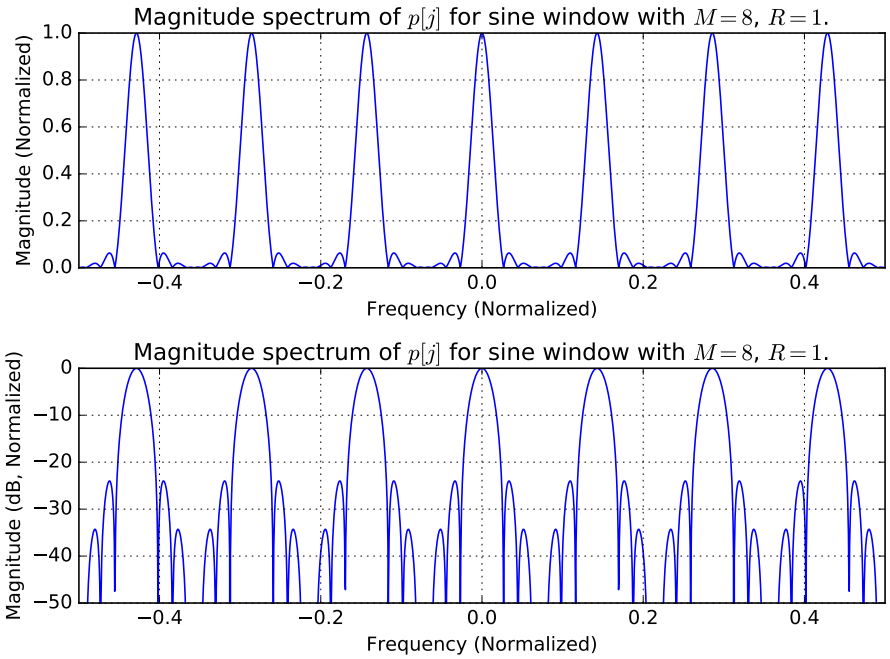

Figure 6.3: Magnitude spectrum of $p[j]$ for sine window with $M = 8$, $R = 1$. Shown in linear (top) and dB scale (bottom).

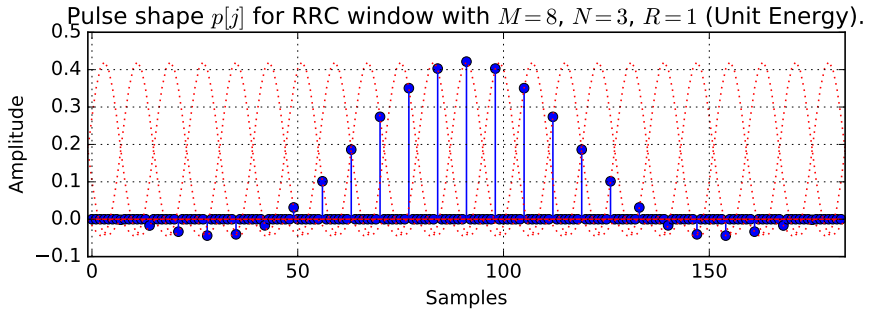

Figure 6.4: Unit-energy pulse shape $p[j]$ for RRC window with $M = 8$, $R = 1$. Window function shown in dotted line for context. Note that the RRC window functions overlap at the channel rate.

only point out here that the overlap-add method is equivalent to a matched filter correlation receiver.

For the sine window shape discussed above, windows functions are orthogonal by the simple fact that they do not overlap in time. One can expect that it is possible for transmitted segments to overlap in time if orthogonality is maintained. One such window shape is the root raised cosine (RRC) window, which should come as no surprise to those familiar with digital communications. The equivalent pulse for this case is shown in Figure 6.4. Although this approach spreads the pulse over a longer period, it can also reduce the PAPR of the transmitted signal and reduce the spectral side lobes of the pulse as shown in Figure 6.5.

The theoretical performance of this scheme can be evaluated on the basis of $\frac{E_s}{N_0}$ using the equivalent unit-energy pulse shapes and a defined a symbol constellation. However, this is not seen to be the most useful or interesting interpretation of TC-OLA.

6.1.2 As a Spread Spectrum Method

As we have described in Chapter 2, the basic effect of playing back a signal sampled at rate f_m at a higher rate f_c is that the spectrum of the message signal $m_u[k]$ is spread in bandwidth by the ratio $\frac{f_c}{f_m}$. This is indeed the case over the observation period of one window, assuming the window function has only negligible effect.

In this way TC-OLA can be considered a spread spectrum technique. As a spread-spectrum technique it can be expected to have a processing gain in AWGN channels, which was derived for sine windows in Chapter 3 and shown to be independent of the

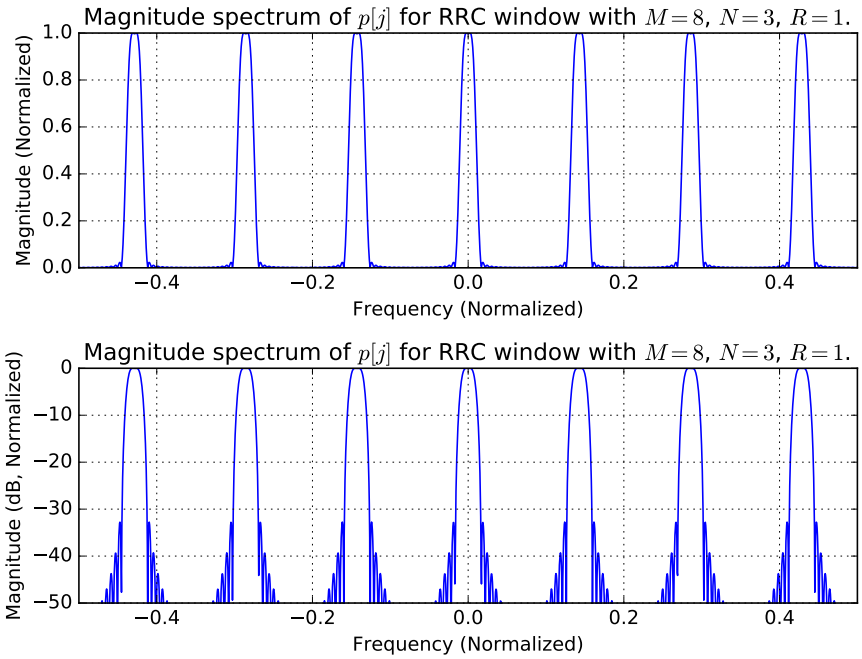

Figure 6.5: Magnitude spectrum of $p[j]$ for RRC window with $M = 8$, $N = 3$, $R = 1$. Shown in linear (top) and dB scale (bottom).

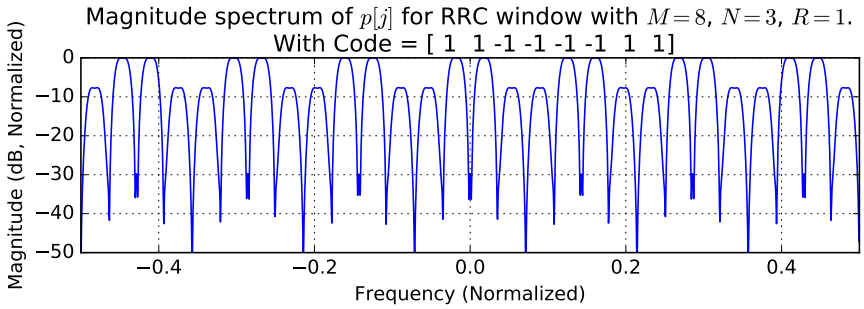

Figure 6.6: Magnitude spectrum of $p[j]$ for RRC window with $M = 8$, $N = 3$, $R = 1$. Code symbols are applied to each window. Compare this with Figure 6.5, where all of the transmitted signal energy is concentrated in narrow bands.

window shape in Chapter 4.

Consider the magnitude spectrum of the pulse $p[j]$ generated in the previous section (Figure 6.3). Although the spectrum of $m_u[k]$ is spread by $\frac{f_c}{f_m}$ in the short observation period, the repetitive nature of the transmitted signal causes the signal power to be concentrated in regularly-spaced narrow bands over a longer observation period. As a spread spectrum method, this implies that the message signal is susceptible to interference within these bands. However, adding a code to the transmitted segments is one way to redistribute the energy, as shown in Figure 6.6.

6.1.3 As a Multicarrier and Cyclic Prefix Block Processing Method

There exist several variants of block transmission wherein a CP is prepended to the modulated signal block. Some of these methods are multicarrier-oriented, while some are single-carrier oriented. Based on Figure 6.5, we might consider uncoded TC-OLA as a multicarrier method where the carriers are spread uniformly across the channel bandwidth. Each carrier conveys a portion of the information contained in the message signal. It has been shown possible to recover TC-OLA by combining each of the carriers through appropriate filter and frequency-shift operations.

Provided the channel length is shorter than the CP and the channel is stable over the length of the CP and modulated signal block then the linear convolution with the channel can be converted into a circular convolution and processed with FFT. OFDM perhaps most famously makes uses of this technique, but other techniques in this family include SC-FDMA and its variants: IFDMA, LFDMA, DFDMA [46] and

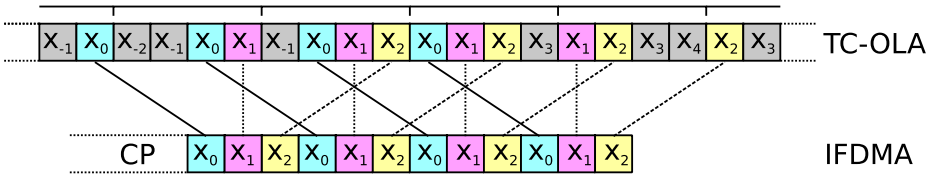

Figure 6.7: Illustrating the time-domain mapping between TC-OLA (top) and IFDMA (bottom) [46]. Shaded symbols are not part of the IFDMA block shown but could be mapped to an adjacent IFDMA block.

others. Overlap FDE attempts to use FFT processing techniques without a CP by playing BER floor against processing load [61].

As we have shown in Chapter 5, the time-domain arrangement of samples used by TC-OLA can be used to reduce the CP overhead as redundancy is added. It some cases it can be completely eliminated, without the issues associated with overlap FDE.

6.1.4 Sample Rearrangement and SC-FDMA

As the name implies, SC-FDMA is inspired by frequency division schemes. Specific time-domain patterns illustrated in [46] emerge from particular subcarrier mappings in frequency. For example, IFDMA distributes the subcarriers evenly over the bandwidth while localized FDMA (LFDMA) gathers them together in a contiguous block. Yet another scheme called B-IFDMA distributes blocks of two or more subcarriers evenly over the bandwidth [64] as a compromise between these two schemes. The basic structure of the transmitter and receiver for these schemes is the same, with the main difference being the subcarrier mapping procedure.

TC-OLA was initially motivated by arrangements of samples in the time domain. In contrast to the relationship above, certain frequency-domain patterns emerge based on the particular arrangement of samples in the time domain. The basic TC-OLA arrangement leads to the frequency domain pattern shown in Figure 6.5 which we could interpret as evenly spaced subcarriers, very similar to the frequency-domain construction of IFDMA. The time-domain mapping between these two schemes is shown in Figure 6.7. Time-domain rearrangement of samples was also used to illustrate the connection to CDMA in Figure 4.3 and will be used to illustrate the connection to OFDM in Section 6.3.2.

6.2 System Parameter Relationships

Throughout the previous chapters there are various examples of relationships between the TC-OLA parameters and channel parameters. A summary of these relationships is given here as a guide for the system designer.

A basic unit is the window time T_w (in seconds) which we define as

$$T_w = \frac{M}{f_c}. \tag{6.2}$$

Another measure is the averaging time T_{avg}, which we can consider to be the effective "rolling average" window on the channel response. This averaging effect is discussed in Chapter 2, particularly the comparisons of Figures 2.5-2.7. Therefore

$$T_{avg} = \frac{M}{R} T_w = \frac{M^2}{R f_c} = \frac{M}{f_m}, \tag{6.3}$$

assuming no timing markers are used in the transmission.

Although the channel transformation created by multipath delays longer than T_w were discussed in Section 3.2.2 and it does have some interesting implications, this case was not considered in detail. In the time-domain equalization case considered in Chapter 4, any significant multipath components are assumed to arrive within about

$$\tau_{max} \approx 0.1 T_w \tag{6.4}$$

to minimize interference between users and maintain (approximately) the constant overlap add property. This figure was arrived at through simulation and some additional analysis could expose the tradeoff between the spread of multipath delays and the SIR given the TC-OLA parameters. This figure is used to justify the window size given the round-trip propagation time over the cell radius.

In comparison, the frequency-domain equalization case considered in Chapter 5 requires that significant multipath components arrive within L_{CP} in order for the circular convolution to work. In the method of Figure 5.1 the length of the CP and the length of the block are the same, and both are shorter than the window. In other words we can tolerate multipath delays up to

$$\tau_{max} = \left(1 - \frac{R}{M}\right) T_w. \tag{6.5}$$

The method of Figure 5.2 means that significant multipath delays up to

$$\tau_{max} = \left(1 - \frac{2R}{M}\right) T_w \tag{6.6}$$

may be tolerated. The value of τ_{max} can be estimated from the common channel parameter RMS delay spread τ_{RMS} as $\tau_{max} \approx 3\tau_{RMS}$ [47].

6.3 Multiple Access

In this section well-known multiple access methods are applied to the basic TC-OLA concept. The multiuser TC-OLA system is assumed here to be a wireless star network. In the downlink (base station to remote terminal) the aggregate signal of all users is transmitted by the base station in a *window synchronous* manner. All of the signals arrive at the remote terminal having experienced the same channel distortions. In the uplink (remote terminal to base station) not only have signals experienced different channels but are also subject to differences in arrival time at the base station.

6.3.1 Time Division

Multiple access by time division was considered in Chapter 2 but was not treated mathematically. A baseband time division TC-OLA waveform for N users can be described as in (6.9) by modifying the original equation in (5.1). Construction of the baseband waveform is illustrated in Figure 6.8.

$$s_u^{(t)}[j] = s_u[j - i(N-1)M] \tag{6.7}$$

$$= \sum_{i=-\infty}^{\infty} w[j - iNM] m_u[j - i(NM - R)] \tag{6.8}$$

$$s^{(t)}[j] = \sum_{u=0}^{N-1} s_u^{(t)}[j - uM] \tag{6.9}$$

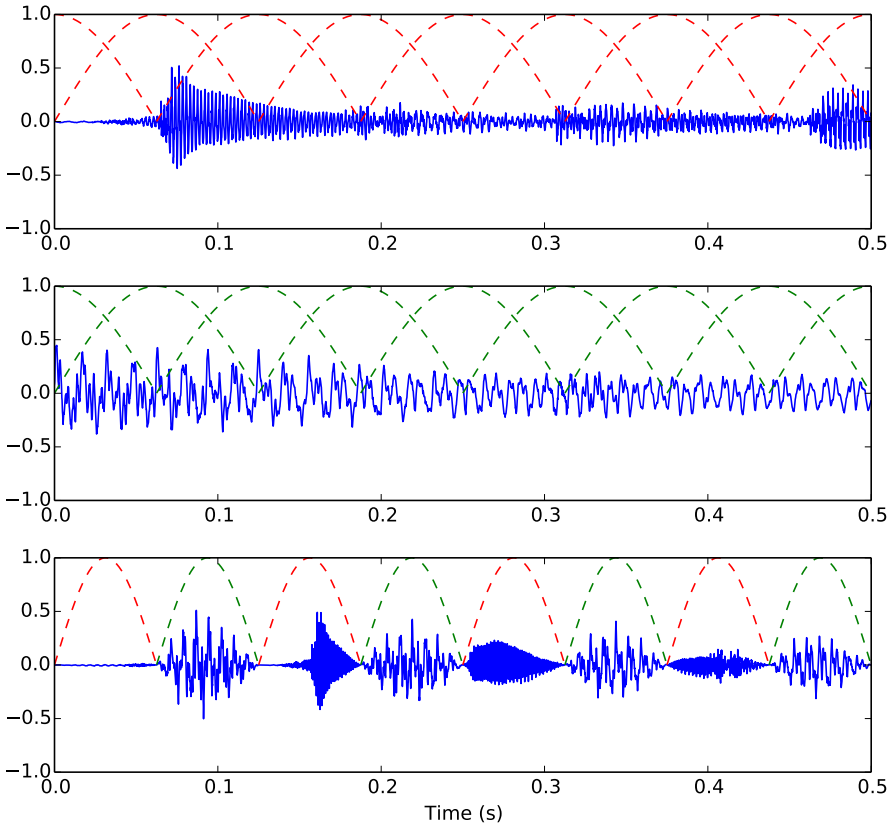

Figure 6.8: Time-division TC-OLA system with two users. Segments from $m_0[k]$ and $m_1[k]$ are interleaved to form the transmitted signal.

$$\widehat{m}_u[k] = \sum_{i=-\infty}^{\infty} w[k - iR] s^{(t)}[k + i(NM - R) + uM] \tag{6.10}$$

$$= Cm[k] \tag{6.11}$$

This scheme is the basis for the classical TCM systems where the window function is assumed to be rectangular as in (4.5). These systems may operate with $R = M$ or $R = M - G$ where G is the number of samples that overlap in order to protect against *grouping noise* [5]. Another common scheme to prevent grouping noise in classical TCM is zero crossing detection. We could interpret this scheme as having a variable window length $M'[i]$ such that $\mathrm{E}\left[M'\left[i\right]\right] = M$.

In this scenario the noise bandwidth (and consequently the noise power) at the receiver must be increased by a factor of $N\frac{M}{R}$. For classical TCM systems where

$\frac{M}{R} \approx 1$ the increase in noise bandwidth is approximately a factor of N.

It is possible to relate [8] to a N-user TCM system with only one active user. The noise bandwidth at the receiver must be expanded by a factor of N and to compensate the transmit power must be increased by the same factor to maintain the signal-to-noise ratio (SNR). Although the average transmit power remains the same, we must build into our system an amplifier capable of producing NP_{tx} with a $1/N$ duty cycle. To the system designer this tradeoff may be worth the proposed advantage of the system [8], which is to spread the analog voice signal such that frequency-selective fading is experienced. The equivalent TC-OLA system is easily shown to experience much the same frequency-selective fading but with a continuous duty-cycle power amplifier operating at P_{tx} to achieve the same received SNR.

In Chapter 2 a practical system with a spreading factor of $\frac{M}{R} = 4$ was demonstrated, in a time division configuration with $N = 4999$ users. We observe here that although increasing the overlap further expands the bandwidth, it does not degrade the AWGN performance given the process gain derived in (3.18). Thus we are losing only to increasing the number of users N. This observation motivates the investigation of other multiple access methods for use with TC-OLA.

6.3.2 Code Division

Multiple access by code division was described in detail in Chapter 4. It was also shown that TC-OLA is equivalent to direct-sequence CDMA through a consistent pattern of time-domain sample rearrangement. Here we show that the same is true of OFDM, if the CP component is neglected.

Equivalence with OFDM

Consider the code division TC-OLA signal construction from (4.12). If we were to choose the code in (4.15) as the set of polyphase sequences such that

$$a_{i,u} = e^{\imath \frac{2\pi iu}{M}} \tag{6.12}$$

it is possible to show that the TC-OLA output is a time-domain rearrangement of the OFDM modulator output. The code sequences are made up of samples of the sinusoidal components that make up the OFDM symbol, which we would usually consider a frequency division scheme. This relates TC-OLA to both OFDM and CDMA

simply by choice of code sequences. Another scheme that can be easily connected to both CDMA and OFDM is IFDMA [45]. It is shown in [65] that OFDM can be considered as a set of spreading sequences which meet certain constraints.

As an example, consider four discrete time series x_k, y_k, z_k, and w_k. The codes in (6.12) are applied to generate four coded TC-OLA signals using (4.11) with rectangular windows to yield (6.13). The columns are summed to produce samples of the transmitted signal s_j as in (4.12).

0	1	2	3	4	5	6	7	8	9	10	11	12	13	14	15	j
0	0	0	0	1	1	1	1	2	2	2	2	3	3	3	3	i
x_0	x_1	x_2	x_3	x_1	x_2	x_3	x_4	x_2	x_3	x_4	x_5	x_3	x_4	x_5	x_6	$\times 1$
y_0	y_1	y_2	y_3	y_1	y_2	y_3	y_4	y_2	y_3	y_4	y_5	y_3	y_4	y_5	y_6	$\times e^{\imath\frac{\pi i}{2}}$
z_0	z_1	z_2	z_3	z_1	z_2	z_3	z_4	z_2	z_3	z_4	z_5	z_3	z_4	z_5	z_6	$\times e^{\imath\pi i}$
w_0	w_1	w_2	w_3	w_1	w_2	w_3	w_4	w_2	w_3	w_4	w_5	w_3	w_4	w_5	w_6	$\times e^{\imath\frac{3\pi i}{2}}$

(6.13)

The vector of frequency-domain symbols $\mathbf{A} = \{x_3, y_3, z_3, w_3\}$ is applied to the input of an OFDM modulator to obtain the output vector $\mathbf{a}$ as

$$\mathbf{a} = DFT^{-1}\{\mathbf{A}\} \leftrightarrow a_n = \sum_{k=0}^{3} A_k e^{\imath\frac{2\pi kn}{4}}. \tag{6.14}$$

Now we compare $\mathbf{a}$ with the samples of s_j that contain $\{x_3, y_3, z_3, w_3\}$:

$$s_3 = x_3 + y_3 + z_3 + w_3 \qquad = a_0 \tag{6.15}$$

$$s_6 = x_3 + y_3 e^{\imath\frac{\pi}{2}} + z_3 e^{\imath\pi} + w_3 e^{\imath\frac{3\pi}{2}} \qquad = a_1 \tag{6.16}$$

$$s_9 = x_3 + y_3 e^{\imath\pi} + z_3 + w_3 e^{\imath\pi} \qquad = a_2 \tag{6.17}$$

$$s_{12} = x_3 + y_3 e^{\imath\frac{3\pi}{2}} + z_3 e^{\imath\pi} + w_3 e^{\imath\frac{\pi}{2}} \qquad = a_3 \tag{6.18}$$

From the example, it is clear to see that this instance of TC-OLA could be produced from the output of an OFDM modulator (before application of the CP) by choosing the code sequences in (6.12) applying the regular pattern of sample rearrangement.

6.3.3 Frequency Division

A frequency division scheme can be described as

$$s^{(f)}[j] = \sum_{u=0}^{N-1} s_u[j] e^{\imath 2\pi j u \Delta_f}, \tag{6.19}$$

where Δ_f is the frequency offset between users. The received version of this signal is

$$\widehat{m}_t[k] = \sum_{i=-\infty}^{\infty} e^{-\imath 2\pi j t \Delta_f} w[k - iR] s^{(f)}[k + i(M - R)] \tag{6.20}$$

$$= \sum_{u=0}^{N-1} m_u[k] \sum_{i=-\infty}^{\infty} e^{\imath 2\pi j (u-t) \Delta_f} w^2[k - iR] \tag{6.21}$$

Similar to the previous section, this scheme can also be shown to be a rearrangement of OFDM samples for $\Delta_f = u\frac{M}{R}$ when using rectangular windows.

6.3.4 Multicarrier Code Division

The multicarrier CDMA concept provides multiple ways that we might create a communications system by combining aspects of CDMA and OFDM. Just as there are multiple ways to assign chips to carriers in the multicarrier CDMA concept [66], there are also multiple ways to assign coded TC-OLA windows to carriers. These methods are essentially combinations of the code and frequency division multiple access schemes discussed above.

As an example, we might assign the same coded windows to each carrier, where the code symbol is assigned based on the carrier index as

$$s_u^{(mc,1)}[j] = \sum_{i=-\infty}^{\infty} w[j - iM] m_u[j - i(M - R)] \sum_{c=0}^{C-1} a_{c,u} e^{\imath 2\pi j c \Delta_f}, \tag{6.22}$$

$$s^{(mc,1)}[j] = \sum_{u=0}^{N-1} s_u^{(mc,1)}[j]. \tag{6.23}$$

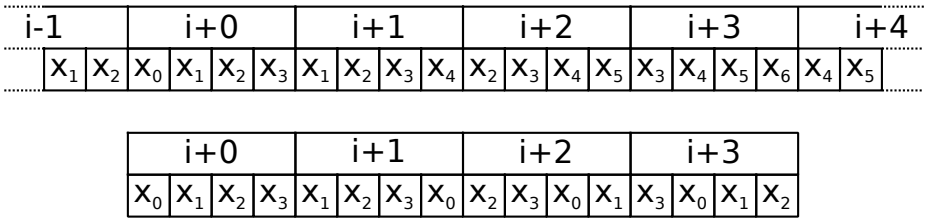

Figure 6.9: Illustrating stream (top) and circular (bottom) TC-OLA.

In a second instance we might assign sequential windows to sequential carriers as

$$s_u^{(mc,2)}[j] = \sum_{i=-\infty}^{\infty} w[j - iM] \sum_{c=0}^{C-1} a_{c,u} m_u[j - (Ci + c)(M - R)] e^{\imath 2\pi j c \Delta_f}, \tag{6.24}$$

$$s^{(mc,2)}[j] = \sum_{u=0}^{N-1} s_u^{(mc,2)}[j]. \tag{6.25}$$

All of the combinations in [66] should have a parallel for TC-OLA. Analysis of any potential benefits resulting from the combination of code and frequency division in a TC-OLA context is identified as an area for future work in Section 6.11.2.

6.4 Circular TC-OLA

It was recognized early on in this work that the process of transmitting a burst of data (rather than a continuous stream) was incredibly inefficient, especially when the burst size is short and the spreading ratio is high. At the beginning of transmission windows are initially empty and new sample values are shifted in, creating a "head" of $\frac{M}{R}$ windows. Similarly, there is a "tail" of $\frac{M}{R}$ windows as the final samples are shifted out. A variant called circular TC-OLA was developed to improve this burst efficiency problem. The scheme is illustrated in Figure 6.9.

This construction makes it easier to support bursty or packet-based transmission, with the constraint that at least $\frac{M}{R}$ windows must be sent. These $\frac{M}{R}$ windows are overlap added into a circular buffer (instead of a linear buffer) to recover the message signal.

6.5 Offset TC-OLA

In Chapter 2 the windows were separated by a short exponential sine sweep, Barker code, or other timing marker. This had the advantage of providing a straightforward method of timing recovery as well as a coarse estimate of the channel condition. However, this scheme in not efficient in terms of channel utilization. The real TC-OLA signal developed in Chapter 3 removes the space between windows to increase the efficiency in terms of channel utilization but creates a DSB-SC type signal which has only 50% spectral efficiency. This real TC-OLA signal can be used to create a more efficient scheme by multiplexing two signals in quadrature, similar to the way that QPSK can be considered as two BPSK signals in quadrature. Consider the discrete complex baseband signal consisting of two independent TC-OLA signals $s_1[j]$ and $s_2[j]$ which are transmitted in phase and in quadrature, respectively:

$$s[j] = s_1[j] + is_2\left[j - \frac{M}{2}\right] \tag{6.26}$$

$$= s_I[j] + is_Q[j] \tag{6.27}$$

In this formulation, the transmitted signal will have a constant envelope in the case that the input signals $m_1[k]$ and $m_2[k]$ also have equal constant envelopes as illustrated in (6.28) and Figure 6.10. Another way to obtain a more constant envelope and more efficient channel utilization is to make use of the overlapping RRC windows described in Section 6.1.1 with a complex input signal.

$$\left|A\left|\cos\frac{\pi j}{M}\right| + i\left|\sin\frac{\pi j}{M}\right|\right| = A \tag{6.28}$$

The advantage of constant envelope is to reduce the linearity requirements for the power amplifier stage. The other benefit of this scheme is that the periodic phase shift between the in-phase and quadrature axes allows the receiver to track the frequency and phase of the signal and to determine the window boundaries.

In (6.26) the quadrature component is delayed by $\frac{M}{2}$. At the receiver, we can delay the in-phase component by $\frac{M}{2}$ in order to regain the original relative time alignment of $m_1[k]$ and $m_2[k]$. However, it is ambiguous at the receiver as to which series of windows is intended to be in phase and which is in quadrature. Consider the case where

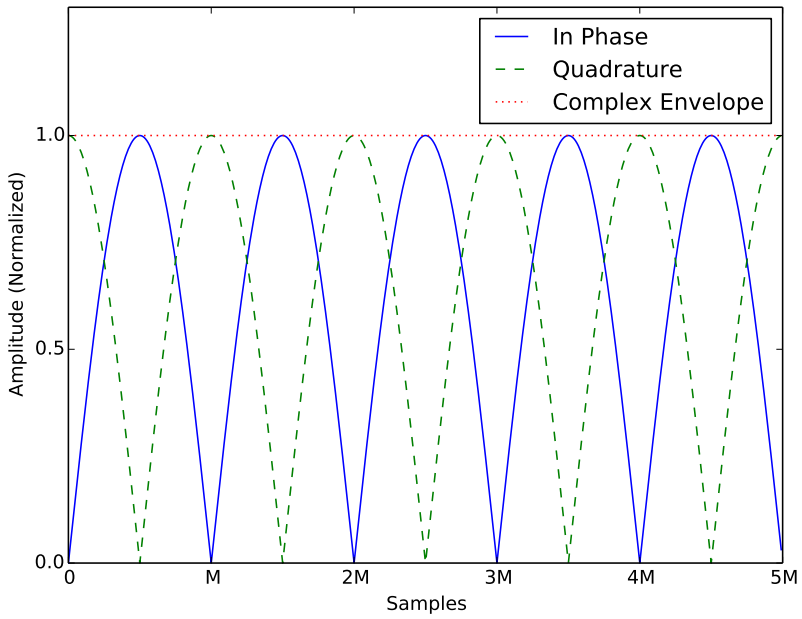

Figure 6.10: Offset Window Functions Showing Constant Envelope

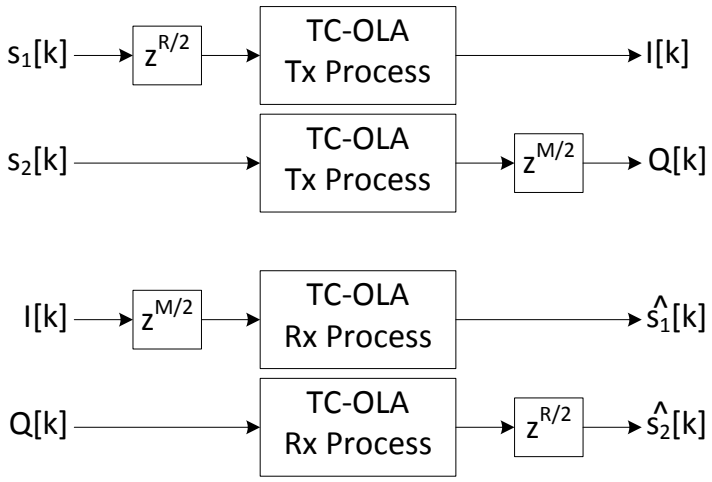

Figure 6.11: Offset TC-OLA transmitter and receiver, showing additional delays to maintain time alignment.

the transmitter's in-phase channel is received on the quadrature channel. Instead of both channels experiencing an additional delay of $\frac{M}{2}$, this channel experiences an additional delay of M while the other channel experiences none. To solve this issue we note that a delay of M at f_2 is equivalent to a delay of R at f_1. An additional delay of $\frac{R}{2}$ is added to both the transmitter and the receiver (Figure 6.11). This ensures that relative time alignment between $\widehat{m}_1[k]$ and $\widehat{m}_2[k]$ is maintained at the receiver output regardless of the receiver's channel orientation relative to the transmitter. This adds an additional constraint to Offset TC-OLA that the hop size must be divisible by 2. This system is considered in Section 6.11.1 regarding potential patent claims.

6.5.1 Phase and Frequency Synchronization

To synchronize phase and frequency offset we first consider the periodic phase shift of the window functions introduced in Figure 6.10. The phase relative to a copy of the signal delayed by $\frac{M}{2}$ samples produces a triangle wave with amplitude $\frac{\pi}{2}$ as shown in Figure 6.12. This triangle wave can be produced by multiplying with the conjugate of the delayed version and taking the argument as in (6.30).

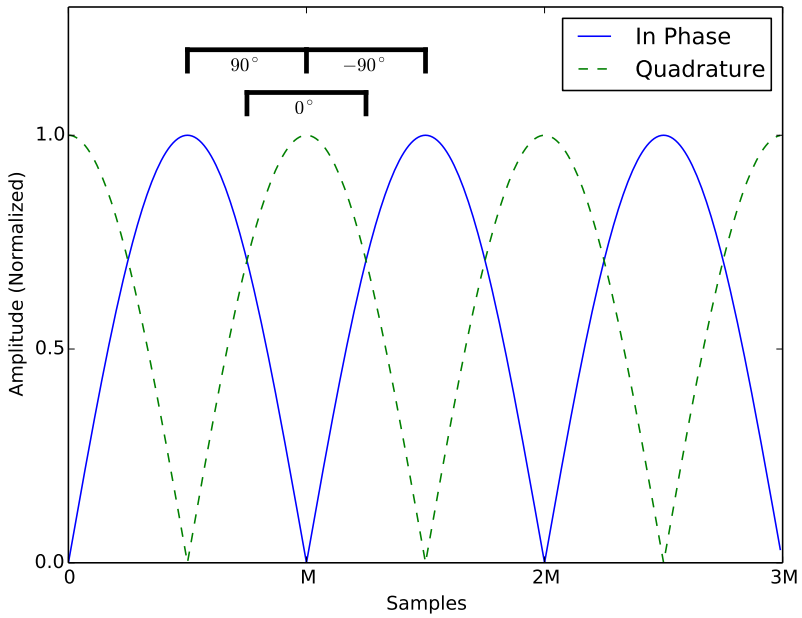

Figure 6.12: Offset Window Functions Showing Relative Angle at a distance of $\frac{M}{2}$ samples. This periodic phase shift is used to track phase offset of the TC-OLA signal.

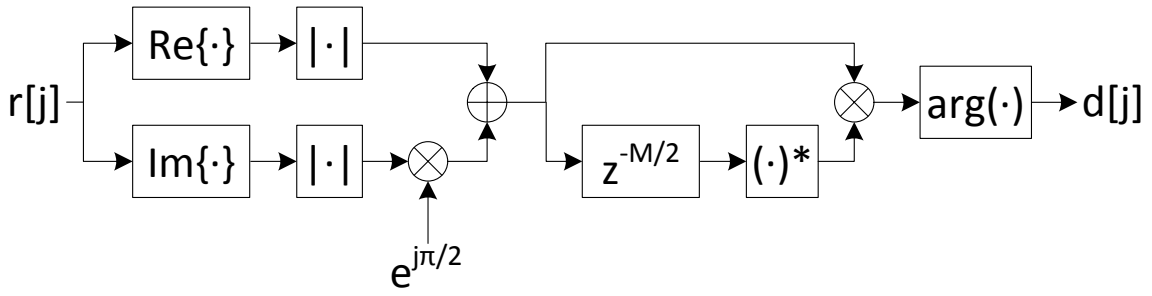

Figure 6.13: Offset TC-OLA detector circuit. Produces a triangle wave at the window frequency when the TC-OLA signal is aligned with the I/Q axes.

$$sync[j] = \angle \left[\left(\left| \cos \frac{\pi j}{M} \right| + \imath \left| \sin \frac{\pi j}{M} \right| \right) \left(\left| \sin \frac{\pi j}{M} \right| - \imath \left| \cos \frac{\pi j}{M} \right| \right) \right] \tag{6.29}$$

$$= \angle \left[\left| \sin \frac{2\pi j}{M} \right| - \imath \cos \frac{2\pi j}{M} \right] \tag{6.30}$$

In practice the TC-OLA signal will carry a bipolar signal. To manage this we add an absolute value operation, resulting in the detector circuit of Figure 6.13. This circuit produces a triangle wave at the window frequency only when the TC-OLA signal is aligned with the I/Q axes.

Assume that the transmitted signal has rotated in the channel by angle θ such that the signal is received as in (6.31). Given an input signal of unmodulated windows, the output of the detection circuit shall be as in (6.32). For a TC-OLA transporting a practical signal such as QPSK this can be made approximately true by the use of a short smoothing filter at the output of each of the absolute value operations in Figure 6.13.

$$r[j] = (s_I[j] + i s_Q[j]) e^{i\theta} \tag{6.31}$$

$$d[j] = \angle \left[\frac{1}{2} \left(\left| \sin \frac{2\pi j}{M} - \sin 2\theta \right| + \left| \sin \frac{2\pi j}{M} + \sin 2\theta \right| \right) + i \frac{1}{2} \left(\left| \cos \frac{2\pi j}{M} - \cos 2\theta \right| - \left| \cos \frac{2\pi j}{M} + \cos 2\theta \right| \right) \right] \tag{6.32}$$

We shall now inspect two cases. The first is for $\theta = n\frac{\pi}{2}$:

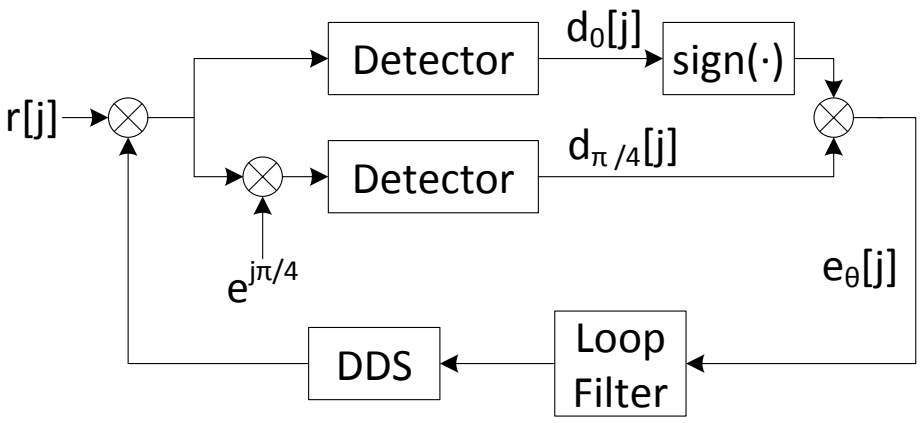

Figure 6.14: TC-OLA Phase Synchronizer. Two detectors are used, one at $0\,rad$ and the other at $\frac{\pi}{4}\,rad$. Their outputs are used to drive the error signal to a phase locked loop.

$$d[j]|_{\theta=n\frac{\pi}{2}} = \angle\left[\left|\sin\frac{2\pi j}{M}\right| - \imath\cos\frac{2\pi j}{M}\right] \tag{6.33}$$

The other case is for $\theta = \frac{\pi}{4} + n\frac{\pi}{2}$ which can easily be shown to be zero. It is with these two cases that we develop a phase synchronizer as in Figure 6.14. By duplicating the input signal with an I/Q rotation of $\frac{\pi}{4}$ it is possible to create a bipolar error signal using a simple rule:

$$e_\theta[j] = sign(d_0[j])d_{\pi/4}[j] \tag{6.34}$$

Standard PLL techniques [67] can then be used to synchronize to the phase of the received TC-OLA signal. It is clear that there is a $\frac{\pi}{2}$ ambiguity in the phase detector that must be resolved by the transported signal. However, the recovery circuit for the transported signal does not need to track all possible orientations, only the four possible axis alignments. This recovery circuit is considered in Section 6.11.1 regarding potential patent claims.

6.5.2 Window Synchronization

We observe that the triangle wave $d_0[j]$ generated by the phase synchronization circuit in the previous section maintains a constant alignment with the incoming window functions. The proposed solution is to track this generated triangle wave using a phase

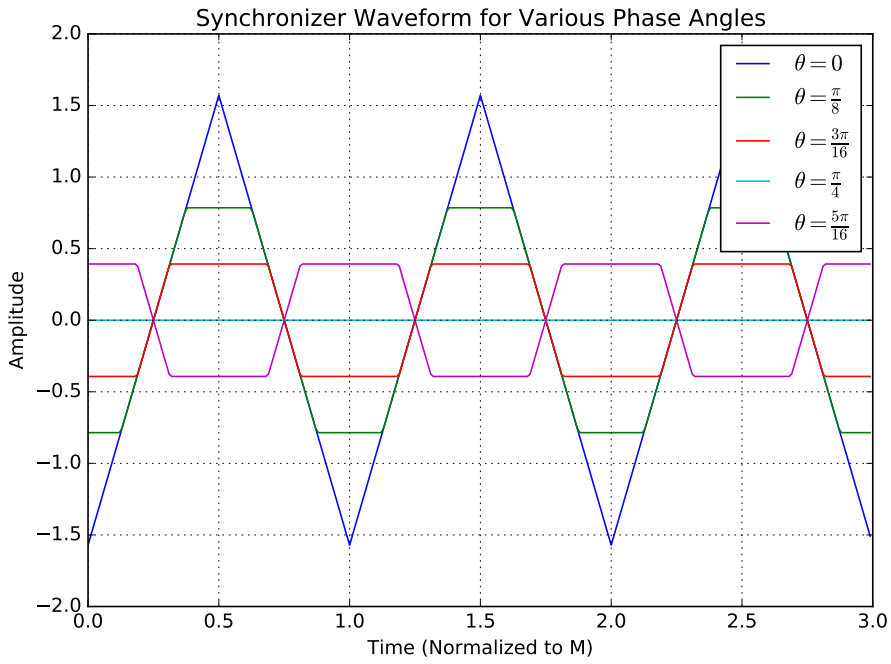

Figure 6.15: Synchronization waveform for different phase offsets. The synchronizer attempts to maximize the 0 radian branch and minimize the $\frac{\pi}{4}$ branch.

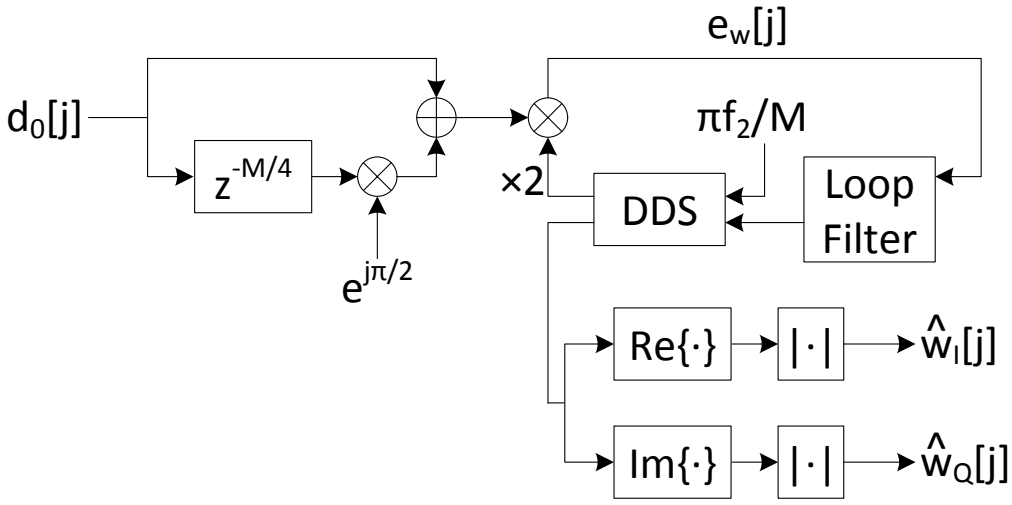

Figure 6.16: TC-OLA Window Synchronizer. A quadrature triangle wave is produced by means of additional delays. Estimates of the window functions are produced by taking the absolute value of the real and imaginary components separately.

locked loop as in Figure 6.16. A secondary output of the DDS provides estimates of the window functions $\widehat{w}_I[j]$ and $\widehat{w}_Q[j]$ by taking the absolute value.

A quadrature triangle wave is produced by means of additional delay. This mimics the quadrature component of a sine wave and helps to reduce oscillations in the error term $e_w[j]$ when the actual window frequency is near to the nominal frequency. When the actual window frequency differs from the nominal window frequency (due to sample rate mismatch) the magnitude of oscillations increases. This mismatch in rate also causes a phase shift between the received and locally generated window functions.

6.6 Timing Recovery

One method to recover timing in a multiuser downlink scenario where signals from all users are transmitted in a window-synchronous manner is to dedicate one channel to timing recovery and broadcast/control information. In the simplest case a known message sequence of $M - R$ samples can be transmitted on the trivial user's channel (code $\{1, 1, ...\}$ for code division or no frequency offset for frequency division). Due to the structure of the transmitted signal, the sequence repeats every $M - R$ samples

at the channel rate as well, completing $\frac{M}{R}+1$ repetitions every $\frac{M}{R}$ windows. This can be considered a special case of TC-OLA where, when rectangular windows are used, the low-rate message signal and the high-rate transmitted signal are identical except for the sample rate.

The known sequence should ideally cover most of the message bandwidth and have good correlation properties. A Chu sequence [68] is a good candidate for the known sequence as it meets these criteria and can also usefully be used to estimate the equivalent low rate channel $\widehat{c}[k]$ by correlating the known sequence against the receiver output for the trivial user.

6.6.1 Sample Frequency Offset

In Chapter 2 the sample clock drift is mentioned as a possible issue. In the practical sections of that chapter, independent GPS disciplined oscillators were used and found to be stable enough to perform the experiments. Some applications may not be able to use GPS easily, such as industrial networks, underground networks, etc. These applications may require some method of synchronizing the sample frequencies.

Audio-motivated procedures such as resampling may be too processor-intensive to be practical. Another method is to provide feedback to the ADC sample clock oscillator based on the synchronization state. Another method is to manipulate the offset of the window function at the channel rate. For example, the basic time-shifting receiver model could be modified as

$$\widehat{m}[k] = \sum_{i=-\infty}^{\infty} w[k - iR]r[k + i(M - R) + \xi_i], \tag{6.35}$$

where ξ_i is some small (positive or negative) integer. Ideally ξ_i is limited to the values $\{-1, 0, 1\}$ which mimics the periodic insertion or deletion of a sample (rob/stuff) used to maintain timing in some OFDM synchronizers [69]. From the analogous OFDM results, one might expect this approach to haver lower complexity than feedback correction of the oscillator frequency while also having lower performance.

6.6.2 Parameter Estimation

A simple method for estimation of the TC-OLA spreading parameter $\frac{M}{R}$ for a single user is sometimes possible by inspecting the autocorrelation function. Assume a

message signal with a range of frequency content and an autocorrelation function that is much shorter than the window time T_w. Based on the structure of the transmitted signal, one can expect $\frac{M}{R}$ autocorrelation peaks would be observed, spaced by $M-R$ samples. Each peak has lower amplitude than the last as the repeated portion in each successive window is reduced and more new content is added. This method can also be used to estimate the frequency offset within a certain range by phase rotation of successive peaks, and window timing. Once multiple users are involved this simple method is no longer reliable.

6.7 Window Weighting

Applying a weighting function to each window as a method of optimizing some aspect of TC-OLA was mentioned in Chapter 2 and is also granted in claim 41 of the patent. Until now windows have been combined without any weighting which we can liken to an equal gain combining (EGC) scheme. Other diversity combining schemes such as MRC could be explored in this context. Two window weighting concepts that were explored in the course of this work are channel inversion, where the weight is the inverse of the channel gain, and window discard, where the weight is simply a binary mask.

6.7.1 Channel Inversion

Under Rayleigh fading, the output SNR with channel inversion is distributed as the harmonic mean of exponential random variables. This problem bears similarity to the problems encountered in the context of multihop relay systems [70, 71]. Using the results for the linear combination of inverse Gamma distributed random variables from [72] we can write the characteristic function for the distribution of $X = \frac{1}{G^2}$ as

$$\phi_X(t) = \frac{\sqrt{-\mathrm{j}\,2t}}{\sigma} K_1\left(\frac{\sqrt{-\mathrm{j}\,2t}}{\sigma}\right) \tag{6.36}$$

where $K_1(\cdot)$ is the first-order modified Bessel function of the second kind.

To simplify the SINR analysis for non-rectangular windows, a weighting coefficient $w_c^2[k]$ is defined that measures the contribution from each overlapping window at the *centre* of the current window as shown in Figure 6.17. SINR values are then computed for the centre of the window only. This calculation is exact when $R = 1$ or

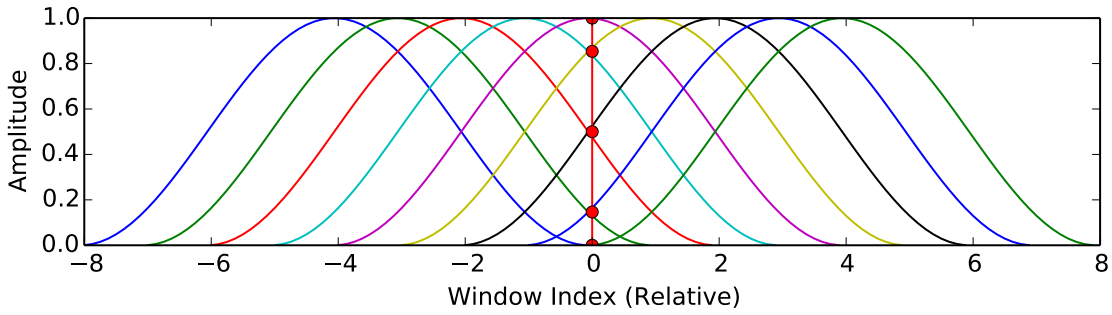

Figure 6.17: Illustrating values of the weighting function $w_c^2[k]$ as the contribution from each window that overlaps the current window.

a rectangular window is used, otherwise is a subsampled approximation.

The characteristic function of the weighted sum

$$Y = \sum_{j=-\frac{M}{2R}}^{\frac{M}{2R}} w_c^2[j]X \tag{6.37}$$

can be expressed as

$$\phi_Y(t) = \prod_{j=-\frac{M}{2R}}^{\frac{M}{2R}} \phi_X\left(w_c^2\left[j\right]t\right) \tag{6.38}$$

The output SNR can then be written as

$$\gamma = \frac{\left(\frac{M}{2R}\right)^2 \mathrm{E}\left[m_t^2[k]\right]}{\sigma_n^2}\frac{1}{Y} \tag{6.39}$$

$$= \frac{\left(\frac{M}{2R}\right) \mathrm{E}\left[m_t^2[k]\right]}{\sigma_n^2}\frac{M}{2R}Z \tag{6.40}$$

$$= \gamma_0 \frac{M}{2R}Z \tag{6.41}$$

where we have the product of the SNR expression for AWGN as derived in Chapter 3 and the random variable Z scaled by $\frac{M}{2R}$.

Once again using the results from [72], the cumulative density function (cdf) of Z is:

$$F_Z(z) = \frac{1}{2} + \frac{1}{\pi}\int_0^\infty \Im\left(\frac{e^{-\mathrm{j}\frac{t}{z}}\phi_Y(t)}{t}\right)dt \tag{6.42}$$

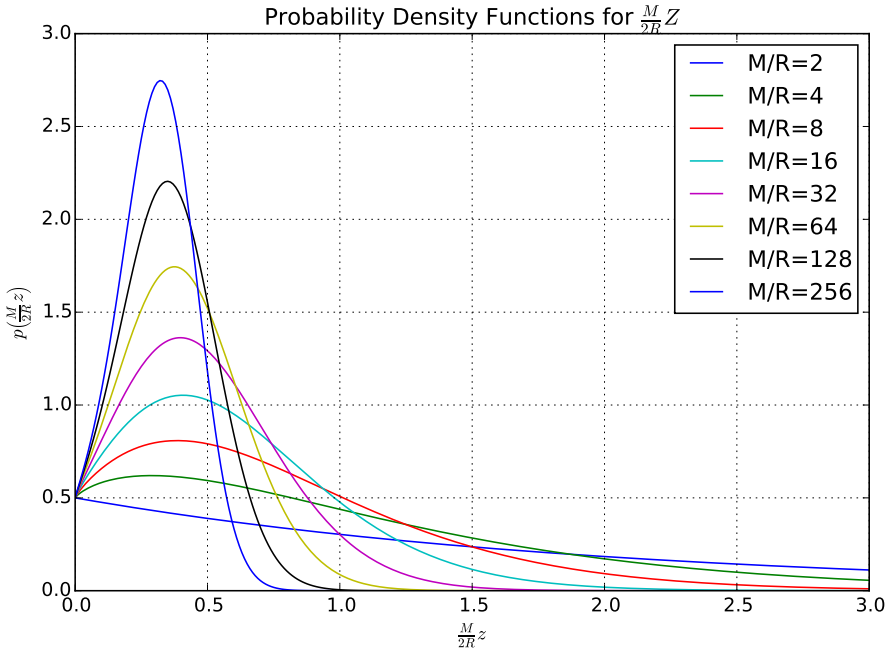

Figure 6.18: Probability density function of SNR with channel inversion, using sine windows.

and the probability density function (pdf) of Z can be written:

$$f_Z(z) = \frac{1}{\pi z^2} \int_0^\infty \Re\left(e^{-\mathrm{j}\frac{t}{z}}\phi_Y(t)\right) dt \tag{6.43}$$

The integral can be evaluated numerically. This has been plotted in Figure 6.18 for several values of $\frac{M}{R}$ with the pdf of Z scaled by $\frac{M}{2R}$. We can compare with the plotted results for two variables in [70] which have a similar characteristic shape. The pdf can then be used to compute the Shannon (ergodic) capacity of the system or the more practically useful capacity with outage [47].

6.7.2 Window Discard

There is an optimization problem to be solved where we may choose the weight (or discard) of a window based on its received SNR in order to maximize the output SINR. For a multiuser system this includes balancing the noise enhancement effect of simple channel inversion against the interference power impact of imperfect cancellation (loss of orthogonality) due to varying channel gain.

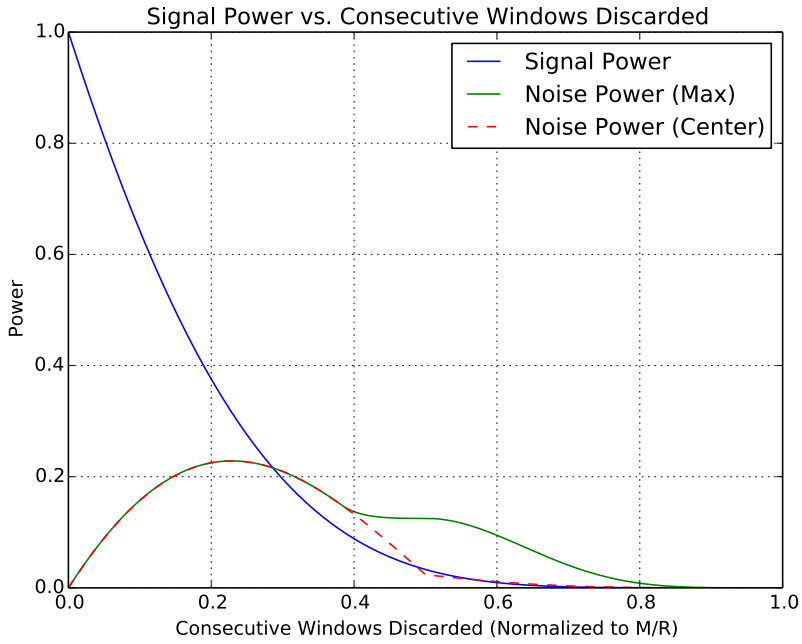

Figure 6.19: Signal and interference (noise) power for consecutive discarded windows.

To begin researching this approach, the signal and (interference) noise power as a function of the number of consecutive discarded windows was recorded as in Figure 6.19. One discard strategy is to allow up to 25% of any $\frac{M}{R}$ windows to be discarded, based on the peak interference power given in Figure 6.19. The discard decision is made by computing the output SINR with and without including the received window.

A basic simulation was done using this strategy, with results in Figure 6.20, showing ≈ 4 dB SINR gain over simple channel inversion. It was observed through experimentation that higher discard rates did not improve the mean output SINR but did increase the output SINR variance. Ideally an optimal weighting or discard strategy could be developed for multiuser systems that accounts for the received SNR and the impact of interference on the output due to time-varying channel gain.

6.8 Hardware Implementation

Although TC-OLA has been presented as a SDR-centric approach, there are some advantages to a hardware implementation. An example of the transmit hardware is shown in Figure 6.21. In an LPWAN scenario the endpoint could initiate a transfer

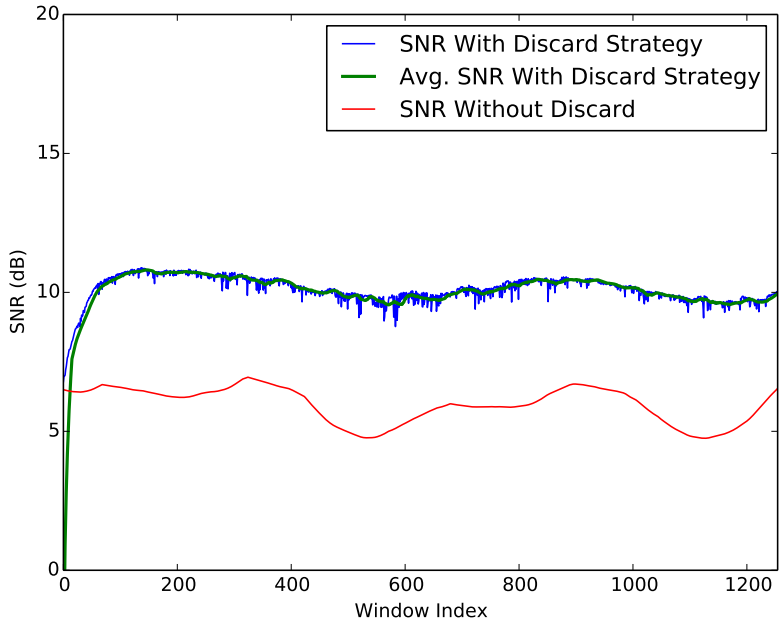

Figure 6.20: Simple discard strategy allowing up to 25% of windows to be discarded. This limit relates to the peak of the noise power curve in Figure 6.19. Above this discard rate the mean SNR was observed to stay relatively constant, but the variance increased, making higher discard rates impractical.

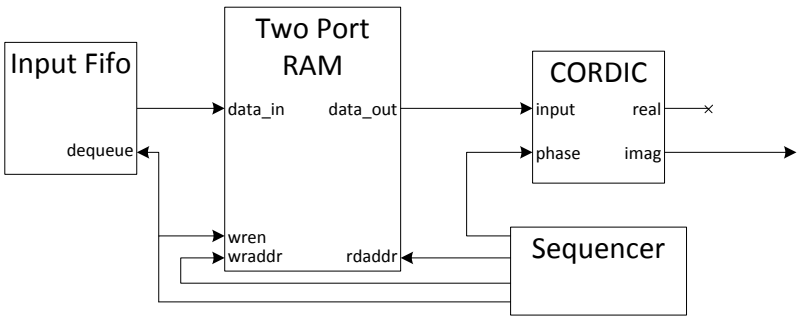

Figure 6.21: General Transmit Hardware. Data entering the input FIFO is written into the two-port RAM. The sequencer generates the read and write addresses while the CORDIC applies the sine window. In a rectangular window system the CORDIC is replaced with a pulse shaping filter.

of one packet using the circular TC-OLA concept of Section 6.4. The packet can then be transmitted without processor intervention. The processor can sleep (be powered down) for this interval as a method of energy savings working toward the goals of green communications [73, 74].

The coordinate rotation digital computer (CORDIC) block is used to apply the sine window without requiring a hardware multiplier. In a system using rectangular windows, this block is replaced by a pulse shaping filter.

When the system uses rectangular windows and transmits simple binary symbols (BPSK), a simplified hardware configuration can be used. This is shown in Figure 6.22 for $R = 1$, $M \in [4, 8]$. This configuration resembles a feedback shift register with $M - 1$ elements. Every M clock cycles the oldest symbol is replaced by a new symbol from the buffer. This approach easily generalizes to other values of M, $R > 1$, and the complex (QPSK) case. This is how the transmitter for the LPWAN system of Chapter 4 or the UWB system of Chapter 5 might be realized in practice. To perform circular TC-OLA as described in Section 6.4 the shift register can be preloaded with the first full window, which may include some predetermined pattern for the receiver to synchronize to.

The receiver hardware is shown in Figure 6.23. Phase and window synchronizers drive the phase to the sequencer and CORDIC if used. Once a memory cell's overlap-add operation is complete, the *valid* signal is asserted and the memory cell is reset to zero. The valid signal can be used to enqueue the data into a FIFO which can trigger

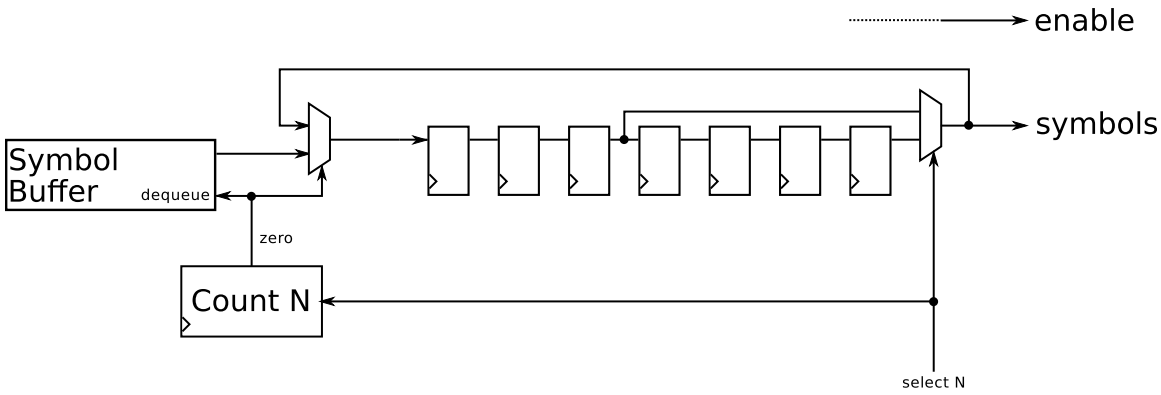

Figure 6.22: Transmit Hardware for Digital Symbols. Every M clock cycles the oldest symbol is replaced with a new symbol from the symbol buffer.

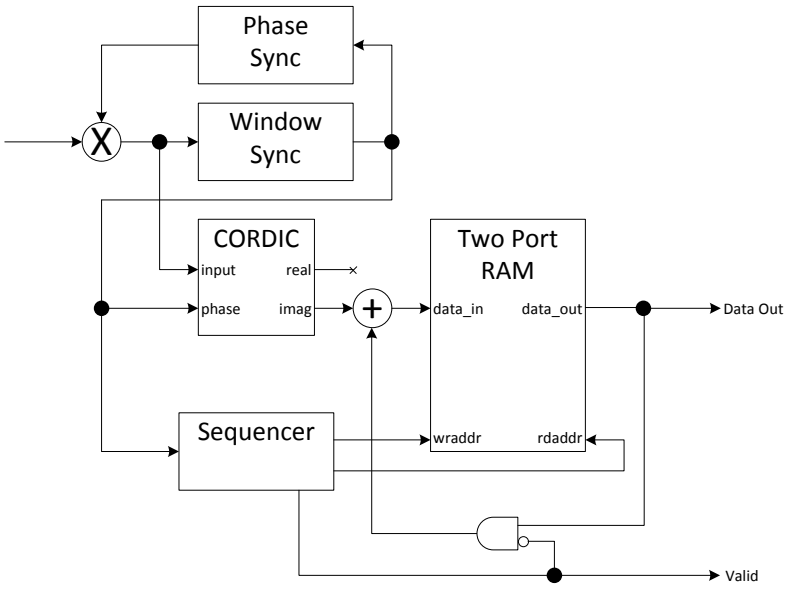

Figure 6.23: Receive Hardware. Phase and window synchronizers correct the phase rotation and drive the window phase to the sequencer. The sequencer controls the read and write addresses to the two-port RAM. When a memory cell's overlap-add accumulation is complete, the sequencer asserts the *valid* signal and resets the memory cell.

an interrupt at a certain fill level. The processor can then be woken up to process the received packet or stream.

6.9 Multiuser FDE

In Chapter 5 we explore extending the link budget through repetition under the specified UWB power constraints. The assumption is that adding another user (or stream, depending on the application) reduces the power available to each user under the total power constraint and thus does not improve the situation.

However, it is useful to note that this method can work with multiple streams. For the linear convolution to act as circular convolution, the phases at the beginning and end of the block must match. In reference to the construction of Figure 5.2, the codes $\{1, 1\}$ and $\{1, -1\}$ would satisfy this condition. It is possible that we generalize

this method to N users or streams with CP length

$$L_{CP} = M - NR \tag{6.44}$$

end block length

$$L_B = N\left(M - R\right), \tag{6.45}$$

with the additional constraint

$$\frac{M}{R} = kN, \;\; k = 1, 2, 3, ... \tag{6.46}$$

Where power constraints are not the main consideration, this approach has possibilities as a multiple access method applicable to UWB systems.

6.10 Novel Applications

This section summarizes some applications of TC-OLA which have not been considered in any of the previous work.

6.10.1 Multiple Antenna Systems

The use of multiple input multiple output (MIMO) in conjunction with TC-OLA is an obvious extension that has not been investigated in detail. Simple antenna selection combining was explored briefly in Chapter 4. This analysis could be extended to more general diversity combining techniques, possibly in combination with the window weighting techniques mentioned in Section 6.7.

Another multi-antenna concept is to consider the TC-OLA spreading in the spatial domain. One could place $\frac{M}{R}$ antennas, spaced at a distance d of

$$d = \frac{c\left(M - R\right)}{f_c}\, m, \tag{6.47}$$

where c is the speed of light, $c \approx 3 \times 10^8\, m/s$. For the case where $R = 1$, each antenna may be sampled at the message rate and then added, effectively performing the overlap-add process. With a proper phasing network it would be possible to sum the signals in the RF domain and then use only a single ADC to sample the line.

Technical challenges with this approach include the length of the required array,

alignment of the array elements with the propagation vector of the transmitted signal, and design of the phasing network if applicable. The overall length could be in the range of tens to hundreds of meters depending on the TC-OLA parameters. A deep space concept where a long array antenna trails behind a satellite could be one application of this technology.

6.10.2 Radar

Schemes such as pulse radar and pulse compression radar are essentially concerned with measuring the channel impulse response along some direction. The channel impulse response is then used to make estimates of target range, size, and velocity.

In Chapter 2 an exponential sweep waveform (similar to a chirp) was used to measure the impulse response of the laboratory as seen by the message signal, which is referred to as the equivalent channel. The equivalent channel concept is explored in depth in Chapter 4 in an LPWAN context. A basic approach is the special case of TC-OLA discussed in Section 6.6.

In principle, this same procedure can be used in a radar context. However, it remains to be seen whether the TC-OLA features of channel averaging and splitting of delayed components into two paths as per the analysis in Chapter 4 will be a benefit or a hindrance to radar processing.

6.10.3 Cognitive Radio

Dynamic manipulation of the TC-OLA parameters based on channel condition is granted in claim 6 of the patent. Changing the TC-OLA spreading factor $\frac{M}{R}$ while maintaining the message rate f_m naturally changes the bandwidth of the transmitted signal, which may logically extend into cognitive radio (CR) applications. During the course of operation, the CR may decide on a lower spreading ratio in order to act as a narrowband signal while the spectrum is free of primary users. When the spectrum contains active primary users it could transition to a higher spreading ratio in order to minimize interference.

This process could be made transparent to the underlying modulation format. For example, the underlying modulation could be a legacy baseband quadrature phase shift keying (QPSK) modulator which is not aware of the action of the CR component of the system.

To operate in the wideband mode with narrowband primary users it is necessary to understand the impact of the interference to the TC-OLA system as well as to the primary users. This type of analysis approach has been undertaken for coexistence of IR-UWB and narrowband users in [75] and could be extended to the TC-OLA case.

6.10.4 Audio Reverb

This technique could be used to construct a simulated reverb processing unit for audio recording applications as a complement to plate, spring, and convolution reverb processing. In much the same way that objects are scaled down for radar cross-section measurement, a scaled-down reverb environment could be constructed. The transmit and receive antennas as well as objects in the environment could be manipulated manually or mechanically to change the arrangement of reflections.

The ability to change the spreading ratio (and thus the bandwidth) makes it possible to scale the effective size of the reverb environment. The redundancy added during the spreading ensures that a high RF power is not required, which would not be welcome in an audio recording studio.

6.10.5 Hybrid Analog/Digital Broadcast

In some scenarios we might use this technique to transmit a digital version and an analog version of the same program material. Since the TC-OLA technique is amenable to either, the analog version may be used as a failover in the case that equalization or accurate timing recovery become difficult and the receiver can not maintain an acceptable BER.

As with [8], the perceived echo added to the analog signal does not make the speech unintelligible whereas the same effect in digital transmission requires an equalizer to limit the ISI to an acceptable level. In early experiments, the observed effect of jitter in timing recovery for analog signals is a random modulation effect. This does not make the speech signal unintelligible either. Another effect of timing jitter is the cancellation of higher frequency components, which are important for digital signals but less important for analog voice signals.

6.11 Conclusions

This chapter summarizes aspects of this research that were not explored in Chapters 2–5. As this is somewhat of a "green field" area, there is a wide range of ideas here. Potential patent and analysis topics based on the ideas described here are summarized below. Some suggested publication topics based on the material presented here can be found at the end of this section.

6.11.1 Patent Concepts

Specific ideas identified for patent potential are:

Overlapping windows at channel rate as described in Section 6.1.1 using RRC windows. This is weakly covered by claim 1, which was granted, using the language *"transmitting the segments serially at a channel rate f_c that is higher than the message rate f_m, wherein the channel rate f_c is selected based on the predetermined length and overlap so as to accommodate redundancy associated with the division into overlapping segments."* While this does not explicitly state that the windows do not overlap at the channel rate, it is explicitly stated in claim 4. Several claims depend on claim 4, leaving this method somewhat open as it relates to the other possible techniques that are claimed.

Frequency domain equalization as described in Chapter 5 and Section 6.1.3. Although adaptive equalization is addressed in claim 8, it is dependent upon claim 4 which is a *transmitter* claim. Therefore, one could argue that this claim covers equalization at the transmitter only (precompensation) and does not cover the FDE receiver method leveraging the distributed CP property which has been shown to have advantages in Chapter 5.

Adaptive frequency domain equalization where the receiver may choose between the two methods presented in Chapter 5 without any change in the transmitted signal.

Scheduled TC-OLA as described in Chapter 4. Claim 11 and other code division claims can be extended to state that the particular codes in use may be assigned by a predetermined scheduling algorithm, random choice, or other method.

Frequency division multiplexing as described in Section 6.3.3. Claims 11, 12, 27 and 40 cover multiple access by code division. However, frequency offset is an alternative way to create orthogonal streams or users in this context which is not protected.

Hardware architecture described in Section 6.8 as an apparatus claim. A generalization on this arrangement of components is thought to be the minimal set required to create a TC-OLA hardware implementation.

Offset TC-OLA enhancements beyond claim 20, including the compensation circuit in Figure 6.11 and the timing recovery method and circuits described in Figures 6.13-6.16.

Circular TC-OLA as described in Section 6.4. This is essential as it solves the burst efficiency problem in TC-OLA but may only have weak protection under the existing claims.

CR applications as described in Section 6.10.3 as an extension to claim 6. The underlying modulation format may or may not be aware of the CR action. The application of dynamic window sizing allows the scheme to transition between narrowband operation and wideband "underlay" type applications without changing the underlying signal processing.

Hybrid analog/digital broadcast as described in Section 6.10.5.

Spatial spreading application as described in Section 6.10.1.

Audio reverb application as described in Section 6.10.4.

6.11.2 Analysis and Design Activities

Specific ideas identified for further analysis and design projects are:

Hardware implementation as described in Section 6.8. This system, especially the transmitter, could be realized in an FPGA. Receiver timing recovery may require software-based feedback to maintain synchronization as was done in Chapter 2, or some other scheme. This is an opportunity to do some SDR-oriented FPGA design, possibly making use of RF network-on-chip (RFNoC) technology. A flexible FPGA-based transmitter model makes it possible to move beyond simulation to a wide variety of practical experiments.

Synchronous TC-OLA/CDMA as a hybrid system where a TC-OLA and CDMA-type modulations coexist in a single base station at a single frequency. It can be expected that the TC-OLA window appears as a random sequence to the CDMA receiver. The overlap-add of $\frac{M}{R}$ coded CDMA symbols with random values are expected to appear to the TC-OLA receiver as a zero-mean random variable. An analysis of the mutual interference is valuable for determining coexistence with current-generation RPMA systems.

Timing recovery as described in Section 6.6 or another reliable method to find and maintain window and phase alignment. The analysis opportunity here is to develop and test a method of timing recovery that exploits the repetitive nature of the TC-OLA signal. This may have a completely novel implementation but would likely draw on synchronizers for both CDMA and OFDM.

Window weighting as described in Section 6.7. There are opportunities for analysis of overlap-add schemes beyond EGC, and for development of weighting or discard strategies that optimize the output SINR.

Radar applications as described in Section 6.10.2. The ability of TC-OLA to measure the average impulse response at the low rate (the *equivalent channel* from Chapter 4) without a high-speed correlator is a potential implementation advantage. The opportunity here is to see what benefit can be extracted from TC-OLA in this context and to further develop the equivalent channel analysis described in Chapter 4.

MIMO extensions to TC-OLA and exploration of any potential benefit of the combination of these techniques.

Multicarrier code division extension as described in Section 6.3.4. Opportunities include extension of the physical layer signal design in this direction, analysis of any potential advantages of this combination, system design and simulation.

IBI analysis when FDE is used as described in Chapter 5. We expect that the construction of TC-OLA prevents the effects of interblock interference (IBI) from disproportionately affecting symbols at the beginning of the block. Instead, we expect the effect of IBI to manifest more like OFDM, where the interference power is spread over the carriers. A more rigorous analysis of this effect is valuable in illustrating the benefit of TC-OLA.

Complexity analysis showing an in-depth comparison between TC-OLA with a software equalizer and a multi-finger rake receiver design.

Multiuser FDE as described in Section 6.9. There is an opportunity to fully explore the parameter space of this method and to find ideal applications, which are not necessarily limited to UWB applications.

Audio reverb device as described in Section 6.10.4. This project could be used as a useful opportunity to develop an FPGA-based TC-OLA system (Tx/Rx) which does not require timing recovery. This development is also useful as a TC-OLA-based radar system. Ideally the timing recovery portion could be added at a later time to create a working communications system.

6.11.3 Suggested Publications

Specific ideas presented here which are identified for future publications are:

An overview paper, in the style of an IEEE magazine article. The proposed article will summarize the work presented here and will help to address some of the publishing challenges we have faced. Some of the challenges are described in Appendix F.

An LPWAN implementation paper, using an array of USRPs to simulate a wireless sensor network using the bandwidths and frequencies of the system described in Chapter 4. The results from this exercise can then be compared against the theoretical results from Chapter 4. It should be noted that this was originally proposed and approved by the committee during the candidacy exam. However, discovery of the distributed CP property covered in Chapter 5 and the connections with IFDMA and other SC-FDE schemes was thought to be a more novel concept for inclusion in this dissertation.

A wideband implementation paper, ideally but not necessarily fitting the UWB 500 MHz criteria, depending on availability of suitable test hardware. What is required is a scenario where the delay spread is significant relative to the window time, in order to verify the FDE scheme proposed in Chapter 5. This could be seen as an extension to the experiment in Chapter 2, transmitting digital symbols instead of a sampled analog waveform and using FDE techniques to recover the symbols.

A more thorough analysis of narrowband TC-OLA, including:

- a comparison of offset TC-OLA as in Section 6.5 vs. RRC-windowed TC-OLA as in Section 6.1.1.
- an analysis of window weighting schemes beyond EGC, as in Section 6.7. This should include suggested algorithms for optimizing the output SINR.
- an exploration of the "code capacity" concept mentioned in Chapter 3, where the number of possible users in exceeds the number of orthogonal codes under some low Doppler conditions.

Although this scenario is not the ideal application for TC-OLA, some weakly time-dispersive channels such as the SUI models used in Chapter 4 approximate it. Additionally, the CR application described in Section 6.10.3 is conceived to operate in a narrowband regime when necessary. For these reasons it is worth exploring the narrowband performance of multiuser TC-OLA in some more detail.

Chapter 7

Conclusions

In this work a novel modulation scheme based on time compression and overlap-add was conceived as a simple way to create a wideband signal. In Chapter 2 we explore the method experimentally and provide some of the groundwork for further investigation. Specifically we look at the averaging effect of TC-OLA on time-varying channels, interference rejection, multiple access extensions, and two reference implementations. One implementation uses the wideband SDR receiver described in Appendix C to transmit over a very wideband channel, while the other uses off-the-shelf USRP hardware to transmit over a narrower bandwidth. With this work we experimentally confirm the practical applicability of this modulation scheme to SDR-based radio communications before setting out to perform further analytical work.

In Chapter 3 we develop the basic analytical tools in order to compute the AWGN processing gain and the basic performance in Rayleigh flat fading. The AWGN processing gain leads to the spread-spectrum interpretation of TC-OLA discussed in Section 6.1.2. We also develop a $\mathcal{Z}$-domain model which is used to compute the transmitted spectrum over a longer observation period. Although not explicitly stated in this chapter, the $\mathcal{Z}$-domain model also leads us to the matched filter interpretation discussed in Section 6.1.1.

In Chapter 4 we look at the LPWAN scenario as a potential application area for this technology. To evaluate this scenario we develop a matrix formulation for TC-OLA in time-dispersive channels. This greatly simplifies the analysis of the equivalent channel as seen by the message signal. We take advantage of the fact that channel models for this application are characterized by relatively low delay spread and very low Doppler spread. In this case the window time can easily be much longer than the delay spread, ensuring that mutual interference between users is kept to a min-

imum. A linear time-domain equalizer is applied at the message rate to reduce the intersymbol interference (ISI), which can easily be a flexible software-based implementation. We point out again the contrast with a rake receiver, where the number of fingers is typically a hardware parameter, which may be over- or under-designed for a particular situation.

We also contrast with [15], which states that scheduling is a system overhead that they wish to avoid in order to keep the system efficient. While it is true that scheduling is an unwanted overhead, there is also a significant technical burden in scheduling a Gold code system to chip-level accuracy and accounting for propagation times. Furthermore, even in a scheduled system, the practical maximum number of users in the uplink is limited by the dispersion of the channel. A TC-OLA system where codes are assigned randomly is subject to the same random access issues described in Appendix E.3, but not the time dispersion issue. A scheduled TC-OLA system has neither of these issues and as we have shown, more relaxed synchronization requirements.

Chapter 5 returns to the original UWB motivation, illustrating two ways in which the added redundancy can act as a built-in CP for use with FDE techniques. In the case where TC-OLA processing gain is used to extend the link budget, we have shown that the CP overhead can be eliminated. When the delay spread is very high it may not be practical to eliminate the CP completely, but we have shown that it is possible to obtain reasonable efficiency while using an fast Fourier transform (FFT) block length that is on the order of the maximum delay of the channel. We contrast this with typical SC-FDE systems, which require a CP on the order of the maximum delay of the channel and an FFT block length that is four or more times longer to maintain efficiency.

Chapter 6 provides a discussion on additional topics related to TC-OLA that were not investigated in detail or developed for publication. Many of these are still-open ended and hopefully lead to more detailed investigation resulting in further publications on this topic.

Finally, we again point out that at the time of this writing, 40 of the original 41 patent claims on this technology were allowed by the United States Patent and Trademark Office (USPTO) and the patent has been issued as U.S. Patent 9,479,216 [13].

Appendix A

Glossary of Symbols

Symbol	Description	Appears
M	Window size, in samples.	(2.1)
R	Hop size, in samples.	(2.1)
δ	Fractional hop size.	(2.1)
f_m	Message sample rate.	(2.2)
f_c	Channel sample rate.	(2.2)
β	Bandwidth spreading ratio.	(2.3)
$w[\cdot]$	Window function used in signal transmission.	(2.4)
k	Discrete time index for signals sampled at message or symbol rate, f_m.	(2.5)
C	COLA sum based on window shape $w[k]$, M and R.	(2.5)
i	Window index.	(2.5)
$\mathcal{F}(\cdot)$	Discrete Fourier Transform.	(2.8)
j	Discrete time index for signals sampled at channel rate, f_c.	(3.5)
$s[\cdot]$	Transmitted signal.	(3.5)
$r[\cdot]$	Received signal.	(3.6)
$n[\cdot]$	Additive white Gaussian noise (AWGN) process with variance σ_n^2.	(3.6)
$x_q[\cdot]$	Time varying channel gain, path q.	(3.6)
$\widehat{m}[\cdot]$	Recovered estimate of the message signal $m[\cdot]$.	(3.7)
σ_n^2	Variance of additive white Gaussian noise term at receiver input.	(3.12)

$\widehat{\sigma}_n^2$	Variance of additive white Gaussian noise term at receiver output.	(3.12)
G	TC-OLA AWGN processing gain.	(3.18)
μ_q	Mean of fading multipath component q.	(3.20)
$\widehat{\mu}_q$	Mean of fading multipath component q referenced to receiver output.	(3.20)
σ_q^2	Variance of fading multipath component q.	(3.21)
$\widehat{\sigma}_q^2$	Variance of fading multipath component q referenced to receiver output.	(3.21)
$H(z, M)$	TC-OLA equivalent filter for $R = 1$	(3.22)
$H(z, M, R, \phi)$	TC-OLA equivalent filter for phase ϕ, $\phi \in \{0..R-1\}$	(3.23)
$m_u[\cdot]$	Message signal associated with general user u.	(4.1)
$\widehat{n}[\cdot]$	Additive white Gaussian noise (AWGN) process with variance $\widehat{\sigma}_n^2$.	(4.9)
$a_{i,u}$	Code symbol associated with window i and user u.	(4.11)
$m_t[\cdot]$	Message signal associated with specific user t.	(4.14)
N_c	Number of chips in CDMA system.	(4.17)
N	Number of users in the system.	(4.17)
$c_{t,u}[\cdot]$	Channel experienced by user u referred to the phase and delay of user t.	(4.26)
$g_{n,u}[i]$	Gain of the n^{th} multipath component associated with segment i of user u.	(4.26)
$\tau_{n,u}[i]$	Delay of the n^{th} multipath component associated with segment i of user u.	(4.26)
$\widehat{c}_t[\cdot]$	Equivalent channel experienced by user t.	(4.39)
$\alpha_{n,t}$	Coefficient of delayed component n for equivalent channel $\widehat{c}_t[\cdot]$.	(4.39)
$\beta_{n,t}$	Coefficient of pre-echo component n for equivalent channel $\widehat{c}_t[\cdot]$.	(4.39)
$\widehat{i}_{t,u}[\cdot]$	Interference signal at the output of the receiver for user t due to user u.	(4.41)
μ_r	Mean of Rician fading channel envelope.	(4.44)
σ_r^2	Variance of Rician channel envelope.	(4.48)
$\bar{\gamma}$	Average SINR.	(4.50)
σ_g^2	Variance of complex Gaussian channel gain.	(4.51)

K	Rician K factor.	(4.54)
$R(\cdot)$	Autocorrelation function of fading process.	(4.59)
T_w	Window period, $T_w = \frac{M}{f_c}$.	(4.59)
η	Receiver efficiency.	(5.8)
L_B	Length of FFT block.	(5.9)
L_{CP}	Effective CP length.	(5.9)

Table A.1: General Symbols

Symbol	**Description**	**Appears**
$\mathbf{m}_{i,u}$	M-element column vector representing the i^{th} segment of $m_u[k]$.	(4.28)
$\mathbf{W}$	$M \times M$ matrix with the M-point window function $w[k]$ in each column.	(4.29)
$\mathbf{A}_{i,u}$	$M \times M$ diagonal matrix representing the set of code symbols for user u.	(4.30)
$\mathbf{S}_{a,u}$	$M \times M$ matrix representing the M most recently transmitted segments of $m_u[k]$.	(4.31)
$\mathbf{G}_{i,u}^{(n)}$	$M \times M$ diagonal matrix representing the most recent M block channel gains for multipath component n of $m_u[k]$.	(4.32)
$\mathbf{P}^{\tau}()$	Permutation operator for delay τ.	(4.33)
$\mathbf{C}_i$	Frequency-domain equalizer taps.	(5.14)

Table A.2: Vectors and Matrices

Appendix B

Generic Multipath Model

To study the system performance and behaviour in a variety of scenarios we assume a generic multipath channel with a continuous-time baseband model [47] as in (B.1). There are $P(t)$ *resolvable* multipath components, each with independent time-varying gain $|g_n(t)|$, phase $\phi'_n(t)$, and delay $\tau'_n(t)$.

$$c(\tau, t) = \sum_{n=0}^{P(t)} |g_n(t)| e^{-j\phi'_n(t)} \delta(\tau - \tau'_n(t)) \tag{B.1}$$

To simplify the analysis we make the assumption that these values are relatively constant over the duration of window i (block fading). The simplified discrete time model is expressed in (B.2) where the discrete version of τ'_n is specified in integer *samples*. To model a continuous time tap with arbitrary delay we may need to create additional adjacent taps with different gains in the discrete time model.

$$c[j, i] = \sum_{n=0}^{P[i]} |g_n[i]| e^{-j\phi'_n[i]} \delta[j - \tau'_n[i]] \tag{B.2}$$

Let us assume that we can recover timing and phase of one of the paths for user t. Without loss of generality we choose $n = 0$ as there is no constraint that $\tau'_n[i]|_{n\neq 0} > \tau'_0[i]$. However, in a variety of practical scenarios we expect this to be the case. For example, we may have a partial LOS (Rician) main path associated with $n = 0$ and a few Rayleigh fading paths that arrive later in time. The simplified model

with timing and phase recovery is then

$$c_{t,u}[j,i] = \sum_{n=0}^{P_t[i]} g_{n,u}[i]\delta[j - \tau_{n,u}[i]], \tag{B.3}$$

where

$$\tau_{n,u}[i] = \tau'_{n,u}[i] - \tau'_{0,t}[i] \tag{B.4}$$

and

$$e^{-\imath\phi_{n,u}[i]} = e^{-\imath(\phi'_{n,u}[i]-\phi'_{0,t}[i])}. \tag{B.5}$$

Appendix C

Wideband SDR Receiver

This appendix captures the design details of the wideband direct-sampling SDR used in the experiments described in Chapter 2. This design document was prepared as part of a directed study course entitled *ELEC 590: Advanced Software-Defined Radio*. It leverages my past professional experience as a VLSI engineer as well as knowledge of the SDR architectures studied in *ELEC 539A: Selected Topics in DSP: Software Defined Radio*.

This document does not describe the Linux kernel module developed for the device, which is heavily based on `user-peripheral-kmod` by Moritz Fischer [76]. It was extended for this project with guidance from [77] and help from Jonathon Pendlum, who had previously created some GNURadio hardware accelerators for the Zynq [78] as a stepping stone toward RFNoC [79]. The user API that interacts with the driver is also undocumented but a minimal usage example is provided below, along with the associated enumerated type definitions.

Listing C.1: Minimal Usage Example

```
1  ////////////////////////////////////////////////////////////////////////////
2  // Minimal ZRF Setup Example
3
4  ...
5  #include "zrf_sdr_api.h"
6
7  ////////////////////////////////////////////////////////////////////////////
8  // Callback data structure.
9  //
10 // Holds all context relevent to processing radio data for this application.
11 // If you have open file or socket handles, filter state, or other data that is
12 // updated in the callback it should be placed in this struct.
13 //
14 typedef struct cb_struct_t {
```

```
15      ...
16  } cb_struct_t;
17
18  ////////////////////////////////////////////////////////////////////////////
19  // Capture callback.
20  //
21  // This function is called whenever a buffer is filled.
22  // A single interleaved buffer is delivered except in 450MHz mode.
23  //
24  void rx_callback(UINT32 nsamples, UINT32 nbuffers, SINT16 **bufs, void *user_data)
25  {
26      cb_struct_t *cb_struct = (cb_struct_t *)user_data;
27      ...
28
29      // This function may perform some useful signal processing, write the data
30      // to a file, or write the data to a UDP socket for connecting with a
31      // GNURadio flowgraph running elsewhere.
32  }
33
34  ////////////////////////////////////////////////////////////////////////////
35  // Main program loop.
36  int main (int argc, char **argv)
37  {
38      ...
39      ZRF_ERROR        rc;        // Error code
40      zrf_sdr_handle_t h;         // SDR Handle
41      zrf_sdr_cfg_t    cfg;       // SDR Config Struct
42      cb_struct_t      cb_struct; // Callback struct
43
44      // Initialize the device handle
45      rc = zrf_sdr_handle_create(&h);
46
47      // Configure the device
48      if (ZRF_SUCCESS == rc)
49      {
50          cfg.zrf_sdr_cb    = rx_callback; // Pointer to callback function
51          cfg.cb_user_data  = &cb_struct;  // Pointer to callback user context
52          cfg.src_mode      = ...          // Input source (zrf_sdr_src_mode_t)
53          cfg.xfer_mode     = ...          // Transfer mode (zrf_sdr_xfer_mode_t)
54          cfg.xfer_size     = ...          // Buffer size (zrf_sdr_xfer_size_t)
55          cfg.frequency     = ...          // NCO Frequency (16 bit signed)
56          cfg.test_mode     = ...          // Test mode (boolean)
57          cfg.prbs_mode     = ...          // PRBS mode (boolean)
58          cfg.gap_count     = ...          // Gap counter (32 bit unsigned)
59          cfg.use_cic       = ...          // Enable CIC (boolean)
60          cfg.cic_rate      = ...          // CIC Decimation rate (8-bit unsigned)
61
62          // Initialize callback struct
63          ...
64
65          // Start the SDR given the handle and parameters
66          rc = zrf_sdr_start(h, &cfg);
67      }
```

```
68
69      // Main Loop.
70      if (ZRF_SUCCESS == rc)
71      {
72          while (run)
73          {
74              // Wait for stop condition
75              ...
76          }
77      }
78
79      // Shut down radio.
80      if (ZRF_SUCCESS == rc)
81      {
82          rc = zrf_sdr_handle_destroy(&h);
83      }
84
85      return rc;
86  }
87
88  //
89  // END OF CODE
90  //
```

Listing C.2: Enumerated Type Definitions

```
1   ////////////////////////////////////////////////////////////////////////////
2   // Data sources supported by the hardware.
3   typedef enum zrf_sdr_src_mode_t
4   {
5                               // Operational Modes:
6       ZRF_SDR_MODE_HB1,       // Halfband 1 (450MHz 2 lanes)
7       ZRF_SDR_MODE_HB2,       // Halfband 2 (225MHz 1 lane)
8       ZRF_SDR_MODE_HB3,       // Halfband 3 (<= 112.5MHz 1 lane)
9       ZRF_SDR_MODE_USER,      // From user-defined logic
10
11                              // Debug Modes:
12      ZRF_SDR_MODE_DIRECT0,   // Direct from RFRB lane 0
13      ZRF_SDR_MODE_DIRECT1,   // Direct from RFRB lane 1
14      ZRF_SDR_MODE_DIRECT2,   // Direct from RFRB lane 2
15      ZRF_SDR_MODE_DIRECT3,   // Direct from RFRB lane 3
16      ZRF_SDR_MODE_CONST,     // Constant value
17      ZRF_SDR_MODE_DIRECT0IQ, // Phase 0 900 MHz I/Q (lanes 0/1)
18      ZRF_SDR_MODE_DIRECT1IQ, // Phase 1 900 MHz I/Q (lanes 2/3)
19      ZRF_SDR_MODE_DIRECT01I, // 900 MHz I (lanes 0/2)
20      ZRF_SDR_MODE_DIRECT01Q, // 900 MHz Q (lanes 1/3)
21
22      LAST_SRC_MODE = ZRF_SDR_MODE_DIRECT01Q
23  } zrf_sdr_src_mode_t;
24
25  ////////////////////////////////////////////////////////////////////////////
26  // Transfer Sizes supported by the hardware. Smaller sizes may be supported,
27  // but are of little practical use.
```

```
28 typedef enum zrf_xfer_size_t
29 {
30     XFER_SIZE_1K = 12, // 2**12 bytes gives 2**10 complex 16-bit samples
31     XFER_SIZE_2K,
32     XFER_SIZE_4K,
33     XFER_SIZE_8K,
34     XFER_SIZE_16K,
35     XFER_SIZE_32K,
36     XFER_SIZE_64K,
37     XFER_SIZE_128K,
38     XFER_SIZE_256K,
39     XFER_SIZE_512K,
40     XFER_SIZE_1M,
41
42     LAST_XFER_SIZE = XFER_SIZE_1M
43 } zrf_xfer_size_t;
44
45 ////////////////////////////////////////////////////////////////////////////
46 // Transfer modes supported by the hardware.
47 typedef enum zrf_xfer_mode_t
48 {
49     XFER_MODE_SNGL, // Single Transfer
50     XFER_MODE_FILL, // Fill Region
51     XFER_MODE_CONT, // Continuous Transfer
52     XFER_MODE_GAP,  // Continuous Gapped Transfer
53
54     LAST_XFER_MODE = XFER_MODE_GAP
55 } zrf_xfer_mode_t;
56
57 //
58 // END OF CODE
59 //
```

RFRB-SDR FPGA Design Document

Stephen Harrison

Contents

1 Technical References **3**

2 Design Features **4**

3 Design Description **4**
3.1 Top-level Description . . . 4
3.2 Block Diagram . . . 5
3.3 Digital Mixer . . . 5
3.3.1 Functional Description . . . 5
3.3.2 Implementation Description . . . 6
3.4 4:1 Downsampler . . . 7
3.4.1 Functional Description . . . 7
3.4.2 Implementation Description . . . 9
3.5 Halfband Filters . . . 10
3.5.1 Functional Description . . . 10
3.5.2 Implementation Description . . . 10
3.6 Capture Controller . . . 11
3.6.1 Functional Description . . . 11
3.6.2 Implementation Description . . . 11

4 Register Description **12**
4.1 Virtex-4 Register File . . . 12
4.2 Zynq Register File . . . 13

5 Operation **15**
5.1 Power-On Sequence . . . 15
5.2 Interface Alignment . . . 16
5.3 Tuning Frequency . . . 16
5.4 Configuring Decimation . . . 17
5.5 Capture . . . 17

6 Clocking Description **18**
6.1 Virtex-4 Clocking . . . 18
6.2 Zynq Clocking . . . 19

7 Connector Description **19**
7.1 FMC Connector Description . . . 19

8 Debug Features **20**
8.1 PRBS Generators . . . 20
8.2 ADC Constant Value Input . . . 21
8.3 AXI Data Override . . . 21
8.4 LED Override . . . 21

List of Figures

1 RFRB-SDR Simplified Block Diagram 5
2 Digital Mixer Operation: Shifting the Spectrum -430 MHz 6
3 Digital Mixer Block Diagram 6
4 4:1 Downsampling Filter Frequency Response 8
5 4:1 Downsampling Filter Frequency Response, Illustrating Aliasing Effect 8
6 4:1 Downsampler Block Diagram 9
7 Halfband Filter Frequency Response, Illustrating Aliasing Effect 10
8 Single Capture Mode State Diagram 12
9 Virtex-4 Clocking Diagram 18
10 Zynq Clocking Diagram 19
11 Board-to-Board Connectivity Diagram 20

List of Tables

1 Virtex-4 Register Description 12
2 Zynq Register Description 14
3 User Logic Input Select 14
4 Lane 0 Input Select 14
5 Lane 1 Input Select 15
6 Transfer Modes 15
7 PRBS Generator Polynomials 20

1 Technical References

[1] *ADC12D1X00RFRB Reference Board Users' Guide.* Revision 1.0. National Semiconductor Corp., July 13, 2011.

[2] *ADC12D1800RF 12-Bit, Single 3.6 GSPS RF Sampling ADC Data Manual.* Texas Instruments, Inc., April 2013.

[3] *Zedboard Hardware User's Guide.* v1.1. Avnet, Inc., August 1, 2012.

[4] *Zynq-7000 All Programmable SoC Technical Reference Manual.* UG585 (v1.6.1). Xilinx, Inc., September 10, 2013.

[5] *7-Series FPGAs SelectIO Resources User Guide.* UG471 (v1.3). Xilinx, Inc., October 31, 2012.

[6] *7-Series FPGAs Clocking Resources User Guide.* UG472 (v1.8). Xilinx, Inc., August 7, 2013.

[7] *7-Series FPGAs Memory Resources User Guide.* UG473 (v1.8). Xilinx, Inc., August 7, 2013.

[8] *7-Series FPGAs Configurable Logic Block User Guide.* UG474 (v1.5). Xilinx, Inc., August 6, 2013.

[9] *7-Series FPGAs DSP48E1 Slice User Guide.* UG479 (v1.6). Xilinx, Inc., August 7, 2013.

[10] *XtremeDSP for Virtex-4 FPGAs.* UG073 (v2.7). Xilinx, Inc., May 15, 2008.

[11] *LogiCORE IP AXI DataMover v3.00a.* PG022 (v5.1). Xilinx, Inc., October 16, 2012.

2 Design Features

The RFRB-SDR receiver is a wideband direct-sampling software-defined radio receiver created from available evaluation modules. Features of the device include:

- 12-bit sampling at 3.6 GHz using interleaved 1.8 GHz ADCs.
- Tunable digital mixer with $\approx$ 55 kHz tuning step from DC to 1.8 GHz.
- Selectable output decimation from 8 (f_s = 450 MHz) to 4096 ($f_s \approx$ 879 kHz).
- Provisions for inserting custom FPGA processing blocks into the receive chain.

Potential applications for this device include:

- Wideband propagation experiments.
- Spectrum monitoring and detection of rare events.
- Wideband communications modes.
- High-speed data acquisition.
- Narrowband radio reception covering a wide frequency range.

3 Design Description

3.1 Top-level Description

The RFRB-SDR integrates the ADC12D1800RFRB from Texas Instruments and with the Zedboard from Avnet as shown in Figure 1. The ADC12D1800RFRB is an evaluation module for for the ADC12D1800 high-speed ADC and also carries a Virtex-4 XC4VLX25 FPGA. The Zedboard carries a Zynq 7Z020 all-programmable System on Chip (SoC) device which integrates programmable logic with two ARM processor cores. This document describes the design of the digital signal processing chain developed for this device.

The digital signal processing chain consists of a digital mixer, 4:1 downsampler, a series of halfband filters, and a CIC filter. Each of these filters can be bypassed to select different output bandwidths. The CIC filter has a programmable decimation rate from 1 to 256. Custom processing blocks can be connected into the datapath via AXI stream connections.

For status and control of the datapath there are register files in both FPGA devices that can be accessed by the ARM processor. The Virtex-4 register file is accessed through an SPI interface

while the register file in the Zynq is accessed through the system bus via an APB connection. Register descriptions are given in Section 4.

The capture controller manages data transfer into the on-board DDR memory and asserting the interrupt request line to the ARM processor. It has four flexible capture modes: single, fill, continuous, and gap. Buffer sizes up to $2^{20} \approx 1$ million complex 16-bit samples per transfer are supported.

3.2 Block Diagram

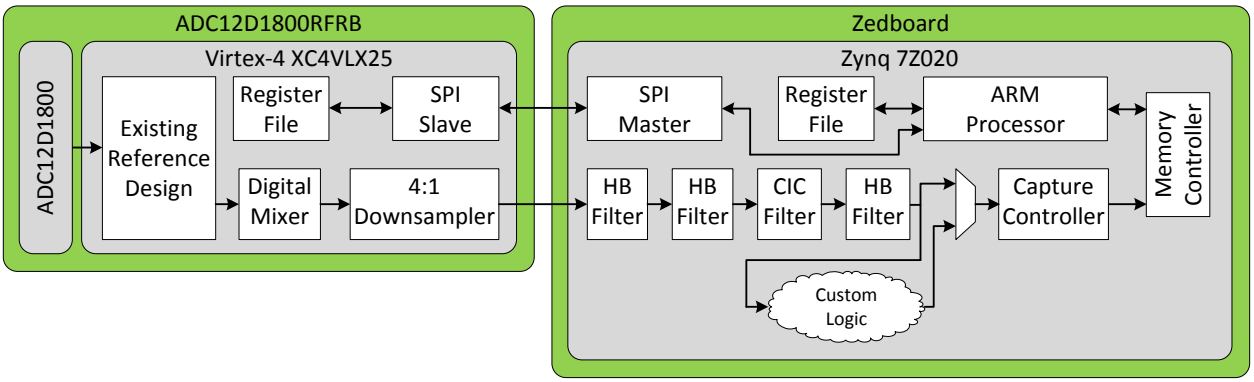

Figure 1: RFRB-SDR Simplified Block Diagram

3.3 Digital Mixer

3.3.1 Functional Description

The digital mixer receives a real data stream $x[n]$ sampled at 3.6 GHz and multiplies it with a complex exponential at frequency f_c as in Equation (1). This has the effect of shifting the spectrum by f_c, resulting in a complex output $y[n]$. This operation is the basis for creating a receiver that can easily be tuned to different frequencies. Figure 2 illustrates shifting the real (symmetric) input spectrum by -430 MHz to create a complex (asymmetric) output spectrum.

$$y[n] = x[n]e^{j\left(\frac{2\pi f_c n}{3.6\times10^9\ Hz}\right)} \tag{1}$$

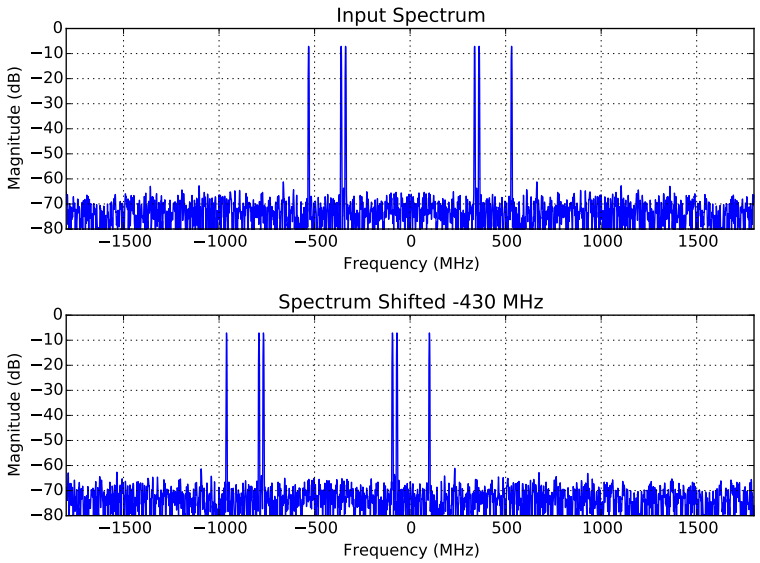

Figure 2: Digital Mixer Operation: Shifting the Spectrum -430 MHz

3.3.2 Implementation Description

The digital mixer is implemented using an array of 16 pipelined 12-bit CORDIC processors. The output is extended to 13 bits to accommodate the CORDIC gain factor of ≈ 1.647. Figure 3 shows a block diagram of the digital mixer implementation.

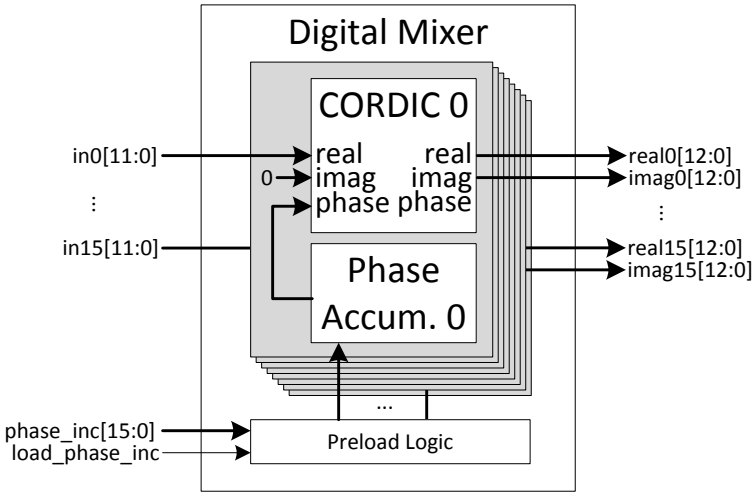

Figure 3: Digital Mixer Block Diagram

Each CORDIC processor has its own 16-bit phase accumulator. When `load_phase_inc` is asserted, the phase accumulators are preset to $N \times$`phase_inc` (where N is the phase number from 0 to 15). The phase accumulator for each CORDIC then adds 16$\times$`phase_inc` each clock cycle. The `phase_inc` value for a desired centre frequency f_c is calculated as in Equation (2).

$$phase\_inc = -Round\left(\frac{f_c\,Hz}{3.6 \times 10^9\,Hz} \times 2^{16}\right) \tag{2}$$

The minimum tuning step is calculated as in Equation (3). It should be noted that although the minimum tuning step is large, it is a factor of 16 smaller than the minimum output sample rate. Finer tuning increments can be realized with custom processing blocks or in software.

$$\frac{3.6 \times 10^9\,Hz}{2^{16}} = 54931.640625\,Hz \tag{3}$$

3.4 4:1 Downsampler

3.4.1 Functional Description

The 4:1 downsampler section reduces the sample rate from 3.6 GHz to 900 MHz. The design target for the cutoff frequency f_1 is 74% of the Nyquist rate at the lowest decimation setting as in Equation (4). The minimum stop band loss target is the signal to quantization noise (SQNR) of the ADC as in Equation (5).

$$f_1 = \frac{450\,MHz}{2} \times 0.74 = 166.5\,MHz \tag{4}$$

$$L_{stop} = 12\,bits \times 6.021\,dB/bit + 1.763\,dB = 74.015\,dB \tag{5}$$

The filter design uses the Remez exchange algorithm with one pass band and two stop bands to achieve the required performance with the available resources. The frequency response for the FIR filter is shown in Figure 4. An alternate view illustrating the aliasing effects after downsampling is shown in Figure 5.

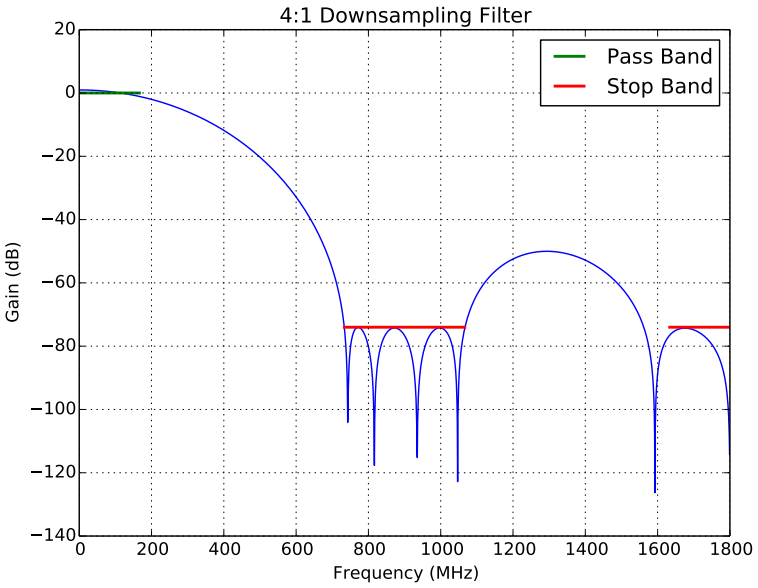

Figure 4: 4:1 Downsampling Filter Frequency Response

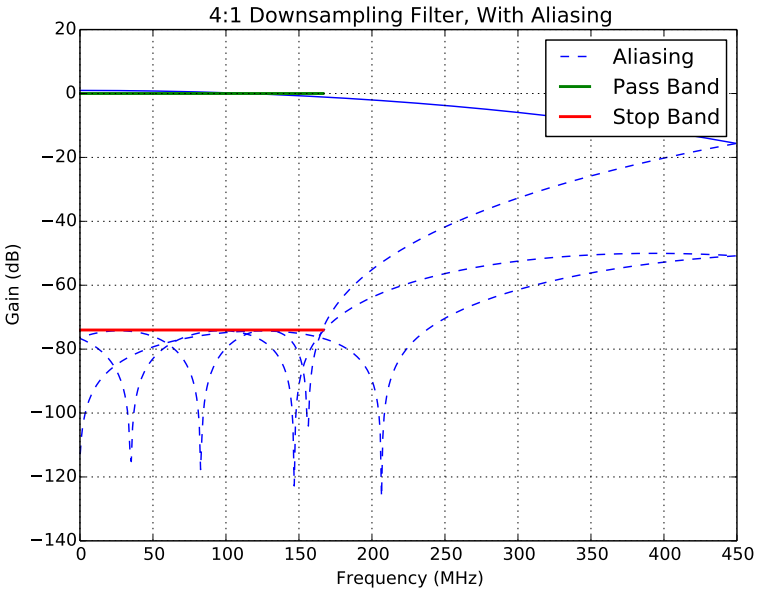

Figure 5: 4:1 Downsampling Filter Frequency Response, Illustrating Aliasing Effect

3.4.2 Implementation Description

The 4:1 downsampler is implemented using four 16:1 downsampler instances as shown in Figure 6. Each instance uses the 14-tap filter design described in the previous section, with a four-sample offset between each instance. Each instance uses six Virtex-4 DSP48 slices with a seventh coefficient realized by bit shifting. With eight total instances of the filter (four each for the in-phase and quadrature channels) the 4:1 downsampler block utilizes all 48 available DSP48 slices in the device. As the Virtex-4 version of the Xilinx DSP48 slice lacks a pre-adder, all pre-adders are implemented in the FPGA fabric.

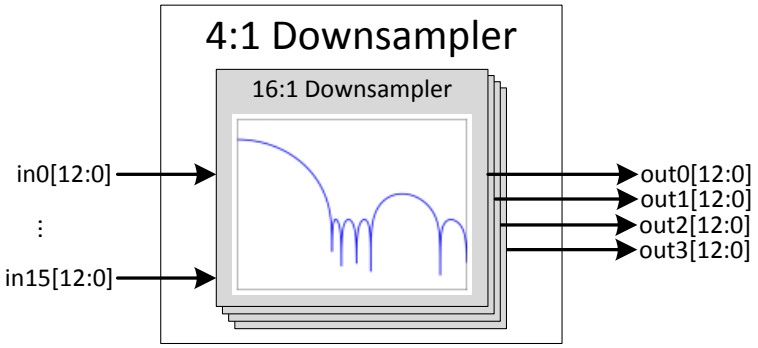

Figure 6: 4:1 Downsampler Block Diagram

Realizing one coefficient by bit shifting requires scaling all coefficients such that one coefficient is a power of two, which changes the overall gain of the filter. As mentioned previously, the data bus has been extended by one bit to accommodate the CORDIC gain. The maximum gain of this filter combined with the CORDIC gain must be less than 2. Thus the maximum gain of this filter after scaling can be calculated as in Equation (7).

$$G_{max} \leq \frac{2}{1.647} \tag{6}$$

$$\leq 1.214 \tag{7}$$

In this design the maximum filter gain after scaling was found to be 1.118 with an overall gain of 1.841 when accounting for the CORDIC gain.

3.5 Halfband Filters

3.5.1 Functional Description

Three halfband filters are implemented in the Zynq programmable logic. All three filters use the same design procedure although their implementation details differ. The band edge is configured for 74% of the Nyquist rate at the output of each filter. The frequency responses are shown in Figure 7.

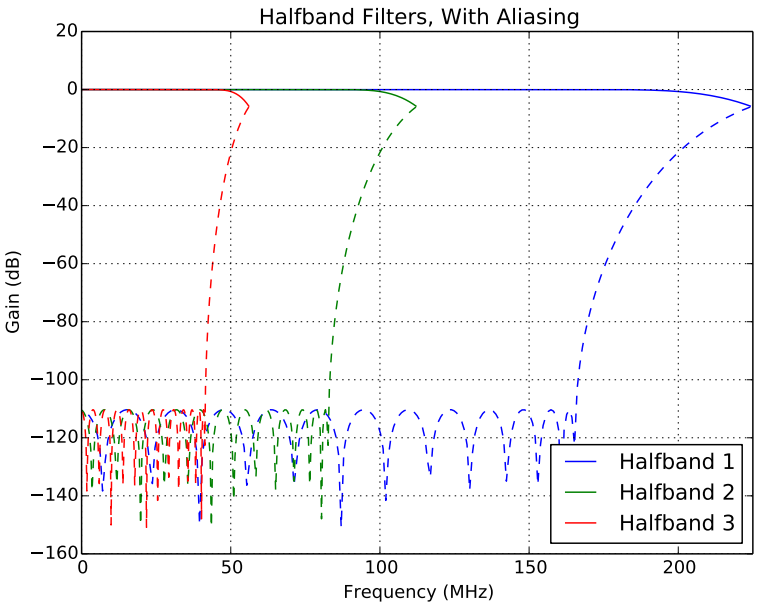

Figure 7: Halfband Filter Frequency Response, Illustrating Aliasing Effect

3.5.2 Implementation Description

Halfband 1 steps the sample rate down from 900 MHz to 450 MHz and steps the datapath down from four phases to two. Halfband 2 steps the sample rate down from 450 MHz to 225 MHz and steps the datapath down from two phases to one. Halfband 3 steps the sample rate down from 225 MHz to 125 MHz and is standard single phase filter. Halfband 3 has a `data_valid` input that is used to signal valid data at the input when the CIC decimation filter is enabled.

Each filter has 51 taps, with 24 taps equal to 0. The center coefficient of 0.5 is implemented by bit shifting. The remaining 26 taps are implemented using DSP48 resources. The 7-Series version of the DSP48 slice includes a preadder, and the symmetric filter is implemented using this technique. Each filter instance uses 13 DSP48 slices. In total the three complex halfband filters use 104 of the 220 available DSP48 slices in the Zynq 7Z020 device.

3.6 Capture Controller

3.6.1 Functional Description

The capture controller includes all the logic that manages transferring complex data samples to the Zynq memory subsystem. These samples are transferred by the memory subsystem into the on-board DDR memory where they can be retrieved by the ARM processor.

The controller has four capture modes which can be used for different applications. The single capture mode transfers a single buffer of data and stops. Similarly, the fill mode captures one or more buffers of data and transfers them to a contiguous block of memory. The continuous and gap modes transfer data until requested to stop. This is done using a double buffer scheme where one buffer is filled by the hardware while the other is processed by the software. The gap mode has an additional timer that must expire before the next transfer begins. This allows the user to take snapshots at a specified interval up to 28.6 seconds.

3.6.2 Implementation Description

The capture controller consists of the capture state machine and Xilinx AXI datamover IP. The capture state machine is used start and stop data capture by generating commands for the datamover based on the register configurations for address, transfer size, and capture mode. The AXI datamover is used to convert the 64-bit AXI data stream into 64-bit AXI memory-map format based on the commands it receives from the state machine.

When halfband 1 is selected as the data source ($f_s = 450MHz$) the quadrature channel is placed on a second 64-bit AXI bus connection to the memory subsystem. The in-phase and quadrature samples are written to different memory locations in this mode ($I \leftarrow$ `lane0_addrX`, $Q \leftarrow$ `lane1_addrX`). In all other modes in-phase and quadrature samples are interleaved in the buffers specified by `lane0_addrX`.

The single capture mode Mealy machine state diagram is shown as an example in Figure 8. Other modes have similar state diagrams with different state transition criteria. The gap mode has an additional state that waits for the timer to expire. The `cnt_preload` register value for a desired capture interval t_c can be calculated as in Equation (8). The maximum time interval can be calculated as in Equation (9).

$$cnt\_preload = Round\left(t_c \times 150\,MHz\right) \tag{8}$$

$$t_{c(max)} = \frac{2^{32} - 1}{150\,MHz} = 28.6331153\,s \tag{9}$$

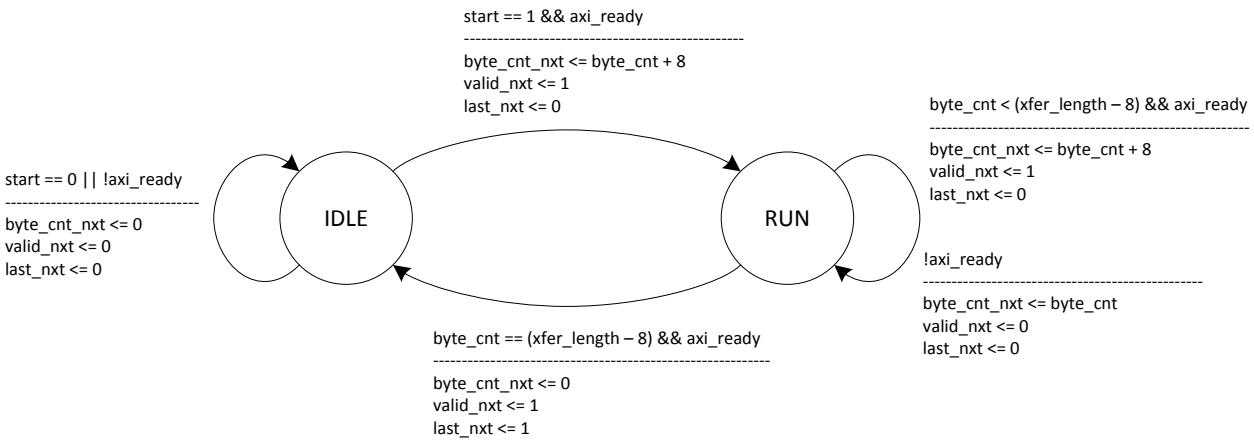

Figure 8: Single Capture Mode State Diagram

4 Register Description

4.1 Virtex-4 Register File

Address	Bits	Default	Type	Field	Description
0x0	24:16	0x0	R/W	led_override	Debug Feature: Enable override of on-board status LEDs (active high).
	8:0	0x0	R/W	led_value	Debug Feature: Set value of on-board status LEDs (active high).
0x1	4	0x0	R/W	zero_input	Debug Feature: Override ADC data with all zeros. Corresponds to a full-scale negative value after converting to signed two's-complement format.
	3:0	0x0	R/W	prbs_en	Debug Feature: Enable PRBS generator (one bit per lane, active high).
0x2	16	0x0	R/W	load_phase_inc	Load phase accumulator. Write to logic 1, write desired phase increment to phase_inc, write logic 0 to release.
	15:0	0x0	R/W	phase_inc	Phase increment for CORDIC.

Table 1: Virtex-4 Register Description

4.2 Zynq Register File

Address	Bits	Default	Type	Field	Description
0x00	3	0x0	R/W	axi_data_override	Debug Feature: Set lane 0 and lane 1 inputs to constant values.
	0	0x0	R/W	rfrb_if_iorstb	Input serdes IO reset (active low).
0x04	3:0	0xF	R/W	prbs_clr	Clear PRBS error counter, one bit per lane (active high).
0x08	31:0	X	R	err_cnt0	Lane 0 PRBS error count value.
0x0C	31:0	X	R	err_cnt1	Lane 1 PRBS error count value.
0x10	31:0	X	R	err_cnt2	Lane 2 PRBS error count value.
0x14	31:0	X	R	err_cnt3	Lane 3 PRBS error count value.
0x18	9:8	0x0	R/W	user_sel	Custom user logic input select. See Table 3.
	6:4	0x0	R/W	lane1_sel	Lane 1 input select. See Table 4.
	2:0	0x0	R/W	lane0_sel	Lane 0 input select. See Table 5.
0x1C	8	0x0	S/C	lane_en_update	Lane enable update. Self-clearing bit: Operation is complete when bit reads as logic 0.
	2	X	R	sm_busy	Capture state machine busy. Transfer is done when read as logic 0.
	1:0	0x0	R/W	lane_en	Lane enable, one bit per lane (active high).
0x20	6:5	0x0	R/W	xfer_mode	Set capture controller state machine transfer mode. See Table 6.
	4:0	0xC	R/W	xfer_length	Set capture controller transfer length in bytes. Buffer size is 2^{xfer_length} bytes. Each complex 16-bit sample is 4 bytes.
0x24	31:0	0x0	R/W	lane0_addr0	Physical memory address of buffer 0 on lane 0.
0x28	31:0	0x0	R/W	lane0_addr1	Physical memory address of buffer 1 on lane 0.
0x2C	31:0	0x0	R/W	lane1_addr0	Physical memory address of buffer 0 on lane 1.
0x30	31:0	0x0	R/W	lane1_addr1	Physical memory address of buffer 1 on lane 1.

Address	Bits	Default	Type	Field	Description
0x34	0	0x0	S/C	ps_en	Phase shifter enable. Self-clearing bit: Write logic 1 to clear. Operation is complete when bit reads as logic 0.
	1	0x0	R/W	psincdec	Phase shifter mode. 0 = Decrement, 1 = Increment.
	2	X	R	locked	MMCM locked status bit.
0x44	0	X	R	lane_state	Indicates which buffer is currently being filled by the hardware.
0x48	0	X	S/C	irq_clr	Interrupt clear. Self-clearing bit: Write logic 1 to clear. Operation is complete when bit reads logic 0.
0x4C	0	0x0	R/W	cnt_preload	Gap mode timer preload value.
0x50	8	0x0	R/W	use_cic	Enable CIC. 0 = Bypass, 1 = Enable.
	7:0	0x0	R/W	cic_decim_rate	CIC Decimation Rate. Real decimation rate is cic_decim_rate + 1.

Table 2: Zynq Register Description

Value	Description
0x0	Halfband 1 output is sent to custom user logic bus.
0x1	Halfband 2 output is sent to custom user logic bus.
0x2	Halfband 3 output is sent to custom user logic bus.
0x3	Unused

Table 3: User Logic Input Select

Value	Description
0x0	AXI memory lane 0 input is data lane 0
0x1	AXI memory lane 0 input is data lane 1
0x2	AXI memory lane 0 input is data lane 2
0x3	AXI memory lane 0 input is data lane 3
0x4	AXI memory lane 0 input is halfband 1, in-phase
0x5	AXI memory lane 0 input is halfband 2
0x6	AXI memory lane 0 input is halfband 3
0x7	AXI memory lane 0 input is custom user logic, bits 31:0

Table 4: Lane 0 Input Select

Value	Description
0x0	AXI memory lane 1 input is data lane 0
0x1	AXI memory lane 1 input is data lane 1
0x2	AXI memory lane 1 input is data lane 2
0x3	AXI memory lane 1 input is data lane 3
0x4	AXI memory lane 1 input is halfband 1, quadrature
0x5	Unused
0x6	Unused
0x7	AXI memory lane 1 input is custom user logic, bits 63:32

Table 5: Lane 1 Input Select

Value	Description
0x0	Single transfer mode. Transfer one buffer of size `xfer_length` bytes to address `laneX_addr0` and stop. Assert interrupt request when done.
0x1	Fill mode. Transfer buffers of size `xfer_length` bytes starting at address `laneX_addr0` and stopping at address `laneX_addr1`. Assert interrupt request when done.
0x2	Continuous transfer mode. Transfer buffers of size 2^{xfer_length} bytes alternating between addresses `laneX_addr0` and `laneX_addr1`. Assert the interrupt request after each transfer.
0x3	Gap transfer mode. The same as continuous mode, but wait for the gap timer to expire before starting the next transfer. The gap counter starts at the *beginning* of each capture cycle and must not be set to a value less than the time required to capture the buffer.

Table 6: Transfer Modes

5 Operation

5.1 Power-On Sequence

To release the device from reset, perform the following sequence:

1. Poll `locked` until the value reads logic 1 to ensure Zynq MMCM is locked to 450 MHz clock from Virtex-4.
2. Write logic 1 to `rfrb_if_iorstb` to release input SERDES from reset.

5.2 Interface Alignment

This sequence ensures the data and clock signals arriving from the ADC12D1800RFRB are correctly aligned in the Zynq device. To begin, write logic 1 to all bits of `prbs_en` to enable the PRBS generators on the ADC12D1800RFRB board. Write logic 1 to `psincdec` to increment the phase shift delay.

Repeat the following sequence until the error count on one or more lanes is non-zero:

1. Write logic 1 to `psen`.
2. Poll `psen` until logic 0 is read.
3. Write logic 1 to all bits of `prbs_clr` to clear PRBS error counts.
4. Write logic 0 to all bits of `prbs_clr` to release counters.
5. Read PRBS error counts from `err_cntX`.

Repeat the above sequence until the error count on all lanes is zero. Repeat the sequence below 20 times to center the clock transition in the data eye.

1. Write logic 1 to `psen`.
2. Poll `psen` until logic 0 is read.

Clear and check the PRBS error counters one last time, and then disable the PRBS generators by writing logic 0 to all bits of `prbs_en`.

5.3 Tuning Frequency

To tune the receiver, execute the following sequence:

1. Write logic 1 to `load_phase_inc`.
2. Write the desired value to `phase_inc` as in Equation (2).
3. Write logic 0 to `load_phase_inc`.

5.4 Configuring Decimation

To enable programmable decimation, execute the following sequence:

1. Write `0x6` to `lane0_sel` to source from halfband 3.
2. Write logic 1 to `use_cic` to enable the CIC filter.
3. Write the desired value to `cic_decim_rate`. Note that the actual decimation rate is `cic_decim_rate` + 1.

5.5 Capture

To begin a capture, ensure that the `laneX_addrX` fields are configured appropriately. 450 MHz output rate requires both lanes to be configured. All other modes require only lane 0. A contiguous memory region of size 2^{xfer_length} bytes must be allocated by the processor at each of the configured physical addresses. The memory regions may not overlap.

Select a transfer mode by writing to `xfer_mode`. The mode may be single, fill, gap or continuous as described in Table 6. The processor must be able to service the interrupt request and process the buffers fast enough for the selected combination of `xfer_length`, `xfer_mode`, configured decimation rate and capture interval.

To capture, execute the following sequence:

1. Poll `sm_busy` until it reads as logic 0.
2. Write `0x0` to `lane_en`.
3. Write logic 1 to `lane_en_update`.
4. If using halfband 1 as the data source, enable both lanes by writing `0x3` to `lane_en`, otherwise write `0x1`.
5. Write logic 1 to `lane_en_update`.

In single and fill modes the transfer is complete when `sm_busy` reads as logic 0.

In continuous and gap modes the interrupt request must be serviced after each transfer. To clear the interrupt request, write logic 1 to `irq_clr`.

In continuous and gap modes the transfer will stop when requested. To stop the capture, execute the following sequence:

1. Write `0x0` to `lane_en`.
2. Write logic 1 to `lane_en_update`.

The capture has stopped completely when `sm_busy` reads as logic 0.

6 Clocking Description

6.1 Virtex-4 Clocking

The clocking structure in the Virtex-4 device is shown in Figure 9. A 450 MHz clock is received from the ADC by a digital clock manager (DCM) tile and is used to operate the DDR I/O pads. The data is transferred to the 225 MHz clock domain through a FIFO that doubles the data width. Digital signal processing occurs in the 225 MHz domain.

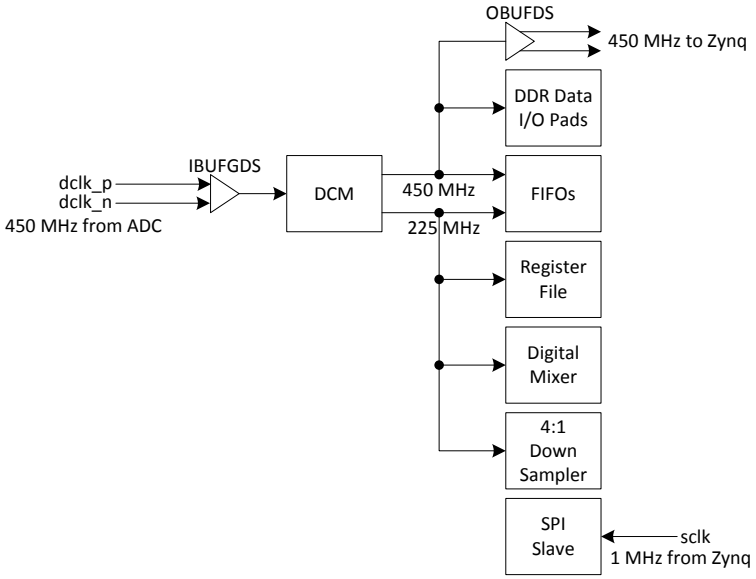

Figure 9: Virtex-4 Clocking Diagram

The SPI slave receives a 1 MHz clock from the Zynq device. This clock is not contrained to the 450 or 225 MHz clock. A bus synchronizer transfers data between the 1 MHz SPI clock domain and the 225 MHz register file clock domain.

6.2 Zynq Clocking

The clocking structure in the Zynq device is shown in Figure 10. The Zynq device receives a differential 450 MHz clock from the FMC port into a mixed-mode clock manager (MMCM) tile that produces 450 and 225 MHz clocks. The MMCM has dynamic phase shifting enabled to align the output clock with the data. Digital signal processing occurs in the 225 MHz clock domain.

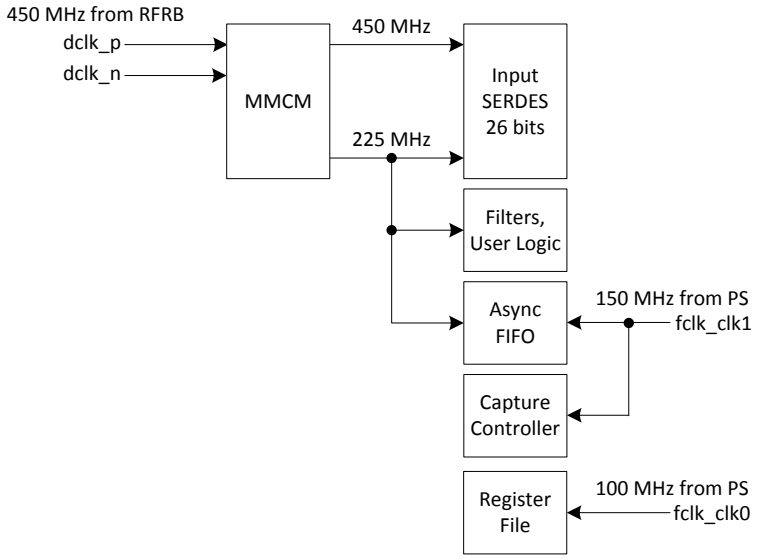

Figure 10: Zynq Clocking Diagram

The Zynq processing system (PS) bus operates at 150 MHz. An asynchronous FIFO transports data from the 225 MHz into the 150 MHz clock domain by doubling the data width.

The Zynq register file operates on the PS 100 MHz APB clock. Bit fields in this register file are synchronized to the appropriate clock domain as necessary.

7 Connector Description

7.1 FMC Connector Description

The connections between the ADC12D1800RFRB and the Zedboard are shown in Figure 11. Data lanes 0-3 are DDR differential pairs switching at 900 MHz. The 450 MHz clock is also provided as a differential pair. 100Ω differential termination must be enabled for these signals.

SPI signals are single-ended. The SPI interface operates at 1 MHz.

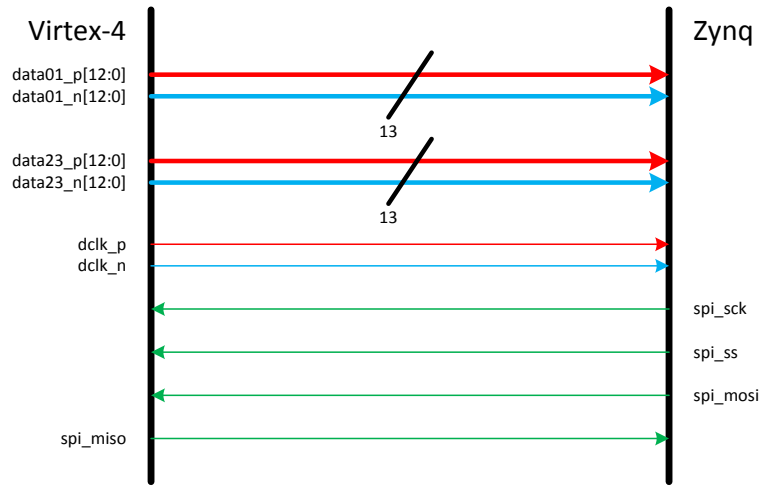

Figure 11: Board-to-Board Connectivity Diagram

8 Debug Features

8.1 PRBS Generators

Each of the four 13-bit data lanes crossing the FMC interface between boards has a PRBS generator that can override the data from the ADC. The PRBS generator on each lane is enabled by writing logic 1 to the corresponding bit in `prbs_en`. Each lane uses a different generator polynomial, given in Table 7.

Lane	Polynomial
0	0x101A
1	0x1046
2	0x1032
3	0x1052

Table 7: PRBS Generator Polynomials

This feature can be used to test the alignment of the data and clock signals crossing the FMC interface by checking the corresponding PRBS error count register `err_cntX`. It can also be used as a known data source to test the operation of the software by selecting a particular lane as the data source (see Tables 4 and 5).

8.2 ADC Constant Value Input

By writing logic 1 to `zero_input` the values from the ADC are overwritten with all zeros. Since the ADC uses an unsigned offset number format, this represents a full-scale negative value when it is converted to signed format. This feature can be used to test the system DSP performance by generating a complex cosine waveform at the frequency set by `phase_inc`.

8.3 AXI Data Override

By writing logic 1 to `axi_data_override` the AXI bus inputs to the memory controller are set to constant values. Lane 0 is set to the 64-bit value 0x0011223344556677 and lane 1 is set to the 64-bit value 0x8899AABBCCDDEEFF. This function is useful for testing various transfer modes without any need to engage with the Virtex-4 device.

8.4 LED Override

The nine status LEDs on the ADC12D1800RFRB board may be overridden to provide software-controlled feedback about different events. Individual LEDs may be enabled for override by setting the corresponding bit in `led_override` to logic 1. This LED may then be controlled by setting the value of the corresponding bit in `led_value`.

Appendix D

Patent Document

This appendix archives the series of actions filed with the United States Patent and Trademark Office (USPTO) in regards to this invention. The full text of the patent is available online and is not repeated here. In this section we present the original claims, the first office action allowing 27 of the original 41 claims, and the amended claims.

CLAIMS AS PENDING
Title: SPREAD SPECTRUM METHOD AND APPARATUS
Application No. 14/811,662, Filed: 7/28/2015
Your Ref. No. *Please advise*
Klarquist Ref. No. 2847-93354-02

---

1. (Original) A method, comprising:

dividing a first message signal associated with a message rate f_m into a series of overlapping segments having a predetermined length and overlap; and

transmitting the segments serially at a channel rate f_C that is higher than the message rate f_m, wherein the channel rate f_C is selected based on the predetermined length and overlap so as to accommodate redundancy associated with the division into overlapping segments.

2. (Original) The method of claim 1, further comprising applying a window function to each segment of the first message signal.

3. (Original) The method of claim 2, wherein the window function is a sine, Hanning, trapezoidal, rectangular, or Blackman window function.

4. (Original) The method of claim 2, wherein the channel rate f_C is selected based on the predetermined length M and overlap R and the message rate f_m such that $f_C \geq (M/R)\, f_m$ so that the segments are transmitted without overlap.

5. (Original) The method of claim 4, further comprising;

dividing a second message signal into a series of overlapping segments having a second predetermined length and overlap;

applying a window function to each segment of the second message signal;

interleaving the windowed segments of the first message signal with the windowed segments of the second message signal; and

transmitting the interleaved segments or data elements serially.

6. (Original) The method of claim 4, wherein the channel rate, overlap and segment length are modified dynamically based on channel conditions.

7. (Original) The method of claim 4, wherein synchronization markers are used to identify the beginning of a segment or group of segments.

8. (Original) The method of claim 4, wherein adaptive equalization is used to compensate for frequency-selective fading.

9. (Original) The method of claim 1, wherein the message rate is a first message rate, and further comprising:

dividing a plurality of message signals associated with at least the first message rate and a second message rate into respective series of overlapping segments having the predetermined length and overlap; and

transmitting the segments of the plurality of message signals serially at the channel rate.

10. (Original) The method of claim 9, wherein the channel rate f_C is at least $\sum_{i=1}^{2} \frac{f_i}{\delta_i}$, wherein f_1 is the first message rate, f_2 is the second message rate, $\delta_i = R_i / M_i$, and M_1, M_2 and R_1, R_2 and are the predetermined lengths and overlaps associated with the first message signal and the second message signal, respectively.

11. (Original) The method of claim 4, further comprising;

dividing a second message signal into a series of overlapping segments having a second predetermined length and overlap;

applying a window function to each segment of the second message signal; and

applying a first code sequence of length N and a second code sequence of length N to the respective series of windowed segments associated with the first message signal and the second message signal, respectively, so as to define corresponding coded series of segments, wherein the serially transmitted code segments includes N coded series of segments, wherein N is a positive integer.

12. (Original) The method of claim 11, wherein the code sequences correspond to rows of a Hadamard matrix $H(2^k)$, wherein *k* is a positive integer.

13. (Original) The method of claim 1, further comprising dividing a plurality of message signals associated with at least one message rate into a series of overlapping segments having predetermined lengths and overlaps; and

transmitting the segments serially at a channel rate that is higher than a combined message rate, wherein the channel rate is selected based on the predetermined lengths and overlaps so as to accommodate redundancy associated with the division into overlapping segments.

14. (Original) The method of claim 4, wherein the segments are transmitted serially by modulating the segments onto a carrier wave.

15. (Original) The method of claim 14, where the modulation is done by creating an analytic complex baseband signal with a Hilbert transform and then upconverting to make a single sideband real passband signal.

16. (Original) The method of claim 4, where the segments are divided into two groups, and I/Q multiplexing the two groups of segments.

17. (Original) The method of claim 4, further comprising:

dividing a second message signal into a series of overlapping segments having a second predetermined length and overlap; and

I/Q multiplexing the segments of the first message signal with the segments of the second message signal; and transmitting the segments serially.

18. (Original) The method of claim 17, wherein the second message signal is corresponds to the first message signal with a time-delay.

19. (Original) The method of claim 16, wherein segments associated with the I and Q channels are temporally offset.

20. (Original) The method of claim 19, wherein the segments associated with the I and Q channels are offset by 50% of the segment length so that amplitude nulls in an I channel and amplitude peaks in a Q channel occur at a common time so as to reduce signal envelope amplitude variations.

21. (Original) The method of claim 4, wherein the message is a real passband output of a digital modulator.

22. (Original) The method of claim 4, wherein the message is a complex baseband output of a digital modulator.

23. (Original) A method, comprising:

identifying a plurality of segments in a serially received data signal at a channel rate;

processing the segments based on a segment length and overlap to obtain the message signal, wherein a message rate associated with the message signal is less than the channel rate, wherein the channel rate is selected based on the predetermined length and overlap so as to accommodate redundancy associated with the division into overlapping segments.

24. (Original) The method of claim 23, further comprising windowing each of the segments prior to processing to obtain the message signal.

25. (Original) The method of claim 23, wherein the message rate f_m is selected such that $f_m \leq \delta f_c$, wherein f_c is the channel rate, $\delta = R / M$, R is the overlap and M is the segment length.

26. (Original) The method of claim 23, wherein the serially received data signal at the channel rate includes segments associated with at least a first message signal and a second

message signal, wherein the processing produces the at least one of the first message signal and the second message signal based on the predetermined length and overlap.

27. (Original) The method of claim 25 wherein at least one of the first message signal and the second message signal are produced based on associated code sequences.

28. (Original) The method of claim 23, wherein the channel rate f_C corresponds to a sum $\sum_{i=1}^{2} \frac{f_i}{\delta_i}$, wherein f_1 is a first rate associated with the first message signal, f_2 is a second rate associated with the second message signal, $\delta_1 = R_1 / M_1$, $\delta_2 = R_2 / M_2$ and R_1, R_2 and M_1, M_2 are predetermined overlaps and segment lengths associated with the first message signal and the second message signal, respectively.

29. (Original) The method of claim 23, further comprising:

identifying a plurality of segments in a serially received data signal at a channel rate, the plurality of segments associated with two or more message signals;

processing the segments based on a segment length and overlap to obtain at least one of the message signals.

30. (Original) The method of claim 23, further comprising:

processing the segments based on segment lengths and overlaps associated with corresponding message signals to obtain the at least two message signals.

31. (Original) An apparatus, comprising:

a data input that receives a sequence of data samples;

a data processor that receives the sequence of data samples and defines a series of overlapping segments having a predetermined length and overlap; and

a data convertor that produces a serial data signal based on the series of overlapping segments, wherein the received sequence of data samples is received at a message data rate, and the serial data signal is at a channel data rate, wherein the channel data rate is greater than the message data rate.

32. (Original) The apparatus of claim 31, wherein the channel data rate is f_C is at least $f_C = \frac{f_m}{\delta}$, wherein f_m is the message data rate, $\delta = R / M$, R is the overlap and M is a segment length.

33. (Original) The apparatus of claim 31, further comprising an analog to digital converter that produces the sequence of data samples.

34. (Original) The apparatus of claim 31, further comprising a modulator that receives the serial data signal and modulates a carrier signal based on the received serial data signal.

35. (Original) The apparatus of claim 31, wherein the sequence of data samples is associated with a plurality of data signal such that segments of the plurality of data signals are interleaved, and further comprising a demultiplexer that processes the received sequence of data samples such that the serial data signal is based on overlapping segments associated with a selected data signal of the plurality of data signals.

36. (Original) An apparatus, comprising:

a data input that receives a serial data signal based on a series of segments having a predetermined length; and

a data processor that receives the serial data signal from the data input and identifies overlapping segments in the serial data signal and produces a de-overlapped serial data signal.

37. (Original) The apparatus of claim 36, wherein the serial data signal is received at a first data rate, and the de-overlapped serial data signal is at a message data rate, wherein the message data rate is less than the channel data rate.

38. (Original) The apparatus of claim 36, wherein the message data rate is f_m is less than or equal to δf_C, wherein f_C is the channel data rate, $\delta = R / M$, R is a segment overlap and M is the predetermined segment length.

39. (Original) The apparatus of claim 36, wherein the sequence of data samples is associated with a plurality of data signals such that segments of the plurality of data signals are interleaved, wherein the data processor produces the de-overlapped serial data signal based on a selected data signal of the plurality of data signals.

40. (Original) The apparatus of claim 36, wherein the sequence of data samples is associated with a plurality of data signals, wherein each of the plurality of data signals is associated with a respective code sequence, and the data processor produces the de-overlapped serial data signal based on a selected data signal of the plurality of data signals and the corresponding code sequence.

41. (Original) The apparatus of claim 37, wherein the data processor that receives the serial data signal from the data input and identifies the overlapping segments in the serial data signal, assigns a weight to each segment based on its quality and produces a de-overlapped serial data signal.

UNITED STATES PATENT AND TRADEMARK OFFICE

UNITED STATES DEPARTMENT OF COMMERCE
United States Patent and Trademark Office
Address: COMMISSIONER FOR PATENTS
P.O. Box 1450
Alexandria, Virginia 22313-1450
www.uspto.gov

APPLICATION NO.	FILING DATE	FIRST NAMED INVENTOR	ATTORNEY DOCKET NO.	CONFIRMATION NO.
14/811,662	07/28/2015	Stephen Harrison	2847-93354-02	1722

24197 7590 04/28/2016

KLARQUIST SPARKMAN, LLP
121 SW SALMON STREET
SUITE 1600
PORTLAND, OR 97204

EXAMINER	
BAYARD, EMMANUEL	

ART UNIT	PAPER NUMBER
2633	

NOTIFICATION DATE	DELIVERY MODE
04/28/2016	ELECTRONIC

Please find below and/or attached an Office communication concerning this application or proceeding.

The time period for reply, if any, is set in the attached communication.

Notice of the Office communication was sent electronically on above-indicated "Notification Date" to the following e-mail address(es):

tanya.harding@klarquist.com
docketing@klarquist.com

Office Action Summary	Application No. 14/811,662	Applicant(s) HARRISON ET AL.	
	Examiner EMMANUEL BAYARD	Art Unit 2633	AIA (First Inventor to File) Status Yes

-- The MAILING DATE of this communication appears on the cover sheet with the correspondence address --

Period for Reply

A SHORTENED STATUTORY PERIOD FOR REPLY IS SET TO EXPIRE 3 MONTHS FROM THE MAILING DATE OF THIS COMMUNICATION.

- Extensions of time may be available under the provisions of 37 CFR 1.136(a). In no event, however, may a reply be timely filed after SIX (6) MONTHS from the mailing date of this communication.
- If NO period for reply is specified above, the maximum statutory period will apply and will expire SIX (6) MONTHS from the mailing date of this communication.
- Failure to reply within the set or extended period for reply will, by statute, cause the application to become ABANDONED (35 U.S.C. § 133). Any reply received by the Office later than three months after the mailing date of this communication, even if timely filed, may reduce any earned patent term adjustment. See 37 CFR 1.704(b).

Status

1)☒ Responsive to communication(s) filed on *7/28/15*.

☐ A declaration(s)/affidavit(s) under **37 CFR 1.130(b)** was/were filed on _____.

2a)☐ This action is **FINAL**. 2b)☒ This action is non-final.

3)☐ An election was made by the applicant in response to a restriction requirement set forth during the interview on _____; the restriction requirement and election have been incorporated into this action.

4)☐ Since this application is in condition for allowance except for formal matters, prosecution as to the merits is closed in accordance with the practice under *Ex parte Quayle*, 1935 C.D. 11, 453 O.G. 213.

Disposition of Claims*

5)☒ Claim(s) *1-41* is/are pending in the application.

5a) Of the above claim(s) _____ is/are withdrawn from consideration.

6)☒ Claim(s) *1-22 and 31-35* is/are allowed.

7)☒ Claim(s) *23-30 and 36-41* is/are rejected.

8)☐ Claim(s) _____ is/are objected to.

9)☐ Claim(s) _____ are subject to restriction and/or election requirement.

* If any claims have been determined allowable, you may be eligible to benefit from the **Patent Prosecution Highway** program at a participating intellectual property office for the corresponding application. For more information, please see http://www.uspto.gov/patents/init_events/pph/index.jsp or send an inquiry to PPHfeedback@uspto.gov.

Application Papers

10)☐ The specification is objected to by the Examiner.

11)☐ The drawing(s) filed on _____ is/are: a)☐ accepted or b)☐ objected to by the Examiner.

Applicant may not request that any objection to the drawing(s) be held in abeyance. See 37 CFR 1.85(a).

Replacement drawing sheet(s) including the correction is required if the drawing(s) is objected to. See 37 CFR 1.121(d).

Priority under 35 U.S.C. § 119

12)☐ Acknowledgment is made of a claim for foreign priority under 35 U.S.C. § 119(a)-(d) or (f).

Certified copies:

a)☐ All b)☐ Some** c)☐ None of the:

1.☐ Certified copies of the priority documents have been received.

2.☐ Certified copies of the priority documents have been received in Application No. _____.

3.☐ Copies of the certified copies of the priority documents have been received in this National Stage application from the International Bureau (PCT Rule 17.2(a)).

** See the attached detailed Office action for a list of the certified copies not received.

Attachment(s)

1) ☒ Notice of References Cited (PTO-892)

2) ☒ Information Disclosure Statement(s) (PTO/SB/08a and/or PTO/SB/08b) Paper No(s)/Mail Date _____.

3) ☐ Interview Summary (PTO-413) Paper No(s)/Mail Date. _____ .

4) ☐ Other: _____.

1. The present application, filed on or after March 16, 2013, is being examined under the first inventor to file provisions of the AIA.

DETAILED ACTION

Claim Rejections - 35 USC § 112

1. The following is a quotation of 35 U.S.C. 112(b):
(b) CONCLUSION.—The specification shall conclude with one or more claims particularly pointing out and distinctly claiming the subject matter which the inventor or a joint inventor regards as the invention.

The following is a quotation of 35 U.S.C. 112 (pre-AIA), second paragraph:
The specification shall conclude with one or more claims particularly pointing out and distinctly claiming the subject matter which the applicant regards as his invention.

2. Claims 23-30, 37-39 and 41 are rejected under 35 U.S.C. 112(b) or 35 U.S.C. 112 (pre-AIA), second paragraph, as being indefinite for failing to particularly point out and distinctly claim the subject matter which the inventor or a joint inventor, or for pre-AIA the applicant regards as the invention.

3. Claim 23 recites the limitation "the division" in line 5. There is insufficient antecedent basis for this limitation in the claim.

4. Claim 23 recites the limitation "the message signal" in lines 4-5. There is insufficient antecedent basis for this limitation in the claim.

5. Claim 27 recites the limitation "the first message signal", " the second message signal" in lines 1-2. There is insufficient antecedent basis for this limitation in the claim.

6. Claim 28 recites the limitation "the first message signal and the second message signal" in lines 3-4. There is insufficient antecedent basis for this limitation in the claim.

7. Claim 30 recites the limitation "the at least two message signals" in line 3. There is insufficient antecedent basis for this limitation in the claim.

8. Claim 37 recites the limitation "the channel data rate" in line 3. There is insufficient antecedent basis for this limitation in the claim.

9. Claim 38 recites the limitation "the channel data rate" in line 2. There is insufficient antecedent basis for this limitation in the claim.

10. Claim 38 recites the limitation "the message data rate" in line 1. There is insufficient antecedent basis for this limitation in the claim.

11. Claim 39 recites the limitation "the sequence of data samples" in line 1. There is insufficient antecedent basis for this limitation in the claim.

12. Claim 24-25, 26, 29 and 41 is also rejected to as being dependent upon a rejected base claim.

13.

Claim Rejections - 35 USC § 102

14. In the event the determination of the status of the application as subject to AIA 35 U.S.C. 102 and 103 (or as subject to pre-AIA 35 U.S.C. 102 and 103) is incorrect, any correction of the statutory basis for the rejection will not be considered a new ground of rejection if the prior art relied upon, and the rationale supporting the rejection, would be the same under either status.

15. The following is a quotation of the appropriate paragraphs of 35 U.S.C. 102 that form the basis for the rejections under this section made in this Office action:

> A person shall be entitled to a patent unless –

16. The following is a quotation of the appropriate paragraphs of 35 U.S.C. 102 that form the basis for the rejections under this section made in this Office action:

> A person shall be entitled to a patent unless –

> (a)(1) the claimed invention was patented, described in a printed publication, or in public use, on sale or otherwise available to the public before the effective filing date of the claimed invention.

17. Claims 36-37 and 40 is rejected under 35 U.S.C. 102(a)(1) as being anticipated by Yost et al U.S. Patent No 5,010,558.

As per claim 36, Yost et al teaches an apparatus, comprising: a data input that receives a serial data signal based on a series of segments having a predetermined length (see col.2, lines 4-36 and col.3, lines 20-35, 42-55); and a data processor that receives the serial data signal from the data input and identifies overlapping segments in the serial data signal (col.3, lines 30-35, 42-55) and produces a de-overlapped serial data signal (see col.2, lines 30-34).

As per claim 37, Yost et al does teach wherein the serial data signal is received at a first data rate, and the de-overlapped serial data signal is at a message data rate (which is equivalent to the decoding rate), wherein the message data rate (the decoding rate) is less than the channel data rate (which is equivalent to the encoding rate) (see abstract and col.1, lines 33-40 and col.1, lines 60-67 and col.4, lines 64-67).

As per claim 40, Yost et al does teach wherein the sequence of data samples is associated with a plurality of data signals, wherein each of the plurality of data signals is associated with a respective code sequence (see col.1, lines 30-35, 53-55 and col.3, lines 45-65), and the data processor produces the de- overlapped serial data signal based on a selected data signal of the plurality of data signals and the corresponding code sequence (see col.2, lines 4-36 and col.3, lines 20-35, 42-55).

Claim Rejections - 35 USC § 103

18. In the event the determination of the status of the application as subject to AIA 35 U.S.C. 102 and 103 (or as subject to pre-AIA 35 U.S.C. 102 and 103) is incorrect, any correction of the statutory basis for the rejection will not be considered a new ground of rejection if the prior art relied upon, and the rationale supporting the rejection, would be the same under either status.

19. The following is a quotation of 35 U.S.C. 103 which forms the basis for all obviousness rejections set forth in this Office action:

> A patent for a claimed invention may not be obtained, notwithstanding that the claimed invention is not identically disclosed as set forth in section 102 of this title, if the differences between the claimed invention and the prior art are such that the claimed invention as a whole would have been obvious before the effective filing date of the claimed invention to a person having ordinary skill in the art to which the claimed invention pertains. Patentability shall not be negated by the manner in which the invention was made.

20. The following is a quotation of 35 U.S.C. 103 which forms the basis for all obviousness rejections set forth in this Office action:

> A patent for a claimed invention may not be obtained, notwithstanding that the claimed invention is not identically disclosed as set forth in section 102 of this title, if the differences between the claimed invention and the prior art are such that the claimed invention as a whole would have been obvious before the effective filing date of the claimed invention to a person having ordinary skill in the art to which the claimed invention pertains. Patentability shall not be negated by the manner in which the invention was made.

21. Claims 39 and 41 are rejected under 35 U.S.C. 103 as being unpatentable over Yost et al U.S. Patent No 5,010,558 in view of Koishida et al U.S. Pub No 20150213804.

As per claim 39 Yost et al teaches all the features of the claimed invention wherein the sequence of data samples is associated with a plurality of data signals, wherein the data processor produces the de-overlapped serial data signal based on a

selected data signal of the plurality of data signals, except that segments of the plurality of data signals are interleaved.

Koishida et al teaches segments of the plurality of data signals are interleaved (see paragraph [0095-0096]).

It would have been obvious to one of ordinary skill in the art to implement the teaching of Koishida into Yost as to apply inverse frequency transform to different modes of encoded audio data as taught by Koishida (see paragraph [0095-0096]).

As per claim 41, Yost et al teaches all the features of the claimed invention wherein the data processor that receives the serial 25 data signal from the data input and identifies the overlapping segments in the serial data signal, and produces a de-overlapped serial data signal except assigns a weight to each segment based on its quality.

Koishida et al teaches assigns a weight to each segment based on its quality (see paragraph ([0004] [0057] [0074]).

It would have been obvious to one of ordinary skill in the art to implement the teaching of Koishida into Yost as to apply inverse frequency transform to different modes of encoded audio data and also determine high quality bitrate compression, as taught by Koishida (see paragraph [0074] [0095-0096]).

Allowable Subject Matter

22. Claims 1-22 and 31-35 are allowed over the prior arts of record.

23. The following is a statement of reasons for the indication of allowable subject matter: transmitting the segments serially at a channel rate fc that is higher than the message rate fm, wherein the channel rate fc is selected based on the predetermined length and overlap so as to accommodate redundancy associated with the division into overlapping segments, as recited in claim 1. A data convertor that produces a serial data signal based on the series of overlapping segments wherein the received sequence of data samples is received at a message data rate, and the serial data signal is at a channel data rate, wherein the channel data rate is greater than the message data rate, as recited in claim 31.

Conclusion

24. The prior art made of record and not relied upon is considered pertinent to applicant's disclosure.

25. (US-20090238578-$ or US-20070299657-$).did. or (US-8630861-$ or US-5977991-$ or US-5394473-$).did.

Any inquiry concerning this communication or earlier communications from the examiner should be directed to EMMANUEL BAYARD whose telephone number is (571)272-3016. The examiner can normally be reached on Monday-Friday (7:Am-4:30PM) Alternate Friday off.

If attempts to reach the examiner by telephone are unsuccessful, the examiner's supervisor, Sam Ahn can be reached on 571 272 3044. The fax phone number for the organization where this application or proceeding is assigned is 571-273-8300.

Information regarding the status of an application may be obtained from the Patent Application Information Retrieval (PAIR) system. Status information for published applications may be obtained from either Private PAIR or Public PAIR. Status information for unpublished applications is available through Private PAIR only. For more information about the PAIR system, see http://pair-direct.uspto.gov. Should you have questions on access to the Private PAIR system, contact the Electronic Business Center (EBC) at 866-217-9197 (toll-free). If you would like assistance from a USPTO Customer Service Representative or access to the automated information system, call 800-786-9199 (IN USA OR CANADA) or 571-272-1000.

Emmanuel Bayard
Primary Examiner
Art Unit 2633

/EMMANUEL BAYARD/
Primary Examiner, Art Unit 2633

Notice of References Cited	Application/Control No. 14/811,662	Applicant(s)/Patent Under Reexamination HARRISON ET AL.	
	Examiner EMMANUEL BAYARD	Art Unit 2633	Page 1 of 1

U.S. PATENT DOCUMENTS

*		Document Number Country Code-Number-Kind Code	Date MM-YYYY	Name	CPC Classification	US Classification
*	A	US-5,010,558 A	04-1991	Yost; Richard A.	H03M13/05	375/259
*	B	US-5,394,473 A	02-1995	Davidson; Grant A.	G10L19/0212	375/240
*	C	US-5,977,991 A	11-1999	DeGoricija; Darko	G09G5/395	345/536
*	D	US-2007/0299657 A1	12-2007	Kang; George S.	G10L19/008	704/207
*	E	US-2009/0238578 A1	09-2009	Taylor; Michael George	H04B10/25133	398/147
*	F	US-8,630,861 B2	01-2014	Chen; Wei-Ge	G10L19/0017	341/51
*	G	US-2015/0213804 A1	07-2015	Koishida; Kazuhito	G10L19/167	704/500
	H	US-				
	I	US-				
	J	US-				
	K	US-				
	L	US-				
	M	US-				

FOREIGN PATENT DOCUMENTS

*		Document Number Country Code-Number-Kind Code	Date MM-YYYY	Country	Name	CPC Classification
	N					
	O					
	P					
	Q					
	R					
	S					
	T					

NON-PATENT DOCUMENTS

*		Include as applicable: Author, Title Date, Publisher, Edition or Volume, Pertinent Pages)
	U	
	V	
	W	
	X	

*A copy of this reference is not being furnished with this Office action. (See MPEP § 707.05(a).)
Dates in MM-YYYY format are publication dates. Classifications may be US or foreign.

MDJ:syc 01/07/16 2847-93354-02 3613077

INFORMATION DISCLOSURE STATEMENT BY APPLICANT		
	Attorney Docket Number	2847-93354-02
	Application Number	14/811,662
	Filing Date	July 28, 2015
	First Named Inventor	Stephen Harrison
	Art Unit	2658
	Examiner Name	Not yet assigned

U.S. PATENT DOCUMENTS				
Examiner Initials*	**Cite No.** (optional)	**Document Number** Number-Kind Code (if known)	**Issue or Publication Date** MM-DD-YYYY	**Name of Patentee or Applicant**
		6,606,312	08-12-2003	McGibney

Examiner Initials*	Cite No. (optional)	OTHER DOCUMENTS	T**
		Alimohammad et al., "Compact Rayleigh and Rician fading simulator based on random walk processes," IET Communications, **3**:1333-1342 (2009).	
		Kourtis et al., "Analogue time division multiplexing," *Int. J. Elect.*, 74:6, pp. 901-907 (1993).	
		Martin and Thepault, "An analog time-division multiplexing system," 3rd European Solid State Circuits Conference (ESSCIRC'77), pp. 162-163 (1977).	

EXAMINER SIGNATURE: /Emmanuel Bayard/	DATE CONSIDERED: 04/16/2016

* Examiner: Initial if reference considered, whether or not in conformance with MPEP 609. Draw line through cite if not in conformance and not considered. Include copy of this form with next communication to applicant.
**Please place an "X" in this column if English translation is attached.

ALL REFERENCES CONSIDERED EXCEPT WHERE LINED THROUGH. /E.B./

IN THE UNITED STATES PATENT AND TRADEMARK OFFICE

First Named Inventor: Stephen Harrison
Application No. 14/811,662
Filed: July 28, 2015
Confirmation No. 1722
For: SPREAD SPECTRUM METHOD AND APPARATUS
Examiner: Emmanuel Bayard
Art Unit: 2658
Attorney Reference No. 2847-93354-02

FILED VIA EFS ON JULY 28, 2016

FILED VIA ELECTRONIC FILING SYSTEM
COMMISSIONER FOR PATENTS

TRANSMITTAL LETTER

Submitted herewith is an Amendment for the above application. The fee has been calculated as shown below.

CLAIMS AS AMENDED						
For	No. after amendment	No. paid for previously		Present Extra	Rate	Fee
Total Claims	40	- 41*	=	0	$40.00	$0.00
Indep. Claims	4	- 4**	=	0	$210.00	$0.00
TOTAL ADDITIONAL FEE(S) FOR THIS FILING						$0.00

* greater of twenty or number for which fee has been paid.
** greater of three or number for which fee has been paid.

☒ No additional fee is required.

Respectfully submitted,

KLARQUIST SPARKMAN, LLP

One World Trade Center, Suite 1600
121 S.W. Salmon Street
Portland, Oregon 97204
Telephone: (503) 595-5300
Facsimile: (503) 595-5301

By /Derrick W. Toddy/
Derrick W. Toddy
Registration No. 74,591

cc: Docketing

IN THE UNITED STATES PATENT AND TRADEMARK OFFICE

First Named Inventor: Stephen Harrison
Application No. 14/811,662
Filed: July 28, 2015
Confirmation No. 1722
For: SPREAD SPECTRUM METHOD AND APPARATUS
Examiner: Emmanuel Bayard
Art Unit: 2658
Attorney Reference No. 2847-93354-02

FILED VIA EFS ON JULY 28, 2016

FILED VIA ELECTRONIC FILING SYSTEM
COMMISSIONER FOR PATENTS

AMENDMENT

This responds to the Office action dated April 28, 2016 (the "Action"). A three-month shortened period of response was set, making a response timely if filed on or before July 28, 2016. It is believed that no fees are required for this filing. However, if the Commissioner determines that fees are required, Applicant hereby gives permission to take such fees from Deposit Account 02-4550.

Please amend the referenced application as follows:

Amendments to the Claims are reflected in the listing of claims, which begins on page 2.

Remarks begin on page 9.

Listing of Claims

1. (Original) A method, comprising:

dividing a first message signal associated with a message rate f_m into a series of overlapping segments having a predetermined length and overlap; and

transmitting the segments serially at a channel rate f_C that is higher than the message rate f_m, wherein the channel rate f_C is selected based on the predetermined length and overlap so as to accommodate redundancy associated with the division into overlapping segments.

2. (Original) The method of claim 1, further comprising applying a window function to each segment of the first message signal.

3. (Original) The method of claim 2, wherein the window function is a sine, Hanning, trapezoidal, rectangular, or Blackman window function.

4. (Original) The method of claim 2, wherein the channel rate f_C is selected based on the predetermined length M and overlap R and the message rate f_m such that $f_C \geq (M/R)\, f_m$ so that the segments are transmitted without overlap.

5. (Original) The method of claim 4, further comprising;

dividing a second message signal into a series of overlapping segments having a second predetermined length and overlap;

applying a window function to each segment of the second message signal;

interleaving the windowed segments of the first message signal with the windowed segments of the second message signal; and

transmitting the interleaved segments or data elements serially.

6. (Original) The method of claim 4, wherein the channel rate, overlap and segment length are modified dynamically based on channel conditions.

7. (Original) The method of claim 4, wherein synchronization markers are used to identify the beginning of a segment or group of segments.

8. (Original) The method of claim 4, wherein adaptive equalization is used to compensate for frequency-selective fading.

9. (Original) The method of claim 1, wherein the message rate is a first message rate, and further comprising:

dividing a plurality of message signals associated with at least the first message rate and a second message rate into respective series of overlapping segments having the predetermined length and overlap; and

transmitting the segments of the plurality of message signals serially at the channel rate.

10. (Original) The method of claim 9, wherein the channel rate f_C is at least $\sum_{i=1}^{2} \frac{f_i}{\delta_i}$,

wherein f_1 is the first message rate, f_2 is the second message rate, $\delta_i = R_i / M_i$, and M_1, M_2 and R_1, R_2 and are the predetermined lengths and overlaps associated with the first message signal and the second message signal, respectively.

11. (Original) The method of claim 4, further comprising;

dividing a second message signal into a series of overlapping segments having a second predetermined length and overlap;

applying a window function to each segment of the second message signal; and

applying a first code sequence of length N and a second code sequence of length N to the respective series of windowed segments associated with the first message signal and the second message signal, respectively, so as to define corresponding coded series of segments, wherein the serially transmitted code segments includes N coded series of segments, wherein N is a positive integer.

12. (Original) The method of claim 11, wherein the code sequences correspond to rows of a Hadamard matrix $H(2^k)$, wherein k is a positive integer.

13. (Original) The method of claim 1, further comprising dividing a plurality of message signals associated with at least one message rate into a series of overlapping segments having predetermined lengths and overlaps; and

transmitting the segments serially at a channel rate that is higher than a combined message rate, wherein the channel rate is selected based on the predetermined lengths and overlaps so as to accommodate redundancy associated with the division into overlapping segments.

14. (Original) The method of claim 4, wherein the segments are transmitted serially by modulating the segments onto a carrier wave.

15. (Original) The method of claim 14, where the modulation is done by creating an analytic complex baseband signal with a Hilbert transform and then upconverting to make a single sideband real passband signal.

16. (Original) The method of claim 4, where the segments are divided into two groups, and I/Q multiplexing the two groups of segments.

17. (Original) The method of claim 4, further comprising:

dividing a second message signal into a series of overlapping segments having a second predetermined length and overlap; and

I/Q multiplexing the segments of the first message signal with the segments of the second message signal; and transmitting the segments serially.

18. (Currently Amended) The method of claim 17, wherein the second message signal ~~is~~ corresponds to the first message signal with a time-delay.

19. (Original) The method of claim 16, wherein segments associated with the I and Q channels are temporally offset.

20. (Original) The method of claim 19, wherein the segments associated with the I and Q channels are offset by 50% of the segment length so that amplitude nulls in an I channel and amplitude peaks in a Q channel occur at a common time so as to reduce signal envelope amplitude variations.

21. (Original) The method of claim 4, wherein the message is a real passband output of a digital modulator.

22. (Original) The method of claim 4, wherein the message is a complex baseband output of a digital modulator.

23. (Currently Amended) A method, comprising:

identifying a plurality of segments in a serially received data signal at a channel rate;

processing the segments based on a segment length and overlap to obtain ~~the~~ a message signal, wherein a message rate associated with the message signal is less than the channel rate, wherein the channel rate is selected based on the predetermined length and overlap so as to accommodate redundancy associated with ~~the~~ a division into overlapping segments.

24. (Original) The method of claim 23, further comprising windowing each of the segments prior to processing to obtain the message signal.

25. (Original) The method of claim 23, wherein the message rate f_m is selected such that $f_m \leq \delta f_C$, wherein f_C is the channel rate, $\delta = R / M$, R is the overlap and M is the segment length.

26. (Original) The method of claim 23, wherein the serially received data signal at the channel rate includes segments associated with at least a first message signal and a second message signal, wherein the processing produces the at least one of the first message signal and the second message signal based on the predetermined length and overlap.

27. (Currently Amended) The method of claim ~~25~~26 wherein at least one of the first message signal and the second message signal are produced based on associated code sequences.

28. (Currently Amended) The method of claim 23, wherein the channel rate f_C corresponds to a sum $\sum_{i=1}^{2} \frac{f_i}{\delta_i}$, wherein f_1 is a first rate associated with ~~the~~ a first message signal, f_2 is a second rate associated with ~~the~~ a second message signal, $\delta_1 = R_1 / M_1$, $\delta_2 = R_2 / M_2$ and R_1, R_2 and M_1, M_2 are predetermined overlaps and segment lengths associated with the first message signal and the second message signal, respectively.

29. (Original) The method of claim 23, further comprising:

identifying a plurality of segments in a serially received data signal at a channel rate, the plurality of segments associated with two or more message signals;

processing the segments based on a segment length and overlap to obtain at least one of the message signals.

30. (Currently Amended) The method of claim 23, further comprising:

processing the segments based on segment lengths and overlaps associated with corresponding message signals to obtain ~~the~~ at least two message signals.

31. (Original) An apparatus, comprising:

a data input that receives a sequence of data samples;

a data processor that receives the sequence of data samples and defines a series of overlapping segments having a predetermined length and overlap; and

a data convertor that produces a serial data signal based on the series of overlapping segments, wherein the received sequence of data samples is received at a message data rate, and the serial data signal is at a channel data rate, wherein the channel data rate is greater than the message data rate.

32. (Currently Amended) The apparatus of claim 31, wherein the channel data rate ~~is~~ f_C is at least $f_C = \frac{f_m}{\delta}$, wherein f_m is the message data rate, $\delta = R / M$, R is the overlap and M is a segment length.

33. (Original) The apparatus of claim 31, further comprising an analog to digital converter that produces the sequence of data samples.

34. (Original) The apparatus of claim 31, further comprising a modulator that receives the serial data signal and modulates a carrier signal based on the received serial data signal.

35. (Original) The apparatus of claim 31, wherein the sequence of data samples is associated with a plurality of data signal such that segments of the plurality of data signals are interleaved, and further comprising a demultiplexer that processes the received sequence of data samples such that the serial data signal is based on overlapping segments associated with a selected data signal of the plurality of data signals.

36. (Currently Amended) An apparatus, comprising:

a data input that receives a serial data signal based on a series of segments having a predetermined length; and

a data processor that receives the serial data signal from the data input and identifies overlapping segments in the serial data signal and produces a de-overlapped serial data signal, wherein the de-overlapped serial data signal is at a message data rate, and wherein the message data rate f_m is less than or equal to δf_C, wherein f_C is a channel data rate, $\delta = R / M$, R is a segment overlap and M is the predetermined segment length.

37. (Currently Amended) The apparatus of claim 36, wherein the serial data signal is received at a first data rate, and the de-overlapped serial data signal is at ~~a~~ the message data rate, wherein the message data rate is less than the channel data rate.

38. (Cancelled).

39. (Currently Amended) The apparatus of claim 36, wherein the serial data signal ~~sequence of data samples~~ is associated with a plurality of data signals such that segments of the plurality of data signals are interleaved, wherein the data processor produces the de-overlapped serial data signal based on a selected data signal of the plurality of data signals.

40. (Currently Amended) The apparatus of claim 36, wherein the serial data signal ~~sequence of data samples~~ is associated with a plurality of data signals, wherein each of the plurality of data signals is associated with a respective code sequence, and the data processor produces the de-overlapped serial data signal based on a selected data signal of the plurality of data signals and the corresponding code sequence.

41. (Original) The apparatus of claim 37, wherein the data processor that receives the serial data signal from the data input and identifies the overlapping segments in the serial data signal, assigns a weight to each segment based on its quality and produces a de-overlapped serial data signal.

Remarks

Reconsideration is requested in view of the preceding amendments and the following remarks. By this Amendment, claim 38 is cancelled without prejudice, and its subject matter added to independent claim 36. In addition, claims 18, 23, 27, 28, 30, 32, 39, and 40 are amended. No new matter is added with these amendments. Upon entry of this Amendment, claims 1-37, and 39-41 are pending, of which claims 1, 23, 31, and 36 are independent.

Allowable Subject Matter

The Applicants thank the Examiner for indicating that claims 1-22 and 31-35 are allowed over the prior art of record.

Rejections under 35 U.S.C. § 112

Claims 23-30, 37-39, and 41 are rejected under 35 U.S.C. § 112(b) as being indefinite. Withdrawal of the rejection is respectfully requested in view of the amendment of claims 23, 27, 28, 30, 36, 39, and 40, and the cancellation of claim 38 without prejudice.

Cited Art

The Action cites:

1. Yost et al., U.S. Patent 5,010,558 (hereinafter "*Yost*"); and
2. Koishida et al., U.S. Patent Application Publication 2015/0213804 (hereinafter "*Koishida*").

Rejections under 35 U.S.C. § 102

Claims 36, 37, and 40 are rejected under 35 U.S.C. § 102(b) as being anticipated by *Yost*. (Action at 3-4.) This rejection is respectfully traversed.

Independent claim 36 is amended herein to include the features of original claim 38, as amended for clarification. Claim 38 was not rejected in view of *Yost* and therefore claim 36 is patentable over *Yost*. Claims 37 and 40 depend from claim 36, and are patentable for at least the same reasons, in addition to the novel combination of features recited therein. Therefore, claims 36, 37, and 40 are allowable, and such action is respectfully requested.

Rejections under 35 U.S.C. § 103

Claims 39 and 41 are rejected under 35 U.S.C. § 103(a) as being unpatentable over *Yost* in view of *Koishida*. (Action at 5-6.) This rejection is respectfully traversed.

As stated above, amended claim 36 is patentable over *Yost*. *Koishida* fails to cure these deficiencies of *Yost* with respect to claim 36. Thus, claims 39 and 41 are patentable over the proposed *Yost* and *Koishida* combination as dependent from allowable claim 36, in addition to the novel and non-obvious combination of features recited therein, and withdrawal of this rejection is respectfully requested.

Conclusion

Applicants believe that this application is now in condition for allowance, in view of the above amendments and remarks. Accordingly, Applicants respectfully request that the Examiner issue a Notice of Allowability covering the pending claims. If the Examiner has any questions, or if a telephone interview would in any way advance prosecution of the application, please contact the undersigned attorney of record.

Respectfully submitted,

KLARQUIST SPARKMAN, LLP

One World Trade Center, Suite 1600
121 S.W. Salmon Street
Portland, Oregon 97204
Telephone: (503) 595-5300
Facsimile: (503) 595-5301

By /Derrick W. Toddy/
Derrick W. Toddy
Registration No. 74,591

Notice of Allowability	Application No. 14/811,662	Applicant(s) HARRISON ET AL.	
	Examiner EMMANUEL BAYARD	Art Unit 2633	AIA (First Inventor to File) Status Yes

-- The MAILING DATE of this communication appears on the cover sheet with the correspondence address--

All claims being allowable, PROSECUTION ON THE MERITS IS (OR REMAINS) CLOSED in this application. If not included herewith (or previously mailed), a Notice of Allowance (PTOL-85) or other appropriate communication will be mailed in due course. **THIS NOTICE OF ALLOWABILITY IS NOT A GRANT OF PATENT RIGHTS.** This application is subject to withdrawal from issue at the initiative of the Office or upon petition by the applicant. See 37 CFR 1.313 and MPEP 1308.

1. ☒ This communication is responsive to *7/28/16*.
   ☐ A declaration(s)/affidavit(s) under **37 CFR 1.130(b)** was/were filed on_____.
2. ☐ An election was made by the applicant in response to a restriction requirement set forth during the interview on _____; the restriction requirement and election have been incorporated into this action.
3. ☒ The allowed claim(s) is/are *1-37 and 39-41*. As a result of the allowed claim(s), you may be eligible to benefit from the **Patent Prosecution Highway** program at a participating intellectual property office for the corresponding application. For more information, please see http://www.uspto.gov/patents/init_events/pph/index.jsp or send an inquiry to PPHfeedback@uspto.gov.
4. ☐ Acknowledgment is made of a claim for foreign priority under 35 U.S.C. § 119(a)-(d) or (f).

   Certified copies:

   a) ☐ All b) ☐ Some *c) ☐ None of the:
   1. ☐ Certified copies of the priority documents have been received.
   2. ☐ Certified copies of the priority documents have been received in Application No. _____ .
   3. ☐ Copies of the certified copies of the priority documents have been received in this national stage application from the International Bureau (PCT Rule 17.2(a)).

   * Certified copies not received: _____.

Applicant has THREE MONTHS FROM THE "MAILING DATE" of this communication to file a reply complying with the requirements noted below. Failure to timely comply will result in ABANDONMENT of this application.
THIS THREE-MONTH PERIOD IS NOT EXTENDABLE.

5. ☐ CORRECTED DRAWINGS (as "replacement sheets") must be submitted.
   ☐ including changes required by the attached Examiner's Amendment / Comment or in the Office action of Paper No./Mail Date _____.

   Identifying indicia such as the application number (see 37 CFR 1.84(c)) should be written on the drawings in the front (not the back) of each sheet. Replacement sheet(s) should be labeled as such in the header according to 37 CFR 1.121(d).
6. ☐ DEPOSIT OF and/or INFORMATION about the deposit of BIOLOGICAL MATERIAL must be submitted. Note the attached Examiner's comment regarding REQUIREMENT FOR THE DEPOSIT OF BIOLOGICAL MATERIAL.

Attachment(s)

1. ☒ Notice of References Cited (PTO-892)
2. ☐ Information Disclosure Statements (PTO/SB/08), Paper No./Mail Date _____
3. ☐ Examiner's Comment Regarding Requirement for Deposit of Biological Material
4. ☐ Interview Summary (PTO-413), Paper No./Mail Date _____ .
5. ☐ Examiner's Amendment/Comment
6. ☒ Examiner's Statement of Reasons for Allowance
7. ☐ Other _____.

1. The present application, filed on or after March 16, 2013, is being examined under the first inventor to file provisions of the AIA.

DETAILED ACTION

This is in response to amendment filed on 7/28/16 in which claims 1-37 and 39-41 are pending and claim 38 is cancelled. The applicant's amendments have been fully considered therefore this case is in condition for allowance. In addition the pending claims have been renumbered as 1-40, respectively.

Allowable Subject Matter

2. The following is an examiner's statement of reasons for allowance: The prior arts of record ail to anticipate or render obvious the following recited features: transmitting the segments serially at a channel rate fc that is higher than the message rate Fm, wherein the channel rate fc is selected based on the predetermined length and overlap so as to accommodate redundancy associated with the division into overlapping segments, as recited in all the independent claims.

Any comments considered necessary by applicant must be submitted no later than the payment of the issue fee and, to avoid processing delays, should preferably accompany the issue fee. Such submissions should be clearly labeled "Comments on Statement of Reasons for Allowance."

Conclusion

3. The prior art made of record and not relied upon is considered pertinent to applicant's disclosure.

(US-9368123-$ or US-9031834-$).did.

Any inquiry concerning this communication or earlier communications from the examiner should be directed to EMMANUEL BAYARD whose telephone number is (571)272-3016. The examiner can normally be reached on Monday-Friday (7:Am-4:30PM) Alternate Friday off.

If attempts to reach the examiner by telephone are unsuccessful, the examiner's supervisor, Sam Ahn can be reached on 571 272 3044. The fax phone number for the organization where this application or proceeding is assigned is 571-273-8300.

Information regarding the status of an application may be obtained from the Patent Application Information Retrieval (PAIR) system. Status information for published applications may be obtained from either Private PAIR or Public PAIR. Status information for unpublished applications is available through Private PAIR only. For more information about the PAIR system, see http://pair-direct.uspto.gov. Should you have questions on access to the Private PAIR system, contact the Electronic Business Center (EBC) at 866-217-9197 (toll-free). If you would like assistance from a USPTO Customer Service Representative or access to the automated information system, call 800-786-9199 (IN USA OR CANADA) or 571-272-1000.

Emmanuel Bayard
Primary Examiner
Art Unit 2633

/EMMANUEL BAYARD/
Primary Examiner, Art Unit 2633

US009479216B2

(12) **United States Patent**
Harrison et al.

(10) **Patent No.: US 9,479,216 B2**
(45) **Date of Patent: Oct. 25, 2016**

(54) **SPREAD SPECTRUM METHOD AND APPARATUS**

(71) Applicants: **Stephen Harrison**, Victoria (CA); **Peter F. Driessen**, Victoria (CA)

(72) Inventors: **Stephen Harrison**, Victoria (CA); **Peter F. Driessen**, Victoria (CA)

(73) Assignee: **UVic Industry Partnerships Inc.**, Victoria, BC (CA)

(*) Notice: Subject to any disclaimer, the term of this patent is extended or adjusted under 35 U.S.C. 154(b) by 0 days.

(21) Appl. No.: **14/811,662**

(22) Filed: **Jul. 28, 2015**

(65) **Prior Publication Data**

US 2016/0056858 A1 Feb. 25, 2016

Related U.S. Application Data

(60) Provisional application No. 62/029,856, filed on Jul. 28, 2014.

(51) **Int. Cl.**

H04B 1/707	(2011.01)
H04B 1/692	(2011.01)
H04B 1/69	(2011.01)

(52) **U.S. Cl.**

CPC ***H04B 1/707*** (2013.01); ***H04B 1/692*** (2013.01); *H04B 2001/6908* (2013.01)

(58) **Field of Classification Search**

CPC H04L 29/0604; H04B 1/707; H04B 2201/707; H04J 2011/0006; H04J 2011/0009; H04J 2011/0013; H04J 2011/0016

USPC 375/149, 259, 240, 140, 260, 295

See application file for complete search history.

(56) **References Cited**

U.S. PATENT DOCUMENTS

5,010,558	A *	4/1991	Yost	H03M 13/05 375/259
5,394,473	A *	2/1995	Davidson	G10L 19/0212 375/240
5,977,991	A *	11/1999	DeGoricija	G09G 5/395 345/536
8,630,861	B2 *	1/2014	Chen	G10L 19/0017 341/51
9,031,834	B2 *	5/2015	Coorman	G10L 13/033 704/205
9,368,123	B2 *	6/2016	Srinivasan	G10L 19/018
2007/0299657	A1 *	12/2007	Kang	G10L 19/008 704/207
2009/0238578	A1 *	9/2009	Taylor	H04B 10/25133 398/147
2015/0213804	A1 *	7/2015	Koishida	G10L 19/167 704/500

OTHER PUBLICATIONS

Alimohammad et al., "Compact Rayleigh and Rician fading simulator based on random walk processes," IET Communications, 3:1333-1342 (2009).

Kourtis et al., "Analogue time division multiplexing," *Int. J. Elect.*, 74:6, pp. 901-907 (1993).

Martin and Thepault, "An analog time-division multiplexing system," 3rd European Solid State Circuits Conference (ESSCIRC'77), pp. 162-163 (1977).

* cited by examiner

Primary Examiner — Emmanuel Bayard

(74) *Attorney, Agent, or Firm* — Klarquist Sparkman, LLP

(57) **ABSTRACT**

A spread spectrum communications method is based on time compression in which a sampled message signal at a first rate is transmitted at a higher sampling rate. Robustness is achieved by dividing the signal into overlapping segments, transmitting each segment fast enough so that the segments no longer overlap. The segments are received and the data signal reconstructed by overlap-adding the segments.

40 Claims, 17 Drawing Sheets

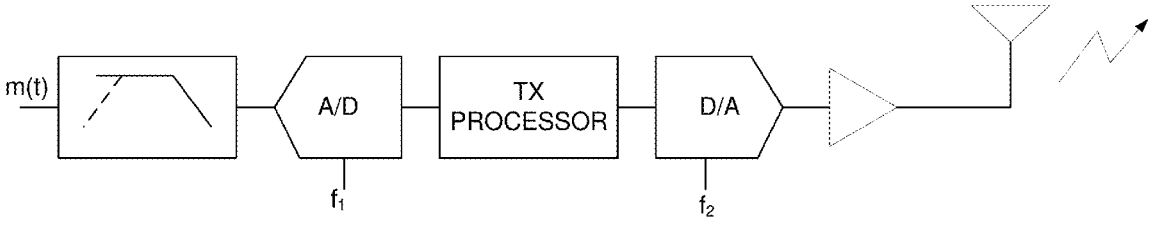

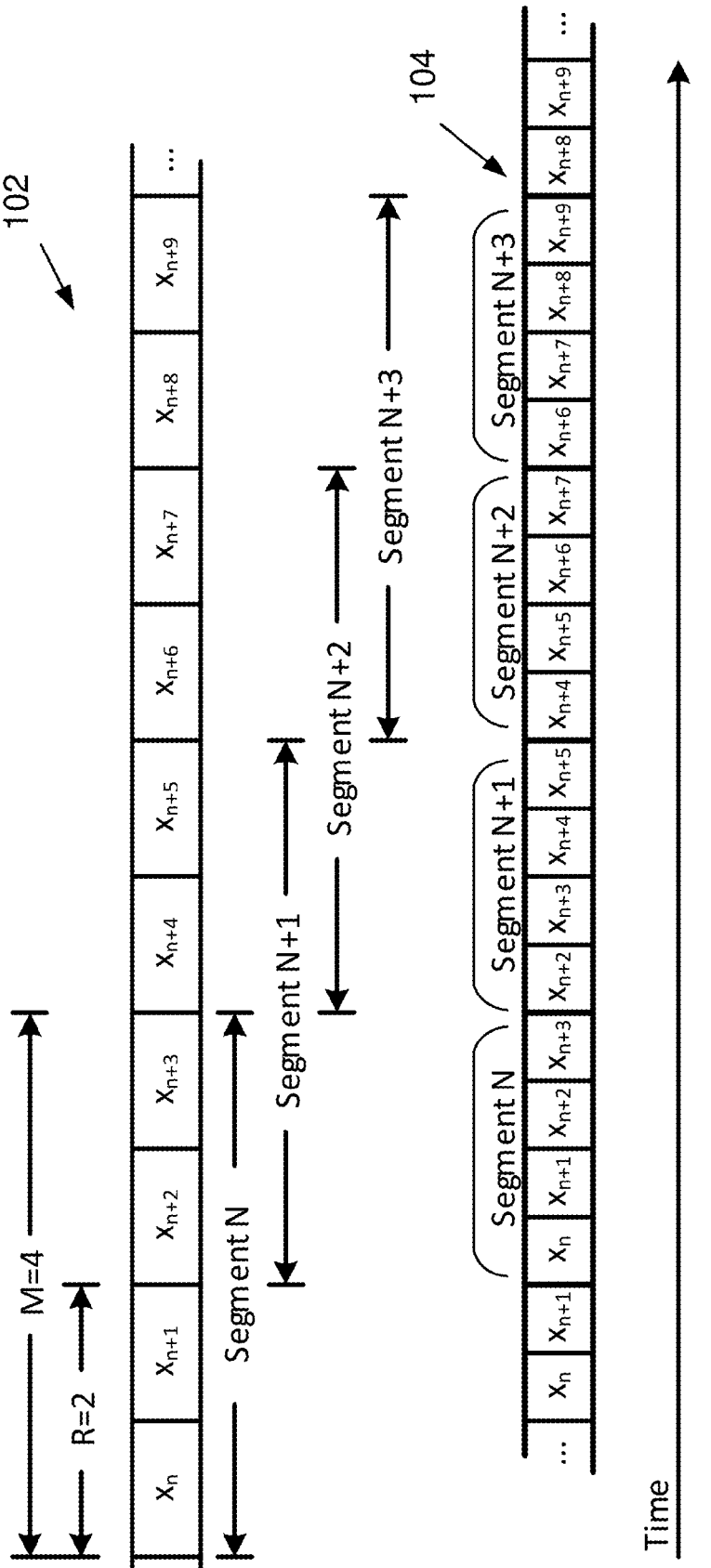

FIG. 1

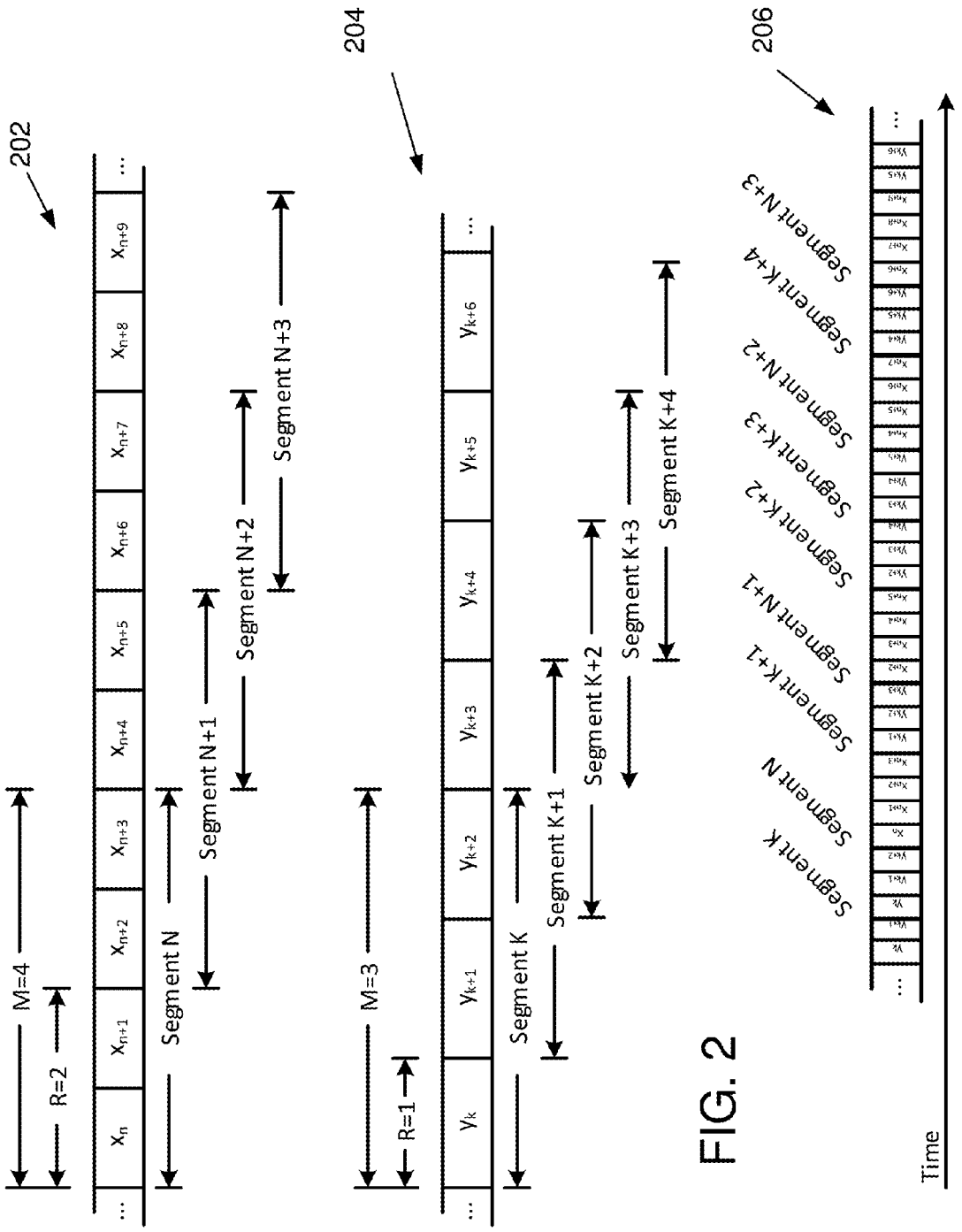
202
204
206
M=4
R=2
M=3
R=1
Segment N
Segment N+1
Segment N+2
Segment N+3
Segment K
Segment K+1
Segment K+2
Segment K+3
Segment K+4
Segment k
Segment N
Segment k+1
Segment N+1
Segment k+2
Segment k+3
Segment N+2
Segment k+4
Segment N+3
Time

FIG. 2

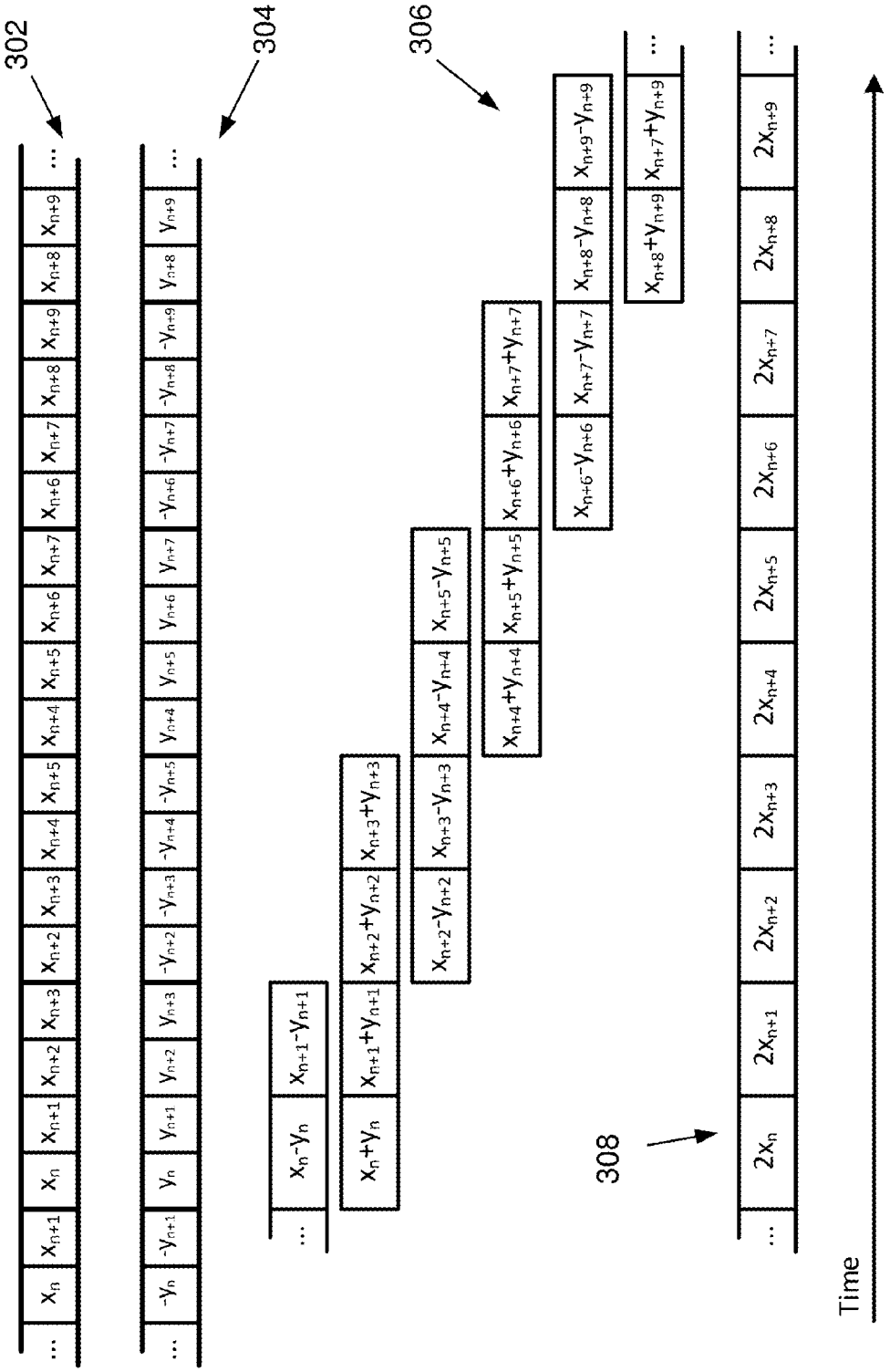

FIG. 3

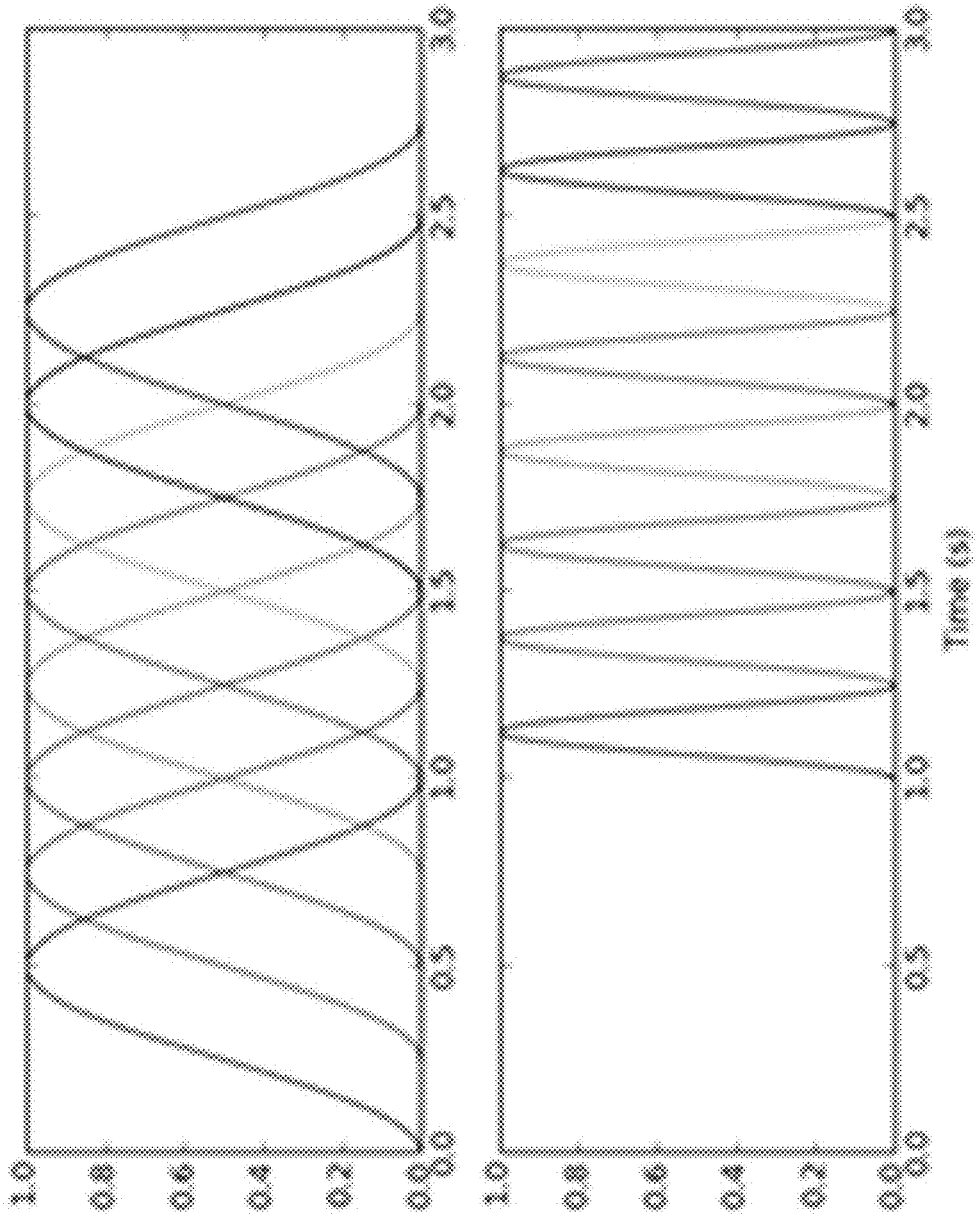

FIG. 4

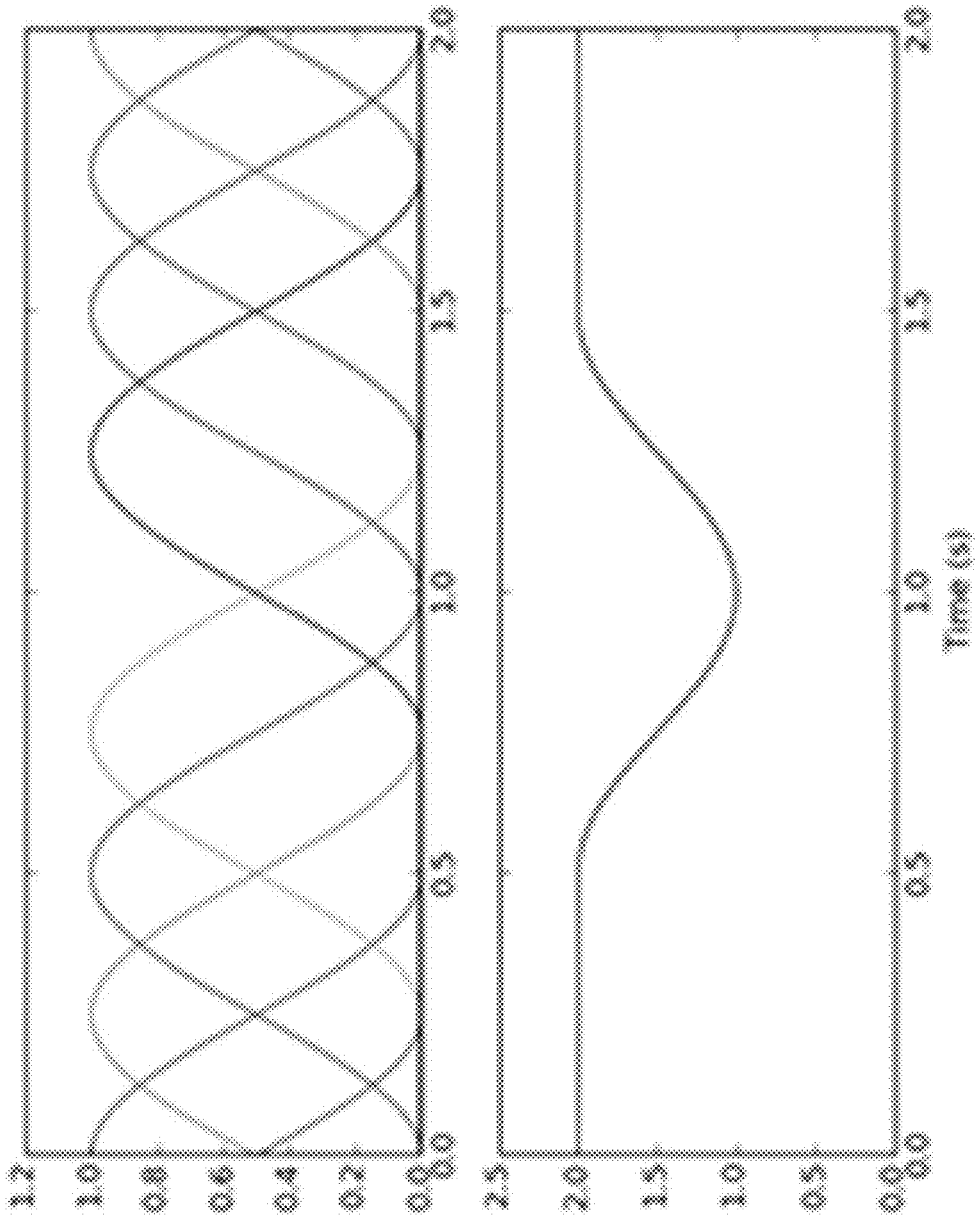

FIG. 5

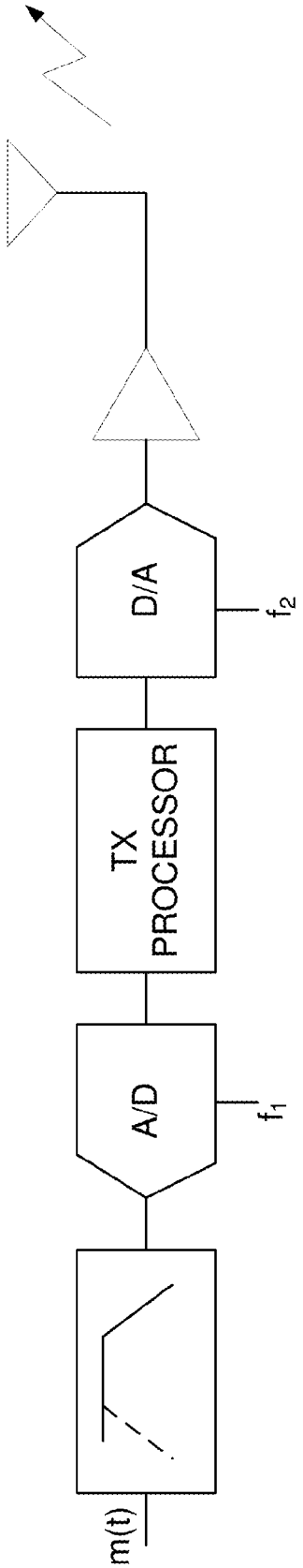

FIG. 6

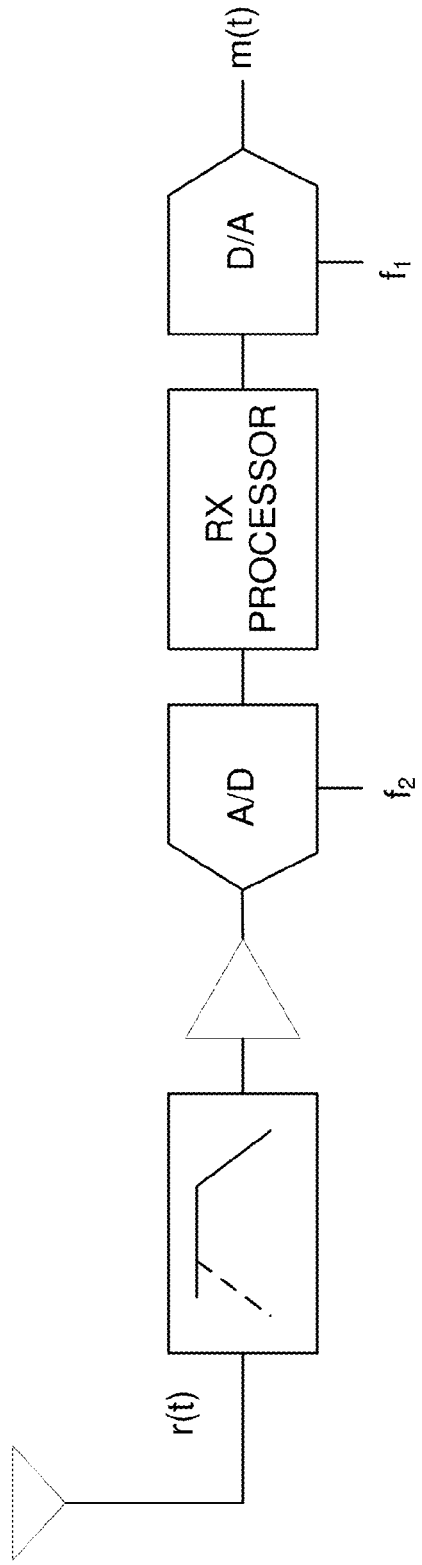

FIG. 7

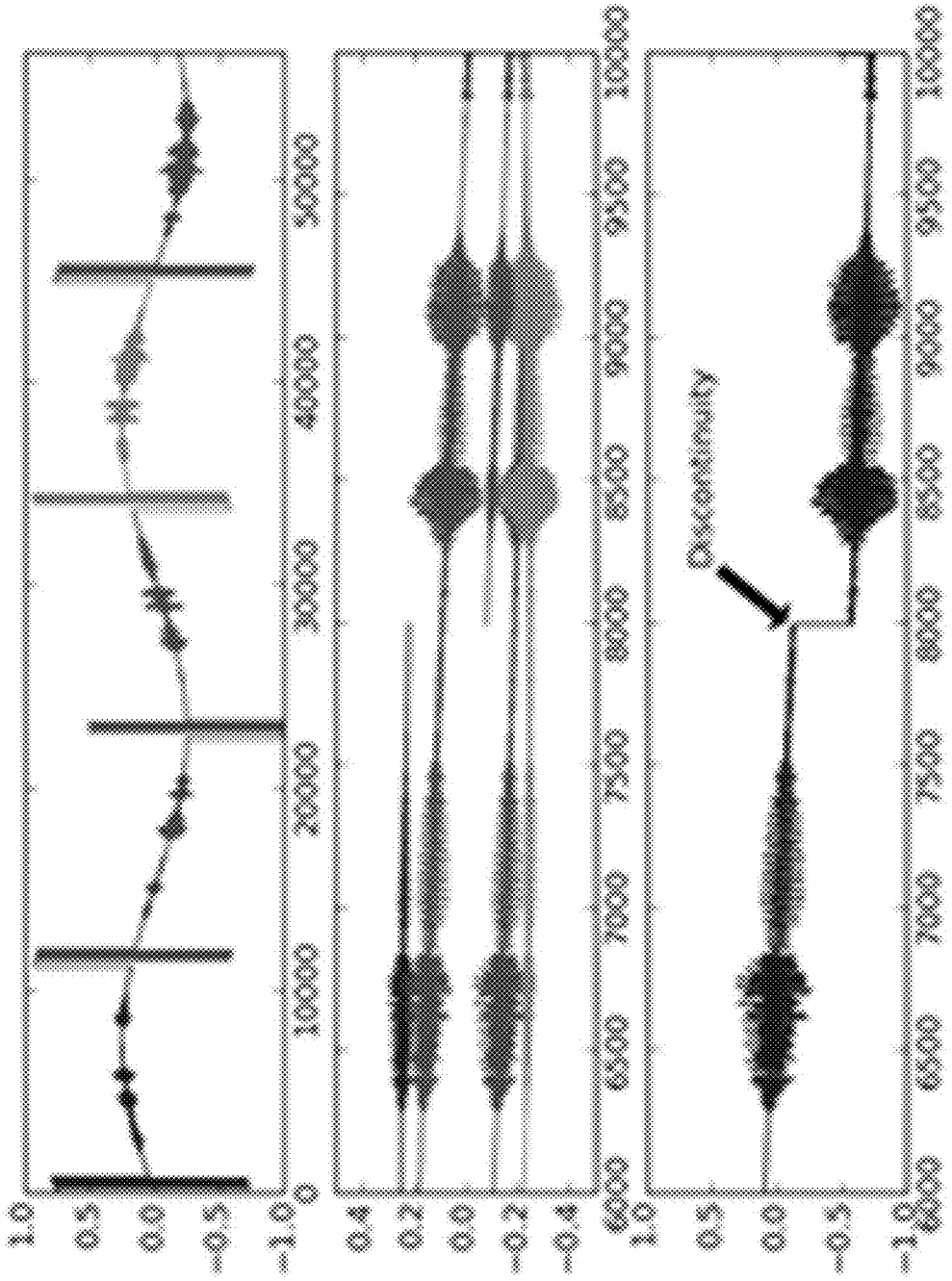
1.0
0.5
0.0
-0.5
-1.0
0
10000
20000
30000
40000
50000
0.4
0.2
0.0
-0.2
-0.4
6000
6500
7000
7500
8000
8500
9000
9500
10000
Eccentricity

FIG. 8

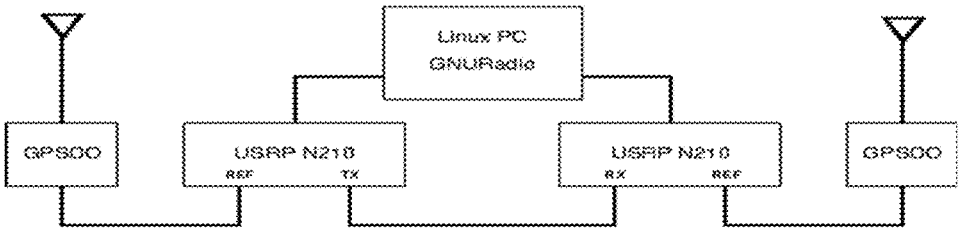
Linux PC
GNURadio
GPSDO
USRP N210
REF
TX
USRP N210
RX
REF
GPSDO

FIG. 9

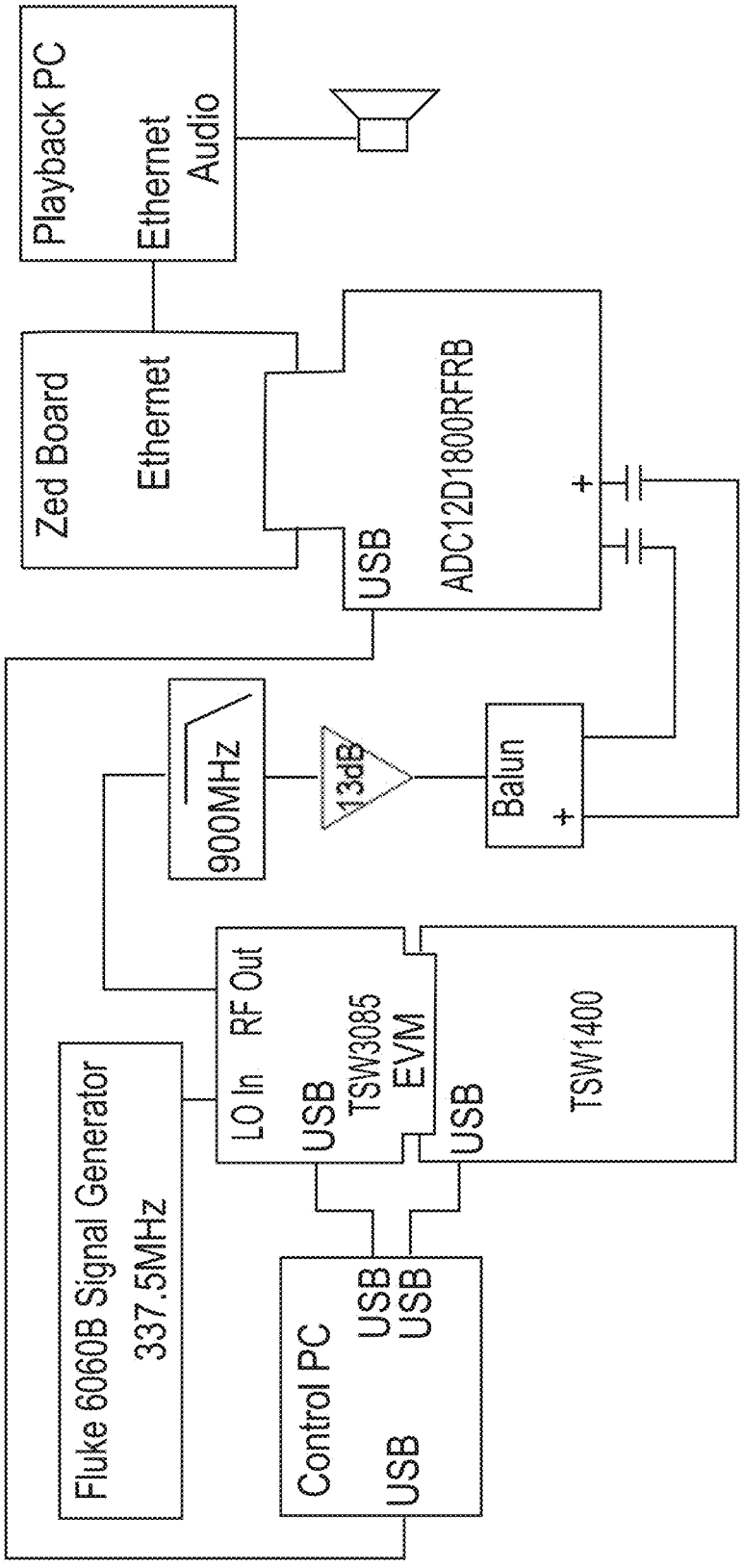
Playback PC
Ethernet
Audio
Zed Board
Ethernet
USB
ADC12D1800RFRB
+
900MHz
13dB
Balun
+
LO In
RF Out
USB
TSW3085
EVM
USB
TSW1400
Fluke 6060B Signal Generator
337.5MHz
Control PC
USB
USB
USB

FIG. 10

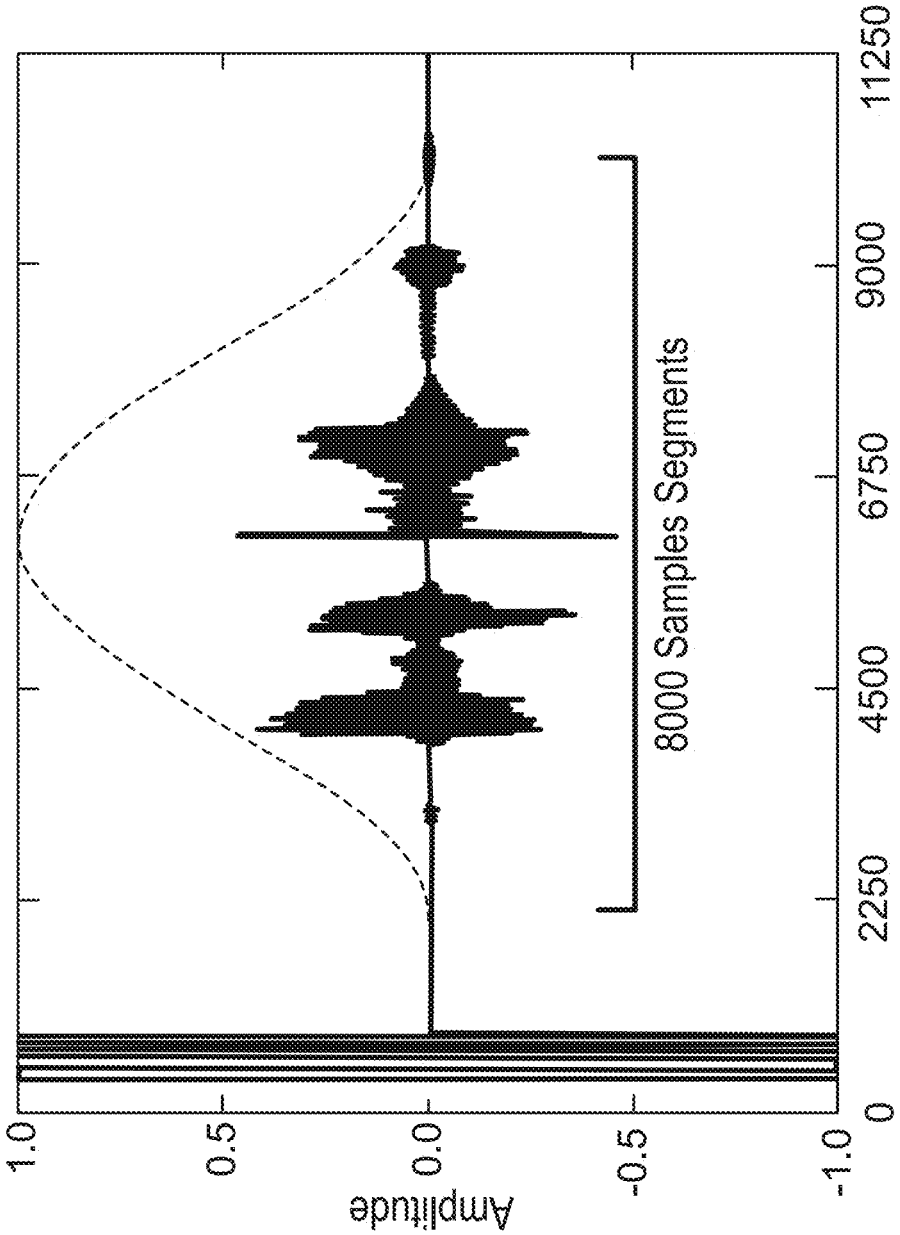
1.0
0.5
0.0
-0.5
-1.0
Amplitude
0
2250
4500
6750
9000
11250
Samples
8000 Samples Segments

FIG. 11

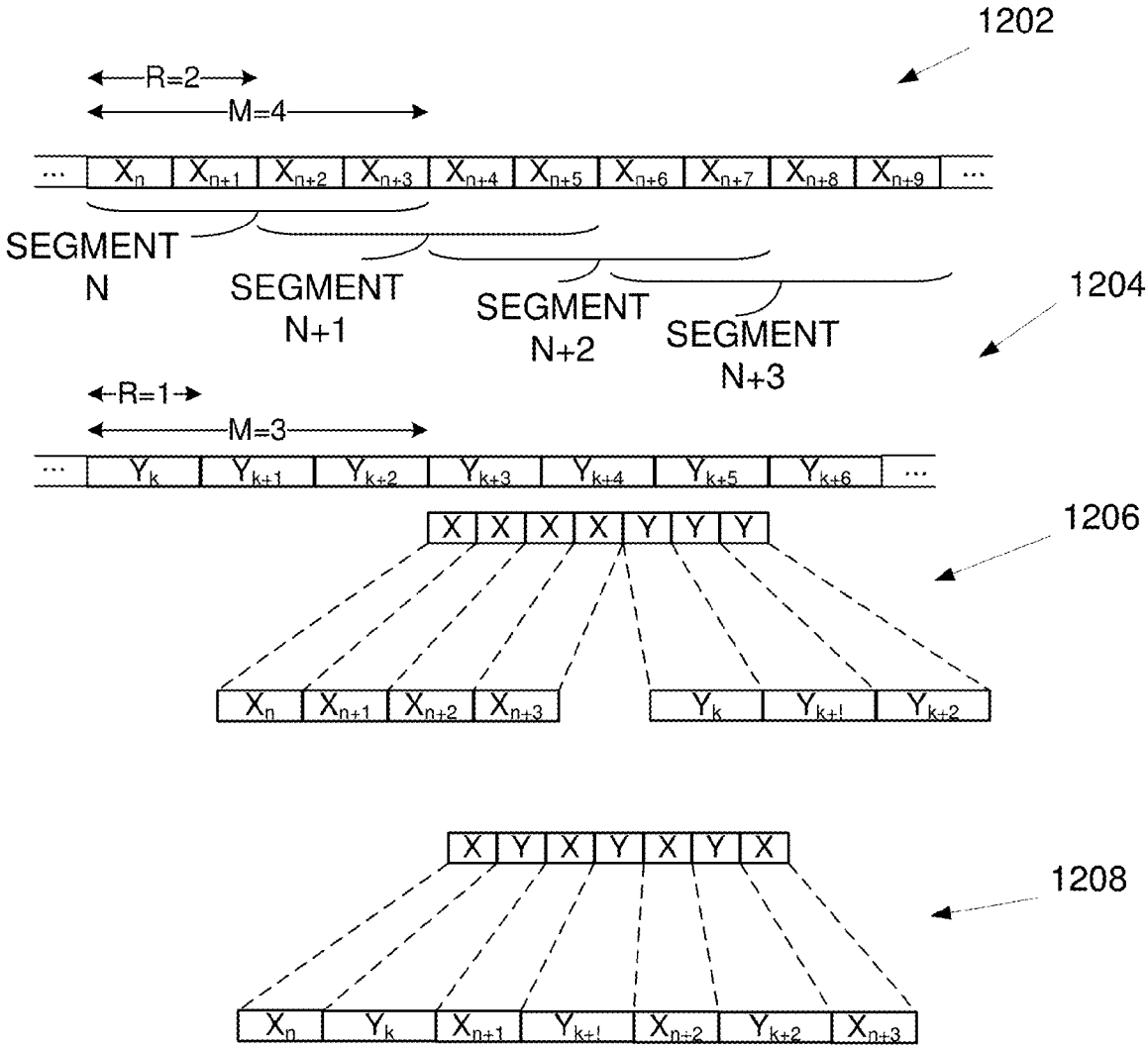
1202
R=2
M=4
... Xn Xn+1 Xn+2 Xn+3 Xn+4 Xn+5 Xn+6 Xn+7 Xn+8 Xn+9 ...
SEGMENT N
SEGMENT N+1
SEGMENT N+2
SEGMENT N+3
1204
R=1
M=3
... Yk Yk+1 Yk+2 Yk+3 Yk+4 Yk+5 Yk+6 ...
1206
X X X X Y Y Y
Xn Xn+1 Xn+2 Xn+3 Yk Yk+! Yk+2
X Y X Y X Y X
1208
Xn Yk Xn+1 Yk+! Xn+2 Yk+2 Xn+3

FIG. 12

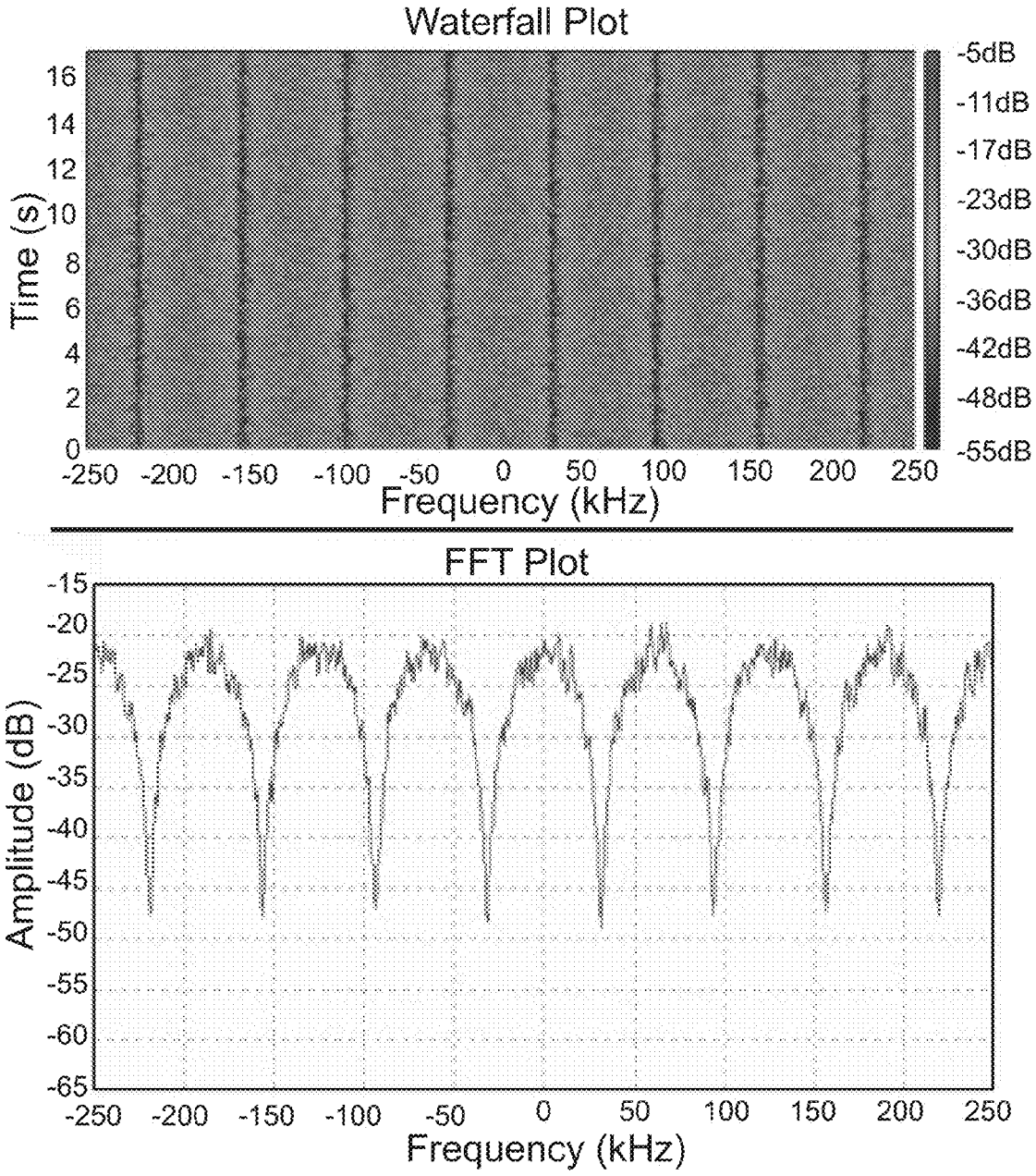
Waterfall Plot
Time (s)
16
14
12
10
8
6
4
2
0
-250 -200 -150 -100 -50 0 50 100 150 200 250
Frequency (kHz)
-5dB
-11dB
-17dB
-23dB
-30dB
-36dB
-42dB
-48dB
-55dB
FFT Plot
Amplitude (dB)
-15
-20
-25
-30
-35
-40
-45
-50
-55
-60
-65
-250 -200 -150 -100 -50 0 50 100 150 200 250
Frequency (kHz)

FIG. 13

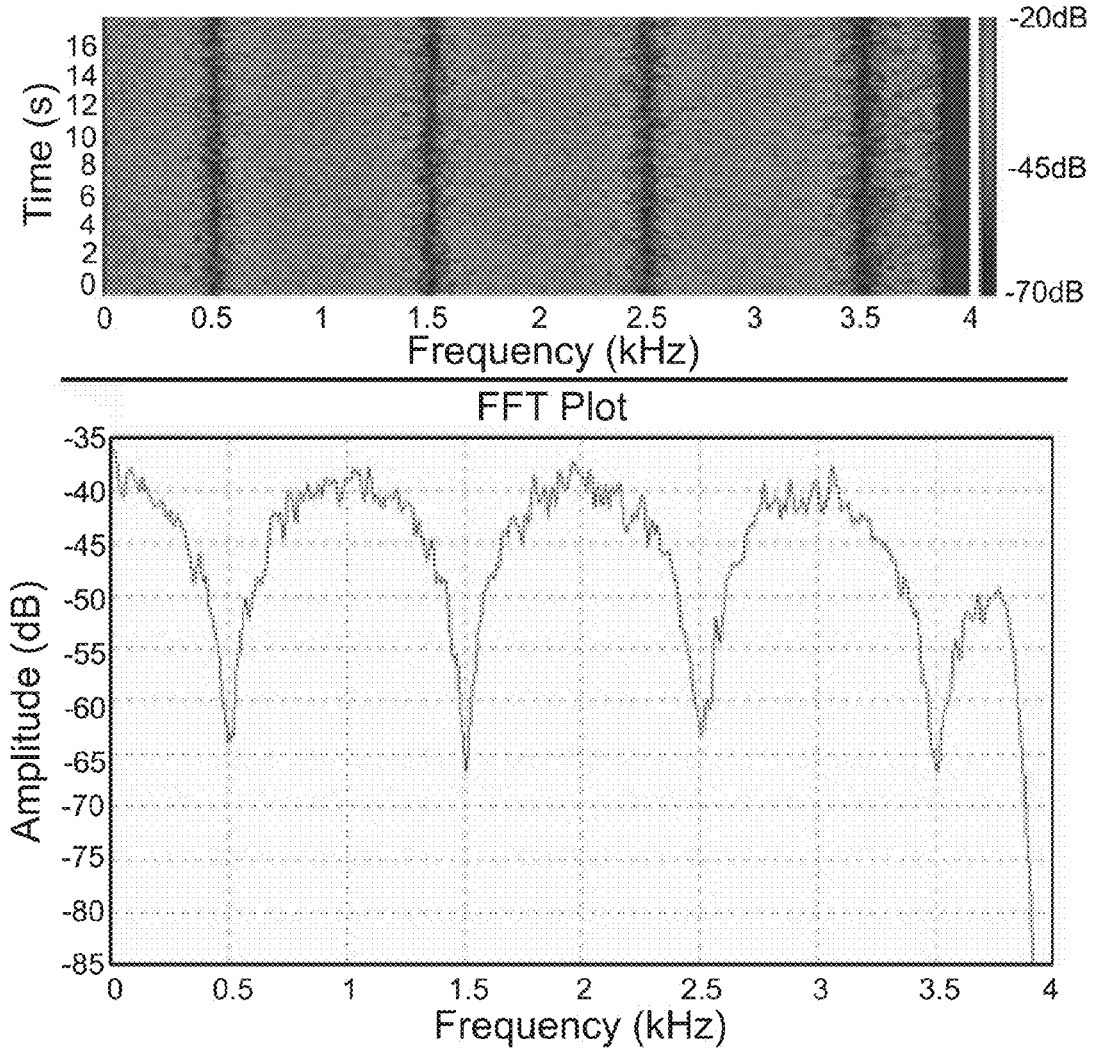
-20dB
-45dB
-70dB
Time (s)
16
14
12
10
8
6
4
2
0
0
0.5
1
1.5
2
2.5
3
3.5
4
Frequency (kHz)
FFT Plot
Amplitude (dB)
-35
-40
-45
-50
-55
-60
-65
-70
-75
-80
-85
0
0.5
1
1.5
2
2.5
3
3.5
4
Frequency (kHz)

FIG. 14

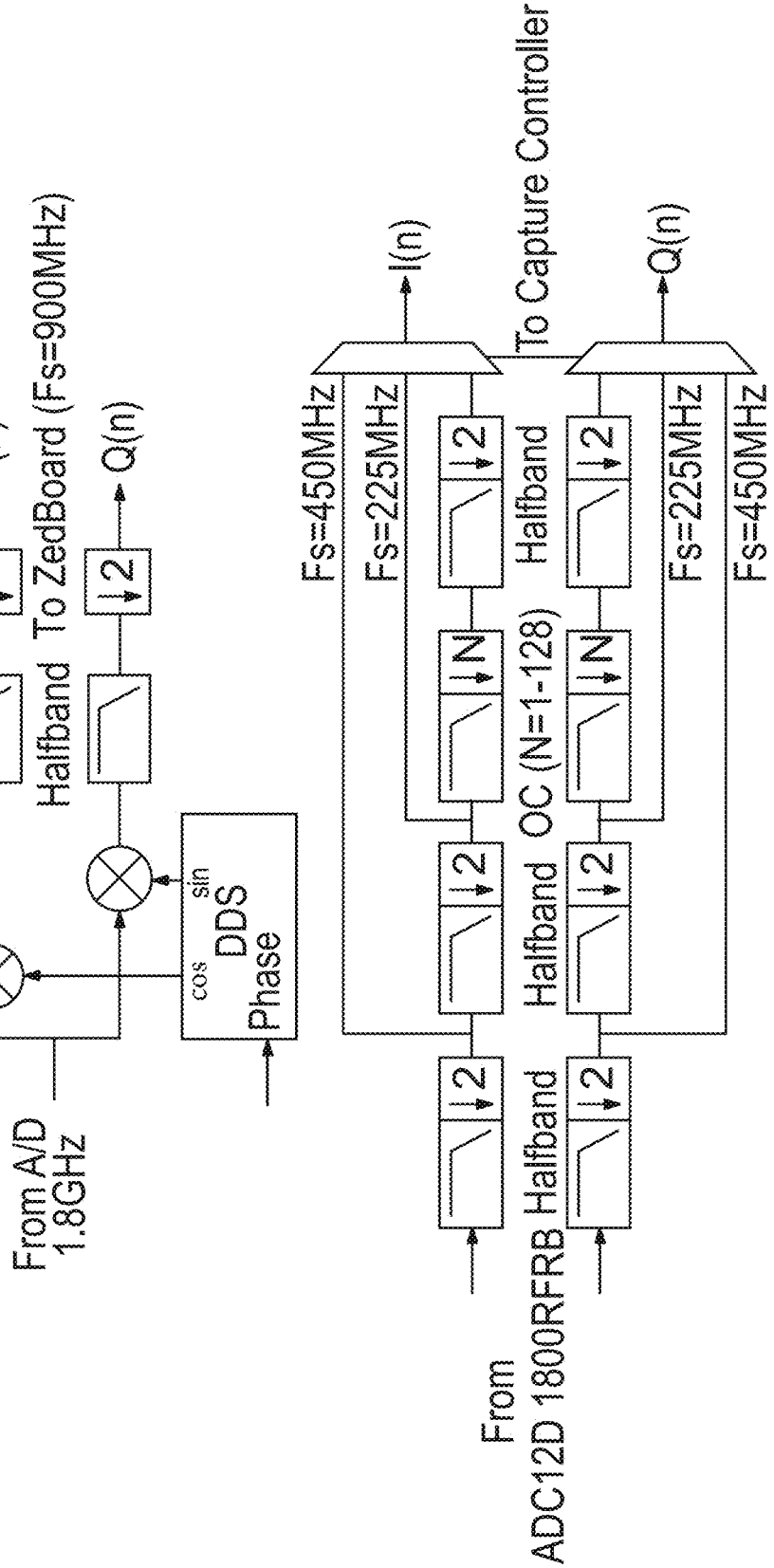
From A/D
1.8GHz
Halfband
To ZedBoard (Fs=900MHz)
I(n)
Q(n)
↓2
DDS
Phase
cos
sin
From
ADC12D 1800RFRB
Halfband
OC (N=1-128)
↓N
Fs=450MHz
Fs=225MHz
To Capture Controller

FIG. 15

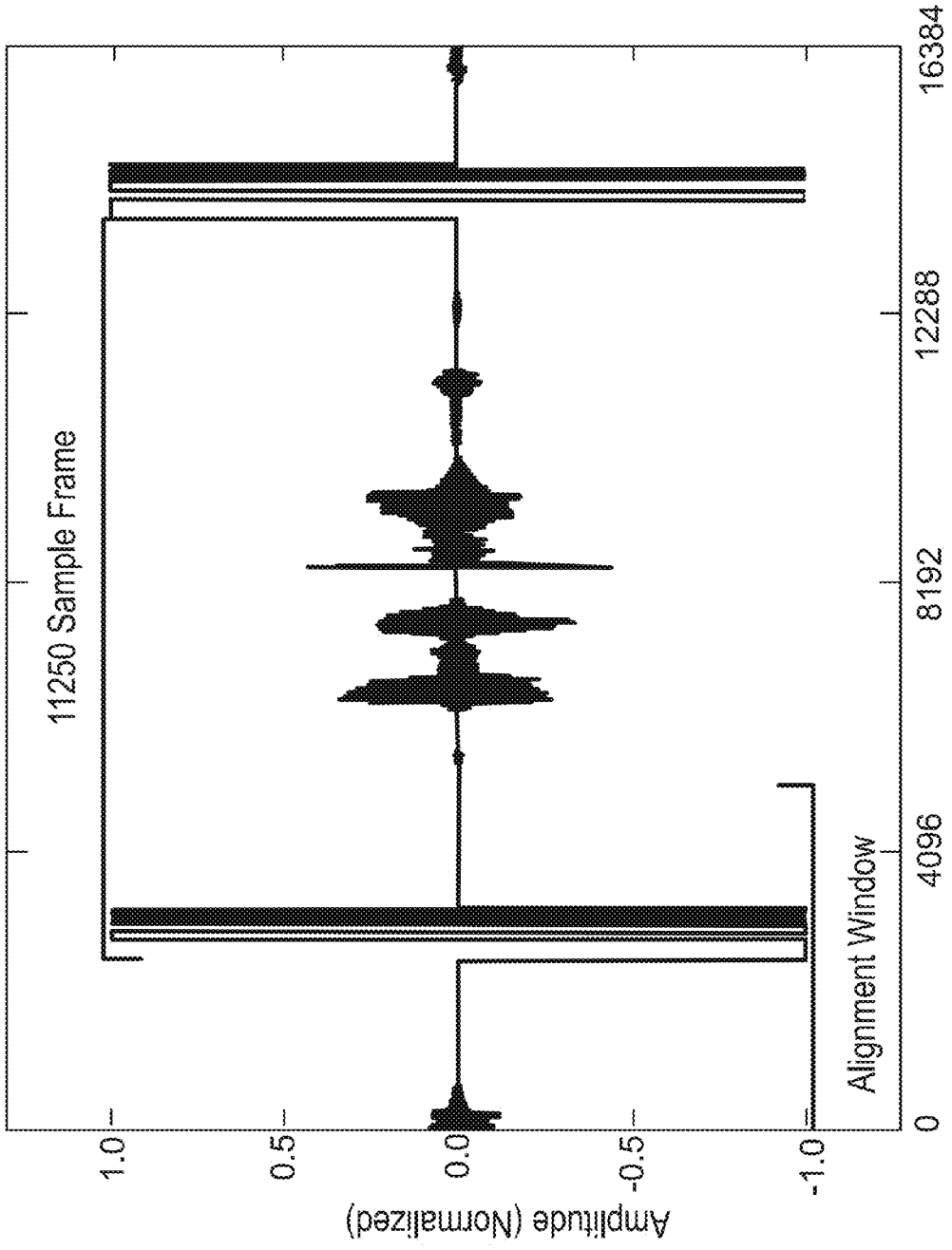
11250 Sample Frame
Alignment Window
Amplitude (Normalized)
1.0
0.5
0.0
-0.5
-1.0
0
4096
8192
12288
16384
Samples

FIG. 16

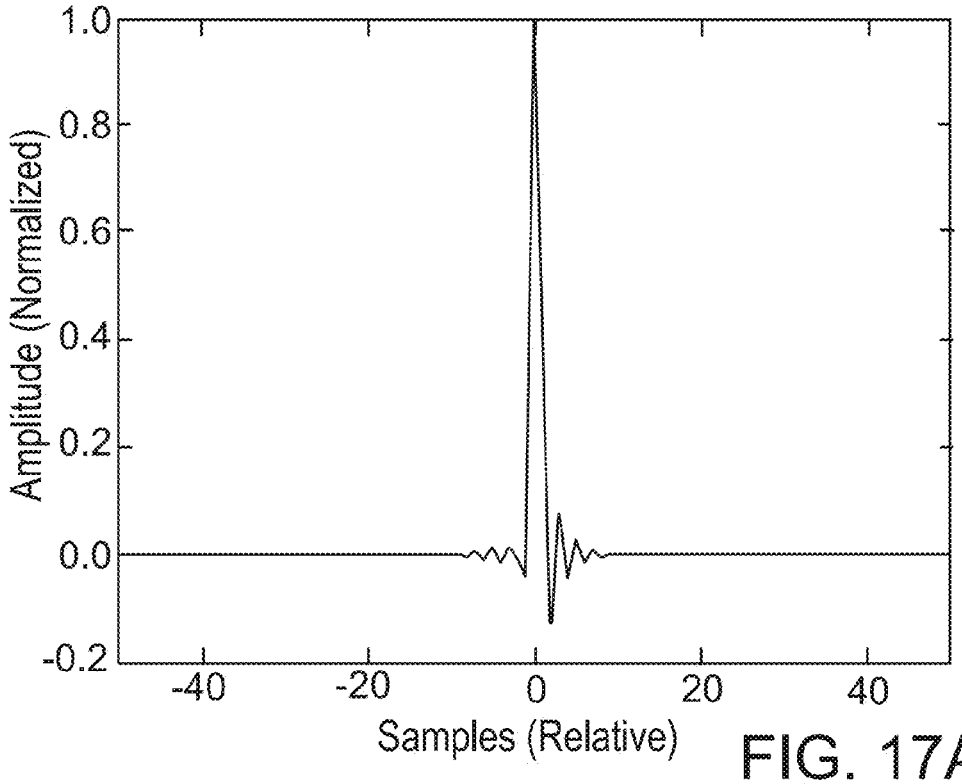

FIG. 17A

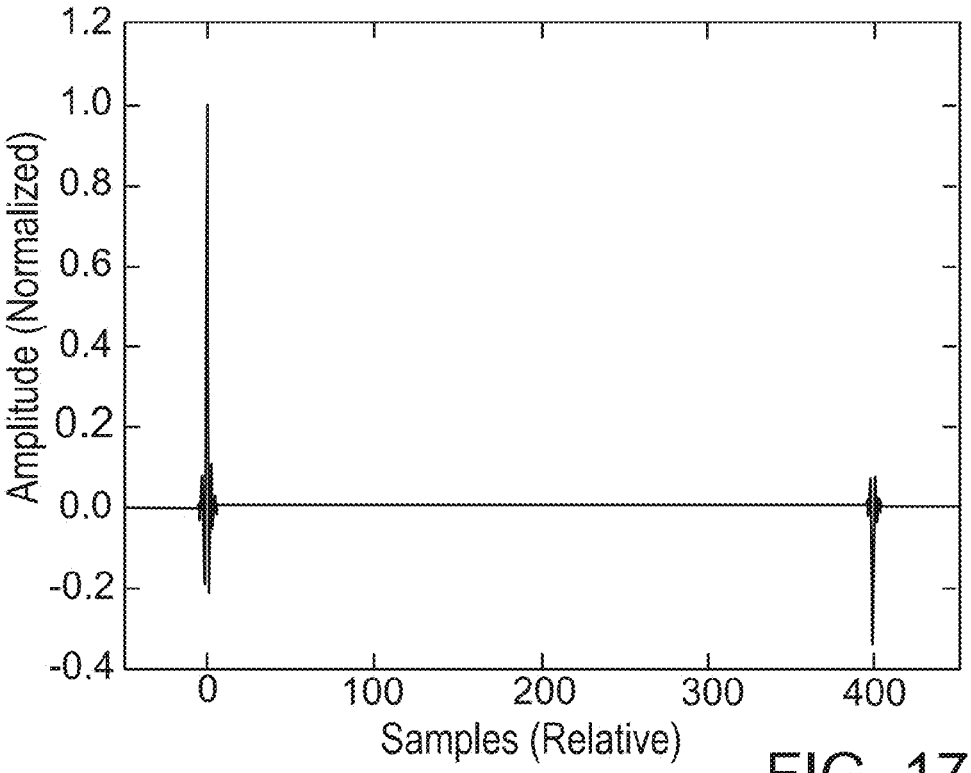

FIG. 17B

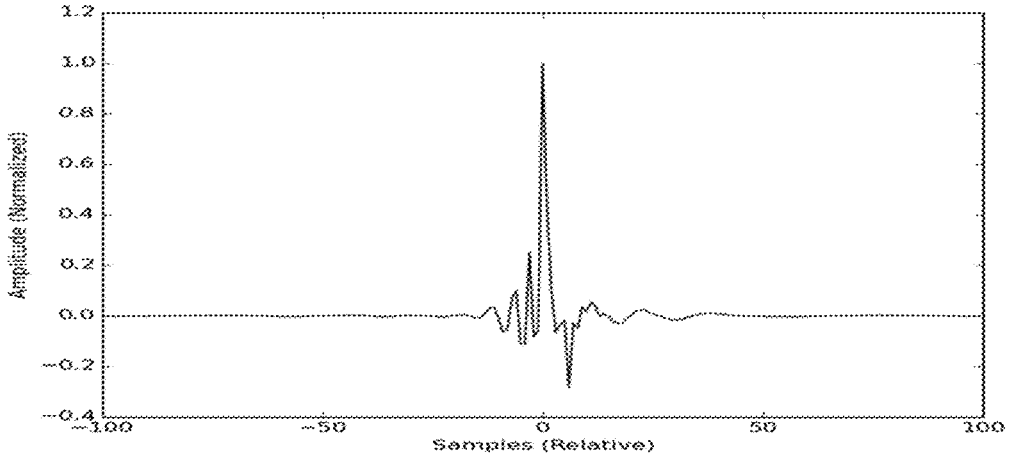
1.2
1.0
0.8
0.6
0.4
0.2
0.0
−0.2
−0.4
Amplitude (Normalized)
−100
−50
0
50
100
Samples (Relative)

FIG. 18

SPREAD SPECTRUM METHOD AND APPARATUS

CROSS REFERENCE TO RELATED APPLICATION

This application claims the benefit of U.S. Provisional Application No. 62/029,856, filed Jul. 28, 2014, which is incorporated herein by reference in its entirety.

FIELD

The disclosure pertains to data communication systems.

BACKGROUND

Communication systems using time compression are described in Martin and Thepault, "An Analog Time-Division Multiplexing System," 3rd European Solid State Circuits Conference (ESSCIRC'77), pp. 162-163 (1977) and Kourtis et al., "Analogue time division multiplexing," Int. J. Elect. 74.6, pp. 901-907 (1993). McGibney, "Analog radio system with acoustic transmission properties," U.S. Pat. No. 6,606,312 discloses segmenting a voice signal and compressing the segments in time before transmission through a radio channel, but is limited to voice transmission. Additional improvements are needed for the realization of practical systems based on time compression.

SUMMARY

Disclosed herein are representative data communication methods and apparatus that offer certain advantages with respect to conventional direct sequence, frequency hopping, chirped, and time hopping spread spectrum techniques, or ultra-wideband pulse radio techniques. The disclosed methods and apparatus can be used with time division multiple access (TDMA) and code division multiple access (CDMA) techniques as well. As disclosed in detail below, overlap-adding segments is used to increase robustness.

In typical examples, time compression is used, wherein a sampled message signal is transmitted at a higher sampling rate than an initial message rate. Robustness is achieved by dividing the message signal into overlapping segments, and transmitting each segment at a rate such that segments no longer overlap, receiving these segments and reconstructing the message by overlap-adding the segments. The spreading factor is the inverse of the fractional hop size, or one minus the normalized amount of overlap relative to the segment length. For segments almost fully overlapping with overlap of all samples but one (a hop size of one sample), the spreading factor is equal to the segment length. The segments may be windowed, tapering to zero at the edges. As an example, for a voice signal sampled at 8 kHz and segments of 8000 samples, and hop size of one sample, the samples are transmitted at 64 Msample/sec. This wideband signal can be transmitted at baseband or on a carrier. The samples could be transmitted at an integer multiple N times 64 Msample/sec to obtain N TDMA channels.

An advantage of some disclosed schemes is that the transmitted samples need not be recovered exactly. The message signal is effectively resampled at the receiver, so sample misalignment and slight clock drift will not significantly alter the quality of the recovered message. Thus frame alignment overhead may not be required, since the periodicity of the windowed frames can define frame boundaries with sufficient accuracy.

In some examples, signals are spread to reduce or eliminate flat fading by spreading over a much wider bandwidth so as to experience frequency-selective fading. Adaptive equalizers for frequency selective channels can then be applied. In the case of a time-varying frequency-selective channel, the overlap-add process naturally reduces the effect of the channel response.

Methods for spread spectrum communication comprise dividing a message signal to be transmitted into a series of overlapping segments having a predetermined length and overlap. The segments are transmitted at a rate at least high enough to accommodate the added redundancy, whereby the transmitted signal bandwidth is spread by a factor proportional to the increase in rate. Received segments are assembled based on the overlap to recover the message signal. In some examples, the rate is increased more than necessary in order to accommodate a plurality of message signals. In other examples, a sequence is applied at the transmitter that permits the receiver to reject interfering signals from among a plurality of transmitted signals.

A spread spectrum modulation apparatus comprises a data input for sequentially inputting a plurality of data samples to be modulated. A data sample separator divides the data samples into a series of overlapping segments having a predetermined length and overlap. A convertor transforms the overlapping segments of the data samples into a continuous waveform, whereby the bandwidth of the signal is spread by a factor related to the overlap of the segments due to the added redundancy. In some examples, the data samples are input by an analog-to-digital converter. In other examples, the data samples are generated digitally. In some examples, the output signal is further modulated onto a carrier signal. Time domain multiplexing can be achieved by spreading the bandwidth of the signal by a factor greater than required by the predetermined overlap, in order to multiplex signals from multiple sources. In some cases, guard time is added between the segments in order to limit the effect of signal impairments due to the physical channel such as multipath. In other embodiments, a marker sequence is added to some or all of the segments and/or the segments are windowed so as to taper to or toward zero at the segment edges.

A spread spectrum demodulation apparatus comprises a data input for converting a continuous waveform into a plurality of data samples so as to produce a data stream. A data processor identifies the data segments in the stream and assembles overlapping data segments into a message signal for communication by a data output. In some examples, the received signal contains signals from multiple sources and a demultiplexer separates the input signal into the associated signals. In some cases, the segments are identified based on a window shape or a marker. In a representative example, the receiver is enabled for a predetermined time interval in a synchronized manner so as to receive segments from one or more desired programs from a plurality of programs contained within a TDMA signal. The remainder of the time the receiver can be in a disabled state allowing it to consume less power than required in the enabled state. Time in the disabled state can be set by a fixed interval or by a predetermined sequence.

The foregoing and other objects, features, and advantages of the disclosed technology will become more apparent from the following detailed description, which proceeds with reference to the accompanying figures.

BRIEF DESCRIPTION OF THE DRAWINGS

FIG. **1** illustrates overlapping segments at a lower sample rate assembled into a stream of non-overlapping segments at a higher sample rate.

FIG. **2** illustrates time-domain interleaving from multiple sources. The sample rate of Y is 3/4 that of X.

FIG. **3** illustrates two systems transmitting simultaneously. Signal X has the sequence {1, 1, . . . } applied while signal Y has the sequence {1, −1, . . . } applied to the transmitted frames. The sequence applied to Y causes it to be cancelled out in the receiver for X.

FIG. **4** illustrates overlapping Hanning windows with fractional hop size of 0.25. These windows sum to k=2. The non-overlapping form is also shown.

FIG. **5** illustrates that a frame centered at t=1.0 s was not recovered, resulting in a drop in amplitude from 2.0 to 1.0. In this example, the fractional hop size is 0.25 and the relative drop in amplitude is 50%.

FIGS. **6-7** illustrate a simplified system. FIG. **6** illustrates a transmitter and FIG. **7** illustrates a receiver.

FIG. **8** illustrates discontinuity caused by interference when a rectangular window is applied at the receiver.

FIG. **9** illustrates a USRP-based system.

FIG. **10** is a block diagram of a representative hardware interconnection diagram. A USB connection between the Control PC and ADC12D1800RFRB is used to load an FPGA image.

FIG. **11** illustrates a transmitted frame format. The dashed line shows the Hanning window function.

FIG. **12** illustrates representative arrangements of segments to form a serial data streams.

FIG. **13** illustrates 500 kHz channel response with nulls spaced every 62.5 kHz.

FIG. **14** illustrates output response to the system using the channel of FIG. **2**. Nulls are spaced by 1 kHz.

FIG. **15** illustrates receiver DSP. The ADC12D1800RFRB image was modified to include a bank of CORDIC processors and a halfband filter. The ZedBoard FPGA image was modified to include a series of halfband filters and a CIC.

FIG. **16** illustrates received data showing the timing marker within the alignment window.

FIG. **17**A illustrates a recovered impulse response with simple wired channel.

FIG. **17**B illustrates a recovered impulse response using two-ray model.

FIG. **18** illustrates averaged impulse response over 8 sweeps.

DETAILED DESCRIPTION

As used in this application and in the claims, the singular forms "a," "an," and "the" include the plural forms unless the context clearly dictates otherwise. Additionally, the term "includes" means "comprises." Further, the term "coupled" does not exclude the presence of intermediate elements between the coupled items.

The systems, apparatus, and methods described herein should not be construed as limiting in any way. Instead, the present disclosure is directed toward all novel and non-obvious features and aspects of the various disclosed embodiments, alone and in various combinations and sub-combinations with one another. The disclosed systems, methods, and apparatus are not limited to any specific aspect or feature or combinations thereof, nor do the disclosed systems, methods, and apparatus require that any one or more specific advantages be present or problems be solved. Any theories of operation are to facilitate explanation, but the disclosed systems, methods, and apparatus are not limited to such theories of operation.

Although the operations of some of the disclosed methods are described in a particular, sequential order for convenient presentation, it should be understood that this manner of description encompasses rearrangement, unless a particular ordering is required by specific language set forth below. For example, operations described sequentially may in some cases be rearranged or performed concurrently. Moreover, for the sake of simplicity, the attached figures may not show the various ways in which the disclosed systems, methods, and apparatus can be used in conjunction with other systems, methods, and apparatus. Additionally, the description sometimes uses terms like "produce" and "provide" to describe the disclosed methods. These terms are high-level abstractions of the actual operations that are performed. The actual operations that correspond to these terms will vary depending on the particular implementation and are readily discernible by one of ordinary skill in the art.

In some examples, values, procedures, or apparatus' are referred to as "lowest", "best", "minimum," or the like. It will be appreciated that such descriptions are intended to indicate that a selection among many used functional alternatives can be made, and such selections need not be better, smaller, or otherwise preferable to other selections.

For convenient description, the examples below are described with reference to digital messages, but messages can be provided as analog waveforms. In some cases, the message is produced as an output of a digital to analog convertor, or messages can be formed as sequences of digital symbols.

Overview

A stream of data samples at a message sample rate f_m is divided into a series of overlapping segments with a fractional hop size δ as in Eq. (1), wherein R is the hop size in samples and M is the length of the segment in samples. The samples may be sourced from an analog-to-digital converter (ADC), retrieved based on values stored in a file in a computer-readable medium such as RAM or other memory device, or generated algorithmically.

$$\delta = \frac{R}{M} \tag{1}$$

The overlapping segments are then reassembled into a stream of non-overlapping segments for transmission at some higher channel sample rate f_c as in Eq. (2).

$$f_c = \frac{f_m}{\delta} = \frac{f_m M}{R} \tag{2}$$

This relationship ensures that each segment is compressed in time by a factor of

$$\frac{f_c}{f_m}$$

such that M samples at f_c occupy the same time duration as R samples at f_m. This process is illustrated pictorially in FIG. **1** with the parameters M=4 and R=2. An input data stream **102** is segmented to produce an output data stream **104** with overlapping segments. Discounting (for now) any sharp

discontinuities at the segment boundaries, the signal bandwidth is spread by a factor of δ^{-1}.

A receiver reverses this process by overlapping and adding the segments to reconstruct the original message signal scaled by a constant δ^{-1}, due to the redundancy added in the transmission process. The receiver process performs an expansion in time which is equivalent to a compression in frequency. Thus any channel impairments, including interference, will also be compressed in frequency. For example, FIG. **13** shows the response of a simple static two-ray channel model with a bandwidth of 500 kHz given a white noise input. The nulls in this channel model are spaced by 62.5 kHz.

If white noise in then applied as the input to an interleaving system as described with an input rate of f_1=8 kHz and an output (a serialized, overlapped and segmented rate) f_2=500 kHz and the serialized data transmitted over this channel, the result will be as in FIG. **14**. The nulls are now spaced by 1 kHz, compressed in frequency by exactly the ratio of the sample rates.

Clearly this discussion extends to time-varying channels but the results are not as easy to interpret pictorially as in the static case. This is again due to the averaging effect of the overlap-add process. Consider a time-varying frequency-selective channel where the response is relatively constant over the duration of each frame (at RF) but varies significantly over the duration of each windowed segment (at the original sample rate). The duration of the original segment acts as an averaging period which diminishes the influence of the channel state during any one frame. This effect increases as δ decreases.

Typically, a window function is applied to each segment, either prior to transmission or after segment identification at a receiver (or at both the transmitter and the receiver). Typical windows include trapezoidal, Blackman, Hanning, Hamming, Kaiser, Sleipian,

Tukey, Gaussian, confined Gaussian, sine, or other windows. In general, suitable windows are defined as functions of time that are non-zero during a segment length, typically having small (often zero) values at window ends, and maximum values at or near a window center.

Extension to TDMA

Allowing f_c to be greater than the minimum required in Eq. (2) provides some unused portion of time that can be used to interleave segments from additional sources. Stated another way, frequency f_c can be set to accommodate multiple signals, possibly with differing sample rates and fractional hop size parameters as in Eq. (3).

$$f_c = \sum_{k=1}^{n} \frac{f_{m_k}}{\delta_k} \tag{3}$$

This time interleaving of this manner is illustrated in FIG. **2**, where signal X uses the parameters M=4 and R=2 while signal Y uses the parameters M=3 and R=1. The sample rate of Y is 3/4 that of X. The output sample rate is therefore

$$f_c = \frac{17}{4} f_{m_x}$$

by application of Eq. (3). FIG. **2** illustrates segmentation and overlapping of data streams **202**, **204** to form a combined data stream **206** in which segments of the data stream **202** (the X stream) are interleaved with segments from the data stream **204** (the Y stream). FIG. **12** shows data streams **1202**, **1204** that are segmented and overlapped to form a data stream **1206** in which segments associated with the streams **1202**, **1204** are interleaved segment by segment. In a data stream **1208**, segments associated with the streams **1202**, **1204** are interleaved data element by data element.

Extension to CDMA

In the case that multiple systems are transmitting on a common frequency they can be separated by applying a varying phase to each transmitted segment. The opposite phase is then applied to the segments at the receiver to rotate the segment back to 0 degrees. The sequences can be chosen to maximize rejection of some or all interfering signals.

FIG. **3** illustrates this concept pictorially, in a simple system with two transmitters operating with the same parameters. The sequence {1, 1} is applied to the transmitted frames of X, while the sequence {1, −1} is applied to the transmitted frames of Y. This allows the receiver for X to effectively cancel out Y. This scheme extends to the set of sequences from the Hadamard matrix H (2^k) with the additional constraints that the number of windows that overlap to produce each output sample must be an integer multiple of the sequence length. This can be expressed in terms of the fractional hop size

$$\delta = \frac{1}{n2^k},$$

wherein n is a positive integer, allowing up to 2^k message signals to be separated. However, there are other ways to generalize this concept and it is not limited to binary phase sequences. As shown in FIG. **3**, data streams **302**, **304** are divided into segments **306**, and a recovered data stream **306** corresponds to the data stream **302**. The data stream **304** can be recovered in addition to or instead of the data stream **302**.

This technique differs from direct sequence spread spectrum (DSSS) in that it does not significantly expand the transmitted signal bandwidth. In DSSS, the sequence is applied at a chip rate which is much higher than the symbol rate. In this scheme the sequence is applied at the frame rate.

Windowing

A window function that tapers to zero is applied to each transmitted segment to address practical concerns about synchronization of the segments at the receiver as well as limiting the transmitted bandwidth. Using a rectangular window as in the previous discussion without perfect synchronization at the receiver would result in sharp transients in the output (audible "glitches" in the case of an audio signal) where the windows are not perfectly aligned. The transmitted signal would also contain high frequency and therefore wide bandwidth transients at the segment boundaries.

The Hanning window Eq. (4) is a one choice as the windows sum to some constant positive integer k per Eq. (5) for any hop size R which satisfies the perfect overlap-add criteria of Eq. (6).

$$w(n) = \frac{1}{2}\left(1 - \cos\left(\frac{2\pi n}{M-1}\right)\right) \quad (4)$$

$$\sum_{m=-\infty}^{\infty} w(n - mR) = k \quad (5)$$

$$R = \frac{M}{2k} \quad (6)$$

A drawback of this window choice is that the maximum fractional hop size is 0.5, leading to a minimum SNR loss of 3 dB over conventional transmission. This is due to the doubling the receiver bandwidth simply to recover the message signal at unity gain.

FIG. **4** illustrates overlapping Hanning windows with fractional hop size of 0.25. These windows sum to k=2. The non-overlapping form is also shown, illustrating the waveform as it would appear when the segments are transmitted at the higher rate.

Interference Rejection

Consider the case where the received segments have an interfering signal superimposed on them. Assume that the overlap-add process sufficiently decorrelates the interfering signal in each segment such that they can be assumed to add in power as with noise. In this case the interference is rejected by a factor of $k \propto \delta^{-1}$. Clearly, one can imagine a scenario where the above assumption is not true. For example, consider an interfering carrier where the interference adds up in phase in the overlap-add process. In this situation, the transmitter can apply a random or predetermined phase sequence to each segment. In the process of rotating each segment back to 0 degrees, the receiver effectively decorrelates this carrier.

Synchronization

A synchronization marker can be inserted between the segments to aid in locating the start and end of each segment in the received sample stream. The sample rate f_1 must be increased to accommodate this insertion. Each timing marker then delineates a frame consisting of one or more segments. The marker that is added should have a strong correlation peak in order to locate the segments with minimum jitter. Segments from multiple interleaved sources can be identified with different timing markers or by including some modulated digital data with the timing marker.

In practice, f_m and f_c at the transmitter will vary slightly from f'_m and f'_c at the receiver. In an ideal system, the number of samples between correlation peaks could be used to estimate the transmitter's sample rate and modulate the receiver's sample rate accordingly. Otherwise, there will be some comb filter effect on the reconstructed signal. However, a one feature of this scheme is that an exact sample rate match is not required to recover the signal although the quality will be degraded.

The effect of frame loss is tolerable in that it creates a momentary drop in the amplitude of the output signal as shown in FIG. **5**. This creates a kind of graceful degradation that is not typically present in digital schemes. As the fractional hop size δ decreases, the relative drop in amplitude from the loss of a single frame is reduced.

Complex Signals

Complex signals can also be used beyond simply applying single-sideband modulation. First, there is the possibility of I/Q multiplexing two separate real signals. Since they are orthogonal, they can be separated at the receiver. A second approach is to transmit half of the overlapping windows for a single signal in quadrature. A third and probably most important possibility is to apply the technique to the complex baseband output of a digital modulator. This may be any existing system such as GSM, WiFi, LTE or future communications standard of suitable bandwidth. Complex baseband and the corresponding real passband signals offers several possibilities. Analytic complex baseband signal can be created with a Hilbert transform and upconverted to make a single sideband real passband signal. Two separate real baseband signals can be I/Q multiplexed. Since they are orthogonal, they can be separated at the receiver. Overlapping message windows can be alternated between the I/Q channels. The I and Q windows can be offset by 50% of the window size so that the amplitude nulls in the I channel and amplitude peaks in the Q channel happen at the same time. This will keep the envelope more constant and be less demanding on the power amplifier. This technique would also help to reduce I/Q crosstalk. In other examples, the complex baseband output of a digital modulator such as QAM or OFDM is used.

Representative Implementations

A simplified diagram of the system implementation is shown in FIGS. **6-7**. The TX process frames the overlapping segments while the RX process synchronizes and performs the overlap-add reconstruction of the message signal. Two different implementations of the system are described here.

First, a USRP-based system is described which, combined with the GNURadio software, provides a flexible experimentation platform. This implementation was used to quickly gather elementary results about this type of system.

Second, a wideband SDR system is described, capable of bandwidths approaching that of UWB. This system operates in real time and simulates a TDM system supporting several thousand users.

In both implementations, a square-root Hanning window is applied to the segments at both the transmitter and receiver, giving the desired Hanning window shape overall on the segments. At the transmitter it helps to reduce sharp transients at the segment boundaries, thus limiting the bandwidth of the transmitted signal. At the receiver, it helps to reduce transients caused by interfering signals which would be present if a Hanning window was applied at the transmitter and a simple rectangular window was applied at the receiver as shown in FIG. **8**.

USRP Implementation

A block diagram of this implementation is shown in FIG. **9**. The system consists of two commercially available USRP N210 software defined radios from Ettus Research and two Thunderbolt E GPS-disciplined oscillators (GPSDO) from Trimble.

All segment framing and message recovery were performed offline in software. This system was used simulation the transmission of a single input signal with a very high level of redundancy. The GNURadio software allows quick simulation of various channel scenarios.

The USRPs are synchronized to the 10 MHz outputs of separate GPS units to provide a realistic simulation of frequency and phase offsets between units located at different sites. LF cards covering 0-30 MHz and WBX cards

covering 50 MHz-2200 MHz were available, so some tests were performed at both 10 MHz and at 900 MHz for comparison.

The system parameters were chosen as in Table 1. A timing marker is added to each segment in the form of a 1000-sample exponential sine sweep. Each segment is then padded on either side with 500 samples to create a 10,000-sample frame.

TABLE 1

System parameters for USRP-based implementation.

Parameter	Value
f_m	8 kHz
f_c	500 kHz
M	8000
R	160

Wideband SDR

The system parameters for this implementation are shown in Table 2. The ratio of the sample rates results in bandwidth spreading by a factor of 28,125. A system of this type could support a very high number of users in the TDM case or a very high level of redundancy. In our tests we use it to simulate the TDM case.

TABLE 2

System parameters for wideband SDR implementation.

Parameter	Value
f_m (kHz)	8
f_c (MHz)	225
β	28,125
M	8000
R	2000
δ	0.25
Timing Marker (samples)	1,000
Frame Length (samples)	11,250
Frame Period (us)	50
Processing Delay (ms)	2000

A more detailed diagram of the hardware interconnects is shown in FIG. **10**. The transmit and receive hardware as well as the software are discussed in more detail in the following sections.

Transmitter

The TSW1400 evaluation platform from Texas Instruments is used as a transmitter. It plays samples from a user-specified data file through the attached DAC at a configured rate. To produce the data file, a 30.75 second audio file containing speech sampled at f_m=8 kHz was divided into 119 segments of 8000 samples each with 25% overlap. The window function applied is a square-root Hanning window. In practice this is just a half-cycle of a cosine function. Framing overhead and padding were added such that each frame contains 11250 samples. The frame overhead efficiency is 71% (8000/11250) and more efficient schemes could be developed. This was convenient scheme given the hardware constraints.

FIG. **11** shows the transmitted frame format. As with the previous system implementation, the synchronization marker used is an exponential sine sweep 1000 samples long. It should be noted that the choice of timing marker can be any sequence with good correlation properties. A Barker code sequence of length 13 modulated with binary phase shift keying (BPSK) was also used experimentally.

These samples are played in a continuous loop through the DAC3482 at f_c=225 MHz, resulting in a frame time of 50 μs, frame rate of 20 k frames/sec, and bandwidth up to 112.5 MHz.

An RF modulator was used to mix the output signal s(t) with a carrier frequency f_0=337 MHz , creating a dual sideband suppressed carrier signal with bandwidth up to 225 MHz.

Receiver

In this example, the receiver hardware consists of a ADC12D1800RFRB evaluation board from Texas Instruments and a Zedboard from Digilent. This combination of devices is used as a wideband direct-sampling software-defined radio with a sample rate of 1.8 GHz. The FPGA images have been modified to include a digital down converter with decimation rates from ranging from 4 to 2048, as shown in FIG. **15**.

A hardware timer is programmed to capture buffers of 16,384 samples every 0.25 seconds (corresponding to the audio segment rate) and place the samples in memory. This results in a capture buffer which is larger than the transmitted frame size as in FIG. **16**. This feature of the system allows the frame timing to be imprecise, as long as the timing marker consistently appears within the alignment window.

The receiver software runs a tracking algorithm to center the frame in the capture buffer. The capture timer is manipulated until the timing marker is held stable within the alignment window. The phase and frequency offsets are then estimated from the timing marker. This estimate is used to compensate the frequency and phase offset in the audio samples. The extracted samples are then put into an overlap-add process to recover the original signal. The output from the overlap-add process is chunked into buffers of 1024 samples for live audio playback.

As there are only 119 frames (5.95 ms), the data file will play 42 times +2 frames (5000 frames=0.25 sec). In our example system we actually use 4999 frames=0.24995s (42 times+1 frame). It is acknowledged that this results in a recovered sample rate slightly faster than the nominal audio rate of 8 kHz. This was done to prevent buffer underruns in the playback hardware as the playback clock is not derived from the same source as the ADC sample clock. In an ideal system playback hardware sample rate would be controlled and this issue would not arise.

In this system, the 4998 ignored frames could contain data from additional users. Therefore, this system simulates a TDM system supporting up to 4999 channels where the receiver only processes one of the channels. To create a practical system supporting this many users, some kind of channel identifier needs to be included with the framing overhead. In a system like this where the time between frames is very long relative to the sample time, the receiver's digital down converter (DDC) could be disabled to save power.

USRP Implementation

The exponential sine sweep method of impulse response estimation was applied to evaluate the response of simple

channel. The method used is described in Eq. (7), where $\mathcal{F}$ denotes the discrete Fourier transform (DFT) operation.

$$h[n] = \mathcal{F}^{-1}\left(\frac{\mathcal{F}(y[n])}{\mathcal{F}(x[n])}\right) \quad (7)$$

The discrete-time signal x[n] represents a discrete version of the exponential sweep as in Eq. (8)-(10), where ω_1 and ω_2 are the start and stop frequencies and Tis the duration of the sweep (insert reference). The discrete time signal y[n] is the output of the overlap-add process.

$$s(t) = \sin[K(e^{-t/L} - 1)] \quad (8)$$

$$K = \frac{\omega_1 T}{\ln\left(\frac{\omega_1}{\omega_2}\right)} \quad (9)$$

$$L = \frac{T}{\ln\left(\frac{\omega_1}{\omega_2}\right)} \quad (10)$$

As expected, the channel response is very flat, except for some attenuation at high frequencies. This could be due to digital filters in the USRPs or cancellation due to jitter in window positioning. This result indicates that the transmission and recovery processes are not significantly affecting the message signal. The recovered impulse response is shown in FIG. **17**A.

Additional signals that were tested with this configuration include two audio signals sampled at 8 kHz, wherein segments from the two sources were coded with columns from H(2) to create a simple CDMA signal. The channels were separated at the receiver with no perceptible crosstalk. In a sense, this is analogous to the CDMA downlink situation where all of the coded frames are transmitted in perfect synchronization.

Waveforms of digital modulation schemes were generated using the amateur radio software FlDigi. Modes that use at least 50% of the available bandwidth were considered such as 2xPSK1000R (2.4 kHz). These generated signals were played through the system and the recovered signals were then successfully decoded by FIDigi.

A two-ray model was simulated in the transmission path using an FIR filter implemented in GNURadio having a second tap at 400 samples with an amplitude of −0.35. The channel impulse response was again estimated using the previously-described method. The recovered impulse response agrees with the simulated channel parameters as shown in FIG. **17**B.

To gain an intuitive understanding of this effect, an audio speech signal was transmitted through the system. The delay of 400 samples at the channel sample rate (800 μs) manifests as a delay of 400 samples at the audio (message) sample rate (50 ms). This is precisely as described McGibney, U.S. Pat. No. 6,606,312, where the channel response is expanded in time by the ratio of sampling rates.

As a short exponential sine sweep is used as a synchronization marker in this system, it is possible to estimate and compensate for this channel on a frame-by-frame basis. First, an inverse filter is estimated as in Eq. (11) which is essentially just the opposite of Eq. (7). This filter is then applied to the audio segment samples before putting them into the overlap-add process. The result is that the echo is removed from the audio speech signal.

Of course there are several drawbacks to this approach, including poor estimation of the channel in a deep fade, frequency interpolation, and limitations on the channel delay relative to the frame length. An adaptive equalizer or MSE solution (provide reference) could provide better results. However, this method was shown to be able to adapt to a time-varying frequency-selective channel provided the channel is relatively constant over the frame period.

$$h_{inv} = \mathcal{F}^{-1}\left(\frac{\mathcal{F}(x[n])}{\mathcal{F}(y[n])}\right) \quad (11)$$

Finally, a Rayleigh fading channel is simulated in the transmission path, using the model of Alimohammad, et al., "Compact Rayleigh and Rician fading simulator based on random walk processes," IET Communications, vol. 3, pp. 1333-1342 (2009), as represented in GNURadio version 3.7.3. The normalized Doppler frequency f_D is configured such that the coherence time is on the order of the frame rate of 20 ms but still much faster than the segment time of 1 second. The results indicate that even without any AGC the scheme is robust against slow fading as the result is averaged over many frames.

The coherence time was then modified to be faster than the frame rate. In this test the signal recovery was poor, indicating that the naïve recovery scheme presented here may not be suitable for fast-fading channels. One could investigate recovery schemes that are more robust or, if possible, choose the system parameters such that the channel is slow-fading relative to the frame rate.

On the topic of system parameter choice, it is acknowledged that the choice of $M=f_m=8000$ creates a delay of 1 second in the transmit process and 1 second in the receive process. In a broadcast scenario, this 2-second delay may be tolerable. However, in a two-way communications system this delay would render the system impractical.

A modification to this system was tested wherein the fractional hop size was held constant while the segment length was reduced to 250 samples. This reduces the delay time to a more practical 62.5 ms. Instead of framing each segment, the segments are framed in groups of 32 so that the frame size stays the same. This provides no additional protection to fading, so the system was again modified such that the segment length was 384 and the timing marker was 64 samples with an overall frame time of 1 ms and a hop size of 8 samples. This gives a similar performance but with faster fading tolerance.

While DSB-SC signals generated from real sampled signals have been considered in some examples, complex baseband signals can be used as well.

Wideband System

The primary observation obtained with this system is that the technique can be scaled up to very wideband transmission using modern high-speed DACs and ADCs.

A speech signal was transmitted through the system and found to be intelligible although quality is noticeably degraded. One source of this degradation could be explained by the lack of interpolation used on the DAC. In typical in SDR transmitters the DAC is interpolated by a factor of at least 2.

Another source of degradation is the fact that, unlike the USRP-based system, the sample clocks are not derived from any disciplined clock source. This could also explain the

result of the sine sweep test, where the impulse response appears to vary significantly with each trial. Given that this system has a low level of redundancy, poor synchronization and sample rate mismatch have a greater impact on the recovered signal.

FIG. **18** shows an averaged impulse response over 8 trial sweeps. Although the impulse response still varies significantly, there are definitive features that appear. Working within the constraints of the current hardware setup, a possible way to improve the results is to reduce the fractional hop size to ⅛ by adding an additional window in quadrature with each frame.

In view of the many possible embodiments to which the principles of the disclosed technology may be applied, it should be recognized that the illustrated embodiments are only representative examples and should not be taken as limiting the scope of the disclosure. Alternatives specifically addressed in these sections are merely exemplary and do not constitute all possible alternatives to the embodiments described herein. For instance, various components of systems described herein may be combined in function and use. We therefore claim as our invention all that comes within the scope and spirit of the appended claims.

We claim:

1. A method, comprising:

dividing a first message signal associated with a message rate f_m into a series of overlapping segments having a predetermined length and overlap; and

transmitting the segments serially at a channel rate f_C that is higher than the message rate f_m, wherein the channel rate f_c is selected based on the predetermined length and overlap so as to accommodate redundancy associated with the division into overlapping segments.

2. The method of claim **1**, further comprising applying a window function to each segment of the first message signal.

3. The method of claim **2**, wherein the window function is a sine, Hanning, trapezoidal, rectangular, or Blackman window function.

4. The method of claim **2**, wherein the channel rate f_C is selected based on the predetermined length M and overlap R and the message rate f_m such that $f_C>(M/R)f_m$ so that the segments are transmitted without overlap.

5. The method of claim **4**, further comprising;

dividing a second message signal into a series of overlapping segments having a second predetermined length and overlap;

applying a window function to each segment of the second message signal;

interleaving the windowed segments of the first message signal with the windowed segments of the second message signal; and

transmitting the interleaved segments or data elements serially.

6. The method of claim **4**, wherein the channel rate, overlap and segment length are modified dynamically based on channel conditions.

7. The method of claim **4**, wherein synchronization markers are used to identify the beginning of a segment or group of segments.

8. The method of claim **4**, wherein adaptive equalization is used to compensate for frequency-selective fading.

9. The method of claim **1**, wherein the message rate is a first message rate, and further comprising:

dividing a plurality of message signals associated with at least the first message rate and a second message rate into respective series of overlapping segments having the predetermined length and overlap; and

transmitting the segments of the plurality of message signals serially at the channel rate.

10. The method of claim **9**, wherein the channel rate f_C is at least

$$\sum_{i=1}^{2} \frac{f_i}{\delta_i},$$

wherein f_1 is the first message rate, f_2 is the second message rate, $\delta_i=R_i/M_i$, and M_1, M_2 and R_1, R_2 and are the predetermined lengths and overlaps associated with the first message signal and the second message signal, respectively.

11. The method of claim **4**, further comprising;

dividing a second message signal into a series of overlapping segments having a second predetermined length and overlap;

applying a window function to each segment of the second message signal; and

applying a first code sequence of length N and a second code sequence of length N to the respective series of windowed segments associated with the first message signal and the second message signal, respectively, so as to define corresponding coded series of segments, wherein the serially transmitted code segments includes N coded series of segments, wherein N is a positive integer.

12. The method of claim **11**, wherein the code sequences correspond to rows of a Hadamard matrix H (2^k), wherein k is a positive integer.

13. The method of claim **1**, further comprising dividing a plurality of message signals associated with at least one message rate into a series of overlapping segments having predetermined lengths and overlaps; and

transmitting the segments serially at a channel rate that is higher than a combined message rate, wherein the channel rate is selected based on the predetermined lengths and overlaps so as to accommodate redundancy associated with the division into overlapping segments.

14. The method of claimer **4**, wherein the segments are transmitted serially by modulating the segments onto a carrier wave.

15. The method of claim **14**, where the modulation is done by creating an analytic complex baseband signal with a Hilbert transform and then upconverting to make a single sideband real passband signal.

16. The method of claim **4**, where the segments are divided into two groups, and I/Q multiplexing the two groups of segments.

17. The method of claim **4**, further comprising:

dividing a second message signal into a series of overlapping segments having a second predetermined length and overlap; and

I/Q multiplexing the segments of the first message signal with the segments of the second message signal; and transmitting the segments serially.

18. The method of claim **17**, wherein the second message signal corresponds to the first message signal with a time-delay.

19. The method of claim **16**, wherein segments associated with the I and Q channels are temporally offset.

20. The method of claim **19**, wherein the segments associated with the I and Q channels are offset by 50% of the segment length so that amplitude nulls in an I channel and

amplitude peaks in a Q channel occur at a common time so as to reduce signal envelope amplitude variations.

21. The method of claim **4**, wherein the message is a real passband output of a digital modulator.

22. The method of claim **4**, wherein the message is a complex baseband output of a digital modulator.

23. A method, comprising:

identifying a plurality of segments in a serially received data signal at a channel rate;

processing the segments based on a segment length and overlap to obtain a message signal, wherein a message rate associated with the message signal is less than the channel rate, wherein the channel rate is selected based on the predetermined length and overlap so as to accommodate redundancy associated with a division into overlapping segments.

24. The method of claim **23**, further comprising windowing each of the segments prior to processing to obtain the message signal.

25. The method of claim **23**, wherein the message rate f_m is selected such that $F_m<\delta f_C$, wherein f_C is the channel rate, $\delta=R/M$, R is the overlap and M is the segment length.

26. The method of claim **23**, wherein the serially received data signal at the channel rate includes segments associated with at least a first message signal and a second message signal, wherein the processing produces the at least one of the first message signal and the second message signal based on the predetermined length and overlap.

27. The method of claim **26** wherein at least one of the first message signal and the second message signal are produced based on associated code sequences.

28. The method of claim **23**, wherein the channel rate f_C corresponds to a sum

$$\sum_{i=1}^{2} \frac{f_i}{\delta_i},$$

wherein f_1 is a first rate associated with a first message signal, f_2 is a second rate associated with a second message signal, $\delta_1=R_1/M_1$, $\delta_2=R_2/M_2$and R_1, $R_2$and M_1, M_2 are predetermined overlaps and segment lengths associated with the first message signal and the second message signal, respectively.

29. The method of claim **23**, further comprising:

identifying a plurality of segments in a serially received data signa a channel rate, the plurality of segments associated with two or more message signals;

processing the segments based on a segment length and overlap to obtain at least one of the message signals.

30. The method of claim **23**, further comprising:

processing the segments based on segment lengths and overlaps associated with corresponding message signals to obtain at least two message signals.

31. An apparatus, comprising:

a data input that receives a sequence of data samples;

a data processor that receives the sequence of data samples and defines a series of overlapping segments having a predetermined length and overlap; and

a data convertor that produces a serial data signal based on the series of overlapping segments, wherein the received sequence of data samples is received at a message data rate, and the serial data signal is at a channel data rate, wherein the channel data rate is greater than the message data rate.

32. The apparatus of claim **31**, wherein the channel data rate is f_C is at least

$$f_C = \frac{f_m}{\delta},$$

wherein f_m is the message data rate, $\delta=R/M$, R is the overlap and M is a segment length.

33. The apparatus of claim **31**, further comprising an analog to digital converter that produces the sequence of data samples.

34. The apparatus of claim **31**, further comprising a modulator that receives the serial data signal and modulates a carrier signal based on the received serial data signal.

35. The apparatus of claim **31**, wherein the sequence of data samples is associated with a plurality of data signal such that segments of the plurality of data signals are interleaved, and further comprising a demultiplexer that processes the received sequence of data samples such that the serial data signal is based on overlapping segments associated with a selected data signal of the plurality of data signals.

36. An apparatus, comprising:

a data input that receives a serial data signal based on a series of segments having a predetermined length and

a data processor that receives the serial data signal from the data input and identifies overlapping segments in the serial data signal and produces a de-overlapped serial data signal, wherein the de-overlapped serial data signal is at a message data rate, and wherein the message data rate f_m is less than or equal to δf_C wherein f_C is a channel data rate, $\delta=R/M$, R is a segment overlap and M is the predetermined segment length.

37. The apparatus of claim **36**, wherein the serial data signal is received at a first data rate, and the de-overlapped serial data signal is at the message data rate, wherein the message data rate is less than the channel data rate.

38. The apparatus of claim **36**, wherein the serial data signal is associated with a plurality of data signals such that segments of the plurality of data signals are interleaved, wherein the data processor produces that de-overlapped serial data signal based on a selected data signal of the plurality of data signals.

39. The apparatus of claim **36**, wherein the serial data signal is associated with a plurality of data signals, wherein each of the plurality of data signals is associated with a respective code sequence, and the data processor produces the de-overlapped serial data signal based on a selected data signal of the plurality of data signals and the corresponding code sequence.

40. The apparatus of claim **37**, wherein the data processor that receives the serial, data signal from the data input and identifies the overlapping segments in the serial data signal, assigns a weight to each segment based on its quality and produces a de-overlapped serial data signal.

* * * * *

Appendix E

Comparison of TC-OLA with RPMA

E.1 Introduction

In this section, we compare TC-OLA with RPMA using metrics taken from RPMA documentation. This work is part of a larger discussion on comparing the two systems, wherein we were asked the following questions:

1. What is the receiver sensitivity you anticipate? I assume its a function of data rate? What data rates did you plan on supporting?
2. Can you quantify the capacity? What is the spectral efficiency?
3. What is the relationship between capacity and receive sensitivity? Is it like DSSS where these quantities are independent.
4. Does the concept of a loading curve apply? If so, what is the pole capacity?
5. ...breaking backward compatibility would be a big problem. Do you have any thoughts to address that concern?

E.2 Uplink Capacity

We can solve for the received power necessary to close the link for TC-OLA as:

$$P_0 = \frac{I_0 SNR_{tgt}}{\frac{M}{R}}. \tag{E.1}$$

In our simulation from Chapter 4,

$$\frac{M}{R} = 1024 = 30.1\,\text{dB} \tag{E.2}$$

$$I_0 = k_B T \Delta_f = (1.38 \times 10^{-23}\text{JK}^{-1})(300\text{K})(2 \times 10^6\text{s}^{-1}) = -110.8\,\text{dBm} \tag{E.3}$$

Assume (for now) that $SNR_{tgt} = 5.5\,\text{dB}$:

$$P_0 = -110.8\,\text{dBm} + 5.5\,\text{dB} - 30.1\,\text{dB} = -135.4\,\text{dBm} \tag{E.4}$$

This is the uplink sensitivity in our simulation assuming this target SNR. Ideally we can go to larger spreading factors such as 8192 (39.1 dB).

The data rate used in the simulation is 977 bps in order to resolve the bandwidth of $B \approx \frac{2}{T_c} \approx 2MHz$ with the processing gain of 1024 and $T_c = 1 \times 10^{-6}$ (1Mchip/second). Other data rates are possible. The spectral efficiency for this case is on the order of $5 \times 10^{-4}\,\text{bps/Hz}$ based on the bandwidth assumptions and spreading gain.

We reason this to be comparable to the raw bit rate in the channel for an RPMA system with a spreading code of 1024. From the RPMA technical overview slides we should have eight 256-bit PDUs plus 16-bit preambles transmitted during the 2.3 second UL slot. The actual bit rate must then be $\frac{8 \times 272}{2.3} = 946$ bps giving around 1Mchip/second when the spreading code is applied.

E.2.1 Pole Capacity

For TC-OLA in AWGN with orthogonal codes we obtain textbook BPSK BER curves. In practice a pole capacity arises due to sources of self-interference in the system. Sources of self interference in TC-OLA include channel fading, carrier frequency offset, timing offset and sample frequency offset. Channel fading and carrier frequency offset manifest in a similar way and can be lumped together into the worst-case SIR limit of 1.96 dB from (4.58), under the assumption that received phase of each interfering user is random from window to window. Timing offsets which are a small fraction of the window time are assumed not to be the limiting factor, evidenced by the results in Figure 4.12 and other simulations. Time dispersion of the channel manifests in the same way as timing offset. Sample frequency offset has not been studied in detail.

To look at the pole capacity due to fading we substitute $I_0 = \sigma_n^2$ and $SNR_{tgt} = \bar{\gamma}$

in (4.64) to obtain

$$P_N^{rx} = \frac{I_0 SNR_{tgt}}{\frac{M}{R}\mu_r^2 - (N-1)SNR_{tgt}\sigma_g^2} \approx \frac{I_0 SNR_{tgt}}{\frac{M}{R}\mu_r^2 - N \cdot SNR_{tgt}\sigma_g^2}, \tag{E.5}$$

where μ_r^2 is the mean square of the fading envelope and σ_g^2 is the fading variance. $\frac{M}{R}$ is the TC-OLA processing gain, equivalent to the CDMA spreading gain G. Although we assume only slow power control, the mean and variance parameters resulting from power control error could be substituted here instead. Compare with the RPMA equation

$$P_N^{rx} = \frac{I_0 SNR_{tgt}}{G - N \cdot SNR_{tgt}} \tag{E.6}$$

which assumes a similar form except for the fading parameters. We can solve for the pole capacity in a similar way as

$$N_{tx} = \frac{\frac{M}{R}}{SNR_{tgt}} \frac{\mu_r^2}{\sigma_g^2}, \tag{E.7}$$

noting that the pole capacity depends on the channel fading parameters. We can similarly solve for pole capacity in terms of N_{rx}:

$$N_{rx} = \frac{\frac{M}{R}}{SNR_{tgt}} \frac{\mu_r^2}{\sigma_g^2}(1 - PER_{ul}(SNR_{tgt})) \tag{E.8}$$

We have used convolutional coding parameters that we believe are similar to the RPMA system to obtain PER as a function of target SNR. We can use this function to plot the pole capacity in terms of N_{rx}. In Figure E.1 we have used $\frac{\mu_r^2}{\sigma_g^2} = 1$ to match the RPMA notes as closely as possible.

For independent Rayleigh fading, $\frac{\mu_r^2}{\sigma_g^2} = \frac{\pi}{2} \approx 1.57$. We could compute the corresponding uplink loading curve as shown below for a hypothetical TC-OLA system with $\frac{M}{R} = 8192$ in *independent* Rayleigh fading based on the loss of link budget as in (E.9) with P_0 from (E.1). The fading has degraded the textbook AWGN BPSK result (no fading, no self-interference) to the values shown below in Figure E.2. This is caused by the self interference due to fading.

$$L_{dB} = 10 \log_{10} \left(P_{rx}(N_{rx}, SNR_{tgt}) \right) - P_0 \tag{E.9}$$

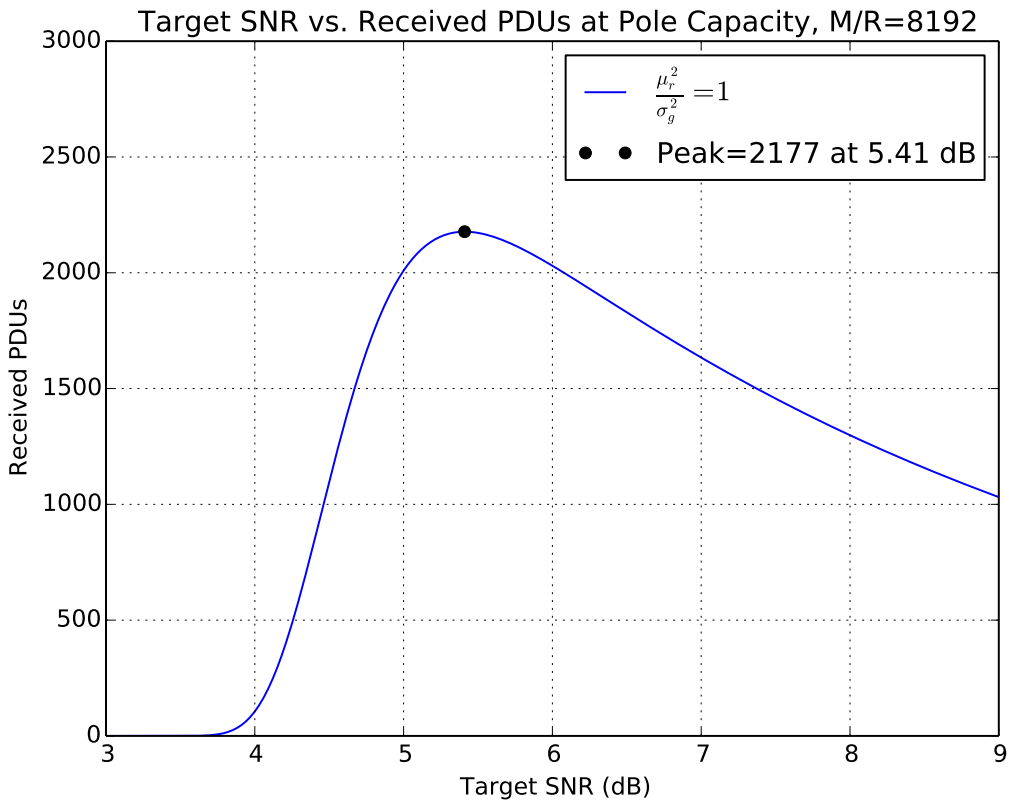

Figure E.1: Pole capacity from (E.8) for $\frac{\mu_r^2}{\sigma_g^2} = 1$.

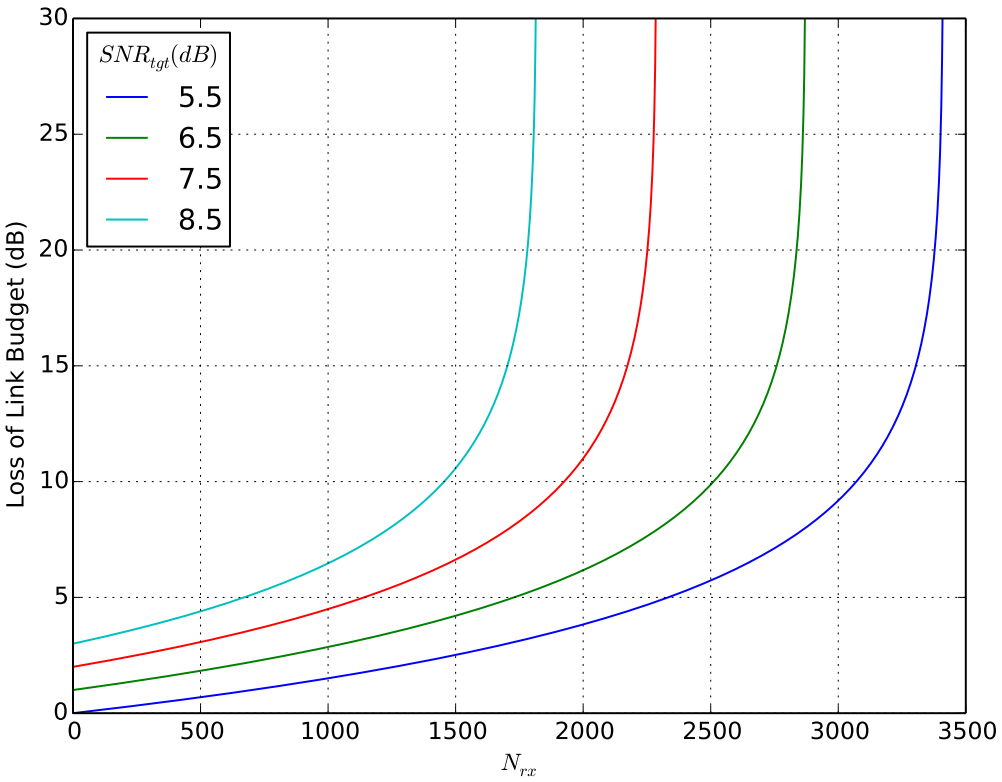

Figure E.2: TC-OLA uplink loading due to independent Rayleigh fading from (E.9) with $\frac{\mu_r^2}{\sigma_g^2} = \frac{\pi}{2}$.

$$P_{rx}(N_{rx}, SNR_{tgt}) = \frac{N_0}{\left(\frac{G}{SNR_{tgt}} - \frac{N_{rx}}{\frac{\mu_r^2}{\sigma_g^2}(1-PER_{ul}(SNR_{tgt}))}\right)} \tag{E.10}$$

If we observe independent Rician fading, the pole capacity is expected to rise by raising the signal to interference ratio (SIR) limit as shown in Figure 4.7. The factor $\frac{\mu_r^2}{\sigma_g^2}$ in (E.8) is related to Rician K by

$$\frac{\mu_r^2}{\sigma_g^2} = \frac{\pi}{2} L_{1/2}^2(-K), \tag{E.11}$$

$$L_{1/2}(x) = e^{x/2}\left[(1-x)\, I_0\left(\frac{-x}{2}\right) - x I_1\left(\frac{-x}{2}\right)\right]. \tag{E.12}$$

When the fading is correlated (the typical case) the pole capacity also rises. In Figure 4.8 below we show the SIR as a function of the normalized Doppler frequency (relative to the window period, analogous to the symbol period). Thus the normalized Doppler is an indicator of pole capacity of this system via equation (E.8).

E.2.2 Power Control

The power control assumption in the above analysis is that users are received with equal average power μ_r^2. Fast power control which tracks the short-term fading may also raise the pole capacity. We might consider this case by creating a log-normal distribution with standard deviation parameter

$$\sigma_{log} = ln\left(10^{\frac{\sigma_e}{20}}\right) \tag{E.13}$$

where σ_e is the power control error deviation in dB. The variance of this "fading" envelope is

$$\sigma_g^2 = (e^{\sigma_{log}^2} - 1)e^{\sigma_{log}^2} \tag{E.14}$$

and the mean is

$$\mu_r = e^{\sigma_{log}^2/2} \tag{E.15}$$

leading to

$$\frac{\mu_r^2}{\sigma_g^2} = \frac{1}{e^{\sigma_{log}^2} - 1}. \tag{E.16}$$

We assume the power control error varies with time and is independent from window to window. As several windows are added together to create the TC-OLA output, the sum of log-normal variables becomes a Gaussian variable with the above parameters. For an error of 2 dB, we obtain

$$\frac{\mu_r^2}{\sigma_g^2} \approx 18.4, \tag{E.17}$$

similar to Rician fading with a high K factor. Therefore, this type of fading alone is not likely to be a limiting factor in a TC-OLA system.

E.2.3 Scheduled vs. Random

In the RPMA uplink, nodes choose a random chip offset to begin transmission. As explained in [15], scheduling is an overhead that reduces network efficiency. However,

there is also a technical challenge in scheduling as it imposes tight timing requirements on the order of T_c to prevent collisions. In a random system there are no tight timing requirements, but the system will be subject to slotted ALOHA type loading that reduces the capacity due to collisions. In [15] it is explained that collisions are dealt with through FEC, which is another overhead that reduces network efficiency. The percentage of successfully received packets at RPMA pole capacity can be computed from (E.21) below as

$$\eta = \left(1 - \frac{1}{N_c}\right)^{N_{tx}-1} \tag{E.18}$$

$$= \left(1 - \frac{1}{8192}\right)^{2100} \tag{E.19}$$

$$= 0.77 \tag{E.20}$$

for the pole capacity scenario described in the ORW uplink capacity slides. The true pole capacity of the RPMA system is reduced by this factor, resulting in about 1625 successfully received packets when accounting for collisions.

TC-OLA can operate in an analogous random mode and will suffer collisions due to codes randomly being the same. However, scheduling does not impose any new timing requirements beyond what is required for a working system. Thus it should be possible to avoid collisions and possibly reduce the necessary FEC overhead.

E.2.4 Time-Dispersive Channels

In a time dispersive channel, the RPMA system will lock onto one (likely the strongest) multipath component. Energy from other multipath components may interfere with other users on nearby chip offsets. In TC-OLA, multipath that is short relative to the window time remains nearly orthogonal to other users and an "equivalent channel" is seen by the desired user. This equivalent channel can be equalized at the symbol rate using standard techniques (MMSE, DFE).

E.3 Comparison of RPMA with Slotted ALOHA

In a slotted ALOHA system with N nodes, a node may transmit in the current slot with probability q such that probability of success is

$$P(success) = q(1-q)^{N-1} \tag{E.21}$$

with efficiency

$$\eta = Nq(1-q)^{N-1}. \tag{E.22}$$

The value that maximizes η in (E.22) is $q = \frac{1}{N}$.

In an RPMA system with N_c chips and N nodes with data to transmit, each node transmits on a specific chip offset with probability $\frac{1}{N_c}$. The probability of success is then

$$P(success) = \frac{1}{N_c}\left(1 - \frac{1}{N_c}\right)^{N-1} \tag{E.23}$$

with efficiency

$$\eta = N\frac{1}{N_c}\left(1 - \frac{1}{N_c}\right)^{N-1}. \tag{E.24}$$

The number of users that maximizes efficiency is $N = N_c$. The primary difference is that in slotted ALOHA we have an unknown probability of transmission q and a known number of users N. Here we have a known transmission probability $\frac{1}{N_c}$ and an unknown number of users N. However, the equations take the same form and are maximized at the same point.

In either case we can obtain the familiar system throughput equation

$$S = Ge^{-G}, \tag{E.25}$$

where G is the normalized traffic load [54].

E.4 TC-OLA Compatibility with RPMA

This section covers some of the initial ideas regarding compatibility of TC-OLA with existing RPMA systems. The two initial ideas are sample rearrangement and coexistance in the same base station.

Sample rearrangement is possible but requires some extra buffer memory to collect all of the symbols before rearranging. Figure 4.3 shows how sample rearrangements converts CDMA (or RPMA) into TC-OLA.

A sample rearrangement approach requires roughly $\approx N^2 b$ SRAM bits, where b is the bit depth of the samples. This is around 64Mbits (2^{26}) for $N = 8192$ with 1-bit symbols. This may not be practically feasible as typical SRAM chips are measbured in Kbits. Some 64Mbit true SRAM products are available on the market but are cost prohibitive (≈$80) at this time.

The overhead to operate a DRAM of this size is probably also not worth it. There are some "Pseudo SRAM" devices on the market which integrate the DRAM control but have a longer access time. These may still be cost prohibitive ($8) at this time, and for this application.

A TC-OLA transmitter design not using sample rearrangement requires N RAM bits. A 1-bit symbol transmitter that could be realized just using N flip flops and a few gates similar to LFSR. A generic transmitter hardware design was shown in Figure 6.21. A transmitter for 1-bit digital symbols was shown in Figure 6.22. The example shows a transmitter for $M = 8, R = 1$ and $M = 4, R = 1$, but can be generalized to a shift register with length $M - 1$ such that a new symbol replaces the oldest symbol whenever the counter is zero. For autonomous operation, a state machine would enable the clock for this circuit until the FIFO runs dry. For circular TC-OLA, you would pre-load the shift register.

The corresponding receiver is not significantly different from what is already drawn in the dissertation document, Figure 6.23. If the incoming signal is sampled with 1 bit (0 = -V, 1 = +V) then an overlap-add RAM is needed with N entries and $\log_2(N + 1)$ bits per entry. A practical receiver would also require an N-bit adder and associated timing recovery circuits.

Alternately, A TC-OLA system can simply coexist with RPMA in the same transmitter. Consider each window is transmitted synchronously with each RPMA symbol. To the RPMA receiver, the synchronous TC-OLA window looks like a random sequence and the correlator should mostly reject it. To the TC-OLA receiver, the

RPMA signal looks like a random sequence and should on average sum to zero in each overlap add column.

Having a dual-mode base station may be a way forward with this, where it could talk to the endpoints in either "language" and some newer installations could be fully TC-OLA while some legacy installs might be a mix.

Appendix F

Publishing Challenges

One difficulty faced in publishing this work has been to convey both the context and the novelty of this method in the span of an IEEE journal article. Reviews of Chapters 2, 3, and 5 were mixed but ultimately accepted for publication. Chapter 4 was ultimately rejected although in our opinion it is the most promising application of TC-OLA that we have found.

As an example of these challenges, the reviewers for Chapter 4 have taken the position that TC-OLA is essentially nothing more than rearrangement of the chips in a DS/CDMA signal. As we have shown in this document, TC-OLA has more facets than this article alone can convey. One way we plan to address the review comments is the aforementioned overview paper in magazine article format. We believe this article will help present the context and novelty of the method without the expectation of deep technical analysis which can be deferred to more focused articles.

The review comments are presented below. The references have been updated to this document.

F.1 Reviews of *Time-Compression Overlap Add for Low Power Wide Area Networks*

F.1.1 Editor's Comments

This paper proposes a code-division variant of time-compression overlap add (TC-OLA) scheme for low power wide area networks and the target key applications are IoT monitoring applications with moderate latency requirements. The proposed

scheme is similar to the traditional CDMA scheme but shows better performance mainly due to the property that it allows the channel to be equalized at the message symbol rate rather than the channel chip rate. The editors detailed comments are as follows.

1. The paper is based on authors previously published work in reference [12] and [44]. It is suggested the authors summarize the key and new contributions of this paper in the introduction section.

2. The paper needs to clearly address how the proposed scheme works well in the low power settings and why its target application IoT monitoring applications with moderate latency requirements instead of just saying so. Detailed performance results are needed to demonstrate these key statements.

3. Regarding the uplink near-far effect, the paper assumes that all the users have the equal received average power at BS thus the issue was not investigated. Since near-far has been one of the key issues in code-division based schemes, the paper at least needs to provide some insights on how the near-far problem impacts the proposed scheme and how that is compared with the traditional CDMA, i.e., is the problem more severe or less severe compared with the traditional CDMA scheme?

4. The system design and results are not sufficiently presented. Some of the simulation assumptions need to be reconsidered so that more comprehensive and realistic performance results, especially the comparison between the proposed scheme and the traditional CDMA, should be provided.

5. The paper should provide clear definitions on some key parameter such as M, R, K, and also need to give their related physical meanings in the system model section, to help better understanding the scheme.

6. The paper needs to improve the writing and fix quite a few grammar mistakes.

F.1.2 Reviewer 1

This paper proposes a physical layer transmission scheme called time-compression overlap add (TC-OLA). The TC-OLA scheme is interesting, which can be regarded as a rearrangement of CDMA signals. Simulation results show that the TC-OLA

scheme outperforms the conventional CDMA system. My major comments are as follows:

1. TC-OLA scheme has been described by the authors as cited in [12], [44], [13]. Furthermore, the authors investigate the TC-OLA performance for different channels. In my opinion, there does not seem to be a sufficient contribution in the performance analysis. They read more like introduction rather than analysis especially for the latter part of frequency flat fading scenario.

2. The authors consider the SUI model for the time-vary frequency selective channels, but the performance analysis seems to be superficially treated. My suggestion is that the authors adopt the multipath Rayleigh fading channel (power delay profile model) to check whether the proposed TC-OLA scheme can collect the multipath diversity.

3. In system model, TC-OLA is viewed as a rearrangement of CDMA signal. In simulations, TC-OLA reduces the BER compared with CDMA. However, it is not clear why such a rearrangement can lead to the improvement of BER performance. The authors say that PRMA-like system suffers more interference between different users. Accordingly, the authors should compare the correlation function of TC-OLA signals and CDMA signals, respectively.

4. Equations (4.33) and (4.34) should be explained more clearly. I understand that the matrix forms of these equations may be complicated due to the convolution operation. It may be better if the authors can formulate simpler equations to decribe these relationships.

In general, although the TC-OLA scheme is interesting, I am afraid I cannot recommend this paper for publication in its current form. The authors still need to do a concrete work beyond the prior knowledge.

F.1.3 Reviewer 2

The paper present a variant of the the modulation scheme called TC-COLA, patented and presented by the authors and presented in reference [12] and [44].

The novelty of the paper is limited since it consists of a variation of such a modulation in the LPWA context. This variation, as presented and evaluated, is compared

to the RPMA only and not in the LPWA scenario at large. Furthermore the comparison with the RPMA technique falls short since it is not taking into in to account the fact that the the packets in RPMA are starts *randomly* in each slot. So RPMA is not as simple as described in the paper.

As far as the presentation the paper needs to be substancially reworked. The notation needs to be greatly improved (basically the paper seems to be adpated from a transmission of digital samples to digital symbols but the notation for digital transmission of bits is much different than that of the transmission of samples of a signal). The system description is quite obscure. The paper starts, for example with the sentence "A baseband TC-OLA signal is generated for a message signal $m_u[k]$ sampled at the message rate f_m using (4.1)": what is u? what is the "message rate"? what is a message signal? is it a sequence of symbols from a constellation? does u stands for user? The reader needs to read trough the paper and then come back to understand the meaning. The suggestion is, as usual, to define first and then use any symbol or term.

The evaluation of the modulation format is done at the raw bit error level. It is pretty known that a fair evaluation must include the coding, as with proper coding the ranking of the different modulation formats can change.

The evaluation of the performances is done in general taking too many shortcuts and gives certainly a first impression of the performances but not robust and rigorous enough for a Transaction paper.

The authors leave the topics related to the synchronization out of their consideration: this is a key aspect since they use a slotted Aloha. Furthermore they leave to another future paper a robust detection for their modulaton scheme. One then remain with a legitimate doubt the the proposed one is fragile.

F.1.4 Reviewer 3

This paper proposed a code-division variant of time-compression overlap add (TC-OLA) and claim that proposed scheme can support a larger number of simultaneous users in the uplink. However, the claimed advantage of proposed scheme is not straightforward based provided results. And the description of proposed scheme is not very clear at many place in the paper. More detail problems I find are listed below.

Time-compression overlap add (TC-OLA) is not such a well known technology yet

hence it is supposed to be at least briefly introduced in the paper like the concept and motivation of it.

The definition of indices k and j make me confused. Are they only used to indicate the change of sample rate? [...], it says "The change in indices from k to j...", but in (4.2) it is changed from j to k. The definition of these two symbol need to be explicitly provided.

From (4.7) to (4.8), I cant understand how $m_u[k]$ comes from, because by looking back on (4.1), it should be $m_u[j]$.

In (4.27), I cant understand the meaning of subscription u here. Why the channel of user t related to other user u? The explicit definition of $c_{t,u}$ is needed. Is it the channel between user t and user u or that between user t and base station.

In the first paragraph of Section 4.3.2, it says $i = k$, if I understand it correctly, I think it should be $j = k$?

The full name of some terminologies such as DS-CDMA and RAKE are not provided.

[...] the function of vec() is not clear.

In Figure 4.11, the difference among SUI models need to be declared in the context. Otherwise the advantage of proposed scheme is not clear from this fig.

The advantage of proposed code-division variant of TC-OLA is not prominent based on the results provided in the paper. There is only one figure compared performance between proposed scheme with existing scheme hence the contribution of proposed scheme is not clear.

Bibliography

[1] M. Z. Win, D. Dardari, A. F. Molisch, W. Wiesbeck, and J. Zhang, "History and applications of UWB," *Proc. IEEE*, vol. 97, no. 2, pp. 198–204, Feb. 2009.

[2] R. L. Freeman, *Telecommunication system engineering*, 4th ed. Hoboken, NJ, USA: Wiley-Interscience, 2004.

[3] "Interfaces for the optical transport network," International Telecommunication Union, ITU-T G.709, 1996.

[4] M. Jacob and J. Mattern, "Time-compressed single-sideband system (Ticoss)," *IRE Trans. Commun. Syst.*, vol. 6, no. 1, pp. 2–8, June 1958.

[5] J. Flood and D. Urquhart-Pullen, "Time-compression-multiplex transmission," *Proc. IEE*, vol. 111, no. 4, pp. 647–668, Apr. 1964.

[6] M. J. Martin and E. Thepault, "An analog time-division multiplexing system," in *Proc. 3rd Eur. Solid State Circuits Conf.*, 1977.

[7] A. Kourtis, K. Dangakis, V. Zacharopoulos, and C. Mantakas, "Analogue time division multiplexing," *Int. J. of Electron.*, vol. 74, no. 6, pp. 901–907, Jan. 1993.

[8] G. McGibney, "Analog radio system with acoustic transmission properties," U.S. Patent 6 606 312 B1, Aug. 12, 2003.

[9] U. Zölzer, *DAFX: digital audio effects*, 2nd ed. Chichester, UK: John Wiley & Sons, 2011.

[10] J. O. Smith, *Spectral Audio Signal Processing*, 2011. [Online]. Available: http://ccrma.stanford.edu/∼jos/sasp/

[11] R. van Nee and R. Prasad, *OFDM for Wireless Multimedia Communications*, 1st ed. Norwood, MA, USA: Artech House, 2000.

[12] S. Harrison and P. Driessen, "Novel UWB and spread spectrum system using time compression and overlap-add techniques," *IEEE Access*, vol. 2, pp. 1092–1105, Sep. 2014.

[13] ——, "Spread spectrum method and apparatus," U.S. Patent 9 479 216 B2, Oct. 25, 2016.

[14] J. G. Andrews *et al.*, "What will 5G be?" *IEEE J. Select. Areas Commun.*, vol. 32, no. 6, pp. 1065–1082, June 2014.

[15] *How RPMA Works: The Making of RPMA*. Ingenu Inc., 2016.

[16] Y. Li, "Channel estimation and signal detection for UWB," Mitsubishi Electric Research Laboratories, TR2003-74, Nov. 2003.

[17] J. del Prado Pavon, S. S. N., V. Gaddam, K. Challapali, and C.-T. Chou, "The MBOA-WiMedia specification for ultra wideband distributed networks," *IEEE Commun. Mag.*, vol. 44, no. 6, pp. 128–134, June 2006.

[18] G. L. Stüber, *Principles of mobile communication*. Berlin, Germany: Springer Science & Business Media, 2011.

[19] K. V. S. Hari, D. S. Baum, A. J. Rustako, R. S. Roman, and D. Trinkwon, "Channel models for fixed wireless applications," *IEEE 802.16 Broadband Wireless Access Working Group*, July 2001.

[20] R. Jain, *Channel models: A tutorial*, 2007. [Online]. Available: https://www.cse.wustl.edu/∼jain/cse574-08/ftp/channel_model_tutorial.pdf

[21] A. F. Molisch *et al.*, "A comprehensive standardized model for ultrawideband propagation channels," *IEEE Trans. Antennas Propagat.*, vol. 54, no. 11, pp. 3151–3166, Nov. 2006.

[22] *Spectrum Allocations for Ultra Wide Band Communication Devices*. New Zealand Ministry of Economic Development, 2008.

[23] "Revision of part 15 of the commission's rule regarding ultra-wideband transmission systems, first report and order (ET Docket 98-153)," Federal Communications Commision, Washington, DC, USA, FCC 02-48, Feb. 2002.

[24] "IMT-2000 third generation cellular networks," European Telecommunications Standards Institute, EN 301 908, 2002.

[25] "LTE; evolved universal terrestrial radio access (E-UTRA); LTE physical layer; general description," European Telecommunications Standards Institute, 3GPP 136.201, 2003.

[26] T. J. Myers, "Random phase multiple access communication interface system and method," U.S. Patent 7 782 926 B2, Aug. 24, 2010.

[27] R. J. Holbeche and R. T. Mannings, "Comparison between time-compression multiplexing and frequency-division multiplexing over narrowband radio systems," *Commun., Radar and Signal Process., IEE Proc. F*, vol. 131, no. 2, pp. 130–138, Apr. 1984.

[28] J. K. Cavers, "Pilot symbol assisted modulation and differential detection in fading and delay spread," *IEEE Trans. Commun.*, vol. 43, no. 7, pp. 2206–2212, July 1995.

[29] A. F. Molisch, "Ultra-wide-band propagation channels," *Proc. IEEE*, vol. 97, no. 2, pp. 353–371, Feb. 2009.

[30] "High speed data capture and pattern generation platform - TSW1400EVM," Texas Instruments. [Online]. Available: http://www.ti.com/tool/tsw1400evm

[31] G.-B. Stan, J.-J. Embrechts, and D. Archambeau, "Comparison of different impulse response measurement techniques," *J. Audio Eng. Soc.*, vol. 50, no. 4, pp. 249–262, Dec. 2002.

[32] "Zedboard," ZedBoard.org. [Online]. Available: http://zedboard.org/product/zedboard

[33] "Universal software radio peripheral (USRP)," Ettus Research (National Instruments). [Online]. Available: http://www.ni.com/sdr/usrp/

[34] "Thunderbolt E GPS disciplined clock," Trimble Navigation, Ltd. [Online]. Available: http://www.trimble.com/timing/thunderbolt-e.aspx

[35] A. Alimohammad, S. F. Fard, B. F. Cockburn, and C. Schlegel, "Compact Rayleigh and Rician fading simulator based on random walk processes," *IET Commun.*, vol. 3, no. 8, pp. 1333–1342, Aug. 2009.

[36] F. Ren and Y. R. Zheng, "A low-complexity hardware implementation of discrete-time frequency-selective Rayleigh fading channels," in *Proc. 2009 IEEE Int. Symp. Circuits Syst.*, pp. 1759–1762.

[37] S. Harrison and P. Driessen, "Spread spectrum method and apparatus," U.S. Patent Appl. 20160056858A1, Feb. 25, 2016.

[38] R. E. Ziemer and R. L. Peterson, *Digital communications and spread spectrum systems*. New York, NY, USA: Macmillan, 1985.

[39] W. C. Jakes and D. C. Cox, *Microwave mobile communications*. Hoboken, NJ, USA: Wiley-IEEE Press, 1994.

[40] F. J. Harris, *Multirate signal processing for communication systems*. Upper Saddle River, NJ, USA: Prentice Hall PTR, 2004.

[41] A. V. Oppenheim and R. W. Schafer, *Discrete-time signal processing*. New York, NY, USA: Pearson Higher Education, 2010.

[42] L. Vangelista, A. Zanella, and M. Zorzi, "Long-range IoT technologies: The dawn of LoRa," in *Future Access Enablers of Ubiquitous and Intelligent Infrastructures*. New York, NY, USA: Springer, 2015, pp. 51–58.

[43] "Seven NB-IoT surprises you need to know about," Ingenu Inc., 2016.

[44] S. Harrison and P. Driessen, "Time-compression overlap add: Description and implementation," in *Proc. 2015 IEEE Pacific Rim Conf. Commun., Comput. and Signal Process.*, pp. 64–69.

[45] T. Frank, A. Klein, and E. Costa, "IFDMA: A scheme combining the advantages of OFDMA and CDMA," *IEEE Wireless Commun. Mag.*, vol. 14, no. 3, pp. 9–17, June 2007.

[46] H. G. Myung, "Introduction to single carrier FDMA," in *Proc. 15th Eur. Signal Process. Conf.*, 2007, pp. 2144–2148.

[47] A. Goldsmith, *Wireless communications*. Cambridge, UK: Cambridge University Press, 2005.

[48] Q. Feng, X. Xia, Z. Ye, and N. Zhang, "Sparse multipath channel estimation and decoding for broadband vector OFDM systems," *CoRR*, vol. abs/1512.06502, 2015. [Online]. Available: http://arxiv.org/abs/1512.06502

[49] J. Hu and N. C. Beaulieu, "Accurate closed-form approximations to Ricean sum distributions and densities," *IEEE Commun. Lett.*, vol. 9, no. 2, pp. 133–135, Feb. 2005.

[50] J. G. Proakis and M. Salehi, *Digital communications*, 5th ed. Boston, MA, USA: McGraw-Hill, 2008.

[51] V. V. Veeravalli, A. Sendonaris, and N. Jain, "CDMA coverage, capacity and pole capacity," in *Proc. 1997 IEEE 47th Veh. Technol. Conf.*, vol. 3, pp. 1450–1454.

[52] H.-C. Yang and M.-S. Alouini, *Order statistics in wireless communications: Diversity, adaptation, and scheduling in MIMO and OFDM systems*. Cambridge, UK: Cambridge University Press, 2011.

[53] T. J. Myers, "Uplink transmitter in a random phase multiple access communication system," U.S. Patent 7 593 383 B1, Sep. 22, 2009.

[54] J. Hayes, *Modeling and analysis of computer communications networks*. New York, NY, USA: Springer, 1984.

[55] X. Dong, L. Jin, and P. Orlik, "A new transmitted reference pulse cluster system for UWB communications," *IEEE Trans. Veh. Technol.*, vol. 57, no. 5, pp. 3217–3224, Sep. 2008.

[56] "DS-UWB physical layer submission to 802.15 task group 3a," IEEE P802.15.3a Working Group, P802.15-04/0137r3, July 2004.

[57] "Multi-band OFDM physical layer proposal for IEEE 802.15 task group 3a," IEEE P802.15.3a Working Group, P802.15-03/268r3, Mar. 2004.

[58] P. A. Catherwood and W. G. Scanlon, "Ultrawideband communications–an idea whose time has still yet to come?" *IEEE Antennas Propagat. Mag.*, vol. 57, no. 2, pp. 38–43, Apr. 2015.

[59] H. G. Myung and D. J. Goodman, *Single carrier FDMA: a new air interface for long term evolution*. Chichester, UK: John Wiley & Sons, 2008.

[60] F. Pancaldi, G. M. Vitetta, R. Kalbasi, N. Al-Dhahir, M. Uysal, and H. Mheidat, "Single-carrier frequency domain equalization," *IEEE Signal Processing Mag.*, vol. 25, no. 5, pp. 37–56, Sep. 2008.

[61] T. Obara, K. Takeda, and F. Adachi, "Performance analysis of single-carrier overlap FDE," in *Proc. 2010 IEEE Int. Conf. Commun. Syst.*, pp. 446–450.

[62] Y. Wang, X. Dong, P. H. Wittke, and S. Mo, "Cyclic prefixed single carrier transmission in ultra-wideband communications," *IEEE Trans. Wireless Commun.*, vol. 5, no. 8, pp. 2017–2021, Aug. 2006.

[63] R. Zhang, X. Lu, Z. Zhong, and L. Cai, "A study on spatial-temporal dynamics properties of indoor wireless channels," in *Wireless Algorithms, Systems, and Applications*. Berlin, Germany: Springer, pp. 410–421.

[64] T. Frank, "Block-interleaved frequency division multiple access and its application in the uplink of future mobile radio systems," Ph.D. dissertation, Technische Universität, 2010.

[65] N. Hicheri, M. Terr, and B. Fino, "OFDM and DS-CDMA approaches, analysis of performances on fading multipath channels," in *Proc. 13th IEEE Int. Symp. Personal, Indoor and Mobile Radio Commun.*, vol. 4, 2002, pp. 1498–1501.

[66] S. Hara and R. Prasad, "Overview of multicarrier CDMA," *IEEE Commun. Mag.*, vol. 35, no. 12, pp. 126–133, Dec. 1997.

[67] M. Rice, *Digital Communications: A Discrete-Time Approach*. Upper Saddle River, NJ, USA: Pearson Prentice Hall, 2009.

[68] D. Chu, "Polyphase codes with good periodic correlation properties," *IEEE Trans. Inform. Theory*, vol. 18, no. 4, pp. 531–532, July 1972.

[69] T. Pollet, P. Spruyt, and M. Moeneclaey, "The BER performance of OFDM systems using non-synchronized sampling," in *Proc. 1994 IEEE Global Telecommun. Conf.*, pp. 253–257 vol.1.

[70] M. Hasna and M.-S. Alouini, "End-to-end performance of transmission systems with relays over Rayleigh-fading channels," *IEEE Trans. Wireless Commun.*, vol. 2, no. 6, pp. 1126–1131, Nov. 2003.

[71] ——, "Outage probability of multihop transmission over Nakagami fading channels," *IEEE Commun. Lett.*, vol. 7, no. 5, pp. 216–218, May 2003.

[72] V. Witkovskỳ, "Computing the distribution of a linear combination of inverted gamma variables," *Kybernetika*, vol. 37, no. 1, pp. 79–90, 2001.

[73] Y. Chen, S. Zhang, S. Xu, and G. Y. Li, "Fundamental trade-offs on green wireless networks," *IEEE Commun. Mag.*, vol. 49, no. 6, pp. 30–37, June 2011.

[74] C. Han *et al.*, "Green radio: Radio techniques to enable energy-efficient wireless networks," *IEEE Commun. Mag.*, vol. 49, no. 6, pp. 46–54, June 2011.

[75] M. Chiani and A. Giorgetti, "Coexistence between UWB and narrow-band wireless communication systems," *Proc. IEEE*, vol. 97, no. 2, pp. 231–254, Feb. 2009.

[76] M. Fischer, "user-peripheral-kmod-public," 2013. [Online]. Available: https://bitbucket.org/mfischer/user-peripheral-kmod-public

[77] J. Corbet, A. Rubini, and G. Kroah-Hartman, *Linux device drivers*. Sebastopol, CA, USA: O'Reilly Media, 2005.

[78] J. Pendlum, "FPGA accelerators in GNURadio with Xilinx's Zynq system on chip," 2013. [Online]. Available: http://www.gnuradio.org/redmine/projects/gnuradio/wiki/Zynq/11

[79] ——, "RFNoC tutorial: FPGA design," Aug. 2015. [Online]. Available: https://gnuradio2.squarespace.com/s/3-pendlum_jonathon-rfnoc_tutorial_fpga.pdf